The trace metal content of modern and ancient peritidal and shallow subtidal dolomites: significance and systematics

by

Daniel Alejandro Petrash

A thesis submitted in partial fulfillment of the requirements for the degree of

Doctor of Philosophy

Department of Earth and Atmospheric Sciences

University of Alberta

ABSTRACT

Dolomitization has traditionally been regarded as being related to the interaction of thermally active Mg-rich fluids with poorly ordered carbonate precursors of elusive origin. Our ideas on how such precursors form have evolved rapidly since the late 1990s, and microbes are now considered key players — i.e., by providing nucleation sites and due to their capacity to regulate pore water alkalinity. Outstanding questions include what triggers the low-temperature reactions conducive to dolomite stabilization and whether or not subsurface chemolithotrophs participate in the catalysis of these reactions.

Here these aspects are evaluated throughout three independent but complementary textural and spectroscopic examinations of shallow marine dolomites. First, fine-scale analyses of modern carbonate cements point to biologically mediated manganese and sulfur co-recycling as a necessary control for dolomite stabilization. Second, similar analyses of mid-Cretaceous dolomitic marlstones suggest that in the Aptian-Albian epicontinental sea of northern South America, dolomite precipitation was linked to the utilization of metals and sulfur for organic matter respiration. Reactants were transported to the extended shallow marine setting in association with episodic orbital perturbations, which also triggered high organic matter productivity and burial, and ultimately led to interstitial organogenic dolomite formation. Third, stromatolitic rocks from the Paleoproterozoic Gunflint Formation (Ontario, Canada) were interrogated in order to interpret the variable redox states of pore waters at the time of stromatolite accretion and diagenetic mineral stabilization. This study shows that diagenetic shifts associated with exogenous water mixing, together with variable burial and exhumation histories, led to the development of the temporarily and spatially restricted reaction fronts responsible for the pervasive replacement of early formed

carbonate cements. Such diagenetic complexity adds difficulty to the interpretation of paleomarine geochemical conditions.

Overall, this work reveals that the trace metal content of shallow marine dolomite provides information useful for the evaluation of redox conditions that govern mineral authigenesis. However, autocycles and their effect on the activity of subsurface microbes, and thus over the saturation state of minerals in coastal sediments should be carefully considered prior to regional scale paleoceanographic interpretations.

PREFACE

This thesis is an original work by Daniel A. Petrash. The research conducted for this doctoral dissertation was supervised by Dr. Kurt O. Konhauser at the University of Alberta.

Chapter 2 of this thesis has been published as: Petrash, D.A., Lalonde, S.V., González-Arismendi, G., Gordon, R. A., Méndez, J.A., Gingras, M.K., and Konhauser, K. O., 2015. "Can Mn-S redox cycling drive sedimentary dolomite formation? A hypothesis". *Chemical Geology* 404: 27-40. Dr. S. Lalonde, J.A. Mendez-Dot, and I were responsible for sample collection and *in situ* microelectrode and physcochemical measurements. G. Gonzalez-Arismendi assisted with statistical analyses and geochemical modeling. Dr. R. Gordon was the beamline scientist at the Advanced Light Source. I was responsible for manuscript composition. Dr. M.K Gingras supervised the sedimentological aspects. Dr. S. Lalonde and Dr. K.O. Konhauser contributed to manuscript edits.

Chapter 3 of this thesis has been submitted to the *American Journal of Science* as: "Black shale deposition and early diagenetic dolomite cementation during Oceanic Anoxic Event 1: The mid-Cretaceous Maracaibo Platform, north-western South America" by D.A. Petrash, N. Gueneli, J.J. Brocks, J.A. Mendez-Dot, G. Gonzalez-Arismendi, S.W. Poulton, and K.O. Konhauser. J.A. Mendez-Dot and I were reponsible for core sampling and transmitted light petrographic analyses. G. Gonzalez-Arismendi provided assistance with isotopic analyses. N. Guineli conducted biomarker and Fe-speciation analyses. I conducted high-resolution petrographic and geochemical analyses. N. Guineli and I were responsible for manuscript composition. Dr. K.O Konhauser, Dr. S.W. Poulton, and Dr. J. J. Brocks contributed to manuscript edits.

Chapter 4 of this thesis has been submitted to *Precambrian Research* as: "Chemical and textural overprinting of ancient stromatolites: timing, processes, and implications for their use as paleoenvironmental proxies". I conducted data collection and analysis and was responsible for manuscript composition. L.J. Robbins, Drs. S. Mojzsis, R. Shapiro, and K.O Konhauser contributed to manuscript edits.

The literature review in chapter 1 and concluding analysis in chapter 5 are my original work. This research benefited from the expert advice of reviewers who have taken the time to read and comment on one or more of the chapters.

DEDICATION

To Gabriela del Pilar

All models are wrong, but some models are useful.

George P. E. Box (1919-2013)

ACKNOWLEDGEMENTS

I express sincere thanks to my supervisor Dr. Kurt Konhauser for his guidance, support, patience, and friendship. My gratitude also extends to Dr. Karlis Muehlenbachs, who also played a major role in my scientific development. Professors Dr. Brian Jones and Dr. Murray Gingras are thankfully acknowledged for their constructive comments and guidance over the last five years.

Thanks to my friends from the Geomicrobiology Research Group, especially to Rasmus Haugaard, Leslie Robbins, Dr. Aleksandra Mloszewska, and Dr. Stefan Lalonde for offering me their help and willingness to discuss, review, and improve my manuscripts.

Nur Gueneli and Dr. Jochen Brocks (The Australian National University) conducted biomarkers analyses (Chapter III). Dr. Simon Poulton (University of Leeds) performed iron speciation analyses (also in Chapter III). I cannot be grateful enough to them for their timely contribution to this work. Samples from the Frustration Bay locality were made available by Dr. Stanley Awramik (University of California) thanks to the intercession of Dr. Steve Mojzsis (Univeristy of Colourado).

I am also grateful to the Support Staff at the Department of Earth And Atmospheric Sciences: Dr. Nathan Gerein, Diane Caird, Dr. Guangcheng Chen, Dr. Andrew Locock, Mark Labbe, Martin Von Dollen, and Igor Jakab. I also thank Dr. Lachlan McLean and Dr. Ferenc Borondics (and team members of the mid-IR (beamline 01B1-1) at the Canadian Light Source) for technical advice and support. The expertise of Dr. Robert Gordon (CLS@APS) was critical for successful analyses at beamline 20ID at the Advanced Photon Source (APS). Use of the APS, an Office of Science User Facility operated for the U.S. Department of Energy (DOE) Office of Science by Argonne National Laboratory, was supported by the U.S. DOE under Contract No. DE-AC02-06CH11357.

Last but certainly not least, I want to express sincere thanks to my mother and my beloved Gabriela del Pilar Gonzalez-Arismendi for inspiration. Their emotional support and enthusiasm for my work made the process of acquiring this degree a rewarding experience.

TABLE OF CONTENTS

LIST OF TABLES

LIST OF FIGURES

LIST OF ABBREVIATIONS

2D-XRD: Two Dimensional-X-ray diffraction

AOM: Anoxygenic oxidation of Methane

ATR: Attenuated Total Reflectance

BSEM: Backscatter Scanning Electron Microscopy

DIC: Dissolved Inorganic Carbon

EDS: Energy-Dispersive Spectrometer

EPMA: Electron Probe microanalyses

EPS Exopolymeric substances (exopolymers)

Fe_{HR}: Highly reactive iron

Fe_{Py}: Iron associated with pyrite (Py)

Fe_T: Total iron

FTIR: Fourier Transform Infrared Spectroscopy

ICP-QMS: Inductively Coupled Plasma Quadrupole Mass Spectrometry

IR: Infrared

KB: Kirkpatrick-Baez mirrors

LA-ICP-MS: Laser Ablation ICP-MS

NIST: National Institute of Standards and Technology

OAE: Oceanic Anoxic Event

PCA Principal Component Analysis

REE: Rare earths elements

SEM: Scanning Electron Microscopy

SR: Synchrotron radiation

SRM: Standard Reference Material

TEM: Transmission Electron Microscopy

TOC: Total Organic Carbon

V-PDB: Vienna-Pee Dee Belemnite

WDS: Wavelength Dispersive X-ray Spectroscopy

XANES: X-ray absorption near edge structure

XRD: X-ray Diffraction

CHAPTER I

General Introduction

Dolomite ($CaMg[CO_3]_2$) is a rhombohedral carbonate mineral that can be structurally visualized as alternating layers of calcite and magnesite, with minor elemental substitutions including strontium, sodium, iron, and manganese (Lippmann, 1973; Veizer, 1983; Fig. 1.1). The mineral is an unimportant constituent of modern unconsolidated marine sediments, however, substantial amounts of Ca-rich poorly ordered precursors — collectively referred to as Ca-dolomite, are found in the peritidal to shallow subtidal zone of most Neogene carbonate platforms (Graf and Goldsmith, 1956; Gaines, 1974; Gaines, 1977; Mazzullo et al, 1987; Budd, 1997; Arvidson and Mackenzie, 1999; Warren, 2000).

In modern shallow marine settings, Ca-dolomite typically occurs in association with microbial heterotrophy (Vasconcelos and Mackenzie, 1997; Wright, 1999; Mazzullo, 2000; Warthmann et al., 2000; Van Lith et al., 2003; Moreira et al., 2004; Wright and Wacey, 2005; Sánchez-Román et al., 2008; Bontognalli et al., 2010). In such environments, the involvement of microbes in precursor dolomite nucleation has been largely linked to the bioutilization of sulfur at near-surface conditions (see Table 1.1). Nevertheless, there remains a lack of information on how such metastable precursors stabilize to more stoichiometric crystalline forms in shallow burial diagenetic realms.

Biogeochemical processes in subsurface sediments drive authigenic mineral formation and dissolution (Konhauser, 2007), and chemoheterotrophic pathways relying on the coupled recycling of manganese and iron may play important roles in shallow burial mineral authigenesis (i.e., Macquaker et al., 2014). In the suboxic zone, organic matter is oxidized via Fe(III) or Mn(IV, III) reduction. This may be a direct oxidation process by metal-reducing microbes or an indirect oxidation one via sulfate reduction and sulfide oxidation (Jørgensen and Kasten, 2006). The relevance of these respiration mechanisms deep in anoxic zones contradicts a tenet of

geomicrobiology, that anaerobic life arranges itself into zones according to a thermodynamic ladder. Effectively, the various heterotrophic communities should become zoned based on the coupling of buried organic carbon oxidation to the reduction of available terminal electron acceptors (TEAs) (Konhauser, 2007). These TEAs include (in decreasing order of energy yield), oxygen, nitrate, manganese, iron, sulfate, and ultimately dissolved inorganic carbon (Froelich et al., 1979). Nonetheless, microbial zonation — that is zonation based on the availability of TEAs in the sediment pile — cannot be evaluated in terms of thermodynamics alone (Bethke et al., 2011), as the thermodynamic drive and thus energy for metabolism is dictated by the identity and availability of the electron acceptors (LaRowe and Amend, 2015).

Enhanced rates of biomineralization due to modern subsurface activity may be related to past oceanographic conditions at the time of sediment deposition (Jørgensen and Kasten, 2006). Such paleoceanographic conditions may cause major variations in the stratigraphic availability of oxidized forms of sulfur, and could be instrumental for the subsurface availability of organic matter and Mn- and Fe-oxyhydroxides. However, it is difficult to predict how one net metabolic pathway would be favoured over another in the proximity of a stratigraphic level characterized by a relatively abnormal abundance of electron acceptors (see Marlow et al., 2014).

The stabilization (growth) of dolomite within discrete stratigraphic levels is perhaps a process that may be better explained by using biogeochemical arguments rather than strictly inorganic ones (cf. Hardie, 1987). Geochemical disequilibria are established in any diagenetic environment by the presence of even small supplies of electron donors and acceptors (Kappler et al., 2005). Therefore, the development of a predictive approach to the involvement of subsurface microbes in shallow burial dolomite formation is of foremost importance, since in such geochemical disequilibrium zones subsurface microbes can thrive over extended periods (Hoehler and Jørgensen, 2013). Further, the localized long-term activity of subsurface microbes may be instrumental for the development of a diagenetic condition favourable for dolomite stabilization (Roberts et al., 2013).

An accurate record of the non-steady oxidation states that affect the activity of subsurface communities during the diagenesis of metal reactive organic matter may be the redox-sensitive

transition metal signatures of organogenic minerals. Yet, a combination of analytical challenges, including spatial resolution and sensitivity of conventional methods, as well as spectroscopic and non-spectroscopic interferences has hindered the use of such a record. In this regard, the increasing utilization of rapidly evolving high resolution and sensitivity methods in chemical sedimentology offers a way forward (see Johnson et al., 2013).

This work provides the first example of an *in situ* geochemical assessment of dolomite via synchrotron-based microprobe techniques aimed at paragenetic interpretations. In this study, Xray techniques, such as micro X-Ray Fluorescence (μXRF), two-dimensional X-ray diffraction (2D-XRD), and spatially resolved X-ray Absorption Near-Edge Structure (XANES) are combined with conventional analytical methods, including stable C and O isotopes, biomarker signatures, mass spectrometry, and petrography. The goal is to interpret the diagenetic significance of subtle changes in trace metals contents of three early diagenetic non-replacive peritidal to shallow subtidal (lagoonal) dolomite occurrences.

Here, I first review what is currently known about the formation of dolomite at low temperature, and briefly discuss the potential role of the dark biosphere in dolomite stabilization. The dark biosphere is a region where the unique attributes of microbial life may combine to produce a precipitation environment that may be favourable to authigenic dolomite growth (see Jørgensen and Kasten, 2006). These microbial life attributes are controlled by the absence of photosynthesis, enclosed pore spaces, fluid flow, low energy levels, and a high rate of metal cycling (Fredickson et al., 1989, Fredickson and Fletcher, 2001; Edwards et al., 2012; Hoehler and Jørgensen, 2013).

Small differences in the physicochemical conditions governing the precipitation environment are likely to be recorded by the trace metal content of dolomitic rocks and the individual dolomite crystals within them (see Weber, 1964; Mackenzie and Moore, 1990); therefore, the systematics of minor and trace elemental abundances of dolomite for diagenetic interpretations are also concisely reviewed here. Finally, the general and specific objectives of this study are presented, followed by an overview of the research manuscripts comprising this dissertation.

1.1. Dolomite precipitation in modern shallow marine settings. What do we know?

The precipitation of modern shallow marine dolomite might not be very different from that of their older Phanerozoic counterparts, and the geochemical disequilibrium conditions that led to localized formation of dolomite in Holocene continental margins could have induced early diagenetic dolomitization in the geological past (Tucker, 1982). Still, one of the most persistent debates surrounds the conditions controlling dolomite formation in Precambrian seas (i.e., Tucker, 1982; Lumsden and Lloyd, 1997; Holland and Zimmerman, 2000). At the heart of this debate is the fact that little penecontemporaneous dolomite forms in modern marine environments, but thick accumulations of presumably primary dolomite occur in the Precambrian stromatolitic rock record (Fairbridge, 1957; Tucker, 1982; Given and Wilkinson, 1987; Grotzinger, 1989; Warren, 2000; Machel, 2004).

From an inorganic point of view, five classic dolomite-forming processes have been proposed: (1) the increase in relative concentrations of Mg^{2+} in tidal flats, sabkhas and lagoons, as Ca^{2+} is removed through the formation of gypsum (i.e., Deffeyes et al., 1964; Shinn et al., 1965; Friedman and Sanders, 1967); (2) the mixing of marine and meteoric water to maintain a marine Mg:Ca ratio of about 5:1 (Land, 1973; Badiozamani, 1973; Burns and Rossinsky Jr, 1989); (3) the generation of Mg-rich pore fluids through pressure solution of high-Mg calcite upon increasing burial (Wanless, 1979); (4) the introduction of Mg-rich exogenous fluids (i.e., Friedman and Hall, 1963; Choquette,1971); and (5) the release of Mg^{2+} from clay during burial (McHargue and Price, 1982). When these models are applied to Neogene sequences, however, the problem with dolomite remains its apparently slow kinetics of precipitation at shallow burial conditions. Accordingly, the formation of early diagenetic dolomite in modern settings is of great interest in addressing the question regarding the kinetics of Neogene dolomite formation in ancient analogous environments and the development of criteria for the recognition of similar diagenetic environments in deep geological time.

1.1.1. Low-T dolomite formation: a problem of kinetics?

Three intimately related aspects of carbonate geochemistry are thought to inhibit the near-surface precipitation of dolomite. First, the high enthalpy of hydration of Mg^{2+} cations may limit their availability to take part in dolomite nucleation reactions (Lippmann, 1973). Binding of partially hydrated Mg^{2+} cations to reactive carbonate surfaces systematically alter the morphology of newly formed crystals to limit further dolomite growth (Lippmann, 1973; Mucci and Morse, 1983; Han and Aizenberg, 2003). Second, the relatively low activity of dissolved CO_3^{2-} relative to HCO_3^- anions in seawater limits the rates of dolomite crystal growth in most modern marine environments. Under such conditions, there is insufficient free energy available for carbonate anions to overcome the hydration energy barriers of Mg cations bound at the surfaces of growing dolomite crystals (Lippmann, 1973). A third potentially inhibitory effect is ascribed to the presence of dissolved sulfate at high-temperatures (i.e., T > 100°C) (Baker and Kastner, 1981), and even low concentrations of dissolved SO_4^{2-} anions have been thought to inhibit the replacement of preexisting carbonate phases by dolomite (Baker and Kastner, 1981; Kastner, 1984; Morrow and Ricketts, 1988). Magnesium cations in solution and on the surface of growing crystals can form a neutral complex with SO_4^{2-} anions, thereby reducing the formation of carbonate complexes (Slaughter and Hill, 1991; Kastner, 1999). However, this effect does not appear to operate at low temperature (see Brady et al., 1996, Sánchez Román et al., 2009).

Despite the kinetic constraints depicted above, three modern dolomite-forming systems challenge our current understanding of low temperature dolomite formation. These include: (1) the formation of near-stoichiometric dolomite as uroliths in Dalmatian dogs (Mansfield, 1980); (2) the capacity of sea urchins to rapidly regenerate their specialized dolomitic teeth (Robach et al., 2006); and (3) some microbial systems that have been documented to mediate the nucleation and growth of dolomite precursors (e.g., Vasconcelos and McKenzie, 1997; Warthmann et al., 2000; van Lith et al., 2003; Sánchez-Román et al., 2008; Kenward et al., 2009). Although these examples suggest that the formation of dolomite is biologically catalyzed, they also highlight two outstanding problems. First, the available biogeochemical data is often amenable to a variety of genetic interpretations (e.g., Vasconcelos and McKenzie, 1997; Moreira et al., 2000; Sánchez-Román et al., 2009). Second, the hydrogeological constraints of early-diagenetic dolomite

formation, including the kinetics of the biochemical reactions involved, and the energy levels locally available in shallow burial diagenetic realms remain poorly understood.

In the rock record, early formed dolomite phases (hereafter termed primary) are often found alongside, and are seemingly indistinguishable from those considered secondary (as they are probably associated with the dissolution and recrystallization of precursor metastable phases). Moreover, it has been argued that secondary dolomite phases may also form by the penecontemporaneous (syndepositional) replacement of precursor phases (Friedman and Sanders, 1967; Land and Epstein, 1970; Buchbinder and Friedman, 1971; Muller et al., 1973; Schofield and Nelson, 1978). On the other hand, mineralogical, textural, and geochemical evidence frequently suggest that prior to pervasive dolomitization, most dolostones underwent a critical early diagenetic stage of direct nucleation followed by shallow burial recrystallization. During the recrystallization stage, reactants and products were conceivably transferred to the site of dolomite formation without the dissolution of precursor crystals (Land et al, 1975; Holail et al., 1988; Gregg and Shelton, 1990; Sibley, 1991). Such low-temperature mechanisms also point to the catalyzing roles of subsurface microbes, which can remain active as long as thermodynamic disequilibrium exists within their local diagenetic setting (Fredickson et al., 1989; Parkes et al., 1994; Whitman et al. 1998; Kappler et al., 2005; Jørgensen and Boetius, 2007; Orcutt et al., 2011; Edwards et al., 2012; Kallmeyer et al. 2012).

Studies of Neogene marine sediments reveal subsurface microbial ecosystems with total carbon contents possibly equaling all surface microbial life (Lomstein et al., 2012). These deep and dark biological reservoirs may extend to few hundred meters below the water-sediment interface (Whitman et al., 1998; Edwards et al., 2012). Members of subsurface microbial communities harvest energy from buried refractory organic matter, exploiting small disequilibria between chemical redox states in order to drive the synthesis and utilization of biological macromolecules and reproduction (Edwards et al., 2012). These processes result in large-scale transformations of buried organic and inorganic compounds and have an attendant impact on the carbon cycle (LaRowe and Amend, 2015). Current unanswered questions about organisms that inhabit this largely unexplored habitat include, among others: what is their community structure and dynamics? Which TEAs provide a localized source of energy for microbial growth,

maintenance, and survival? What factors govern their dispersal patterns and how do they adapt to a changing diagenetic environment? The kinetics of formation of dolomite and the rates of trace metal incorporation into this mineral may be intrinsically related to the long-term bioavailability of substrates and other biogeochemical conditions governing the subsurface habitats harboring the chemosynthetic ecosystems where dolomite forms. However, the scientific framework and conceptual models for such studies are still to be established.

1.2 Minor and trace element concentrations of dolomite

The wide variety of minor and trace elements in terms of geochemical behaviour (e.g., lithophile, siderophile, et cetera.) have made them instrumental to diagenetic studies. They provide unique constraints on redox conditions, mineral-fluid reactions, and allow for diagenetic interpretations. Regarding dolomite, it has long been recognized that its trace element composition provides information pertaining to its physicochemical precipitation environment, and as suggested by Weber (1964): "*If dolomite crystallized directly from seawater of normal or perhaps elevated salinity, or crystallized diagenetically in the presence of intrastratal fluids, it might be expected that slight differences in chemical composition reflecting these varied environments might be recorded by the rocks themselves, and by the individual dolomite crystals within the dolostones*". He recognized, however, that the detection and substantiation of such minor differences is an exceedingly difficult task (Weber, 1964).

Despite significant advances in our analytical capabilities, a review of the literature reveals that only a few attempts aimed at understanding the significance of trace elements in dolomite have been made since the 1960's. To this end, several tools have been explored including cathodoluminescence (CL) petrography, electron probe microanalyses, and bulk-rock geochemistry. Notwithstanding the vast number of such analyses conducted, the implications of variable concentration levels of trace metals in dolomite remain elusive. The main obstacle for interpretations is that we do not possessed the proper tools to interpret the significance of our data, and most available data consist only of variable bulk-rock concentrations of elements such as strontium (Sr), sodium (Na), iron (Fe), and manganese (Mn) in the range ~ 200 - 10,000 ppm.

Critically examined in this section are some traditional views essential for the emerging use of *in situ* geochemical analyses, with the ultimate goal of unraveling the nature of the multistep low temperature (i.e., microbially influenced) processes wherein early formed dolomite can be repeatedly overgrown.

With regard to Sr, the higher concentrations generally observed in primary dolomites, both modern and ancient, result from its preferential substitution into Ca sites within poorly ordered Ca-rich precursor dolomite phases (Shukla, 1988). This peculiarity allows the use of the absolute Sr contents of dolomite to predict the nature of the dolomitizing fluids (i.e., Vahrenkamp and Swart, 1990), as well as radiogenic ^{87}Sr isotope abundances to determine the timing of dolomitization (e.g., Vahrenkamp et al., 1991).

In the case of Na, determinations of lattice-bound concentrations are useful to constrain the salinity of dolomitizing fluids and to support isotopic and mineralogical observations regarding the environment of formation and genesis of dolomite (Staudt et al., 1993). As the incorporation of Na in the dolomite lattice is related to the salinity of the dolomitizing brines, dolomite crystals formed in hypersaline environments are expected to be enriched in this metal (see Fritz and Katz, 1972). Sodium, however, may well occur as fluid or solid halite inclusions and as $NaHCO_3$ in crystal defects. Such non-lattice bound Na contents typically makes interpreting Na in dolomite a questionable endeavour (Budd, 1997).

For the redox-sensitive elements Fe and Mn, their reduction by Fe(III)- and Mn(IV, III)utilizing microbes allow these metals to be incorporated in their divalent state in dolomite by the partial substitution of Mg^{2+} and minor Ca^{2+} (Kastner, 1999). Multigenic dolomites include variable levels of divalent Fe and Mn as the reducing conditions that typify pore waters change during burial. However, in general, the concentrations of such elements in dolomite seem to increase with increasing depth of formation (Warren, 2000). Incidentally, it has been observed that the reduction of detrital Fe(III) in reactive minerals causes carbonate and silicate buffering reactions to operate effectively and the pore waters to become Fe(II)-rich. In the presence of free biologically produced sulfide anions (HS^-), however, this condition leads to the coprecipitation of pyrite and iron-poor carbonates (Macquaker et al., 2014). On the other hand, in sediments governed by sulfide oxidation, the reduced availability of Fe leads to poorly buffered pore waters

that result in metastable carbonate dissolution and Fe incorporation into newly formed carbonate overgrowths (Macquaker et al., 2014). As can be deduced from this particular observation, the activity of subsurface microbes can act as a key control over the availability of reactants, and has the ability to regulate the content of Fe, and other bioactive elements in multigenic dolomite crystals.

Dolomite may also incorporate a number of other bioactive redox-sensitive elements with atomic mass >55 in trace concentrations (< 200 ppm). These metals are also able to substitute for the position of either Ca^{2+} and Mg^{2+} in the crystal structure (Lorens, 1981, Mucci and Morse, 1983). The degree to which this substitution occurs can be expressed through a distribution coefficient (K_D), i.e.:

$$K_D = (Tr/Ca)_{carb} / (Tr/Ca)_{soln},$$

where Tr is the trace cation.

Despite the importance of the trace metal inventories of dolomite for understanding biogeochemical processes in the subsurface, few studies have attempted to analyse the significance of its trace element geochemistry, and the K_D values of low-temperature dolomite have yet to be determined. A major analytical difficulty in measuring transition elements at very low abundances in inhomogeneous carbonate matrices results from a number of spectroscopic and nonspectroscopic interferences of first-row transition elements with highly concentrated species typically present in natural carbonates (see Evans and Giglio, 1993 for details). In addition to this challenge, the micrometer size of most synthetic and modern natural dolomite has also prevented the use of currently available Laser Ablation Inductively Coupled Plasma Mass Spectrometry systems for obtaining consistent transition metal concentration data.

1.3. Objectives of this thesis

X-ray photon microprobes are installed at major synchrotron radiation facilities around the world. These microprobes make use of very intense micro-focused monochromatized X-rays tuned at a particular wavelength. Soft X-ray microprobes operate in the energy range between 0.2 keV and

5.0 keV and are useful for resolving the spatial distribution of light elements within small analytical areas. Alternatively, hard X-ray (>5.0 keV) allow for similar mapping of heavy metals, including biologically active transition elements.

In order to assess the paragenesis of peritidal to shallow subtidal, restricted lagoonal dolomite, this research balances data obtained from conventional microscopic and spectroscopic analyses and data collected in highly sensitive third generation synchrotron–based hard X-ray microprobes. Three different shallow marine dolomite occurrences from dissimilar stratigraphic settings are examined in this study. First, peritidal carbonate sediments from the Holocene carbonate build-up from the Archipelago Los Roques, in the Venezuelan Caribbean Sea. Second, dolomitic black shales from the deeply buried Aptian-Albian mixed carbonate-siliciclastic sequences in the subsurface of the Maracaibo Lake area, western Venezuela. Third, Paleoproterozoic dolomite-bearing stromatolites of the Gunflint Formation, Ontario, Canada. The Cretaceous microfacies studied here represent deposits from a low energy inner to middle zone of a distally steepened ramp setting affected by the episodic upwelling of stagnant basinal waters (Ford and Houbolt, 1963; Bartok et al., 1981; Renz, 1981, 1982; Vahrenkamp et al., 1993). The Paleoproterozoic organosedimentary structures interrogated here were accreted on foreshore environments of a shallow non-barred, microtidal shelf (Simonson, 1985, 1987; Winter and Knaut, 1992; Pufahl, 1996; Pufahl et al., 2000). The small size of the hemispheroids and microdigitate stromatolites examined attest to their accretion in a very shallow inner shelf (e.g., Grotzinger, 1989; Kah and Knoll, 1996; Grotzinger and Knoll, 1999; Bartley et al., 1999).

This study collectively focuses on primary peritidal to shallow subtidal dolomite of different ages for four reasons: (1) the precipitation of modern dolomite precursors might not be very different from the modes of precipitation and growth of their older Phanerozoic counterparts (Tucker, 1982); (2) most ancient dolostone occurrences are peritidal in origin (Sun, 1994); (3) the localized geochemical disequilibrium conditions that led to formation of dolomite in modern continental margins would have also induced dolomitization in older Phanerozoic carbonate sequences (Lumsden and Lloyd, 1997); and (4) the conditions of Precambrian dolomite formation remain obscure (Holland and Zimmerman, 2000).

1.3.1 Specific objectives

1. Assess the redox-sensitive metal contents of dolomite that have undergone different stages of diagenesis, and their significance.
2. Elucidate the general mechanism of formation and growth of dolomite precursors in association with the degradation of microbial biomass.
3. Identify the early diagenetic mineral assemblage common to the three peritidal locales evaluated, and discuss their environmental significance within the context of dolomite formation.
4. Explore the utility of dolomite in deep geological time investigations. For this aim, exceptionally well-preserved dolomite-bearing Paleoproterozoic stromatolites (~1.89 Ga) are examined to determine what insights their geochemical trends provide on the puzzle of the redox structure of the Precambrian oceans (i.e., Poulton et al., 2010; Pufhal et al., 2010).

1.4. Overview of manuscripts

This thesis consists of three individual research manuscripts, the first of which deals with the formation of disordered Ca-dolomite precursor in a modern peritidal setting in the Caribbean Sea (**Chapter II**). In this location, spheroidal aggregates comprised of sub-micrometer-scale Ca-rich dolomite rhombohedra are associated with sediments affected by a complex chemical zonation linked to the presence of remnant microbial mats. Multiple analytical tools, including Electron Probe Microanalyses (EPMA), Inductively Coupled Plasma Mass Spectrometry (ICP-MS), synchrotron–based X-ray Fluoresce (μXRF) and spatially resolved X-ray Diffraction (XRD) and X-ray Absorption Near-Edge Structure spectrometry (XANES) show that the dolomite-cemented interval exhibits depleted bulk iron concentrations, but is interstitially enriched in elemental sulfur (S^0). Manganese occurs in several oxidation states, indicating that the dolomite-cemented interval is the locus of complex biological redox transformations characterized by coupled Mn and S cycling. The co-occurrence of S^0 and mixed-valence Mn (Mn(IV)-Mn(III)-Mn(II)) maintains a geochemical disequilibrium zone in which the buried organic matter is more efficiently oxidized, leading to sustained rates of alkalinity generation. Thus, the conditions necessary for dolomite

formation are met (e.g., Mazzullo, 2000). This study is the first to suggest that microbially related processes in the suboxic Mn-recycling zone can facilitate modern dolomite stabilization.

Chapter III details a multi-faceted mineralogical, petrographic, and high-resolution spectroscopic investigation conducted on dolomitic black shales from the mixed carbonate – siliciclastic sequences in the subsurface of the Maracaibo Lake area, northern South America. A bulk rock and *in situ* assessment of trace metals was combined with detailed textural and biomarkers analyses in order to interpret the variable redox states of pore waters at the time of black shale deposition and early diagenetic dolomite cementation. In the resulting paragenetic model, environmental shifts associated with Milankovitch-scale cyclicity led to the development of temporarily and spatially restricted diagenetic microenvironments favourable to dolomite formation in an extended shallow lagoonal to tidal flat realm. Oversaturation with regard to dolomite was triggered by the complex interplay between climatically driven drying and wetting events, high-frequency sea level changes, upwelling, and enhanced subsurface microbial activity.

Chapter IV evaluates well-preserved dolomite- and pyrite-bearing small hemispheroidal and multifurcate stromatolites from the Gunflint Iron Formation, in Ontario, Canada. These stromatolites are compared with coeval hematite- and siderite-rich stromatolites aiming to yield valuable information on the laterally and vertically variable diagenetic conditions prevailing at the time of stromatolite stabilization in the shallow marine zone of the Animikie Basin. As silicification proceeded very soon after stromatolite accretion, it accounted not only for the preservation of benchmark microfossils (Barghoorn and Tyler, 1965), but also of some early diagenetic minerals precipitated as cement in the void spaces of the stromatolitic structures. Analyses conducted as part of this research indicate that, independent of their mineralogy, the bulk-rock trace metal contents of stromatolites must be used with care when interpreting the redox structure of Precambrian oceans. Further, it is suggested that only fine-crystalline dolomite ought to be used for early diagenetic interpretations. For this aim, the increasing use of high spatial resolution and sensitivity photon and ion microprobes should provide relevant insights.

Finally, **Chapter V** places results and major discussion points into a more general context and summarizes the conclusions of this research. It draws together the disparate lines of evidence presented into a working model that describes how the development of reaction fronts,

characterized by the mixture of pore waters of contrasting redox potentials, can lead to an autocatalytic early diagenetic condition involving metal cycling and favourable for dolomite growth.

Table 1.1 Microbial metabolism relevant to dolomite formation

Metabolic pathway (References)	**Mechanism of mediation**	**Organisms identified**
Aerobic heterotrophy (Sánchez- Román et al., 2008)	These microorganisms utilize nitrogenated organic matter coupled to oxygen as a terminal electron acceptor, consuming acidity and producing alkalinity by also reducing nitrate or nitrite to ammonia.	*Halomonas meridiana, Virgibacillus marismortui*
Chemotrophic sulfide oxidation (SO) coupled to **Dissimilatory sulfate reduction** (Moreira et al., 2004)	Microorganisms using sulfide, H_2O and other reduced forms of sulfur as electron donors for the reduction and fixation of CO_2 to cellular carbon at the oxygen/ sulfide interface. A diel fluctuating pH gradient decreases pore water saturation states for high-Mg calcite and aragonite, to favour the precipitation of dolomite precursors at night.	Organisms capable of anoxygenic SO, include *Microcoleus* and *Thiobacillus* growing symbiotically with phototrophic *Thiocapsa*
Dissimilatory sulfate reduction (Vasconcelos and McKenzie, 1997; Warthmann et al., 2000)	This functional group of microbes oxidize organic carbon using sulfate as a terminal electron acceptor, thereby removing the sulfate and generating alkalinity under anaerobic conditions.	*Desulfostipes saporovans* *Desulfosarcina* spp. Desulfovibriae
Methanogenesis coupled to **Anaerobic oxidation of methane** (Moore et al., 2004; Roberts et al., 2004; Kenward et al., 2009)	Methanogenesis alone tends to decrease the saturation state of dolomite; the coupled mechanism, however, utilizes CO_2 and H_2 to increases lithoautotrophically the concentration of CO_3^{2-} via sulfate reduction. Increased alkalinity may thus result in dolomite supersaturation.	Acetoclastic and autotrophic methanogens and S (N)-utilizing methanotrophs

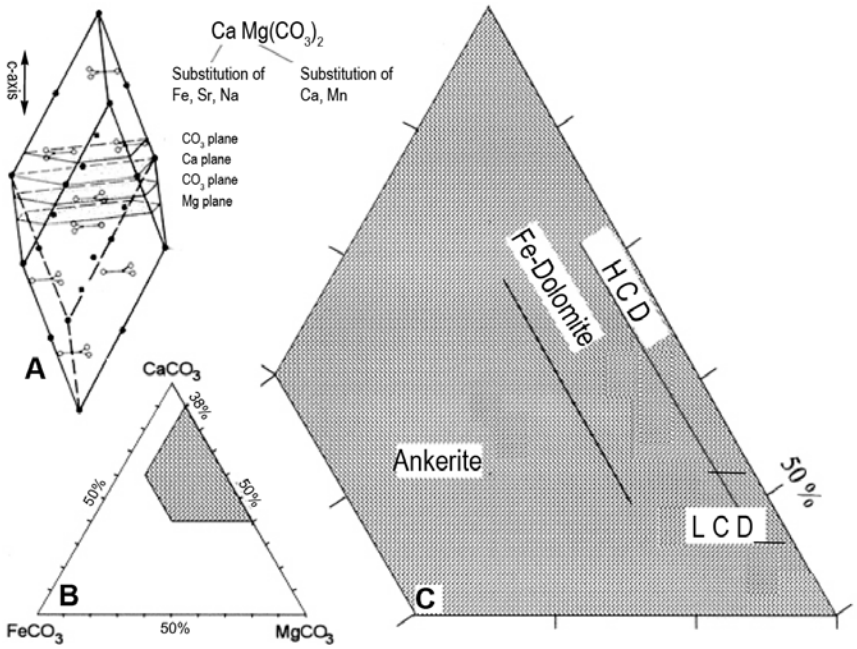

Figure 1.1. Structure and composition of the dolomite-ankerite series. A: crystal structure. B-C: composition of the dolomite-ankerite series, and its compositional thresholds. The International Mineralogical Association guidelines (IMA) suggests the '50% rule' to be applied for this solid solution, so that any Ca-Mg-Fe carbonate containing less than 50 mol% Fe in the Mg sites of the crystal lattice would be called dolomite. Likewise, any mineral with more than 50 mol% Fe would be called ankerite. HCD: High-Ca Dolomite; LCD: Low-Ca dolomite

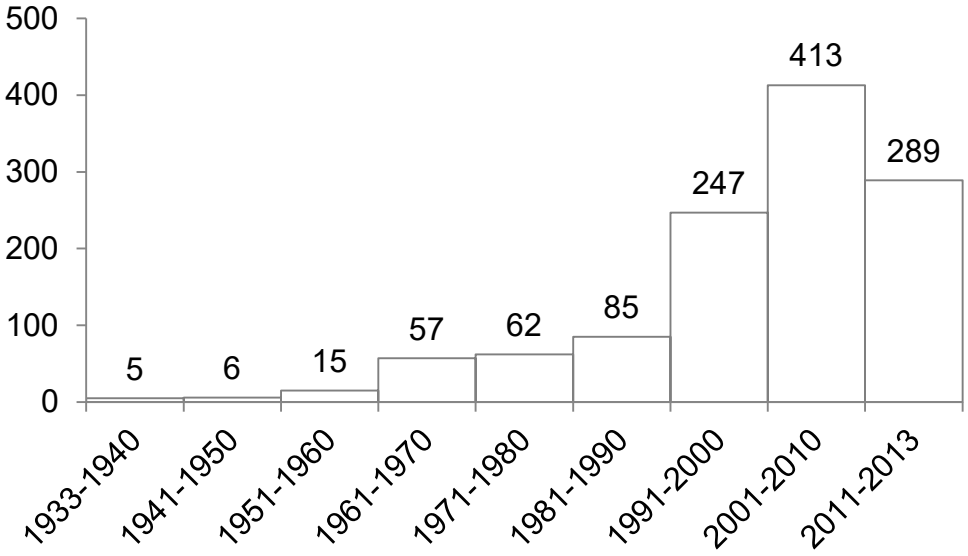

Figure 1.2. GeoRef search: Dolomite ∧ (Algal ∨ Bacteria ∨ Microbial) since 1933 to 2013. Y-axis is number of published peer-reviewed papers (September 2014).

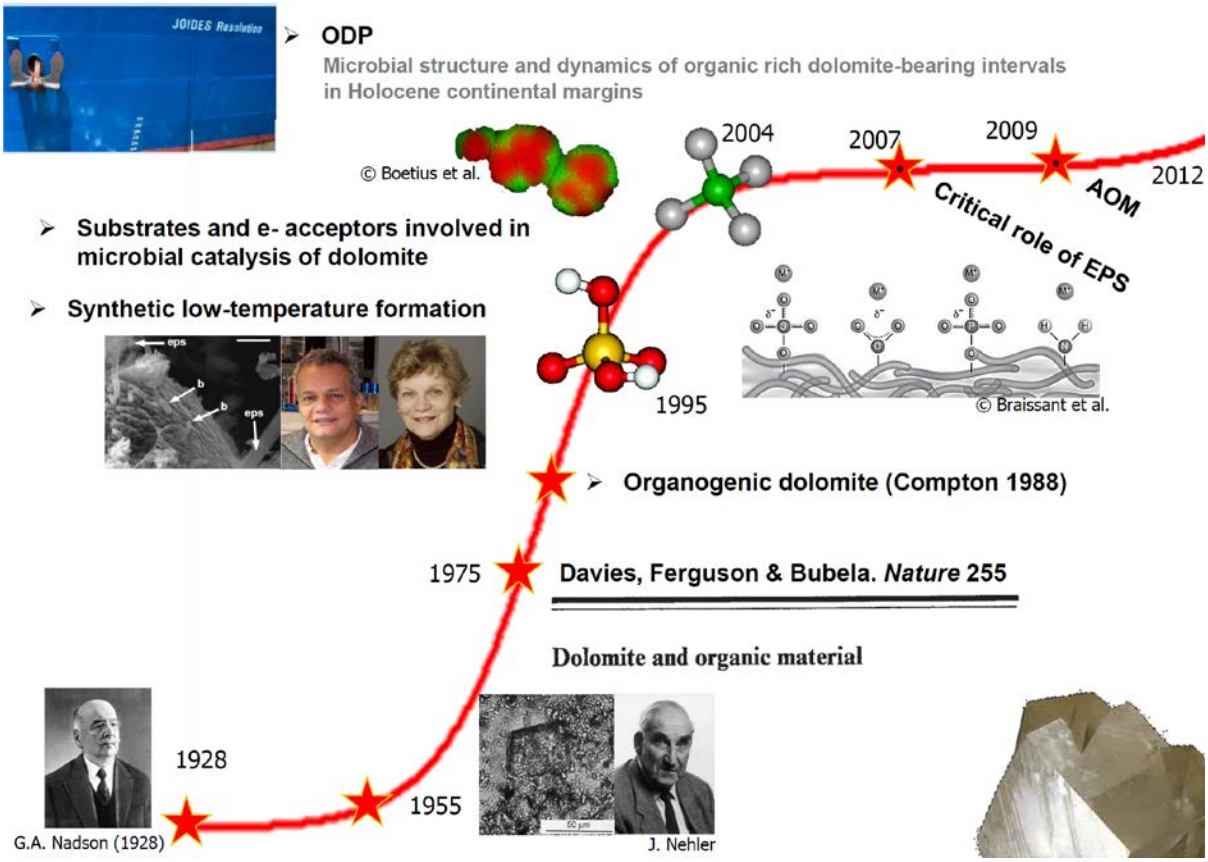

Figure 1.3. A chronological compilation of some milestones in microbial dolomite research.

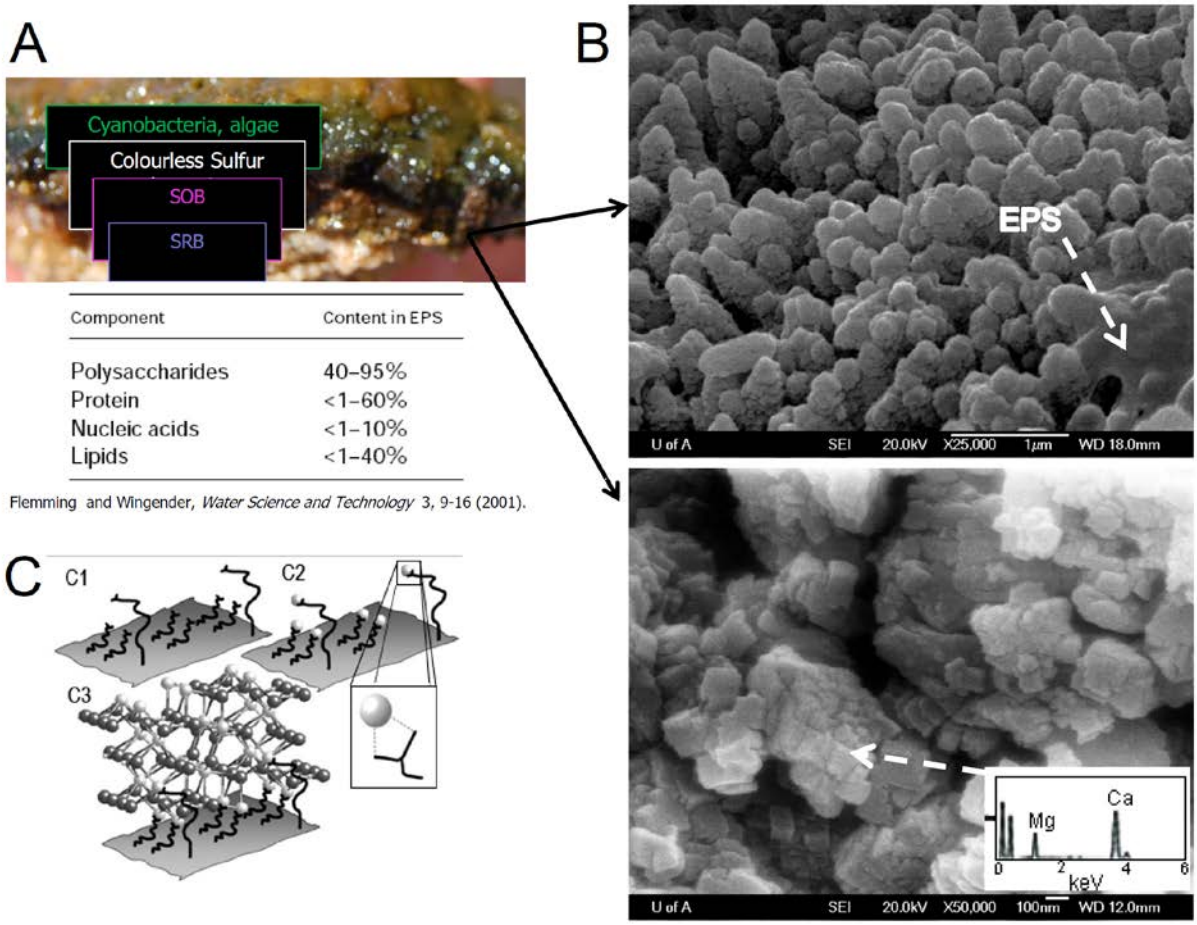

Figure 1.4. Precipitation of dolomite within chemically stratified halophilic microbial mats. A: The biomass on these mats can be comprised in up to 90% by exopolymers (EPS). B: Dolomite and other carbonate phases can grow within decaying organic matrices. C: The various compounds comprising these reactive matrices can act as nucleation template by differential binding of alkali etals in solution, C1: deprotonated ligads, C2: differential binding of Ca and Mg to decaying organic ligands lead to C3: mineral templating (see Petrash, 2010).

1.5. References

Arvidson, R. S; Mackenzie, F.T., 1999. The dolomite problem; control of precipitation kinetics by temperature and saturation state. Am. J. Sci. 299, 257–288.

Baker, P.A., Kastner, M., 1981. Constraints on the formation of sedimentary dolomite. Science 213, 214–216

Barghoorn, E., Tyler, S., 1965. Microorganisms from the Gunflint chert. Science 80, 147, 563–577.

Bartley, J.K., Knoll, A.H., Grotzinger, J.P., Sergeev, V.N., 1999. Lithification and fabric genesis in precipitated stromatolites and associated per- itidal carbonates, Mesoproterozoic Billyakh Group, Siberia. Kah LC, Knoll AH. 1996. Microbenthic distribution of Proterozoic tidal flats: environmental and taphonomic considerations. Geology 24:79–82.

Bartok, P., Reijers, T., and Juhasz, I., 1981. Lower Cretaceous Cogollo Group, Maracaibo Basin, Venezuela: sedimentology, diagenesis, and petrophysics. Am. Assoc. Pet. Geol. Bull. 65, 1110–1134.

Bethke, C.M., Sanford, R. a., Kirk, M.F., Jin, Q., Flynn, T.M., 2011. The thermodynamic ladder in geomicrobiology. Am. J. Sci. 311, 183–210.

Boetius, A., Ravenschlag, K., Schubert, C.J., Rickert, D., Widdel, F., Gieseke, A., Amann, R., Jørgensen, B.B., Witte, U., Pfannkuche, O., 2000. A marine microbial consortium apparently mediating anaerobic oxidation of methane. Nature 407, 623–6.

Bontognalli, T.R.R., Vasconcelos, C., Warthmann, R.J., Dupraz, C., Bernasconi, S.M., McKenzie, J. A., 2008. Microbes produce nanobacteria-like structures, avoiding cell entombment. Geology 36, 663-66.

Bontognalli, T.R.R., Vasconcelos, C., Warthmann, R.J., Bernasconi, S.M., Dupraz, C., Strohmenger, C.J., McKenzie, J.A., 2010. Dolomite formation within microbial mats in the coastal sabkha of Abu Dhabi (United Arab Emirates). Sedimentology 57, 824–844.

Brady, P.V., Krumhansl, J.L., Papenguth, H.W., 1996. Surface complexation clues to dolomite growth. Geochim. Cosmochim. Acta 60, 727–731.

Buchbinder, B., and Friedman, G.M., 1971. Selective dolomitization of micrite envelopes: A possible clue to original mineralogy. Journal of Sedimentary 40, 514-517

Budd, D., 1997. Cenozoic dolomites of carbonate islands: their attributes and origin. Earth-Science Rev. 42, 1–47.

Burns, S.J., Baker, P.A., 1987. A Geochemical Study of Dolomite in the Monterey Formation, California. J. Sediment. Res. 57, 128.

Burns, S.J., Mckenzie, J.A., Vasconcelos, C., 2000. Dolomite formation and biogeochemical cycles in the Phanerozoic. Sedimentology 47, 49–61.

Carballo, J.D., Land, L.S., and Miser, D.E., 1987, Holocene dolomitization of supratidal sediments by active tidal pumping, Sugarloaf Key, Florida: Journal of Sedimentary Petrology 57, 153–165.

Choquette, P.W., 1971, Late ferroan dolomite cement, Mississippian carbonates, Illinois Basin, U.S.A., m Bricker, O.P., editor, Carbonate Cements: Baltimore Johns Hopkins Univ. Studies in Geology 19, 339-346.

Deffeyes, K.S., Lucia, F.J., and Weyl, P.K., 1964, Dolomitization: Observations on the island of Bonaire, Netherlands Antilles: Science, 143,678-679.

Edwards, K. J., Becker, K., and Colwell, F., 2012. The deep, dark energy biosphere: Intraterrestrial life on Earth. Annual Reviews in Earth Planetary Sciences 40, 551–568.

Evans, E., Giglio, J., 1993. Interferences in inductively coupled plasma mass spectrometry. A review. J. Anal. At. Spectrom. 8, 1–18.

Fairbridge, R. W., 1957. The dolomite question, in R. J. Leblanc and J. C. Breeding, editors. Regional aspects of carbonate deposition: SEPM Spec. Pub. 5, 125-178

Ford, A. and Houbolt, J. J. H. C., 1963. The microfacies of the Cretaceous of Western Venezuela. Brill, Leiden, 56 pp.

Fredickson, J. K., Garland, T. R., Hicks, R. J., Thomas, J. M., Li, S. W., and McFadden, K. M., 1989. Lithotrophic and heterotrophic bacteria in deep subsurface sediments and their relation to sediment properties. Geomicrobiology Journal 7, 53–66.

Fredickson, J. K., and Fletcher, M., 2001, Subsurface Microbiology and Biogeochemistry: New York, Wiley & Sons, p. 341.

Friedman, G. M., and Sanders, J. E., 1967, Origin and occurrence of dolostones, in Chilingar, G. V., Bissell, H. J., and Fairbridge, R. W., editors., Carbonate Rocks; Origin, Occurrence and Classification: Amsterdam, Developments in Sedimentology, 9A, Elsevier, 267-348.

Fritz, P., Katz, A., 1972. The sodium distribution of dolomite crystals. Chem. Geol.

Gaines, A.M., 1974. Protodolomite synthesis at 100 °C and atmospheric pressure. Science 183, 518-520.

Gaines, A.M., 1977. Protodolomite redefined. J. Sediment. Petrol. 47, 543-546

Gellatly, A., Lyons, T., 2005. Trace sulfate in mid-Proterozoic carbonates and the sulfur isotope record of biospheric evolution. Geochim. Cosmochim. Acta 69, 3813–3829.

Given, R. K., and Wilkinson, B. H., 1987, Dolomite abundance and stratigraphic age-constraints on rates and mechanisms of Phanerozoic dolostone formation: Journal of Sedimentary Petrology 57, 457-469.

González de Juana C., Arozena J. and Picard X.C., 1980. Geología de Venezuela y de sus Cuencas Petrolíferas, Ediciones Foninves, Caracas, 1031 pp.

Graf, D., Goldsmith, J., 1956. Some hydrothermal syntheses of dolomite and protodolomite. J. Geol. 64, 173–186.

Gregg, J.M. and Shelton, K.L., 1990. Dolomitization and dolomite neomorphism in the backreef facies of the Bonterre and Davis formations (Cambrian), southeastern Missouri. Sediment. Petrol. 60: 549-562.

Grotzinger J.P., 1989. Facies and evolution of Precambrian carbonate depositional systems: emergence of the modern platform archetype. In Crevello, P.D., Wilson, J.L., Sarg, J.F, Read,

J.F., eds., Controls on Carbonate Platform and Basin Development, Soc. Econ.Paleontol. Mineral. Spec. Publ. 44, 79–106.

Grotzinger, J.P., Knoll, a H., 1999. Stromatolites in Precambrian carbonates: evolutionary mileposts or environmental dipsticks? Annu. Rev. Earth Planet. Sci. 27, 313–58.

Han, Y. J., Aizenberg, J., 2003. Effect of magnesium ions on oriented growth of calcite on carboxylic acid functionalized self-assembled monolayer. J. Am. Chem. Soc. 125, 4032–3.

Hardie, L.A., 1987. Dolomitization; a critical view of some current views. J. Sediment. Res. 57, 166.

Hoehler, T.M., Jørgensen, B.B., 2013. Microbial life under extreme energy limitation. Nat. Rev. Microbiol. 11, 83–94.

Holail, H., Lohmann, K.C , Sanderson, I., 1988, Dolomitization and dedolomitization of Upper Cretaceous carbonates: Bahariya Oasis, Egypt, in Shukla, V., and Baker, P. A., editors, Sedimentology and geochemistry of dolostones: SEPM Spec. Publ. 43, 191-207

Holland, H., Zimmermann, H. 2000. The Dolomite Problem Revisited. International Geology Review, 37–41.

Holmden, C., 2009. Ca isotope study of Ordovician dolomite, limestone, and anhydrite in the Williston Basin: Implications for subsurface dolomitization and local Ca cycling. Chem. Geol. 268, 180–188.

Ingerson E., 1962. Problems of the geochemistry of sedimentary carbonate rocks. Geochim. et Coamochim. Acta 26, 815-847.

Irwin, M.L., 1965. General theory of epeiric clear water sedimentation. Am. Assoc. Pet. Geol. Bull., 49: 445-459.

Irwin, H., Curtis, C., and Coleman, M., 1977. Isotopic evidence for source of diagenetic carbonates formed during burial of organic-rich sediments. Nature, 269:209-213.

Johnson, C., McLennan, S., Mcsween, H.Y., Summons, R.E. 2013. Smaller, better, more: Five decades of advances in geochemistry. In M. E. Bickford, editor, The Web of Geological Sciences: Advances, Impacts, and Interactions: Geological Society of America Special Paper 500 1-44.

Jørgensen B. B. and Kasten S., 2006. Sulfur cycling and methane oxidation. In Marine Geochemistry. In Schulz H. D., Zabel M., eds. Springer, Berlin, pp. 271–309

Jørgensen, B. B., Boetius, A., 2007. Feast and famine — microbial life in the deep-sea bed: Nature Reviews Microbiology, 5, 770–781.

Kah, L.C., Knoll, A.H., 1996. Microbenthic distribution of Proterozoic tidal flats: environmen- tal and taphonomic considerations. Geology 24, 79–82.

Kallmeyer, J., Pockalny, R., Adhikari, R. R., Smith, D. C., and D'Hondt, S., 2012, Global distribution of microbial abundance and biomass in subseafloor sediment: PNAS 109, 16213–16216.

Kamber, B.S., Webb, G.E., 2007. Transition metal abundances in microbial carbonate: a pilot study based on *in situ* LA-ICP-MS analysis. Geobiology 5, 375–389.

Kappler A., Emerson D., Edwards, K.J., Amend, J.P., Gralnick, J.A, Grathwohl, P., Hoehler, T.M., Straub, K.L., 2005. Microbial activity in biogeochemical gradients - new aspects of research. Geobiol 3, 229-233.

Kastner, M., Hollander, D., and Garrison, R., 1984. The association of dolomite-phosphorite-chert: causes and possible diagenetic sequences. In Garrison, R. E., Kastner, R. E., and Zenger, D. H., editors, Dolomites of the Monterey Formation and Other Organic-Rich Units. Pac. Sect., Soc. Econ. Paleontol. Mineral. Spec. Publ. 41,75-86.

Kelts, K. R., and McKenzie, J. A., 1982. Diagenetic dolomite formation in Quaternary anoxic diatomaceous muds of Deep Sea Drilling Project Leg 64, Gulf of California. In Curray, J.R., Moore, D., et al., Init. Reports. DSDP, 64: Washington (U.S. Govt. Printing Office), 553-569.

Kenward, P. A, Goldstein, R.H., González, L. A, Roberts, J. A, 2009. Precipitation of low-temperature dolomite from an anaerobic microbial consortium: the role of methanogenic Archaea. Geobiology 7, 556–65.

Kenward, P. A., Fowle, D. A., Goldstein, R.H., Ueshima, M., González, L. A., Roberts, J. A., 2013. Ordered low-temperature dolomite mediated by carboxyl-group density of microbial cell walls. Am. Assoc. Pet. Geol. Bull. 97, 2113–2125.

Kirkland, B., Lynch, F., Rahnis, M., 1999. Alternative origins for nannobacteria-like objects in calcite. Geology 27, 347–350.

Knoll, A., 2003. Biomineralization and evolutionary history. Rev. Mineral. Geochemistry 329–356.

Knoll, A., Swett, K., 1990. Carbonate deposition during the late Proterozoic Era: an example from Spitsbergen. Am. J. Sci. 290, 104–132.

Konhauser, K.O., Introduction to geomicrobiology. John Wiley and Sons, Oxford, 425 pp.

Konhauser, K.O, Phoenix, V., 2001. Microbial–silica interactions in Icelandic hot spring sinter: possible analogues for some Precambrian siliceous stromatolites. Sedimentology 48, 415–433.

Konhauser, K.O. , Gingras, M.K., and Kappler, A., 2011. Diagenesis – Biologically Controlled. In: J. Reitner and V. Thiel, editors, *Encyclopedia of Geobiology*. Springer, Berlin, p. 777-784.

Land, L. S., and Epstein, S., 1970, Late Pleistocene diagenesis and dolomitization, North Jamaica: Sedimentology 14, 187-200.

Land, L.S., 1973. Holocene meteoric dolomitization of Pleistocene limestones, North Jamaica. Sedimentology 20, 411– 424

Land, L.S., 1985. The origin of massive dolomite. J. Geol. Educ, 33:112-125.

Land, L S., Salem, M. R. I., and Morrow, D. W., 1975. Paleohydrology of ancient dolomites: geochemical evidence: Am. Assoc. Petroleum Geologists Bull. 59, 1602-1625.

LaRowe, D.E., Amend, J.P., 2015. Catabolic rates, population sizes and doubling/replacement times of microorganisms in natural settings. Am. J. Sci. 315, 167–203.

Lasemi, Z., Boardman, M.R., Sandberg, P.A., 1989. Cement origin of supratidal dolomite, Andros Island, Bahamas. J. Sediment. Petrol. 59, 249–257.

Lippmann, F., 1973, Sedimentary carbonate minerals: New York, Springer-Verlag, 228 p.

Lomstein, B. A., Langerhuus, A. T., D'Hondt, S., Jørgensen, B. B., and Spivack, A. J., 2012, Endospore abundance, microbial growth and necromass turnover in deep sub-seafloor sediment: Nature 484, 101–104.

Lorens, B., 1980. Sr, Cd, Mn and Co distribution coefficients in calcite as a function of calcite precipitation rate 45.

Lovely, D. R. (2000). Environmental microbe-metal interactions. American Society of Microbiology ASM Press, Washington, D.C.

Lumsden, D.N., 1985. Secular variations in dolomite abundance in deep marine sediments. Geology 13, 766.

Lumsden, D.N., 1988. Characteristics of Deep-Marine Dolomite. J. Sediment. Res 58, 1023-1031

Lumsden, D., Lloyd, R., 1997. Three dolomites. J. Sediment. Res. 67, 391–396.

Machel, H.G., 2004. Concepts and models of dolomitization: a critical reappraisal. Geol. Soc. London, Spec. Publ. 235, 7–63. doi:10.1144/GSL.SP.2004.235.01.02

Machel, H., Mountjoy, E., 1986. Chemistry and environments of dolomitization—a reappraisal. Earth-Science Rev. 23, 175–222.

Machel, H.G., Mountjoy, E.W. and Amthor, J.E. 1996b. Mass balance and fluid flow constraints on regional-scale dolomitization, Late Devonian, Western Canada Sedimentary Basin. Bulletin of Canadian Petroleum Geology 44, 566-571.

Macquaker, J.H.S., Taylor, K.G., Keller, M., and Polya, D., 2014. Compositional controls on early diagenetic pathways in fine-grained sedimentary rocks: Implications for predicting unconventional reservoir attributes of mudstones. Am. Assoc. Pet. Geol. Bull. 98, 587–603. doi:10.1306/08201311176

Major, R.P., Lloyd, R.M., Lucia, F.J., Friedman, G.M., 1992. Oxygen isotope composition of Holocene dolomite formed in a humid hypersaline setting: Comment and Reply. Geology 20, 586.

Mansfield, C., 1980. A urolith of biogenic dolomite—Another clue in the dolomite mystery. Geochim. Cosmochim. Acta 44, 829–839.

Marlow, J.J., Steele, J.A., Case, D.H., Connon, S,A., Levin, L.A., and Orphan, V.J., 2014. Microbial Abundance and Diversity Patterns Associated with Sediments and Carbonates from the Methane Seep Environments of Hydrate Ridge, OR. Front. Mar. Sci. 1:44.

Mazzullo, S., 1992. Geochemical and neomorphic alteration of dolomite: a review. Carbonates and Evaporites 7, 21–37.

Mazzullo, S., 2000. Organogenic Dolomitization in Peritidal to Deep-Sea Sediments: Perspectives. J. Sediment. Res. 70, 10–23.

Mazzullo, S.J., Reid, A. M., and Gregg, J.M., 1987. Dolomitization of Holocene Mg-calcite supratidal deposits, Ambergris Cay, Belize. Geological Soc. of America Bull. 98, 224–231.

McHargue, T., and Price, R., 1982. Dolomite from clay in argillaceous or shale-associated marine carbonates. J. Sediment. Petrol 52, 873–886.

McKenzie, J. A., 1991. The dolomite problem: an outstanding controversy. Controversies in Modern Geology, 37-54.

Melim, L., Scholle, P., 2002. Dolomitization of the Capitan Formation forereef facies (Permian, West Texas and New Mexico): seepage reflux revisited. Sedimentology 49, 1207–1227.

Mizutani, Y., Rafter, T.A., 1969. Oxygen isotopic composition of sulfates: Part 4. Bacteria fractionation of oxygen isotopes in the reduction of sulfate and in the oxidation of sulfur. N. Z. J. Sci.Technol. 12, 60 – 68.

Moore, C.H., 1989. Dolomitization associated with meteoric and mixed meteoric and marine waters, in: Moore, C.H. (Ed.), Developments in Sedimentology 46: Carbonate Diagenesis and Porosity. Elsevier, pp. 219–235.

Moore, T. S., Murray, R. W., Kurtz, A. C., and Schrag, D. P., 2004. Anaerobic methane oxidation and the formation of dolomite. Earth and Planetary Science Letters, 229, 141–154.

Moreira, N. F., Walter, L. M., Vasconcelos, C., McKenzie, J. A., and McCall, P. J., 2004. Role of sulfide oxidation in dolomitization: sediment and porewater geochemistry of a modern hypersaline lagoon system. Geology, 32, 701–704.

Morrow, D.W., Ricketts, B.D., 1988. Experimental investigation of sulfate inhibition of dolomite and its mineral analogues. In: Shukla, V., Baker, P.A. (Eds.), Sedimentology and Geochemistry of Dolostones. Society of Economic Paleontologists and Mineralogists, Tulsa, pp. 25–38.

Mucci, A. and Morse, J.W., 1983. The incorporation of Mg 2+ and Sr 2+ into calcite overgrowths: influences of growth rate and solution composition. Geochim. Cosmochim. Acta, 47: 217-223.

Muller, G., Scoll, W. V., and Tietz, G., 1973, Diagenetic development of a Precambrian limestone as interpreted from a modern analogue: Sedimentology 20, 529-538.

Nadson, G. A., 1928. Breitag zur kenntnis der bakteriogenen kalkablagerungen. Archiv fuer Hydrobiologie, 19, 154–164.

Nickel, E.H. and Grice, J.D., 1998. The IMA Commission on new minerals and mineral names: Procedures and guidelines on mineral nomenclature, 1998. Canadian Mineralogist 36, 913-926.

Nordeng, S., Sibley, D., 1996. A crystal growth rate equation for ancient dolomites: Evidence for millimeter-scale flux-limited growth. J. Sediment. Res. 66, 477–481.

Nyman, S.L., Nelson, C.S., Campbell, K.A., 2010. Miocene tubular concretions in East Coast Basin, New Zealand: analogue for the subsurface plumbing of cold seeps. Marine Geology 272 (1–4), 319–336.

Orcutt, B. N., Sylvan, J. B., Knab, N. J., and Edwards, K. J., 2011. Microbial ecology of the dark ocean above, at, and below the seafloor. Microbiology and Molecular Biology Reviews 75, 361–422.

Parkes, R., Cragg, B., Wellsbury, P., 2000. Recent studies on bacterial populations and processes in subseafloor sediments: A review. Hydrogeol. J. 8, 11–28

Parkes, R.J., Wellsbury, P., Mather, I.D., Cobb, S.J., Cragg, B.A., Hornibrook, E.R.C., Horsfield, B., 2007. Temperature activation of organic matter and minerals during burial has the potential to sustain the deep biosphere over geological time scales. Organic Geochemistry 38, 845–85.

Parkes, R., Linnane, C., Warthmann, G., Sass, H., Weightman, A., Hornibrook, E., Horsfield, B., 2011. Prokaryotes stimulate mineral H_2 formation for the deep biosphere and subsequent thermogenic activity. Geology 39, 219–222.

Parkes, R.J., Cragg, B., Roussel, E., Webster, G., Weightman, A., Sass, H., 2014. A review of prokaryotic populations and processes in sub-seafloor sediments, including biosphere: geosphere interactions. Mar. Geol. 352, 409–425.

Petrash, D.A., 2010. Metal-enrichment in microbial carbonates: The role of carboxylated biomacromolecules. Master Thesis, University of Alberta, Edmonton. (unpublished).

Poulton, S.W., Fralick, P.W., Canfield, D.E., 2004. The transition to a sulphidic ocean, 1.84 billion years ago. Nature 431, 173–177.

Poulton, S.W., Fralick, P.W., Canfield, D.E., 2010. Spatial variability in oceanic redox structure 1.8 billion years ago. Nat. Geosci. 3, 486–490

Pufahl, P.K., Fralick, P.W., Scott, J., 2000. Depositional Environments of the Palaeoproterozoic Gunflint Formation. In: Fralick, P. (Ed.), Institute of Lake Superior Geology Field Guide, p. 46.

Pufahl, P., Hiatt, E., Kyser, T., 2010. Does the Paleoproterozoic Animikie Basin record the sulfidic ocean transition? Geology 98, 659-662.

Renz, O., 1958. Estratigrafia del Cretácico en Venezuela. Bol. Minist. Min. Hidrocarb. 5, 3–48.

Renz, O., 1981. Venezuela in Payment R.A., and Bengtson P., editors, Aspects of Mid-Cretaceous Regional Geology. Academic Press, London 197-22

Renz, O., 1982. The Cretaceous ammonites of Venezuela. Birkhauser Verlag, Basel, 132. (+ 40 pl.)

Ricketts B.D., 1982. Comment on Pecambrian dolomites: Petrographic isotopic evidence that they differ from Phanerozoic dolomites: Geology 10, 663

Robach, J., Stock, S., Veis, A., 2006. Mapping of magnesium and of different protein fragments in sea urchin teeth via secondary ion mass spectroscopy. J. Struct. Biol. 155, 87–95.

Roberts, J, A., Bennett, P.C., Gonzalez, L.A., Macpherson, G,L, Milliken, K.L., 2004. Microbial precipitation of dolomite in methanogenic groundwater. Geology 32, 277–280.

Roberts, J. A, Kenward, P. A, Fowle, D. A, Goldstein, R.H., González, L. A, Moore, D.S., 2013. Surface chemistry allows for abiotic precipitation of dolomite at low temperature. Proc. Natl. Acad. Sci. U. S. A. 110, 14540–5.

Sánchez-Román, M., C. Vasconcelos, T. Schmid, M. Dittrich, J. A. McKenzie, R. Zenobi, and M. A. Rivadeneyra, 2008. Aerobic microbial dolomite at the nanometer scale: Implications for the geological record: Geology 36, 879–882.

Sánchez-Román, M., J. A. McKenzie, A. de Luca Rebello Wagner, M. A. Rivadeneyra, and C. Vasconcelos, 2009. Presence of sulfate does not inhibit low-temperature dolomite precipitation: Earth and Planetary Science Letters 285, 131–139.

Sass, E., Bein, A., Almogi-Labin, A., 1991. Oxygen isotope composition of diagenetic calcite in organic-rich rocks: evidence for 18O depletion in marine anaerobic porewater. Geology 19, 839–842.

Schmoker JW, Krystinik KB, and Halley RB (1985) Selected characteristics of limestone and dolomite reservoirs in the United States. Bulletin American Association Petroleum 69, 733-741

Schofield, J. C., and Nelson, C. S., 1978, Dolomitization and Quaternary climate of Niue Island, Pacific Ocean. Pacific Geology 13, 37-48.

Shima, S., Krueger, M., Weinert, T., Demmer, U., Kahnt, J., Thauer, R.K., Ermler, U., 2012. Structure of a methyl-coenzyme M reductase from Black Sea mats that oxidize methane anaerobically. Nature 481, 98–101. doi:10.1038/nature10663.

Shinn E. A., Ginsburg, R. N., and Lloyd, R. M., 1965, Recent supratidal dolomite from Andros Island, Bahamas, in Pray, L. C., and Murray, R. C., eds., Dolomitization and Limestone Diagenesis: SEPM Spec. Publ. 13, 112-123.

Shinn, E.A., 1983, Tidal flat environments, in Scholle, P.A., Bebout, D.G., and Moore, C.H., eds., Depositional Environments in Carbonate Rocks: American Association of Petroleum Geologists, Memoir 33, 172–210.

Shinn, E.A., Kendall, C.G.S.T.C.G.S.C., 2011. Back to the future. Sediment. Rec. 9, 4–9.

Shukla, 1988. Sedimentology and geochemistry of a regional dolostones: correlation of trace elements with dolomite fabrics, in V.J. Shukla and P.A. Baker, editors, Sedimentology and geochemistry of dolostones.SEPM Spec. Publ., 43, 129–144.

Sibley, D.F., 1991. Secular changes in the amount and texture of dolomite. Geology 19, 151–154.

Simonson B.M., 1985. Sedimentological constraints on the origins of Precambrian iron-formations. Geol. Soc. Am. Bull. 96, 244– 252.

Simonson, B.M., 1987. Early silica cementation and subsequent diagenesis in arenites from four early Proterozoic iron formations of North America. J. Sediment. Res. 57, 494–511.

Staudt, W., Oswald, E., Schoonen, M., 1993. Determination of sodium, chloride and sulfate in dolomites: a new technique to constrain the composition of dolomitizing fluids. Chem. Geol. 107, 97–109.

Sun, S.Q., 1994. A Reappraisal of Dolomite Abundance and Occurrence in the Phanerozoic: Perspective. J. Sediment. Res. 64A 396–404.

Tucker, M., 1982. Precambrian dolomites: petrographic and isotopic evidence that they differ from Phanerozoic dolomites. Geology 7–12.

Tucker, M., 1983. Diagenesis, geochemistry, and origin of a Precambrian dolomite: the Beck Spring Dolomite of eastern California. J. Sediment. Res. 53, 1097-1119.

Tucker, M.E., 1992. The Precambrian-Cambrian boundary: seawater chemistry, ocean circulation and nutrient supply in metazoan evolution, extinction and biomineralization. J. Geol. Soc. London. 149, 655–668.

Tucker, M. E., and Wright, V. P. (2009). Carbonate sedimentology. John Wiley & Sons.

Turchyn, A.V., Brüchert, V., Lyons, T.W., Engel, G.S., Balci, N., Schrag, D.P., Brunner, B., 2010. Kinetic oxygen isotope effects during dissimilatory sulfate reduction: a combined theoretical and experimental approach. Geochimica et Cosmochimica Acta 74, 2011–2024.

Van Lith Y., Warthmann R., Vasconcelos C. and McKenzie J. A., 2003. Sulfate-reducing bacteria induce low-temperature Ca-dolomite and high Mg-calcite formation. Geobiology 1, 71–79.

Vahrenkamp, V. C., Franssen, R.C.W.M., Grötsch, J., Munoz, P. J., 1993, Maracaibo Platform (Aptian-Albian), northwestern Venezuela. In: Simo, J. A. T., Scott, R.W.,Masse,J.P., eds., Cretaceous Carbonate Platforms. AAPG Memoir 25, 25–33.

Vasconcelos C. and McKenzie J. A., 1997.Microbial mediation of modern dolomite precipitation and diagenesis under anoxic conditions (Lagoa Vermelha, Rio de Janeiro, Brazil). J. Sediment. Res. 67, 378–390.

Vasconcelos C., Mckenzie J. A., Bernasconi S., Grujic D. and Tien A.J., 1995. Microbial mediation as a possible mechanism for natural dolomite formation at low-temperatures. Nature 377, 220–222.

Veizer J. 1983. Trace elements and isotopes in sedimentary carbonates. *In* Reeder R.J., ed., Carbonates: Mineralogy and Chemistry, Reviews in Mineralogy, I, pp. 265-300. Mineral. Soc. America, Book Crafters, Incorporated, Chelsea, MI

von der Borch, C.C. and Jones, J.B., 1976. Spherular modern dolomite from the Coorong area, South Australia. Sedimentology 23, 587–591.

Wanless, H. R., 1979, Limestone response to stress: pressure solution and dolomitization: Jour. Sed. Petrology 49, 437-462.

Warren, J., 2000. Dolomite: occurrence, evolution and economically important associations. Earth-Science Rev. 52, 1–81.

Warthmann, R., Y. van Lith, C. Vasconcelos, J. A. McKenzie, and A. M. Karpoff, 2000. Bacterially induced dolomite precipitation in anoxic culture experiments. Geology 28, 1091–1094.

Weber, J., 1964. Trace element composition of dolostones and dolomites and its bearing on the dolomite problem. Geochim. Cosmochim. Acta 28, 1817–1868.

Whitman, W. B., Coleman, D. C., and Wiebe, W. J., 1998, Prokaryotes: The unseen majority: Proceedings of the National Academy of Sciences of the United States of America, v. 95, n. 12, p. 6578–6583.

Winter, B.L., Knauth, L.P., 1992. Stable isotope geochemistry of cherts and carbonates from the 2.0 Ga gunflint iron formation: implications for the depositional setting, and the effects of diagenesis and metamorphism. Precambrian Res. 59, 283–313.

Wright, D.T., 1999. The role of sulphate-reducing bacteria and cyanobacteria in dolomite formation in distal ephemeral lakes of the Coorong region, South Australia. Sediment. Geol. 126, 147–157.

Wright, D.T., Wacey, D., 2005. Precipitation of dolomite using sulphate- reducing bacteria from the Coorong Region, South Australia: significance and implications. Sedimentology 52, 987–1008.

Zenger, D. H., 1972. Dolomitization and uniformitarianism: Journal of Geological Education 20, 107-124.

CHAPTER II

Can Mn-S redox cycling drive sedimentary dolomite formation? A hypothesis[1]

2.1. Introduction

In the peritidal zone of most Holocene carbonate platforms, Ca-dolomite formation has been linked to the near-surface decay of microbial mats (e.g., Kendall and Skipwith, 1968; Gebelein and Hoffman, 1973; Davies et al., 1975*;* von der Borch and Lock, 1979) that were rapidly buried during sediment progradation (Hardie and Shinn, 1986). While modern hypersaline microbial mats are functionally diverse (Des Marais, 2003), their upper trophic structure is generally composed of halophilic cyanobacteria living in close association with halotolerant algae and other oxygenic and anoxygenic autotrophs, while the deeper levels contain various heterotrophic communities which couple the oxidation of buried organic carbon to the reduction of available terminal electron acceptors (TEAs). These TEAs include (in decreasing order of energy yield), oxygen, nitrate, manganese, iron, sulfate, and ultimately dissolved inorganic carbon (Froelich et al., 1979). The progressive depletion of TEAs often leads to sharp biogeochemical interfaces that may favour the

[1] A version of this chapter was published in *Chemical Geology* 404, 27-40.

precipitation of authigenic minerals — i.e., calcite, phosphates, pyrite, and/or dolomite (see Konhauser, 2007).

The fact that dolomite is abundant in the geological record yet is rarely observed forming today (the so-called "dolomite problem") is complicated by the fact that Mg in seawater today is largely found in complexed form (cf. Arvidson and Mackenzie, 1999). In the limited number of modern dolomite-forming systems known today, this is thought to be overcome in several ways. The extracellular polymeric substances (EPS) produced by benthic microbes facilitate the sorption and accumulation of Ca, Mg, and various trace metals, and may also act as a mineral nucleation template (Défarge et al., 1996; Braissant et al., 2007; 2009; Wang et al. 2009). Recent work by Roberts et al. (2013) details how the variety of carboxylated macromolecules comprising EPS may catalyze the precipitation of dolomite through complexation and dehydration of Mg^{2+} ions (see also Kenward et al., 2013). The anaerobic respiration of organic carbon shifts the pH towards alkaline values and increases the activity of CO_3^{2-} ions, both favouring dolomite saturation by displacing water dipoles bonded to the surface of magnesium cations (Lippmann 1973; Slaughter and Hill 1991; Défarge et al., 1996; Castanier et al., 1999; Raz et al., 2000; Decho et al., 2005; Gilbert et al., 2005; Visscher and Stolz, 2005; Kwak et al,. 2005; Braissant et al., 2007; Wang et al., 2009; Gallagher et al., 2012).

It is by this combination of biologically influenced (i.e., ion adsorption and mineral templating) and biologically induced (metabolically controlled) mechanisms (cf. Dupraz et al., 2009) that points to many heterotrophic bacteria being capable of facilitating Ca-dolomite nucleation. Yet, the anaerobic respiratory pathway that has received the most attention in terms of diagenetic carbonate mineral formation is bacterial sulfate reduction (Vasconcelos et al., 1995; Vasconcelos and McKenzie, 1997; Wright, 1999; Wright and Wacey, 2005; Warthmann et al., 2000; Van Lith et al., 2003; Sánchez-Román et al., 2009). While studying dolomite formation in hypersaline mats from Lagoa Vermelha, RJ, Brazil, Moreira et al. (2004) concluded that the mineral actually forms as a result of undersaturation of competing carbonate phases due to sulfide oxidation. Similarly, it has been proposed that sulfide ions or some organic ligands may promote Mg^{2+} dehydration at the surface of a solid precursor phase resulting in dolomite nucleation/precipitation reactions (Zhang et al., 2012; Yang et al., 2012, see also Roberts et al., 2013).

It is thus apparent that a variety of mechanisms, non-exclusive in nature, can act as potential promoters of dolomite formation. In some marine sediments, the activity of subsurface Mn(IV)- and Fe(III)-reducing bacteria exerts a quantitatively substantial control on rates of organic carbon mineralization (Aller and Rude, 1988; Aller, 1990, 1994; Canfield et al., 1993a,b; Thamdrup et al., 1994), and not surprisingly, these microorganisms have also been found potentially associated with dolomite precipitation (see for instance Compton, 1992; Curtis et al., 2000; Breuker et al., 2013). However, sedimentary evidence for links between metal respiration during suboxic diagenesis and dolomite formation has yet to be reported.

In this study we employ a high-resolution chemostratigraphic approach, complemented by synchrotron-based microscale analyses and microbial surface chemical characterization, with the goal of examining the formation of dolomite in association with buried microbial mats, and specifically the potential role of electron acceptors other than sulfate in the dolomitization process. In a hypersaline lagoonal sediments in the Archipelago Los Roques, Venezuela, we describe a surprising relation between the subsurface availability of manganese and the abundance of dolomite at this site, where it appears that progressive degradation of a rapidly buried microbial mat system produced a geochemical disequilibrium zone marked by the availability, and recycling, of intermediate manganese and sulfur species. We propose a reaction model whereby intermediate Mn(III) phases, formed via Mn(IV) reduction or Mn(II) oxidation, reacted with native and evolved S^0, enhanced the degradation of sedimentary organic matter, sustained favourable alkalinity and pH, and ultimately, contributed to the stabilization (i.e., progressive growth) of early formed dolomite precursors as microcrystalline Ca-dolomite cements.

2.2. Study site

Francisqui is one of the many cays comprising the Archipelago Los Roques; a semi-arid isolated carbonate platform located 150 km from the Venezuelan coastline in the Caribbean Sea (see Fig. 2.1A). The platform developed over an uplifted lithospheric block whose age, petrography, geochemistry, and tectono-magmatic history are similar to exposures of the Caribbean Plate on the nearby Leeward Antilles islands (see Wright and Wyld, 2010). The restricted lagoon sampled (Fig. 2.1B) has an areal extent of about 7,100 m^2; it is shallow (average water depth <15 cm), alkaline

(pH = 9.3; $CaCO_{3\ total}$ = 259 meq/L), and hypersaline (salinity = 138 - 141‰). Other relevant chemical features of the lagoon water are summarized in Table 2.1, and its predicted saturation states with regard to a variety of minerals are shown Table 2.2. The lagoon has been infilled by accretion of sediments of both authigenic and allogenic (storm transported) origin (i.e., Hardie and Shinn, 1986). A subaqueous microbial mat, composed of both photosynthetic and non-photosynthetic microbes, has developed across the lagoon due to the suppression of most grazing activity under the hypersaline conditions governing this environment (Fig. 2.1C-D). The organic-rich mud-dominated lagoonal succession reflects annual low amplitude fluctuations of the lagoon water level (Fig. 2.1C). The range of such oscillations is controlled by seepage reflux, and sporadically by storm events. The sedimentary distribution of organic matter is greatly influenced by such autocyclic controls, and fossil analogues to the surficial mat have been buried due to active sediment accumulation.

2.3. Methods

With the goal of investigating the formation of dolomite in association with the oxidation of the buried microbial mats and the potential role of electron acceptors other than sulfate, information obtained via bulk sediment digestion and Inductively Coupled Plasma Quadrupole Mass Spectrometry (ICP-QMS) was combined with a range of textural, mineralogical and *in situ* geochemical analyses. We also evaluated the reactivity of the surficial microbial mats by potentiometric titration and applied a surface complexation model that benefits from complimentary Fourier Transform Infrared Spectroscopy (FTIR) data.

2.3.1. Sample collection

A Glew Gravity Corer (Glew, 1991) was used to collect 30 cm-long vertical cores of lagoon sediments. The cores were then extruded and sliced into 0.5 cm subsamples, for the first 6 cm, and then into 2 cm subsamples for the deeper part of the core. Sub-samples of the organic-rich sediments were placed in sterile 0.5 ml Eppendorf PCR polypropylene tubes containing filtered lagoon water and aqueous glutaraldehyde to a final concentration of 2% v/v. The overlying surface waters were sampled in duplicate and filtered through Spectra micropore 0.22-µm filters. One of the aliquots was immediately acidified with concentrated trace metal-free HNO_3 for cation

analyses, and the other left unacidified for anion analysis. The sediment subsamples were freeze-dried prior to further analyses. The samples were kept refrigerated (3ºC) prior to all sample preparation and analyses.

2.3.2. Bulk mineralogical analysis

The mineralogy of freeze-dried bulk sediments (0-30 cm depth) was determined at a vertical resolution of 2 cm by X-ray Diffraction (XRD), with patterns produced using a Rigaku Geigerflex Power Diffractometer with Co-Kα radiation generated at 50 kV and 25 mA, a step size of 0.5° $2\theta \cdot step^{-1}$, and an accumulation time of $2s \cdot step^{-1}$. In the samples where dolomite was found, we optimized the XRD in the interval 29 to 38° 2θ using the d_{101} peak of quartz for calibration purposes. The refined XRD patterns were obtained at $0.2°2\theta \cdot min^{-1}$, and a step size of 0.004 $°2\theta \cdot step^{-1}$ (after Jones et al. 2001).

2.3.3. Electron microscopy

Scanning Electron Microscopy (SEM) observations of both the surface microbial mat, and the dolomite-bearing sediments, were performed on a JEOL JSM-6301FXV instrument connected to a Norvar Energy-Dispersive Spectrometer (EDS). Freshly broken samples were graphite coated for SEM observation, while others were cryosectioned and observed by Transmission Electron Microscopy (TEM). The SEM analyses were done at accelerating voltages of 5 kV (20 kV for EDS), and at a working distance of 11 mm. The accelerating voltage of TEM was 80 kV. Additional details of the microbial mat preparation for SEM and TEM are provided in Petrash et al. (2012).

2.3.4. Solid phase geochemistry

Samples were freeze-dried and powdered before analysis. For minor and trace element composition, a mass of ~200 mg of each sediment subsample was digested using analytical grade HNO_3 (8N). The transition metal concentrations were determined by inductively coupled plasma mass quadrupole spectrometry ICPQ-MS using a PerkinElmer Elan6000 instrument. The Total Organic Carbon (TOC) and Total Nitrogen (TN) of sediment subsamples were determined using the Dumas Combustion Method in a Costech 4010 Elemental Analyzer. We complemented our bulk ICPQ-MS analyses with laser ablation analyses (28 laser spots) in order to measure Mg, Mn,

Fe, and Sr concentrations of the sediments comprising the interval from 8 to 14 cm depth, where Ca-dolomite was identified via XRD. Ca-concentrations obtained via WDS (see below), were used as internal standards, and the USGS analytical standard MACS-3 was used to derive the trace metal concentrations of the samples. Measuring conditions and detection limits are as described in Petrash et al. (2012).

2.3.4.1 Sorptive properties of the microbial mats and their influence on sediments

In order to evaluate the sorptive properties of individual layers comprising the microbial mat, 500 mg (dry weight) sub-samples of the green (upper) and purple (lower) layers of the mat at the sediment-water interface were examined by acid-base titration. Samples were first washed with four alternating wash and harvest cycles (10-s agitation followed by 10-min soak and centrifugation at 11,050 g) at circumneutral pH with ultra-pure (18.2 MOhms) water in order to replace interstitial waters and release surface-complexed elements (e.g., Lalonde et al., 2007). Samples were then suspended in ~40 ml of 0.01 M $NaNO_3$ titration electrolyte and adjusted to pH ~3 with concentrated analytical grade HNO_3. Sub-samples were titrated up from pH ~3 to pH 11, and a surface complexation model was fitted to the resulting excess charge data following the methods of Lalonde et al. (2007, 2010). Briefly, the set of functional groups (in terms of concentrations and proton stability constants) that best account for the excess charge data for each titration were determined by linear programming over a fixed grid of possible pK_a values (in this case, 4-10 in 0.2 increments). We also conducted synchrotron-based FTIR using a Ge IR attachment for attenuated total internal reflection. These analyses were conducted at the Mid-IR Beamline (01B1-1) at the Canadian Light Source and provide identification of the organic ligands contributing to the surface reactivity of the surficial microbial mat with high spatial resolution and minimum sample preparation.

To evaluate the extent to which biologically important metals are transferred from ambient waters to the surficial microbial mats and subsurface sediments, we examined Ca-normalized distribution coefficients between lagoon water ($[Me]_{lw}/[Ca]_{lw}$) and bulk sediments ($[Me]_{Sed}/[Ca]_{Sed}$). In the context of the uppermost mat layer, this approach provides an indication of the affinity of the mat for certain biologically important metals and variation down core reveal

shifts in the mobility of these elements upon burial and diagenesis. Elemental distribution coefficients for the mat and underlying sediments were calculated using the relation:

$$D_{Me} = ([Me]_{Sed}/[Me]_{lw}) \cdot ([Ca]_{lw}/[Ca]_{Sed}).$$

2.3.4.2. Statistical characterization of the sedimentary chemofacies

A Spearman rank correlation coefficient (r_s, $p<0.001$) was used as a non-parametric measure of the strength and direction of association between any two parameters of interest. Geochemical behaviour and correlation amongst bulk element compositions were further examined by hierarchal cluster analysis, which offers a secondary and objective test of the elemental grouping in each diagenetic zone. The data standardization and clustering protocols implemented here (Filzmoser and Hron, 2008; Montero-Serrano et al., 2010) emphasize the relative similarity between analytes by means of squared normalized Euclidian distances. The analyses were performed using the Multi-Variate Statistical Package R.

2.3.5. Aqueous geochemistry

Overlying water temperatures and pH values were measured immediately after collection using a Ross (Orion) combination pH electrode. Total alkalinity was measured *in situ* by using acid titration. Quantitative analyses of SO_4^{2-} and Cl^- anions in the surficial lagoon water samples were performed using a Dionex DX600 Ion Chromatograph. Filtered non-acidified samples were diluted as required before analysis, to reduce salinity to operational values adequate for the analytical machine. Field measurements of temperature, pH, dissolved oxygen and alkalinity, and the chemical analysis of the water samples were used as input data to calculate the distribution of aqueous species, ion activities, and mineral saturation indices that indicate the tendency of a water to dissolve or precipitate relevant mineral phases (see Drever, 1988). The model was computed using the chemical speciation code WATEQ4F (Ball and Nordstrom, 1991) as implemented in PHREEQC (Parkhurst and Appelo, 1999), and assumes homogeneous aqueous phase equilibria, except for redox species. The thermodynamic database used is Nordstrom et al. (1990), revised by Ball and Nordstrom (1991) for gypsum. Equilibrium with respect to mineral solubilities is not assumed. The program results are used primarily to constraint on interpreting the precipitation conditions at the sediment-water interface.

2.3.5.1. Major and trace metal concentrations

For determination of major and trace metal compositions of the lagoon water, the samples were digested with HNO_3 (8N) and analyzed according to standard procedures (e.g., Windom et al., 1989) using the quadrupole inductively coupled plasma mass spectrometer ICP-MS instrument described above.

2.3.6 Electron Probe microanalyses (EPMA)

The *in situ* distributions and concentrations of major elements Ca, Mg, Mn, S, and P in sediments comprising the dolomite-bearing zone were determined using Wavelength Dispersive X-ray Spectroscopy (WDS) with a JEOL JXA-8900 electron microprobe operated at an accelerating voltage of 15 kV, focused beam diameter of 40 μm, and an average current of 10 nA. Count times were 20 s on each peak and half that for background measurements; detection limits (3σ) from the mean of three analyses were approximately 250 ppm for most of the analyzed oxides. A combination of natural and synthetic mineral, oxide, and metal standards were used to reduce counts to weight percent concentrations using the CITZAF method with φρZ calculation.

2.3.7 Synchrotron-based microanalyses

All synchrotron-based elemental microanalyses were conducted under high-resolution conditions by tuning the excitation energy to desired levels using a Si(111) double-crystal monochromator installed at beamline 20 ID at the Advanced Photon Source (APS) in Argonne, IL.

2.3.7.1. Micro X-ray fluorescence (μ-XRF)

The *in situ* distributions and concentrations of Mn, Fe, Co, Ni, Zn, and Sr in the dolomite-bearing sediment layer were determined via hard X-ray microprobe analyses. The excitation energy was tuned at 20.196 keV and a flux of 10^{10} to 10^{11} photons-per-second micro-focused over an analytical area of ~30 μm^2 using Kirkpatrick-Baez (KB) mirrors. The resulting fluorescence spectra were measured using a 4-element Vortex multi-element Si drift detector located at 90° to the incident beam in the direction of the polarization. The detector was calibrated to ~30 eV per channel. Semi-quantitative μ-XRF results were obtained via calibration of relative element sensitivities against a chemically homogeneous zone of the USGS MACS-3 reference material. The spectral acquisition involved counting for 60 s. Net intensities of the fluorescence peaks were

determined by fitting the complete emission line series of each spectrum in the computer code PyMca v.4.6.2 (Solé et al., 2007).

2.3.7.2. X-ray absorption near edge structure (XANES) and 2D-X-ray diffraction (2D-XRD)

We used XANES for determining the oxidation state and coordination chemistry of Mn in the micritic cement. The pre-edge features were collected in the energy range 6.450−6.690 keV; the main edge crest was collected with 0.50 eV steps, then with 0.05 Å steps (*k*-space) until 200 eV above the absorption edge. XANES results were aligned using the K-edge of a Mn foil standard measured in parallel with the sample (i.e., Kraft et al., 1996), with no energy shifts between scans observed for the simultaneously measured Mn foil reference. Nine individual Mn K-edge XANES scans were averaged in energy before background removal and normalization to unit edge-step using ATHENA (Ravel and Newville, 2005). Semi-quantitative analysis of these bulk merged Mn K-edge XANES spectra was done through a linear combination-least squares fitting using four model compounds: Mn_2O_3, $MnCO_3$, ɣ-MnOOH, and Mn_3O_4. At the end of spectral data collection, the mineralogy of the microanalytical area subjected to XANES was evaluated by integrating its bulk 2D-XRD reflection patterns, produced via a KB micro-focused beam (λ=0.6139 Å), using the computer code FIT2D (Hammersley, 1998). Correction of the experimental geometry and 2θ calibration was made possible by also measuring the reflection patterns of LaB_6.

2.4. Results and Discussion

2.4.1. Sorptive properties of the living microbial mat

Concentrations and acidity constant (pK_a) values of proton binding sites modelled from acid-base titration data reveal very little difference between the upper (green) and lower (purple) layers comprising the living microbial mat (Fig. 2.2A). The total site density in the surficial microbial mat was found to be 3.10 ± 0.63 mol·kg^{-1} (dry). The pK_a distribution of chemical functional groups (Fig. 2.2A) shows three buffering zones that we attribute to carboxyl groups (apparent pK_a at 4.03 ± 0.32), the combined buffering capacity of phosphoryl and thiol groups (apparent pK_a at 6.2 ± 0.85), and amino groups (apparent pK_a at 9.32 ± 0.60) (see Fein et al., 1997; Braissant et al., 2007). A contribution from thiol functional groups is not only supported by the significant accumulation of intra- and extracellular-sulfur in these mats (see Fig. 2.2B), but also by the FTIR spectral data

(Fig. 2.2C) that shows peaks at 2550-2620 cm^{-1} which are characteristic of S-H stretching. While more acidic carboxyl, phosphoryl, and thiol groups are more commonly implicated as the primary sites responsible for metal sorption (e.g., Boyanov et al., 2003; Lalonde et al., 2010), the concentration of the third site (amino groups) was found to exceed the combined concentration of the first and second buffering zones (Fig. 2.2A). This has been previously reported for bacterial cultures producing copious amounts of EPS (Lalonde et al., 2005; Braissant et al., 2007), and is consistent with visual and TEM observations (Fig. 2.2D) affirming the EPS-rich nature of the living microbial mat in this study.

At the pH of the lagoon water (pH 9.3) most of the reactive sites identified here will be in deprotonated state (see Fig. 2.2A) and available to bind dissolved metal cations (Geesey and Jang, 1989: Decho, 2000). The natural abundance and activity of these cations in the alkaline lagoon water, together with competition based on their ionic radii, charge, and specific organic and inorganic ligand-metal binding constants (Fraústo da Silva and Williams, 2001), determines which metals are preferentially sequestered by the microbial mat surface (see Table 2.1, Fig. 2.2D). Based solely on the total concentration of reactive sites determined for the surficial mat biomass, we calculate that the burial of an equivalent ~two cm-thick microbial mat (estimated $\rho = 1.15$ kg/m^3) could sequester and transport between 59 to 86 mmol m^{-2} of alkali and transition metals to the subsurface.

2.4.2. High-resolution chemostratigraphy

Solid phase geochemical data reflects exchange and equilibrium between reactive solid phases and pore fluids. The elemental distribution coefficients in the sediments, D_{Me}, reveal three distinct biogeochemical zones, or chemofacies (Fig. 2.2.3). These reflect the variable redox behaviour down core of transition metals (e.g., Mn, Ni, Co, and Fe) which form highly insoluble oxides in oxic pore waters, and elements that occur as highly soluble anionic species in oxic and suboxic waters (e.g., Mo and Re) and are rendered insoluble under more reducing conditions, where they co-precipitate with sulfides (Tribovillard et al., 2006). These general patterns of metal distribution are also evident in a dendrogram (Fig. 2.4).

2.4.2.1 Chemofacies I

From the water-sediment interface downwards to about 6 cm depth is an interval characterized by a general decrease in the concentrations of various transition metals, including Fe, Mo and Cu. Both Fe(III) and Mn(IV) reduction occur in this zone consisting of the surficial living mat and sediments immediately below, with solid-phase Fe concentrations being about one order of magnitude higher than Mn. The log D trend of Cu closely parallels that of Mo ($r_S = 0.92$, $p < 0.001$) (Fig. 2.3). The trend in Mo and Cu depletion also correlates with that of TOC ($r_S = 0.54$, $p < 0.001$) and C/N values ($r_S = 0.68$, $p < 0.001$), pointing to the role of organic matter as a sink for these metals. The base of this chemofacies is a local minimum in all solid phase redox-sensitive metals (Fig. 2.3).

2.4.2.2 Chemofacies II

Below Chemofacies I is a transitional zone, from ~6 to 12 cm depth, which spans the dolomite-bearing buried microbial mat horizon, and in which bulk sediment Mn exhibits a concentration maximum concomitant with decreased bulk sediment Fe concentration and relatively low levels of Mo and Cu (Fig. 2.3). Chemofacies II exhibits peak bulk sediment Mg concentrations (as MgO) up to 18.9 mol%, with remarkable correspondence between both D_{Me} of Mn and Mg (determined from bulk solid and aqueous phase analyses; Fig. 2.3), as well as the Mn and Mg contents of high-Mg calcite cements (as determined by laser ablation ICPQ-MS; Fig. 2.3 inset). The base of this zone marks a subsequent increase in TOC.

2.4.2.3 Chemofacies III

This zone is defined as being from the base of Chemofacies II to at least 30 cm depth. At the top, bulk sediment concentrations of Zn and Cd are at their highest (Fig. 2.3). The top is also characterized by mottled organic matter-rich zones and exhibits a local maximum in Mo and Cu concentrations. Chemofacies III shows relatively constant concentrations of Fe, which contrast with the progressive depletion of solid-phase Mn. Nickel and cobalt rise above our instrumental detection limits (Fig. 2.3) are indicating that these elements may be dependent on the rates of Fe(III) and Mn(IV)-reduction. These trends are accompanied by increasing concentrations of Cr, V, and U (not shown), whose geochemical behaviours are strongly correlated ($r_S = 0.84$ to 0.93, $p < 0.001$) with those of the redox-sensitive element Re. This redox-sensitive element increases

progressively towards the base, peaking at about 22 cm below the water-sediment interface. The down-core distribution of solid phase-bound Re allows for the identification of the most reducing intervals.

2.4.3 Ca-dolomite distribution

A buried microbial mat hosting a laminar dolomite-bearing horizon was observed at a depth between 8 and 12 cm below the sediment-water interface (Fig. 2.3). At this interval, the mineral assemblage consists of halite, partially replaced gypsum, and aragonite. They are cemented by microcrystalline high-Mg calcite and Ca-dolomite. The latter occurs interstitially as spheroidal aggregates composed of sub-micrometer-scale rhombs that are in direct contact with decaying EPS (Fig. 2.5A). WDS analyses show that the proportion of $CaCO_3$ in micritic Ca-dolomite is between 57.8 to 60.1 wt. % (Fig. 2.5B).

Changes in TOC (Fig. 2.3), total nitrogen (not shown), and Mg, Fe, and Mn concentrations depth profiles (Figs. 2.3, 2.5C), point to a link between heterotrophy, the bulk sediment abundance of Ca-dolomite, and these elements. In addition, within a chemostratigraphic context, it was observed that Zn, Mo, Re, Cu, and As are enriched immediately below the dolomite-cemented interval (see Fig. 2.3). The co-enrichment of siderophile and chalcophile metals at this level suggests co-precipitation with solid phase sulfide minerals, such as pyrite. However, neither pyrite nor its precursor monosulfide phases were observed, and if present, they were below the detection limit of standard XRD analyses (~ 2 wt. %). On this note, a closer observation of the bulk sediment concentration trends (Table 2.1) shows strong correlation ($r_S = 0.907 \pm 0.030$, $p < 0.001$) between chalcophile elements (e.g., Zn and Cd) with P, but not between these elements and Fe (Fig. 2.4). This result points to metal scavenging potential by another mineral phase, such as Ca-hydroxyapatite (e.g., Seaman et al., 2001). The latter occurs as small sub-millimeter-scale concretions below the dolomite-cemented interval (Fig. 2.6).

Petrographic relationships revealed by EPMA indicate that S^0 has accumulated in zones texturally dominated by gypsum and aragonite, while interstitial zones are being occluded by a mixture of microcrystalline Mg-enriched carbonate cement that lack S^0 accumulations (Fig. 2.5D). In order to evaluate the association between Ca-dolomite, Mn accumulations and S^0 depletion, the solid phase chemostratigraphic data were complemented by a number of high-resolution *in situ*

analyses, including LA-ICPQ-MS, μXRD, μXRF and XANES. With a spatial resolution (spot size diameter) of 40 μm, our laser ablation data shows a striking correlation between the concentrations of Mn and Mg (see Fig. 2.3 inset). The integration of our μXRD analyses with μXRF (spatial resolution = 5 x 6 μm) also reveals the co-occurrence of microcrystalline Ca-dolomite (d_{104} = 2.901Å), high-Mg calcite, and aragonite in association with solid phase accumulations of manganese (Figs. 2.7, 2.8). Unfortunately, defining the exact mineralogy of Mn–bearing phases is precluded by the poor crystallinity of the mineral phases comprising this heterogeneous cement and their nanometer crystal size. Moreover, the presence of calcite makes it difficult to detect small amounts of Mn(II)-bearing carbonate phases (cf. Table 2.2). It is important to note that although thermodynamically predicted, no Ca-dolomite was positively identified in sediments directly influenced by the decaying process of the surficial photosynthetic microbial mat system. Indeed, in this peritidal parasequence, the mineral was only identified in the suboxic zone influenced by the subsurface decay of a buried microbial mat.

2.4.4 Evidence for multiple manganese redox states

Electron probe microanalyses demonstrate that the interstitial distribution of Ca-dolomite is accompanied by a decrease in solid-phase sulfur (Fig. 2.5D). Synchrotron–based microanalyses, on the other hand, reveal that Mn occurs in interstitial areas being occlude by heterogeneous carbonate cements (Figs. 2.7, 2.8), and that other transition metals, known for their affinity for reactive manganese species (e.g., Ni, Co, and Zn), are spatially related to the Mn accumulations (Fig. 2.8; Table 2.3). XANES further provides information about the mineralogy of the Mn-bearing phases, as well as the Mn redox states. The presence of Mn(III) is evident by the position and broad white line feature of the K-edge, which exhibits two peaks at 6,545.0 and 6,548.5 eV (Fig. 2.9A, B). A linear combination fit of the sorption edge is only achieved by including Mn_2O_3, $MnCO_3$, ɣ-MnOOH, and Mn_3O_4 as standards (Fig. 2.9C). From the semi-quantitative analysis of the resulting Mn-K edge spectrum it can be concluded that in the dolomite-bearing interval, most manganese occurs interstitially as mixed-valence state oxide minerals, yet a substantial fraction of reduced Mn^{2+} may substitute for Mg^{2+} in the micritic carbonates.

2.4.5 Mn cycling as a factor promoting dolomite stabilization

Several lines of evidence suggest that dolomite growth in the Francisqui lagoon was more likely promoted by cycling of metals (specifically Mn) as opposed to metabolisms more commonly implicated in dolomite formation, such as sulfate reduction or methanotrophy. These include (1) the strong correspondence between sedimentary Mn and $MgCO_3$ enrichments throughout the sedimentary pile, (2) tight correspondence between Mg and Mn contents in micrite cements in the dolomite-cemented interval, and (3) the co-occurrence of elemental sulfur with Mn in multiple valence states in the dolomitized interval. The dolomite-cemented interval occurs at significant depth (8–12 cm) below the sediment–water interface, it is restricted to the buried mat and is located well within the zone of sulfate reduction. These features all point towards the fact that the nucleation of dolomite may not actually be occurring at present, but rather took place while the microbial mat hosting the dolomitized interval was buried.

The robust correspondence between Mn and $MgCO_3$ in bulk sediments and micritic cements, combined with the presence of Mn in mixed valence states in the dolomite interval, suggest an important role for Mn cycling during early diagenetic dolomite growth. Below we expand on the potential operation and efficiency of Mn-driven diagenetic reactions that would act to favour dolomitization. As in ocean surface waters, most dissolved manganese in the lagoon is thought to be maintained in its divalent state (i.e., Sunda and Huntsman, 1988, 1990) due to its slow oxidation rate in the presence of O_2 (Murray and Brewer, 1977). Therefore, Mn^{2+} may potentially form organo-metallic complexes with reactive ligands of the microbial mat (i.e., Petrash et al., 2011a,b). Nonetheless, Mn(II)-oxidizing bacteria could be highly active under conditions of low oxygen, as shown in other hypersaline systems (e.g., Tebo, 1991). Previous work has also demonstrated that both Mn_3O_4 and MnOOH are the primary products of enzyme-catalyzed Mn(II) oxidation reactions (Hasting and Emerson, 1986; Mann et al., 1988; Bargar et al., 2000). These phases may then transform into Mn(IV) oxides abiotically, via the autocatalytic oxidation of Mn(III), leading to disproportionation (Bargar et al., 2000; Tebo et al. 2004). Nucleation of both primary and secondary Mn-bearing oxide phases may also be catalyzed by organic and inorganic ligands comprising microbial mats (i.e., Haack and Warren, 2003). The rapid burial of reactive microbial mats in peritidal settings can thus enable a cascade of aqueous reactions involving

intermediate and reduced forms of manganese and sulfur that allow the metal to be recycled multiple times (Fig. 2.10).

Upon burial, the Mn (oxy)hydroxide phases within the EPS may become solubilized. After oxygen (and nitrate if available) is consumed, the earliest stage of anaerobic respiration in the sedimentary pile involves the progressive reduction of Mn (oxy)hydroxides to soluble Mn(II) (Burdige and Nealson, 1985; Burdige, 1993, Tebo et al., 2004). This dissolved Mn(II) may influence local mineral saturation with respect to Mn-bearing carbonates (e.g., Mucci, 1988), or may diffuse vertically and/or laterally, to be biologically oxidized back to Mn(IV), sometimes accompanied by the formation of solid phase and potentially mixed-valence Mn oxides, including Mn(III)-bearing intermediates (Burdige and Nealson, 1985; Myers and Nealson, 1988; Calvert and Pedersen, 1996; Tebo et al., 2004; Tribovillard et al., 2006; Trouwborst et al., 2006). When the process is linked to reduced, and intermediate sulfur species (e.g., HS^-, S^0), the formation of Mn (oxy)hydroxides promotes reactions that evolve pore waters towards more alkaline conditions. Indeed, Aller and Rude (1988) demonstrated that in normal marine-derived pore waters, most alkalinity produced during the reduction of Mn(IV) is rapidly consumed by the co-precipitation of Ca, and some of the reduced Mn(II), into Mg-rich calcites.

Here we suggest that Mn(IV) reduction and recycling may also lead to the precipitation of Ca-dolomite. In our model, the precipitation potential of dolomite is enhanced by the co-occurrence of reduced sulfur species (e.g., HS^-, S^0) and Mn (oxy)hydroxides within the buried microbial mat, i.e., the dolomite-cemented interval. This occurs during reduction of Mn(IV/III) coupled to sulfur oxidation (reactions 2.1 - 2.2) or during Mn(III)-driven elemental sulfur disproportionation (reaction 3) (Thamdrup et al., 1993; Böttcher and Thamdrup 2001; Schippers and Jørgensen, 2001). Moreover, Mn(III) species produced during sulfide oxidation (e.g., reaction 1) are more active in sedimentary diagenesis than previously thought because they can also act as an electron donor (reaction 4) (Trouwborst et al., 2006; Madison et al., 2013).

$$2MnO_2 + HS^- + H_2O \rightarrow 2MnOOH + S^0 + OH^- (\Delta G_r = -96 \text{ kJ/mol}), \quad (2.1)$$

$$3MnO_2 + S^0 + 2H_2O \rightarrow SO_4^{2-} + 3Mn^{2+} + 4OH^- (\Delta G_r = -107 \text{ kJ/mol}), \quad (2.2)$$

$$Mn_3O_4 + 3S^0 + 2H^+ \rightarrow 3Mn^{2+} + SO_4^{2-} + 2HS^- (\Delta G_r = -118 \text{ kJ/mol}), \quad (2.3)$$

$$2MnOOH + 2H^+ \rightarrow MnO_2 + Mn^{2+} + 2H_2O \ (\Delta G_r = -51 \text{ kJ/mol}). \quad (2.4)$$

These redox reactions are relevant in suboxic near-shore sediments where intermediate and reduced sulfur species are brought into close contact with Mn (oxy)hydroxides by natural depositional or syndiagenetic processes (Aller, 1990). They collectively act to increase total alkalinity (see Aller and Rude, 1988), and as experimentally demonstrated by Böttcher and Thamdrup (2001) lead to a continuous increase in pH (e.g., reactions 2.1 - 2.4). However, for dolomite saturation, equally or perhaps even more important is their role in recycling Mn and assuring for a steady upwards diffusive supply and continual oxidation of Mn^{2+}. This, in turn, yields Mn(IV) oxides that can be reduced anew to sustain long-term conditions that ―because of the high Mg/Ca ratios of the precipitation microenvironment― may be favourable for dolomite growth. Importantly, our semi-quantitative XANES analyses showed that although some of the Mn^{2+} diffuses upwards where it could be re-oxidized, a fraction of it substitutes for Mg into newly formed Ca-dolomite (cf., Fig. 2.9), leaving the imprint of Mn cycling that we believe we are observing in the dolomite cemented interval at Francisqui lagoon. Using published Mn partitioning coefficients (K_D) for carbonates in the rhodochrosite–calcite solid solution series (Mucci, 1988; Böttcher, 1998), we estimate maximal pore water Mn concentrations during carbonate mineral precipitation at between 50 and 700 micromolar (depending on the K_D). These fall within the range observed in sediments where Mn-cycling dominates the pore water alkalinity budget (e.g., Thamdrup and Dalsgaard, 2000).

When coupled with the utilization of sedimentary organic matter (e.g., from the buried microbial mat), Mn(IV) reduction (reaction 2.5) is more efficient than acetoclastic bacterial sulfate reduction (BSR) at generating alkalinity (reaction 2.6). In the presence of intermediate forms of sulfur, the process may continuously consume protons to sustain elevated pH levels in the precipitation environment. Such precipitation conditions have long been thought required for interstitial dolomite nucleation (Lippmann, 1973; Middelburg et al., 1991, 1990; Mazzullo, 2000).

$$CH_3COO^- + 4MnO_2 + 3H_2O \rightarrow 4Mn^{2+} + 2HCO_3^- + 7OH^- \ (\Delta G_r = -569 \text{ kJ/mol}), \quad (2.5)$$

$$CH_3COO^- + SO_4^{2-} + H_2O \rightarrow H_2S + 2HCO_3^- + OH^- \quad (\Delta G_r = -48 \text{ kJ/mol}). \quad (2.6)$$

A key point in this regard is whether the relatively low Mn concentrations characterizing marine sediments are capable of generating sufficient alkalinity as to locally influence carbonate

mineral saturation. Previous data for atypical marine sediments where Mn(IV), rather than sulfate, serves as the primary terminal electron acceptor for anaerobic respiration indicates that very little Mn is required. For example, Canfield et al. (1993a,b) demonstrated that in Danish sediments with solid-phase Mn concentrations roughly two orders of magnitude higher than reported herein, Mn(IV) was more important for respiration, and by proxy the alkalinity budget, than all other electron acceptors combined, including oxygen, by a factor of ~10. In this environment, Mn(IV) reduction accounts for 25–99% of anaerobic carbon oxidation in the upper 10 cm of sediments. Part of the reason is rampant Mn recycling; Mn(IV) is continually regenerated by either spontaneous disproportionation of Mn(III) or by aerobic oxidation of Mn(II), the latter being the product of Mn(IV) reduction and also Mn(III) disproportionation (see reactions 2.1-2.4; Fig. 2.10). In this manner, seemingly small sedimentary Mn enrichments may have contributed to the general underestimation of the role of Mn in organic matter cycling (cf. Canfield et al., 1993a; Sunda and Kieber, 1994), and thus alkalinity generation.

Based on our observations at this novel dolomite-forming site, we speculate that in peritidal settings the burial of metal-reactive microbial mats may act as a barrier capable of localizing upward diffusing species in an autocatalytic feedback between Mn (oxy)hydroxide precipitation, solid phase sulfide dissolution, and carbon turnover (Fig. 2.10). While we consider adsorption of Mn to the reactive mat substrate (promoting greater Mn residence times in the suboxic manganic zone) a microbially-influenced process (cf. Dupraz et al., 2009), we consider Ca-dolomite formation in this setting effectively a microbially-induced process (cf. Dupraz et al., 2009), whereby the initial standing stock of reactive manganese and its efficient redox cycling sustain the elevated alkalinities promoting Ca-dolomite growth. Importantly, as this biochemical process takes place, the rapid oxidation of diffused HS^- (reaction 1) may also act to alleviate the inhibitory effect of Mg coordination by water at the solution–solid interface (see Zhang et al., 2012, and also Yang et al. 2012), and ultimately facilitate interstitial Ca-dolomite growth. It is important also to note that abundant Mn cycling is not likely sufficient on its own; higher initial dissolved Mg/Ca, such as occurs in Francisqui lagoon (~6.1), is likely significant in that it kinetically favours the formation of Ca-dolomite.

The influence of the water activity (a_w) on the crystallization of Mg-rich carbonates may also be necessary for the precipitation of dolomite precursors. In experiments where this effect has

been tested (i.e., at a_w below the life limit, < 0.72), the resulting solid phases are a mixture of magnesian calcite, aragonite, and hydromagnesite, but no dolomite (e.g., Lenders et al., 2012; Radha et al., 2012). The hydrated Mg oxides in such experiments attest to the strong binding of the first hydration shell to Mg. In hypersaline systems where the activity of water does not prevent the growth of microbial life, hydrated Mg oxides are only found in supratidal zones at very high evaporation rates. In such environments, the removal of Ca^{2+} due to the precipitation of gypsum ($CaSO_4 \cdot 2H_2O$) contributes to a rise in pore waters Mg/Ca ratios. It also consumes sulfate from the water column, making it available as an electron acceptor in subsequent shallow burial diagenetic reactions (i.e., Petrash et al., 2012). Gypsum reduction also facilitates dolomitization because it creates high alkalinity via the oxidation of the sedimentary organic matter, and the carboxylic acids liberated can serve as nucleation templates (Roberts et al., 2013; Kenward et al., 2013).

The high dissolved Mg/Ca ratios in our study site clearly favours the precipitation of Mg-rich carbonate, but not Mn-rich carbonate-bearing phases, which are more frequent in sediments exposed to relatively low open marine Mg/Ca ratios and much higher Mn concentrations. Because the mechanism for sustained alkalinity described here would coincide with a zone of relatively high dissolved sulfide concentrations, it is possible that some of the early microbial models ascribing a prominent role to BSR might, in fact, be much more complicated and involve Mn (and S) cycling. As recently suggested by Meister (2013), BSR alone might be ineffective for inducing carbonate saturation (but see Gallagher et al., 2012), and only with an alternative mechanism acting in parallel would BSR lead to a state of localized dolomite supersaturation (i.e., Moreira et al., 2004).

2.6. Summary and Conclusions

At Francisqui, a buried microbial mat appears to have facilitated authigenic dolomite precipitation in three ways: (1) by providing a highly reactive substrate for initial Mn and Mg sorption, (2) by providing the reducing equivalents (as organic carbon) for driving heterotrophic reactions that promote alkalinity and carbonation of Mg ions, and (3) upon rapid burial, bringing the Mn-rich, diffusion-limited mat substrate into the sulfate reduction zone where coupled Mn-S redox cycling auto-catalytically enhanced alkalinity generation given sufficient organic matter. We suggest here that these processes have the potential to increase locally pH and alkaline conditions, which

together with relatively high Mg:Ca ratios observed in the lagoon water and inferred for the pore waters, fulfills the prerequisites for the interstitial stabilization (and growth) of early formed dolomite precursors in shallow burial diagenetic realms. More detailed studies on classic penecontemporaneous dolomite-forming settings should consider the importance of manganese cycling in dolomite authigenesis and the integral role of subsurface microbes in shallow burial dolomite formation.

Table 2.1. Lagoon water and bulk sediment trace element concentrations with depth (cm).

Analyte	Ti	V	Cr	Mn	Fe	Co	Ni	Cu	Zn	Mo
$[Me]_{lw}$	3.0	4.9	0.3	1.3	1.6	0.1	0.5	18.4	1.2	1.6
0.25	159.9	43.3	41.6	140.1	6,179.2	13.4	202.3	39.3	81.23	52.0
0.75	82.7	27.4	25.3	106.9	4,654.6	1.4	N.D.	45.2	74.49	48.2
1.25	78.0	26.8	22.6	94.8	4,253.4	1.1	N.D.	46.6	102.32	69.5
1.75	169.6	66.1	45.0	189.1	7,331.7	1.7	N.D.	122.1	203.37	155.9
2.25	159.5	36.7	29.0	124.9	5,044.4	0.7	N.D.	60.9	113.50	91.3
2.75	117.5	45.6	31.4	151.7	5,507.4	1.1	N.D.	80.7	153.90	105.5
3.25	131.0	51.9	40.1	174.0	6,163.6	1.8	N.D.	107.2	177.66	150.3
3.75	92.4	35.7	26.7	148.7	4,231.9	0.5	N.D.	63.8	129.57	88.8
4.25	87.2	34.6	26.2	145.6	4,041.8	0.6	N.D.	74.3	143.91	92.5
4.75	69.5	25.1	21.5	137.8	3,056.2	N.D.	N.D.	50.4	99.89	60.8
5.25	76.9	25.3	22.0	136.5	3,056.2	N.D.	N.D.	50.0	101.35	59.7
5.75	87.5	20.9	17.9	125.1	2,692.3	N.D.	N.D.	39.1	118.33	107.4
7	127.4	32.8	29.3	178.8	3,613.5	N.D.	N.D.	61.3	150.15	24.3
9	**109.9**	**28.6**	**36.0**	**260.4**	**2,090.9**	**2.1**	**N.D.**	**20.0**	**179.73**	**27.1**
11	**129.6**	**39.3**	**39.9**	**252.3**	**2,207.0**	**3.3**	**5.5**	**27.7**	**195.53**	**57.7**
13	**123.2**	**35.1**	**49.7**	**280.7**	**2,409.7**	**4.7**	**32.1**	**29.0**	**219.64**	**70.3**
15	**630.3**	**58.3**	**70.9**	**155.0**	**1,940.4**	**5.7**	**59.6**	**49.4**	**569.28**	**47.7**
17	452.1	50.7	70.9	119.2	1,940.2	6.8	79.3	39.2	346.77	15.2
19	165.0	50.4	69.5	73.3	1,714.7	8.5	115.3	24.6	172.28	11.5
21	196.2	62.8	74.9	68.2	2,255.8	10.3	147.5	24.3	155.66	10.3
23	206.6	87.5	88.2	76.8	2,615.2	11.4	174.8	30.9	167.64	11.5
25	239.3	89.2	89.5	79.3	2,697.7	13.3	200.0	31.3	165.94	7.0
27	191.2	89.0	80.0	68.1	2,102.6	11.3	180.9	26.6	152.11	7.3
29	117.1	101.6	70.6	56.9	1,686.6	12.1	204.0	18.8	94.51	15.2
SE	7.9	0.6	0.5	1.8	18.9	0.7	9.4	0.7	1.4	0.4

Units in nM for lagoon water and µmol/kg for sediments $[Me]_{lw}$: concentration measured in the surficial lagoon water; SE: Measured standard error (based on 3 sediment replicates) Grey shadowed zone represents the living microbial mat, values in bold the Ca-dolomite cemented interval of buried microbial mat. See also Table 2.4

Table 2.2. Activity of dissolved species and saturation indexes (SI) of predicted mineral phases (Ω>0) in the surficial lagoon water as determined using the chemical speciation code WATEQ4F as implemented in PHREEQC (Parkhurst and Appelo, 1999). deriv.Xμ(E)

Phase		**SI**	**log IAP**	**log KT**
Goethite	$FeOOH$	7.0	5.7	-4.7
Huntite	$CaMg_3(CO_3)_4$	5.8	-24.7	2.7
Maghemite	Fe_2O_3	5.0	11.3	-9.0
Dolomite(d)	$CaMg(CO_3)_2$	4.0	-12.8	-3.0
Hydromagnesite	$Mg_5(CO_3)_4(OH)_2 \cdot 4H_2O$	3.5	-6.4	-30.5
Artinite	$MgCO_3 \cdot Mg(OH)_2 \cdot 3H_2O$	2.6	11.6	6.4
Magnesite	$MgCO_3$	2.2	-6.0	-17.3
Calcite	$CaCO_3$	1.8	-6.8	9.0
Aragonite	$CaCO_3$	1.6	-6.8	-8.2
Brucite	$Mg(OH)_2$	1.4	17.6	6.9
Hausmannite	Mn_3O_4	1.3	60.1	7.3
$Fe(OH)_3(a)$	$Fe(OH)_3$	0.7	5.6	-8.4
Strontianite	$SrCO_3$	0.3	-9.0	16.3
Gypsum	$CaSO_4 \cdot 2H_2O$	0.3	-4.3	58.9
Celestite	$SrSO_4$	0.2	-6.5	8.3
Bixbyite	Mn_2O_3	0.04	-0.9	-6.7

Activity of dissolved species and saturation indexes (SI) of predicted mineral phases in the surficial lagoon waters. SI=log (IAP/ Ksp), with IAP and Ksp being the ion activity product of the dissolved constituents and solubility product, respectively. Calculation were performed using the following parameters: Salinity= 140‰; pH=9.3; $CaCO_{3(Tot)}$ =259 meq/L; $[Cl^-]$ = 77,260 mg/L, $[S0_4^-]$ = 13,269 mg/L; Mg/Ca= 6.1, with dissolved concentrations of [Ca] =1,370; and [Sr]= 274; [Fe] = $9.16 \cdot 10^{-2}$, [Mn] = $6.9 \cdot 10^{-3}$, [Zn] = $7.33 \cdot 10^{-2}$, [Cu] = 1.16 ppm.

Table 2.3. Semi-quantitative μ-XRF concentration data

Zone A (micritized snail)

MCA	Ti	V	Mn	Fe	Co	Ni	Cu
1-1	1.11	1.52	5.82	71.71	0.41	1.16	1.03
1-2	0.80	2.70	3.63	40.87	0.93	1.13	0.52
1-3	0.32	0.25	2.31	41.47	1.34	0.17	0.69
1-4	0.33	0.25	2.66	42.01	1.36	0.17	0.70
1-5	0.44	1.14	1.12	34.59	1.39	0.14	0.37
1-6	1.74	0.96	5.22	35.99	0.36	0.88	0.43
SD	0.56	0.92	1.80	13.71	0.48	0.50	0.24

Zone B: (microcrystalline dolomite-bearing cement)

MCA	Ti	V	Mn	Fe	Co	Ni	Cu
2-1	0.78	0.69	19.96	71.51	3.58	0.12	0.75
2-2	0.28	1.63	18.89	118.31	1.85	0.22	0.73
2-3	1.98	0.28	31.93	156.72	5.57	0.15	1.31
2-4	0.17	0.46	21.26	343.04	2.36	4.49	1.36
2-5	1.30	2.74	18.98	130.38	7.94	0.57	0.56
SD	0.75	1.03	5.52	104.74	2.51	1.90	0.37

Units are ppm

Table 2.4. Concentration values for lagoon water and bulk sediment samples

Depth (cm)	TOC	TN	Mg	P	Ca	Ti	V	Cr	Mn	Fe	Co	Ni	Cu	Zn	As	Sr	Mo	Cd	Ce	Re	U
$[Me]_{lw}$	-	-	200.04	0.03	36.63	2.95	4.87	0.32	1.25	1.64	0.12	0.50	18.41	1.24	0.003	312.71	1.63	0.83	0.83	0.003	0.01
0.25	3.5	0.5	464.1	72.9	7950.9	159.9	43.3	41.6	140.2	6179.2	13.4	203.1	39.3	81.2	21.8	68.3	52.0	1.8	2.4	0.016	7.4
0.75	1.8	0.2	321.4	48.8	5352.1	82.7	27.4	25.3	107.0	4654.7	1.4	<D.L.	45.2	74.5	11.0	51.5	48.3	1.6	2.4	0.023	6.7
1.25	0.7	0.1	280.9	57.2	5263.7	78.0	26.8	22.6	94.8	4253.4	1.1	<D.L.	46.6	102.3	11.9	51.3	69.5	2.4	2.2	0.029	6.2
1.75	0.5	0.1	457.2	122.4	5456.7	169.6	66.1	45.0	189.2	7331.7	1.7	<D.L.	122.1	203.4	14.8	54.6	156.0	6.2	4.0	0.059	10.5
2.25	0.5	0.1	410.4	69.0	5772.6	159.5	36.7	29.0	125.0	5044.5	0.7	<D.L.	65.6	113.5	14.2	59.1	91.3	2.5	2.8	0.035	6.8
2.75	0.3	0.1	426.7	94.5	5642.2	117.5	45.6	31.4	151.8	5507.4	1.1	<D.L.	87.0	153.9	13.8	55.7	105.6	3.9	3.1	0.041	7.4
3.25	0.3	0.1	540.6	110.5	5274.0	131.0	51.9	40.1	174.0	6163.7	1.8	<D.L.	115.6	177.7	16.4	54.9	150.4	4.5	3.3	0.052	9.0
3.75	0.7	0.1	429.3	72.7	5932.4	92.4	35.7	26.7	148.7	4231.9	0.5	<D.L.	68.8	129.6	12.0	53.0	88.8	3.2	2.0	0.032	6.3
4.25	0.3	0.1	462.4	75.0	5559.8	87.2	34.6	26.2	145.6	4041.8	0.6	<D.L.	80.1	143.9	12.2	44.0	92.6	3.4	1.8	0.034	5.9
4.75	0.4	0.1	407.2	74.2	6606.0	69.5	25.1	21.5	137.9	3056.2	0.0	<D.L.	54.3	99.9	10.1	54.1	60.9	1.5	1.4	0.026	5.6
5.25	4.6	0.6	420.7	74.7	6555.4	76.9	25.3	22.0	136.6	3056.2	0.0	<D.L.	53.9	101.3	10.0	53.9	59.8	1.5	1.4	0.022	5.5
5.75	0.3	0.0	278.7	105.5	6751.2	87.5	20.9	17.9	125.2	2692.3	0.0	<D.L.	42.2	118.3	12.1	62.5	107.6	2.5	1.8	0.028	7.0
7	0.2	0.0	460.2	163.7	6685.0	127.4	32.8	29.3	178.9	3613.5	0.0	<D.L.	66.1	150.1	11.3	102.6	24.3	2.1	2.8	0.012	13.7
9	**0.3**	**0.0**	**947.7**	**166.0**	**8701.7**	**109.9**	**28.6**	**36.0**	**260.4**	**2091.0**	**2.1**	<D.L.	**21.6**	**179.7**	**10.9**	**98.6**	**27.1**	**2.8**	**3.0**	**0.011**	**14.6**
11	**1.1**	**0.2**	**979.6**	**166.9**	**8713.9**	**129.6**	**39.3**	**39.9**	**252.4**	**2207.1**	**3.3**	**5.5**	**29.8**	**195.5**	**12.0**	**93.6**	**57.7**	**3.3**	**4.3**	**0.011**	**18.4**
13	**1.8**	**0.3**	**1073.2**	**743.2**	**8580.5**	**123.2**	**35.1**	**49.7**	**280.8**	**2409.7**	**4.7**	**32.1**	**31.2**	**219.6**	**14.4**	**96.4**	**70.4**	**9.1**	**8.4**	**0.014**	**28.6**
15	4.8	0.7	410.2	457.6	9318.5	630.3	58.3	70.9	155.0	1940.5	5.7	59.6	53.3	569.3	12.6	97.0	47.8	7.5	7.0	0.015	26.0
17	5.5	0.8	365.6	176.7	9409.8	452.1	50.7	70.9	119.2	1940.3	6.8	79.3	42.3	346.8	10.9	101.7	15.2	5.3	8.5	0.009	26.9
19	3.8	0.5	235.3	169.8	9466.8	165.0	50.4	69.5	73.4	1714.8	8.5	115.3	26.6	172.3	11.3	101.4	11.5	5.7	8.9	0.012	31.6
21	5.3	0.7	222.1	205.2	9747.4	196.2	62.8	74.9	68.2	2255.9	10.3	147.5	26.2	155.7	11.6	95.1	10.4	5.5	9.0	0.012	37.1
23	5.0	0.7	253.0	149.6	9426.0	206.6	87.5	88.2	76.9	2615.2	11.4	174.8	33.3	167.6	12.8	90.9	11.5	4.2	6.9	0.015	28.4
25	4.5	0.6	258.9	87.9	9392.1	239.3	89.2	89.5	79.3	2697.8	13.3	200.0	33.8	165.9	10.1	89.0	7.1	3.4	5.4	0.022	27.3
27	4.8	0.7	258.0	64.3	9601.4	191.2	89.0	80.0	68.1	2102.6	11.3	180.9	28.7	152.1	10.2	67.7	7.3	3.9	4.6	0.021	26.0
29	2.8	0.4	223.6	34.7	9664.1	117.1	101.6	70.6	57.0	1686.7	12.1	204.0	20.2	94.5	12.9	86.1	15.3	2.7	4.6	0.041	36.6

TOC: Total Organic Carbon, TN: Total Nitrogen (wt. %). Sediment elemental concentrations are $nmol \cdot g^{-1}$ (nM for water); except for magnesium, phosphate, and calcium that are $\mu mol \cdot g^{-1}$ (mM for water). Grey shadowed zone represents the living microbial mat, values in bold the Ca-dolomite cemented interval

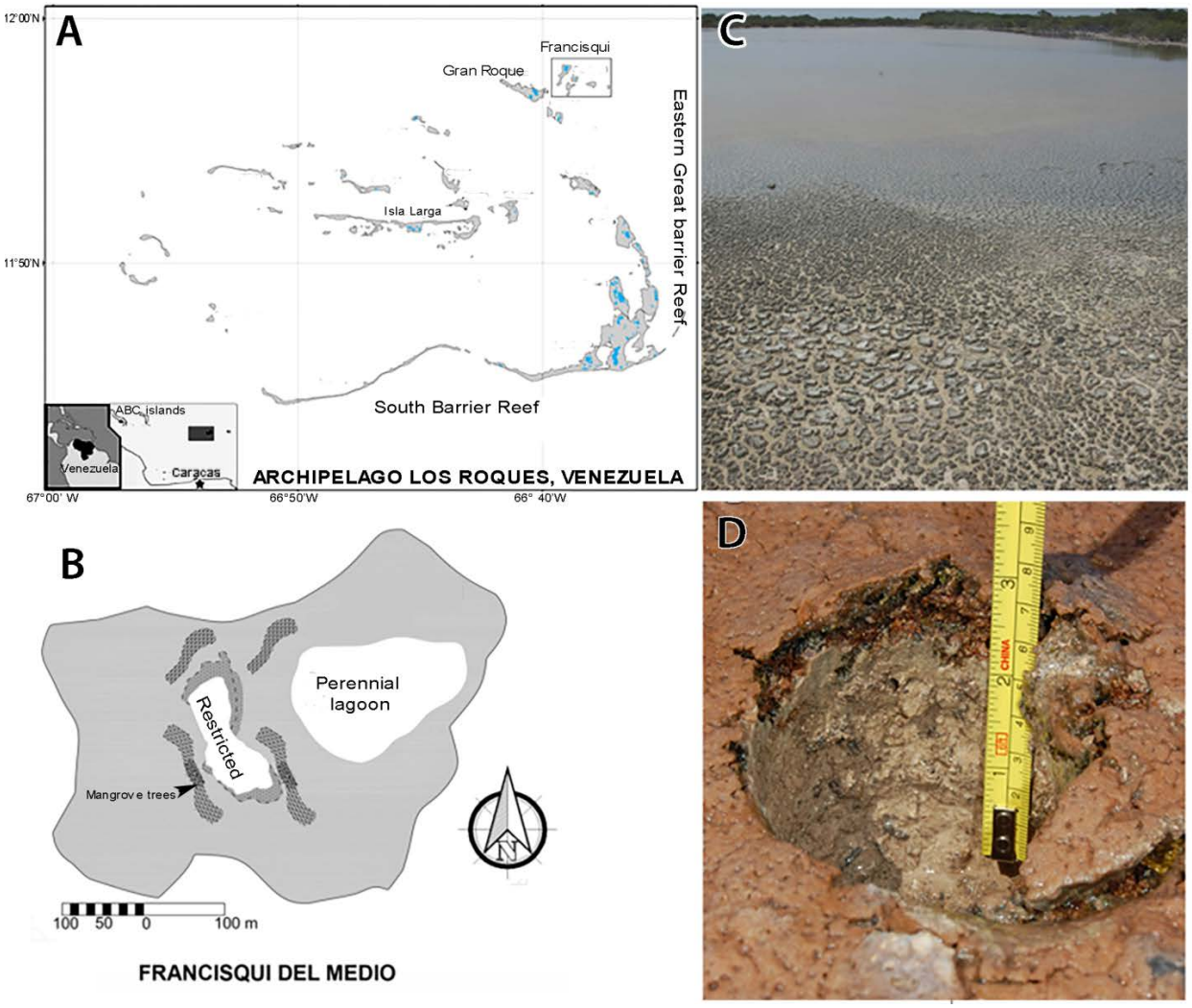

Figure 2.1. Archipiélago Los Roques National Park, Venezuela. A: The Archipelago consists of more than 42 cays, most of them exhibiting at least one restricted lagoon. B: The selected study site is the hypersaline lagoon Francisqui del Medio. C: Desiccated microbial mats remain as evidence of seasonal variations in the lagoonal water level. D: The communities comprising these mats produce copious amounts of exopolymers (EPS).

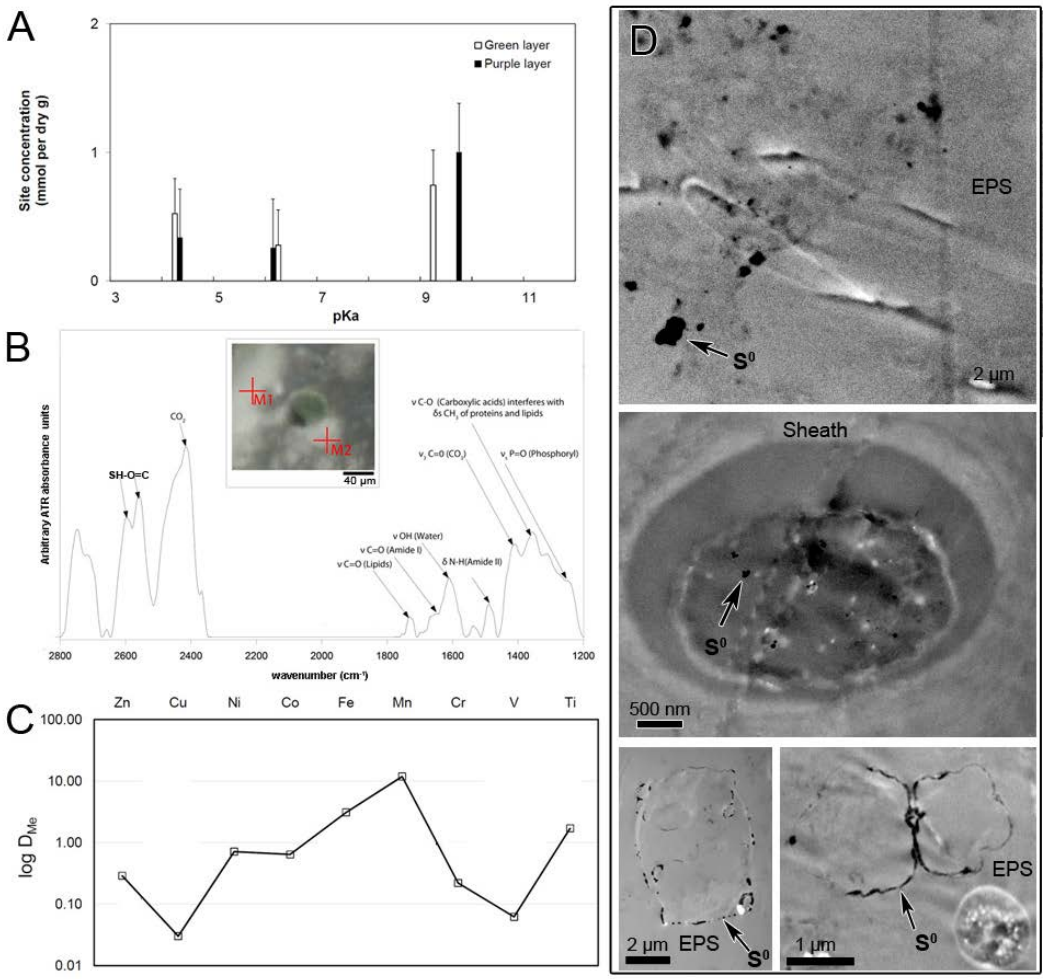

Figure 2.2. Reactivity of the surficial microbial mat. Organic functional groups comprising the microbial biomass confer it with a strong capacity for metal sorption. A: Functional group distribution modelled from titration data for upper (green) and lower (purple) photosynthetic mat layers from the hypersaline lagoon in Francisqui. The model represents the set of functional groups, fitted in terms of concentration (y-axis, normalized to dry weight) over a fixed grid of possible acidity constants (x-axis, in this case from 3 to 11 in 0.2 pK_a increments), that best describes the charge excess data over three titration replicates. B: SR-FTIR-ATR spectrum of microbial biomass. C: Logarithmic plot showing enrichment/depletion factors (D_{Me}= $([Me]_{Sed}/[Me]_{lw})\cdot([Ca]_{lw}/[Ca]_{Sed})$) for the first row transition metals in the sediments and surface mat relative to lagoon waters. D: Transmitted electron micrographs of filamentous and coccoid microorganisms associated with S^0-rich mats. Note extracellular, intracellular, and cytoplasmic membrane sulfur inclusions.

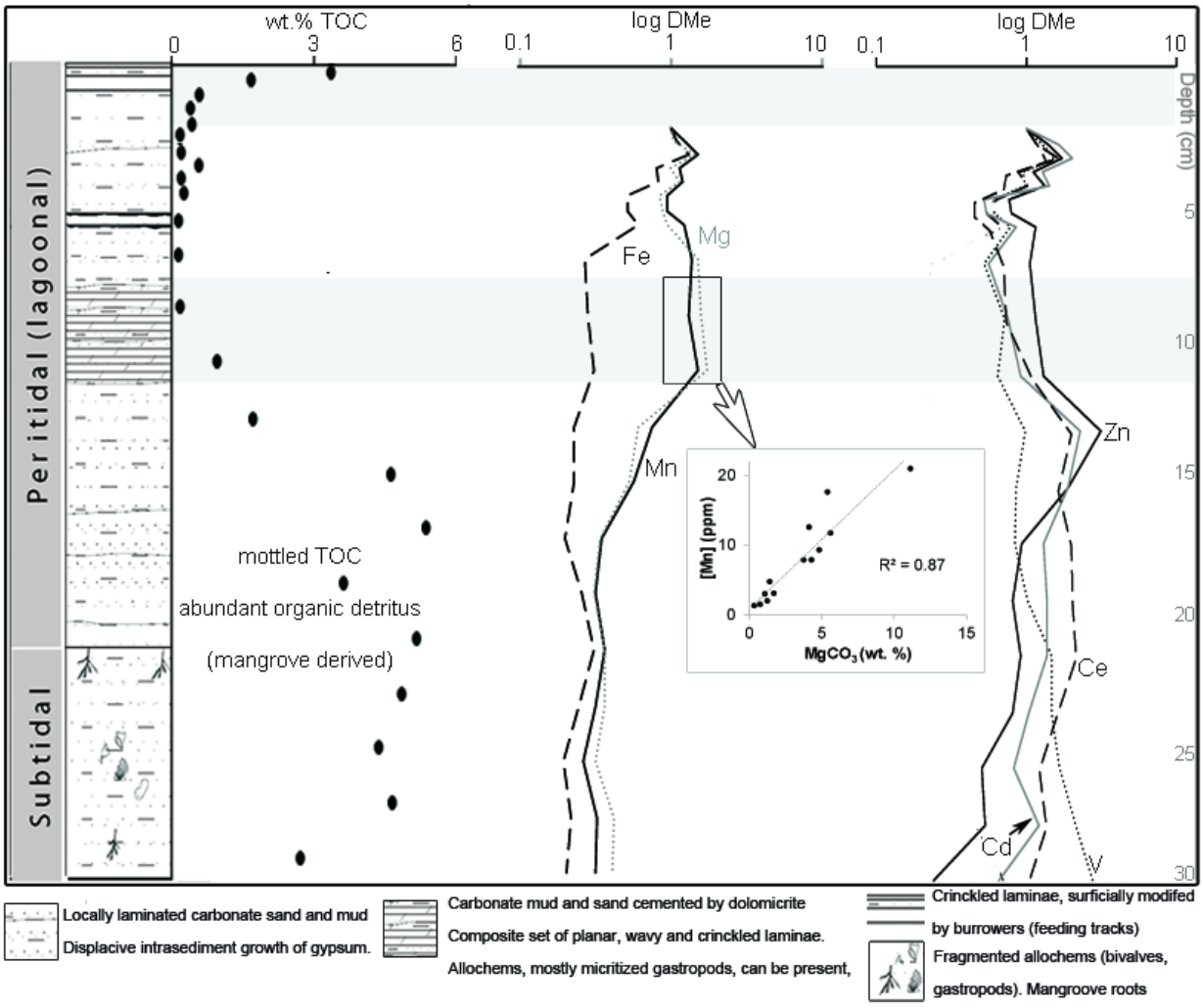

Figure 2.3. Bulk sedimentological and geochemical trends along the studied interval. TOC values of the lagoonal facies range from 0.24 to 4.56 wt%. In the first 10 cm of the sedimentary pile, TOC is approximately equal to the reciprocal of depth$^{-1/2}$; a significant increase in TOC values occurs below 11 cm depth. The bulk sediment trace metal enrichment/depletion trends were normalized using concentrations measured at the microbial mat sediment interface (D_{Me}= $([Me]_{Sed}/[Me]_{lw})\cdot([Ca]_{lw}/[Ca]_{Sed})$, see also Table 2.1). Areas influenced by the microbial mats are shown in light grey, with darker grey showing the living surficial microbial mat.

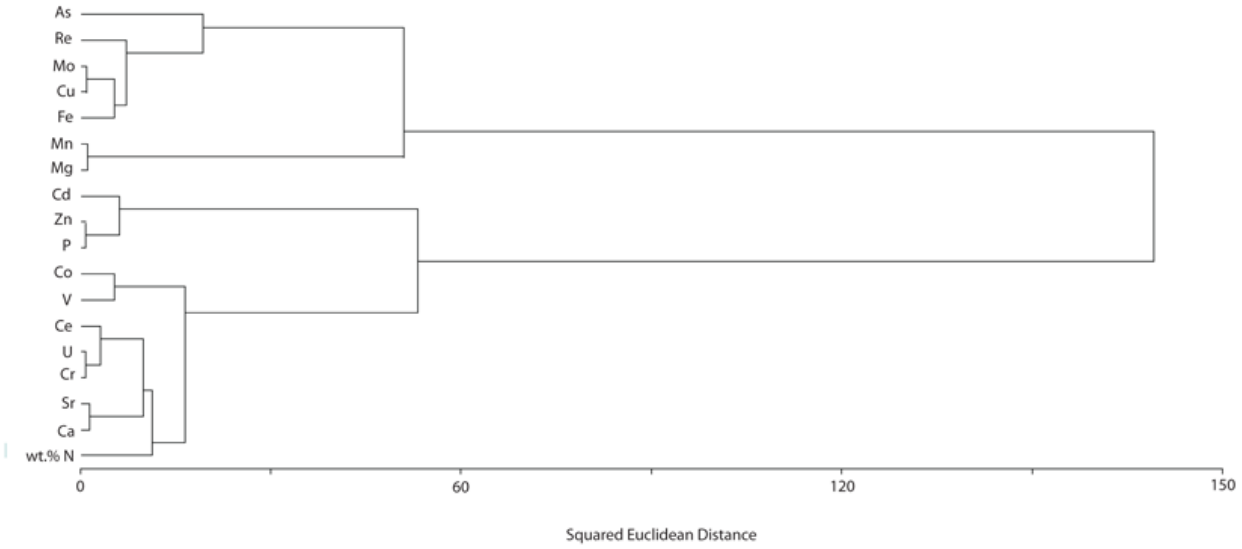

Figure 2.4. Dendrogram representing the outcome of a Hierarchical Cluster Analysis of the bulk sediment ICP-MS data.

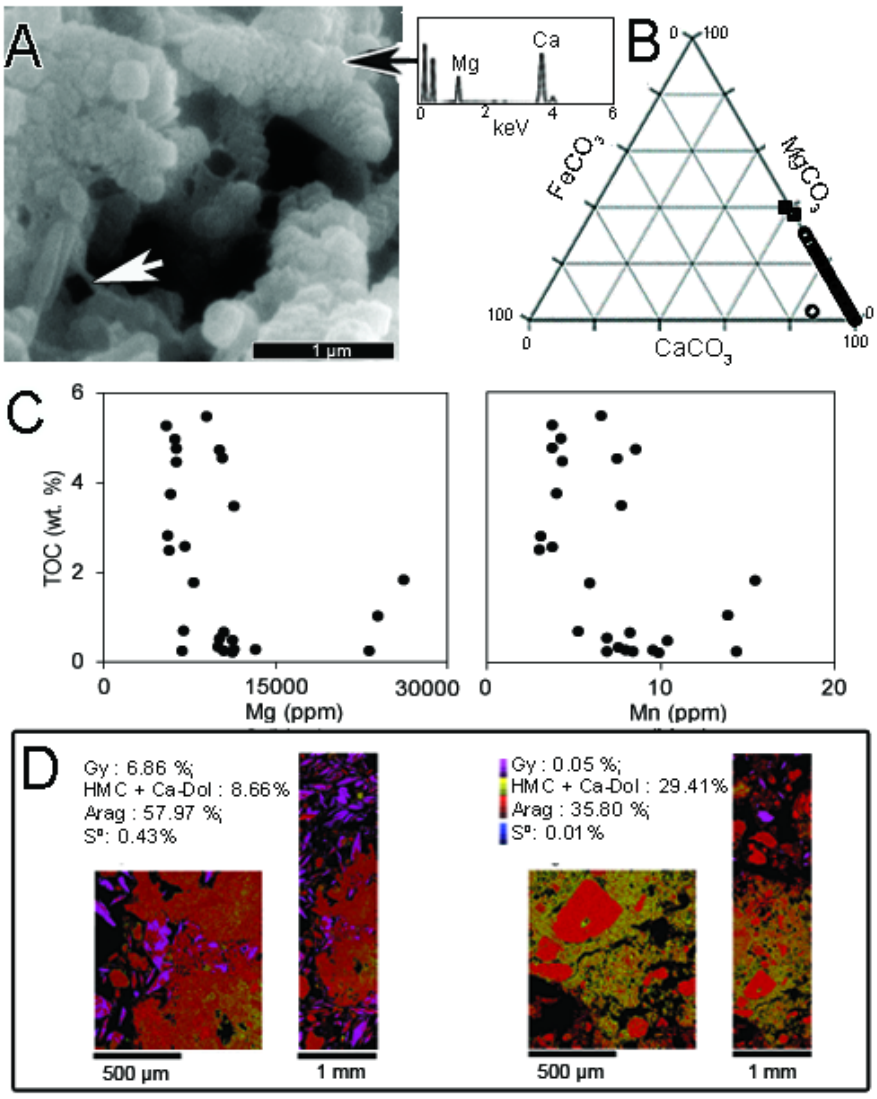

Figure 2.5. Textural and electron probe microanalyses of the dolomite-bearing interval. A: High magnification SEM photomicrograph and EDS spectrum of the Ca-dolomite cement, the latter associated with decaying EPS (arrow). B: $MgCO_3$-$CaCO_3$-$FeCO_3$ triangular plot of cement composition based on WDS data. C: More efficient degradation of the sedimentary organic matter is observed in the Mg and Mn enriched interval (data from ICP-MS). D: Backscattered electron imaging and composite Ca, S, Mg elemental maps (EMPA) provide evidence for the replacement of gypsum by aragonite, and the distribution of Ca-dolomite and elemental sulfur in the 8-10 cm depth interval. Note the decrease in S^0 accumulation in interstitial areas occluded by Mg-enriched carbonates.

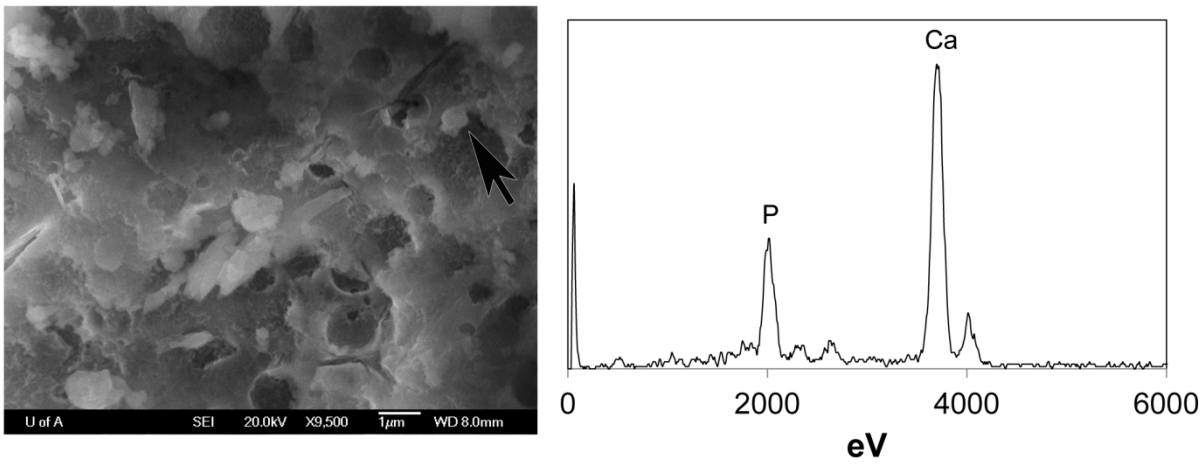

Figure 2.6. SEM micrograph and EDS spectrum of Ca-hydroxyapatite at 13-cm depth.

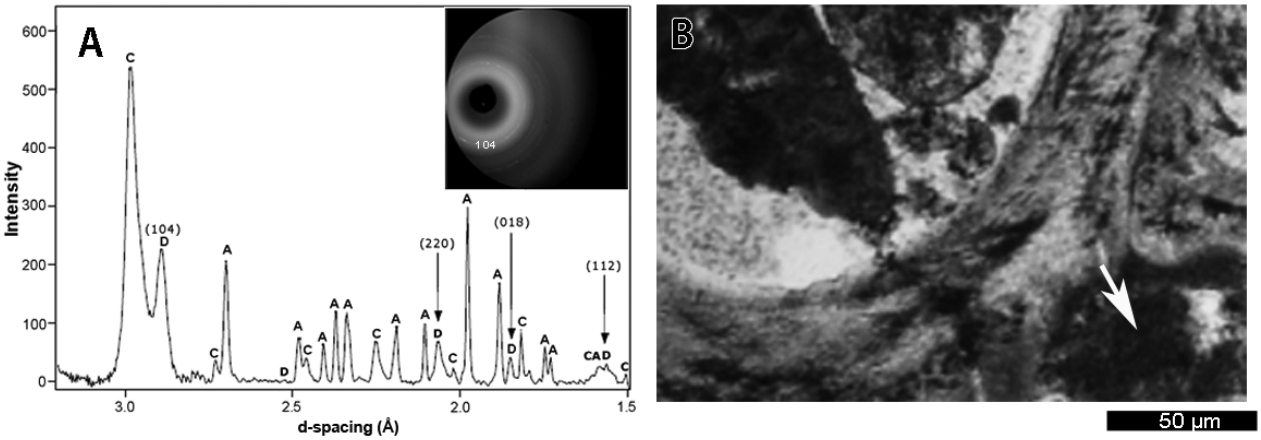

Figure 2.7. Synchrotron-based µ-XRD. A: Close up of the 2D integrated pattern (inset) obtained over the analytical area (~30 µm^2) shown in B (arrow) at this location. The dominant phases are microcrystalline high-Mg calcite, aragonite, and Ca-dolomite (d_{104} = 2.901Å). B: Micrograph showing a micritized hydrobiid gastropod shell and associated micritic cement. See also Fig. 2.8A.

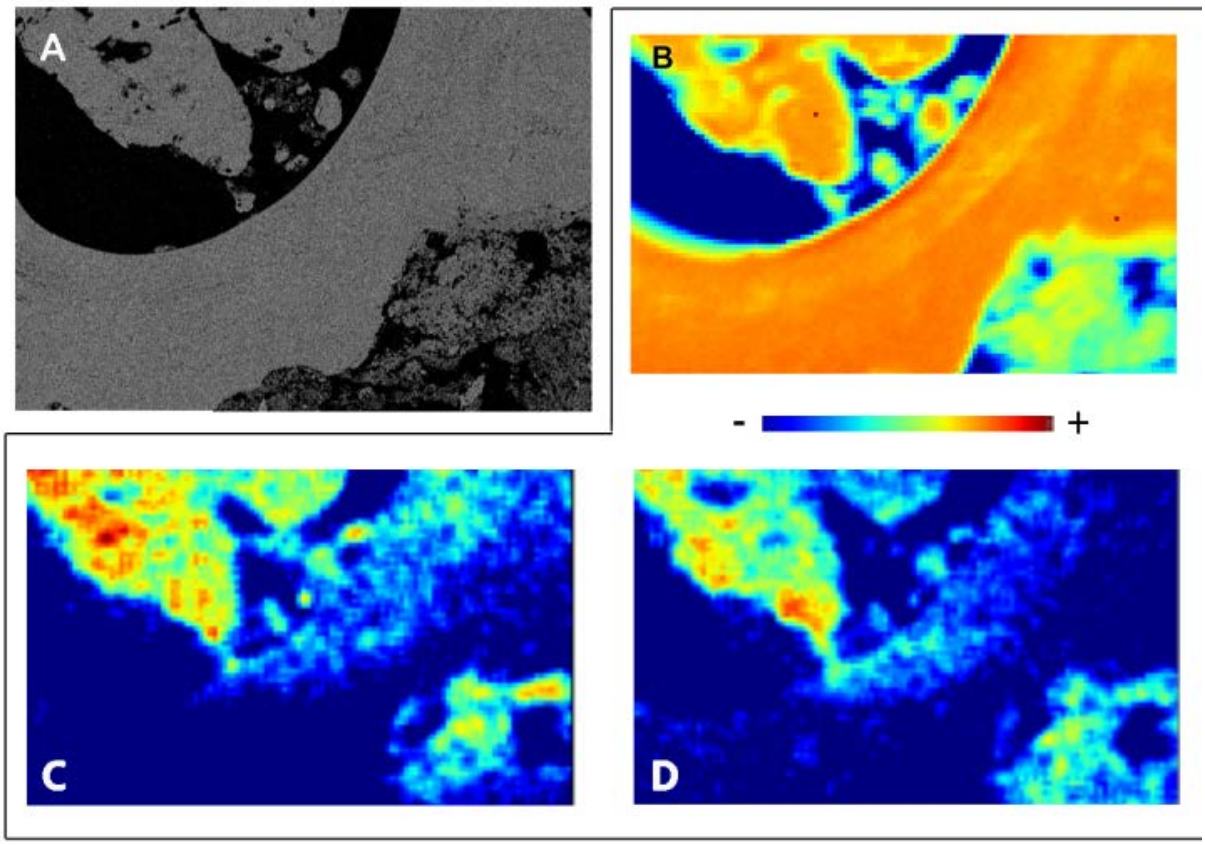

Figure 2.8. Micro-XRF distribution maps (400 × 600 μm^2) showing zones of preferential enrichment of Ca (B) Mn (C) and Ni (D) in the cement. The colour-coding convention is presented by the scale bar (300 μm in size); it assigns blue to the minimum and red to maximum deconvoluted peak area of the element.

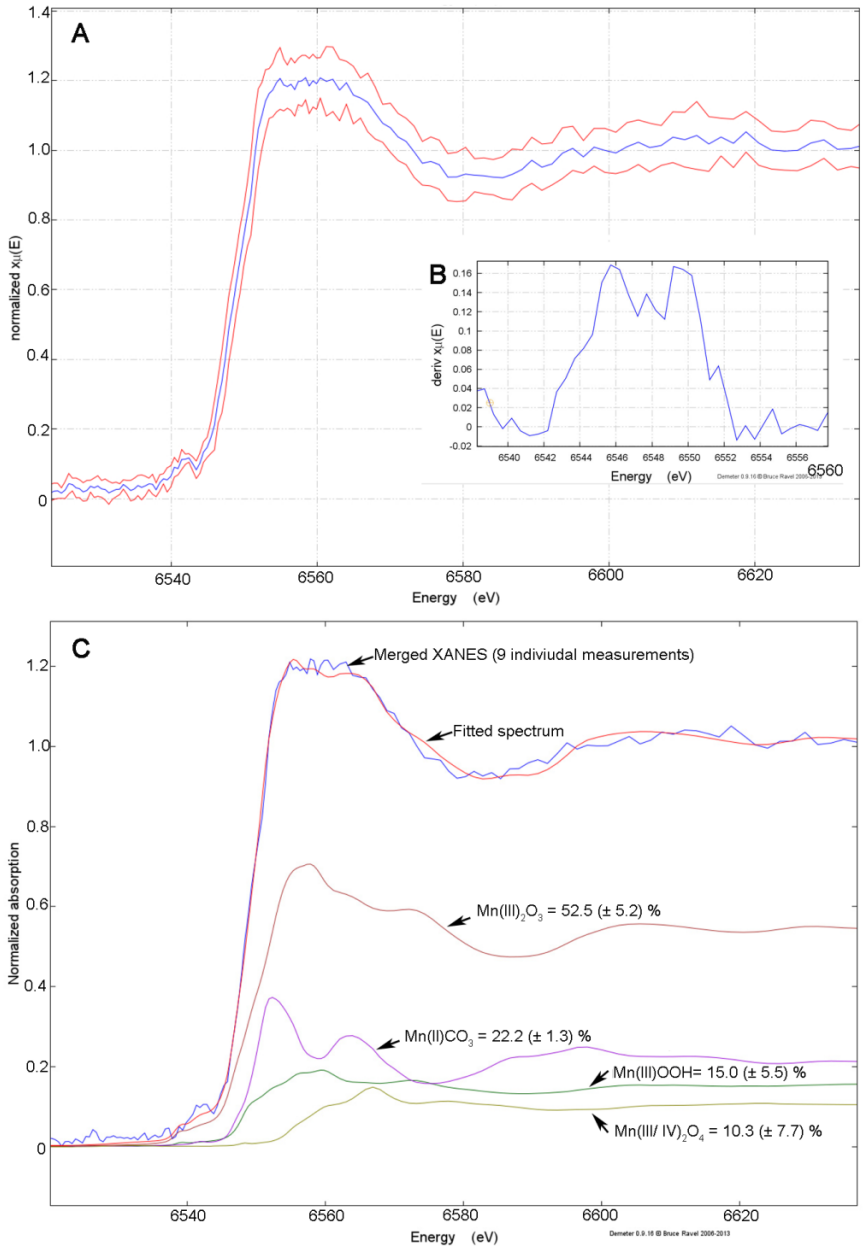

Figure 2.9. Normalized Mn K-edge merged spectra of the analytical area shown in Fig. 2.7B (arrow). A. The K-edge exhibits two main features at about 6554 and 6558 eV. B: Intermediate valence Mn(III) is identified by using the first derivative of the XANES spectra in the interval 6547.9–6549.0 eV (e.g., Manceau et al., 2012). C: A least-square fitting of the spectra was performed to quantify the Mn species present. The spectra can be fitted with four model compounds, Mn_2O_3 (52.5 ± 5.2%), $MnCO_3$ (22.2 ± 1.3%), ɣ-MnOOH (15.0 ± 5.0%), and Mn_3O_4 (10.3 ± 7.7%), suggesting co-occurrence of these phases in the dolomite-bearing microcrystalline cements.

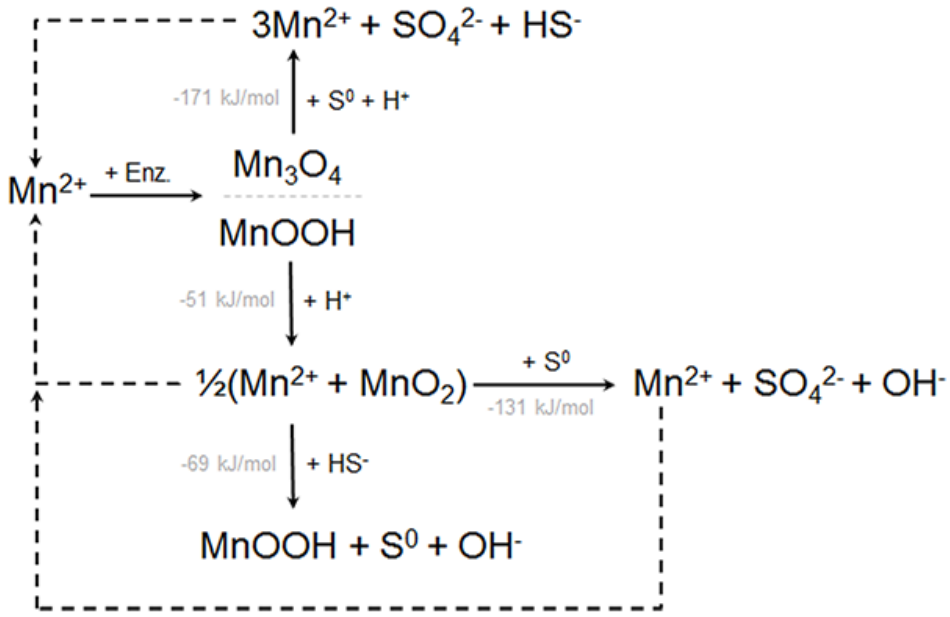

Figure 2.10. Schematic diagram showing a simplified coupled sedimentary manganese - sulfur cycle. The theoretical calculation of energy yield of each reaction is also shown (This diagram is not mass or charge balanced. See details on the text: reactions 2.1 - 2.4.

2.7. References

Aller R. C., 1990. Bioturbation and manganese cycling in hemipelagic sediments. *Philosophical Transactions of the Royal Society A* 331, 51–68

Aller, R. C., 1994. The sedimentary Mn cycle in Long Island Sound. Its role as intermediate oxidant and the influence of bioturbation, O_2, and C_{org} flux on diagenetic reaction balances. *J.Marine Research,* 52, 259–295.

Aller, R.C., and Rude, P.D., 1988. Complete oxidation of solid phase sulfides by manganese and bacteria in anoxic marine sediments. *Geochimica et Cosmochimica Acta* 52, 751–765.

Arvidson, R.S., MacKenzie, F.T., 1999. The dolomite problem: control of precipitation kinetics by temperature and saturation state. *Amer. J. Sci*. 299, 257–288.

Ball, J.W., and Nordstrom, K., 1991. User's manual for WATEQ4F, with revised thermodynamic data base and test cases for calculating speciation of major, trace, and redox elements in natural waters. U.S. Geological Survey Open-File Report 91-183.

Bargar, J., Tebo, B., Villinski, J., 2000. *In situ* characterization of Mn (II) oxidation by spores of the marine *Bacillus* sp. strain SG-1. *Geochimica et Cosmochimica Acta* 64*,* 2775-2778

Braissant, O., Decho, A. W., Dupraz, C., Glunk, C., Przekop, K. M., and Visscher, P. T., 2007. Exopolymeric substances of sulfate-reducing bacteria: Interactions with calcium at alkaline pH and implication for formation of carbonate minerals. *Geobiology* 5, 401–11.

Braissant, O., Decho, A.W., Przekop, K.M., Gallagher, K.L., Glunk, C., Dupraz, C., and Visscher, P.T., 2009. Characteristics and turnover of exopolymeric substances in a hypersaline microbial mat. *FEMS Microbial. Ecol.*67, 2005–2008.

Breuker, A., Stadler, S., and Schippers, A., 2013. Microbial community analysis of deeply buried marine sediments of the New Jersey shallow shelf, IODP Expedition 313. *FEMS Microbial. Ecol.*, doi. 10.1111/1574-6941.12146

Böttcher, M., and Thamdrup, B., 2001. Anaerobic sulfide oxidation and stable isotope fractionation associated with bacterial sulfur disproportionation in the presence of MnO_2. *Geochimica et Cosmochimica Acta* 65, 1573–1581.

Boyanov, M.I., Kelly, S.D., Kemner, K.M., Bunker, B.A., Fein, J.B., and Fowle, D.A., 2003. Adsorption of cadmium to *Bacillus subtilis* bacterial cell walls: A pH-dependent X-ray

absorption fine structure spectroscopy study. *Geochimica et Cosmochimica Acta* 67, 3299-3311.

Burdige, D.J., 1993. The biogeochemistry of manganese and iron reduction in marine sediments. *Earth-Science Reviews* 35, 249-284.

Burdige, D. J., and Nealson, K. H., 1985. Microbial manganese reduction by enrichment cultures from coastal marine sediments. *Applied Environ. Microbiol.* 50, 491–7.

Calvert, S. E., and Pedersen, T. F., 1996. Sedimentary Geochemistry of Manganese: Implications for the Environment of Formation of Manganiferous Black Shales. *Econ. Geol.* 91, 36–47.

Canfield, D. E., Thamdrup, B., and Hansen, J. W., 1993a. The anaerobic degradation of organic matter in Danish coastal sediments: Iron reduction, manganese reduction, and sulfate reduction. *Geochimica et Cosmochimica Acta* 57, 3867–83.

Canfield, D.E., Jørgensen, B.B., Fossing, H., Glud, R., Gundersen, J., Ramsing, N.B., Thamdrup B., Hansen J.W., Nielsen L.P., Hall P.O.J., 1993b. Pathways of organic carbon oxidation in three continental margin sediments. *Marine Geology* 113, 27–40.

Castanier, S., Métayer-Levrel, G. Le, and Perthuisot, J., 1999. Ca-carbonate precipitation and limestone genesis —the microbiogeologist point of view. *Sed.Geol.*126, 9-23

Compton, J., 1992. Early diagenesis and the origin of diagenetic carbonate in sediment recovered from the Argo Basin, Northeastern Indian Ocean, Site 765. *Proceedings of the Ocean Drilling Program, Site 765*, 77–88.

Covington, A.K., Whitfield, M., 1988. Recommendations for the determination of pH in seawater and estuarine waters. *Pure Appl. Chem*. 60, 865–870.

Curtis, C.D., Cope, J.C.W., Plant, D., and Macquaker, J.H.S., 2000. "Instantaneous" sedimentation, early microbial sediment strengthening and a lengthy record of chemical diagenesis preserved in Lower Jurassic ammonitiferous concretions from Dorset. *J. Geol.Soc.* 157, 165–72.

Davies, P., Ferguson, J, and Bubela, B., 1975. Dolomite and organic material. *Nature* 255, 472–74.

Decho, A.W., 2000. Microbial biofilms in intertidal systems: an overview. *Continental Shelf Research* 20, 1257–1273.

Decho, A. W., Visscher, P. T., and Reid, R. P., 2005. Production and cycling of natural microbial exopolymers, EPS, within a marine stromatolite. *Palaeogeog., Palaeoclim., Palaeoecol.* 219, 71 – 86.

Défarge, C., Trichet, J., Jaunet, A.M., Robert, M., and Sansone, F.J., 1996. Texture of microbial sediments revealed by cryo-scanning electron microscopy. *J. Sed. Research* 66, 935–47.

Des Marais, D. J., 2003. Biogeochemistry of hypersaline microbial mats illustrates the dynamics of modern microbial ecosystems and the early evolution of the biosphere. *The Biological Bulletin* 204, 160–167.

Drever, J. I., 1988. The geochemistry of natural waters (2nd ed.). Englewood Cliffs, New Jersey, Prentice-Hall, 437 p.

Dupraz, C., Reid, R.P., Braissant, O., Decho, A.W., Norman, R.S., Visscher, P.T., 2009. Processes of carbonate precipitation in modern microbial mats. *Earth Science Reviews* 96**,** 141–162.

Fein, J., Daughney, C., Yee, N., and Davis, T., 1997. A chemical equilibrium model for metal adsorption onto bacterial surfaces. *Geochimica et Cosmochimica Acta* 61, 3319–3328.

Filzmoser, P., and Hron, K. 2008. Outlier detection for compositional data using robust methods. *Mathematical Geoscience.* 40, 233–248.

Fraústo da Silva, J.J.R., Williams, R.J.P., 2001. The Biological Chemistry of the Elements, second ed. Oxford University Press, Oxford, UK, 575 pp.

Froelich, P.N., Klinkhammer, G.P., Bender, M.L., Luedtke, N.A., Heath, G.R., Cullen, D., Dauphin, P., Hammond, D., Hartman, B., and Maynard, V., 1979. Early oxidation of organic-matter in pelagic sediments of the eastern equatorial Atlantic: Suboxic diagenesis: *Geochimica et Cosmochimica Acta* 43, 1075–1090.

Gallagher, K.L., Kading, T.J., Braissant, O., Dupraz, C., and Visscher, P.T., 2012. Inside the alkalinity engine: the role of electron donors in the organomineralization potential of sulfate-reducing bacteria. Geobiology 10, 518–30.

Gebelein, C.D., and Hoffman, P., 1973. Algal origin of dolomite laminations in stromatolitic limestone. Journal of Sedimentary Petrology 43, 603–613.

Geesey, G.G., and Jang, L., 1989. Interactions between metal ions and capsular polymers. In Beveridge, T.J., and Doyle R., eds., Metal ions and bacteria, 325-357.

Gilbert, P., Abrecht, M., and Frazer, B.H., 2005. The organic-mineral interface in biominerals. Reviews in Mineralogy and Geochemistry 59, 157-185.

Glew, J.R., 1991. Miniature gravity corer for recovering short sediment cores. Journal of Paleolimnology 5, 285-287.

Haack, E.A., Warren, L.A., 2003. Biofilm Hydrous Manganese Oxyhydroxides and Metal Dynamics in Acid Rock Drainage. Environ. Sci. Technol. 37, 4138–4147.

Hammersley A.P., Svensson, S.O., Han, M., Fitch A.N., and Hausermann D., 1996. Two-dimensional detector software: from real detector to idealized image or two-theta scan: High Pressure Research 14, 235-248.

Hardie, L.A., and Shinn, E.A., 1986. Carbonate depositional environments - modern and ancient – part 3. tidal flats. Colourado School of Mines Quarterly 81, 1-74.

Johnson, C.M., Mclennan, S.M., Mcsween, H.Y., Summons, R.E., 2013. Smaller , better , more : Five decades of advances in geochemistry. Geol. Soc. Am. Special Pub, 1–44. doi:10.1130/2013.2500(08).

Jones, B., Luth, R., and MacNeil, A., 2001. Powder X-ray diffraction analysis of homogeneous and heterogeneous sedimentary dolostones. *Journal of Sedimentary Research* 71, 790-799.

Kendall, C.G.St.C., and Skipwith P.S. 1968. Recent algal mats of a Persian Gulf lagoon. *Journal of Sedimentary Petrology* 38, 1040–1058.

Kenward, P., and Goldstein, R., 2009. Precipitation of low-temperature dolomite from an anaerobic microbial consortium: the role of methanogenic Archaea. *Geobiology* 7, 556–565.

Kenward, P., Fowle, D. A., Goldstein, R.H., Ueshima, M., González, L.A., and Roberts, J. A., 2013. Ordered low-temperature dolomite mediated by carboxyl-group density of microbial cell walls. *AAPG Bulletin* 97, 2113–2125.

Konhauser, K.O. 2007. Introduction to Geomicrobiology. Blackwell Publishing. 433 p.

Kraft, S., Stümpel, J., Becker, P., Kuetgens, U. 1996. High-resolution x-ray absorption spectroscopy with absolute energy calibration for the determination of absorption edge energies. *Review of scientific instruments* 67, 681–687.

Kwak, S. Y., DiMasi, E., Han, Y.-J., Aizenberg, J., and Kuzmenko, I., 2005. Orientation and Mg Incorporation of Calcite Grown on Functionalized Self-Assembled Monolayers. A Synchrotron X-ray Study. *Crystal Growth and Design* 5, 2139–2145.

Lalonde, S.V., Konhauser, K.O., Reysenbach, A.-L., and Ferris, F.G., 2005. Thermophilic silicification: The role of *Aquificales* in hot spring sinter formation. *Geobiology* 3, 41-52.

Lalonde, S.V., Amskold, L, McDermott, T.R., Inskeep, W.P., and Konhauser, K.O., 2007. Chemical reactivity of microbe and mineral surfaces in hydrous ferric oxide depositing hydrothermal springs. Geobiology 5, 219–234.

Lalonde, S.V., Dafoe, L.T., Pemberton, S.G., Gingras, M.K., and Konhauser, K.O., 2010. Investigating the geochemical impact of burrowing animals: Proton and cadmium adsorption onto the mucus lining of Terebellid polychaete worms. Chemical Geology 271, 44–51.

Lenders, J.J.M., Dey, A., Bomans, P.H.H., Spielmann, J., Hendrix, M.M.R.M., de With, G., Meldrum, F.C., Harder, S., Sommerdijk, N.A.J.M., With, G. De, 2012. High-Magnesian Calcite Mesocrystals: A Coordination Chemistry Approach. J. Am. Chem. Soc. 134, 1367–73.

Lippmann, F., 1973. Sedimentary carbonate minerals. Berlin, Springer-Verlag, 228

Madison, A.S., Tebo, B.M., Mucci, A., Sundby, B., and Luther, G.W. 2013. Abundant porewater Mn (III) is a major component of the sedimentary redox system. Science 341, 875-878.

Manceau, A., Marcus, M., and Grangeon, S., 2012. Determination of Mn valence states in mixed-valent manganates by XANES spectroscopy. American Mineralogist 97, 816-827.

Mann, S., Sparks N.H.C., Scott, G.H.E., and deVrind-deJong E.W., 1988. Oxidation of manganese and formation of Mn_3O_4 (hausmannite) by spore coats of a marine Bacillus sp. Applied Environmental Microbiology 54, 2140-2143.

Mazzullo, S.J., 2000, Organogenic Dolomitization in Peritidal to Deep-Sea Sediments. J. Sed. Research 70, 10–23.

Meister, P., 2013. Two opposing effects of sulfate reduction on carbonate precipitation in normal marine, hypersaline, and alkaline environments. Geology 41, 499–502.

Middelburg, J., de Lange, G.J., and Kreulen, R., 1990. Dolomite formation in anoxic sediments of Kau Bay, Indonesia. Geology 18, 399-492

Montero-Serrano, J.C., Palarea-Albaladejo, J., Martín-Fernández, J.A., Martínez-Santana, M., and Gutiérrez-Martín, J. V.,2010. Sedimentary chemofacies characterization by means of multivariate analysis. Sedimentary Geology 228, 218-228.

Moreira, N.F., Walter, L.M., Vasconcelos, C., McKenzie, J.A., and Mccall, P.J., 2004. Role of sulfide oxidation in dolomitization: sediment and porewater geochemistry of a modern hypersaline lagoon system. Geology 32, 701–704.

Mucci, A., 1988. Manganese uptake during calcite precipitation from seawater: conditions leading to the formation of a pseudokutnahorite. *Geochimica et Cosmochimica Acta* 52, 1859–1868.

Murray, J.W. and Brewer, P.G., 1977. Mechanism of removal of manganese, iron and other trace metals from seawater, in Glasby, G.P., ed., Marine manganese deposits. Elsevier, Amsterdam, 291- 325.

Myers, C. R., and Nealson, K.H., 1988. Microbial reduction of manganese oxides. Interactions with iron and sulfur. *Geochimica et Cosmochimica Acta* 52, 2727–2732.

Nordstrom, D.K., Plummer, L.N., Langmuir, D., Busenberd, E, May, H. M., Jones, B.F., and Parkhurst, D.L., 1990, Revised chemical equilibrium data for major water-mineral reactions and their limitations, in Melchior, D. C, and Bassett, R. L., eds., Chemical modeling of aqueous systems II: *American Chemical Society Symposium Series* 416, 398-413.

Petrash, D.A., Gingras, M., and Lalonde, S.V., Orange, F., Pecoits, E., and Konhauser, K.O., 2012. Dynamic controls on accretion and lithification of modern gypsum-dominated thrombolites, Los Roques, Venezuela. *Sedimentary Geology* 245–246, 29–47.

Petrash, D.A., Lalonde, S.V., Raudsepp, M., Konhauser, K.O. 2011a. Assessing the importance of organic matrix materials in biofilm chemical reactivity: insights from proton and cadmium adsorption onto the commercially available biopolymer alginate. *Geomicrobiology Journal* 28, 266-273

Petrash, D.A., Lalonde, S.V., Gingras, M.K., and Konhauser, K.O., 2011b. A surrogate approach to studying the chemical reactivity of burrow mucous linings in marine sediments. *Palaios* 26, 594–600.

Radha, A. V, Fernandez-martinez, A., Hu, Y., Jun, Y., Waychunas, G.A., Navrotsky, A., 2012. Energetic and structural studies of amorphous Ca1?xMgxCO3?nH2O(0 6 x 6 1) A.V. 90, 83–95.

Ravel B. and Newville M., 2005, Athena, Artemis, Hephaestus: data analysis for X-ray absorption spectroscopy using IFEFFIT: *J. Synchrotron Rad.* 12, 537-541.

Raz, S., Weiner, S., and Addadi, L., 2000. Formation of High-Magnesian Calcites via an amorphous precursor phase: possible biological implications. *Advanced Materials* 12, 38–42.

Roberts, J. A, Kenward, P. A, Fowle, D. A, Goldstein, R.H., González, L. A, and Moore, D.S., 2013. Surface chemistry allows for abiotic precipitation of dolomite at low temperature. *PNAS* 6–11, doi. 10.1073/pnas.1305403110.

Sánchez-Román, M., Mckenzie, J.A., de Luca Rebello, A., Rivadeneyra, M.A., and Vasconcelos, C., 2009, Presence of sulfate does not inhibit low-temperature dolomite precipitation. *Earth and Planetary Science Letters* 285, 131–139.

Schippers, A., and Jørgensen, B., 2001. Oxidation of pyrite and iron sulfide by manganese dioxide in marine sediments. *Geochimica et Cosmochimica Acta* 65, 915–922.

Seaman, J. C., Arey, J. S. and Bertsch, P. M., 2001. Immobilization of nickel and other metals in contaminated sediments by hydroxyapatite addition. *J. Environ. Qual.*30, 460–469.

Slaughter, M., Hill, R.J., 1991. The influence of organic matter in organogenic dolomitization. J. *Sediment. Petrol.* 61, 296–303.

Solé, V.A. Papillon, E. Cotte, M. Walter Ph., Susini, J. 2007, A multiplatform code for the analysis of energy-dispersive X-ray fluorescence spectra: *Spectrochim. Acta Part B* 62, 63-68.

Sunda, W.G. Huntsman, S.A., 1988. Effect of sunlight on redox cycles of manganese in the southwestern Sargasso Sea. *Deep-Sea Res.* 35, 1297-1317.

Sunda, W.G. Huntsman, S.A., 1990. Diel cycles in microbial manganese oxidation and manganese redox speciation in coastal waters of the Bahama Islands. *Limnol. Oceanogr.* 35, 325-328.

Sunda, W.G., Kieber, D.J., 1994. Oxidation of humic substances by manganese oxides yields low-molecular-weight organic substrates. *Nature* 367, 62–64

Tebo, B.M., 1991. Manganese(II) oxidation in the suboxic zone of the Black Sea. *Deep-Sea Research* 38 *(Suppl. 2)*, S883-S905

Tebo, B. M., Bargar, J. R., Clement, B. G., Dick, G. J., Murray, K. J., Parker, D., Verity, R., and Webb, S.M., 2004. Biogenic Manganese Oxides: Properties and Mechanisms of Formation. *Annual Rev. Earth Planet. Sci.*32, 287–328.

Thamdrup, B, and Finster, K., 1993. Bacterial disproportionation of elemental sulfur coupled to chemical reduction of iron or manganese. *Applied Environ. Microbiol.* 59, 101–108.

Thamdrup, B, Rosselló-Mora, R., and Amann, R., 2000. Microbial manganese and sulfate reduction in Black Sea shelf sediments. *Applied Environ. Microbiol.* 66, 2888–2897.

Thamdrup, B., Fossing, H., and Jørgensen, B., 1994. Manganese, iron and sulfur cycling in a coastal marine sediment, Aarhus Bay, Denmark. Geochimica et Cosmochimica Acta 58, 5115–29.

Tribovillard, N., Algeo, T. J., Lyons, T., and Riboulleau, A., 2006. Trace metals as paleoredox and paleoproductivity proxies: An update. Chemical Geology 232, 12–32.

Trouwborst, R. E., Clement, B. G., Tebo, B. M., Glazer, B. T., and Luther, G. W., 2006. Soluble Mn, III, in suboxic zones. Science 313, 1955-57.

Van Lith, Y., Warthmann, R., Vasconcelos, C., and McKenzie, J. A., 2003. Sulphate-reducing bacteria induce low-temperature Ca-dolomite and high Mg-calcite formation. Geobiology 1, 71–79.

Vasconcelos, C., McKenzie, J.A., Bernasconi, S., Grujic, D., and Tien, A.J., 1995, Microbial mediation as a possible mechanism for natural dolomite formation at low temperatures: Nature 377, 220–222.

Vasconcelos, C. and McKenzie, J. A., 1997. Microbial mediation of modern dolomite precipitation and diagenesis under anoxic conditions (Lagoa Vermelha, Rio de Janeiro, Brazil). J. Sed. Research 67, 378–390.

Visscher, P. T., and Stolz, J. F., 2005. Microbial mats as bioreactors: populations, processes, and products. Palaeogeog., Palaeoclim., Palaeoecol. 219, 87–100.

Von der Borch, C.C., and Lock, D., 1979. Geological significance of Coorong dolomites: Sedimentology 26, 813–824.

Wang, D., Wallace, A. F., De Yoreo, J. J., and Dove, P. M., 2009. Carboxylated molecules regulate magnesium content of amorphous calcium carbonates during calcification. PNAS 106, 21511-16.

Warthmann, R., Van Lith, Y., Vasconcelos, C., McKenzie, J.A., and Karpoff, A., 2000, Bacterially induced dolomite precipitation in anoxic culture experiments. *Geology* 28, 1091–1094.

Windom, H.L., Schropp, S.J., Calder, F.D., Ryan, J.D., Smith Jr., R.G., Burney, F.G., Lewis, L.C., Rawlinson, C.H., 1989. Natural trace metal concentrations in estuarine and coastal marine sediments of the southeastern United States. *Environ. Sci. Technol*. 23, 314–320.

Wright, D.T., and Wacey, D., 2005. Precipitation of dolomite using sulphate-reducing bacteria from the Coorong Region, South Australia: significance and implications. Sedimentology 52, 987–1008.

Wright, J.E., Wyld, S.J., 2011. Late Cretaceous subduction initiation on the eastern margin of the Caribbean-Colombian Oceanic Plateau. One Great Arc of the Caribbean (?). Geosphere 7, 468–493.

Yang, Y., Sahai, N., Romanek, C.S., and Chakraborty, S., 2012. A computational study of Mg^{2+} dehydration in aqueous solution in the presence of HS^- and other monovalent anions – Insights to dolomite formation. Geochimica et Cosmochimica Acta 88, 77–87.

Zhang, F., Xu, H., Konishi, H., Kemp, J.M., Roden, E.E., and Shen, Z., 2012. Dissolved sulfide-catalyzed precipitation of disordered dolomite: Implications for the formation mechanism of sedimentary dolomite. Geochimica et Cosmochimica Acta 97, 148–165.

CHAPTER III

Organic-rich fine-grained sediment deposition and early diagenetic dolomite cementation in the mid-Cretaceous Maracaibo Platform, northwestern South America: Dynamics of Oceanic Anoxic Event 1[2]

3.1. Introduction

The widespread deposition of black shale intervals during the mid-Cretaceous has been linked to multiple paleoenvironmental perturbations, potentially resulting from the emplacement of large igneous provinces (Arthur et al., et al., 1985; Wignall, 2001; Hay et al., et al., 2006; Tejada et al., et al., 2009; Föllmi, 2012; Adams et al., et al., 2010; Barclay et al., et al., 2010; Monteiro et al., et al., 2012). Such tectono-magmatic pulses augmented atmospheric concentrations of CO_2, which led to intensified rates of erosion and phosphate delivery to the oceans (Kump and Arthur, 1999). The hydrothermal activity related to these pulses also increased the concentrations of dissolved bioessential metals in seawater (Larson and Erba, 1999), leading to transient nutrient-rich conditions that fostered greater organic productivity in the upper water column (Kuypers et al., et al., 2001; Leckie et al., et al., 2002; Herrle et al., et al., 2003; see also Karl, 2007). In turn, this led to the development of anoxic bottom waters that were ideal for the deposition of sediments exceptionally rich in organic matter. This sequence of events led to what is generally referred to as an "Oceanic Anoxic Event (OAE) (Schlanger and Jenkyns, 1976; Arthur and Schlanger, 1979; Arthur et al., et al., et al., 1990; Jenkyns, 2010).

Several episodes of oceanic anoxia that occurred between the Aptian and Albian have been collectively grouped within OAE 1 (Arthur et al., 1990). The OEA 1 was a period marked by the beginning of a greenhouse world, with rising sea level, warming global climate, and major turnovers in marine planktonic communities. Probably associated with this warming were major climate shifts that included monsoonal precipitation which augmented continental runoff (Arthur

[2] A version of this manuscript was submitted for publication in *American Journal of Science*

et al., et al., 1990; Wignall, 2001; Erbacher et al., et al., 2001; Kuypers et al., et al., 2001, 2002; Leckie et al., et al., 2002; Hay et al., et al., 2006; Herrle et al., et al., 2003; Browning and Watkins, 2008; Mutterlose et al., et al., 2009; Tejada et al., 2009; Adams et al., 2010; Barclay et al., 2010; Föllmi, 2012; Bottini et al., 2014). The lithofacies resulting from OAE 1 not only include discrete thick hemipelagic black shale intervals of economic importance due to their oil generation potential (Arthur et al., 1990; Wignall, 1994, 1996; Leckie et al., 2002), but also relatively thin organic-rich shales of striking stratigraphic persistence and lateral continuity, interbedded with shallow marine carbonates (for example Ford and Houbolt, 1963; Fisher and Rodda, 1969; Bishop, 1975; Sass and Katz, 1982; Patton et al., 1984; Halley, 1985; Sass and Bein, 1988; Claps et al., 1991; Peterson, 1983; Bellanca et al., 1996, 1997; Lehmann et al., 1998; Bachmann and Hirsch, 2006; Méndez-Baamonde et al., 2009; Gaona-Narvaez et al., 2013). Despite their widespread geographic distribution (see Westphal and Munnecke, 2003 for details), the driving forces controlling the cyclicity and early diagenesis of these intervals remains controversial. Theories ranging from orbital forcing mechanisms to differential microbial zonation processes have been proposed (Arthur et al., 1984; Hallam, 1986; Weedon, 1986, Weedon and Hallam, 1987; Raiswell, 1988; Westphal and Munnecke, 2003).

Within the shallow marine black shales, the presence of dolomite cement is quite common, and thus they have been referred to as dolomitic shales, argillaceous dolomites, and in some cases marlstones (after Rodgers, 1954). The available sedimentological and geochemical evidence suggests that the precipitation of interstitial dolomite could be related to low amplitude (high frequency) relative sea level changes superimposed on the generally transgressive state of the mid-Cretaceous seas (Given and Wilkinson, 1987; Sun, 1994; Erbachaer et al., 1996, 2001; see also Haq et al., 1987). Moreover, the stratabound geometry of these rocks, and the petrographic relationships between dolomite and other early diagenetic mineral phases, typically suggest that dolomite occurred penecontemporaneously, or shortly after deposition (Lehman et al., 1998).

In this study, we explore plausible mechanisms that promoted dolomite precipitation in laterally continuous black shales associated with OAE 1 in the Maracaibo Platform, western Venezuela (Fig. 3.1). The continuous burial history of the epicontinental succession (see Yurewick et al., 1998; Pöppelreiter et al., 2005), together with the stronger compaction of argillaceous intervals comprising mixed carbonate-siliciclastic sequences (i.e., Bathurst, 1986; Dewers and

Ortoleva, 1994), prevented the admixture of late diagenetic waters within the impermeable shales, and thus allowed for the exceptional preservation of textural and geochemical features of the early formed authigenic minerals. Therefore, these intervals provide a unique opportunity to evaluate the timing and controls on dolomite formation in mixed carbonate–siliciclastic shallow marine depositional systems.

The approach implemented here is threefold. First, the microtextural relations between dolomite, other authigenic minerals, and detrital clays were evaluated. Second, a comprehensive bulk geochemical characterization, including biomarker signatures, minor and trace element analyses, Fe-speciation, and stable C-, O-, and Sr-isotopes, was applied. This broad geochemical analysis was necessary to examine the conditions that would have governed the nucleation and pre-compactional growth of dolomite. Third, high-resolution *in situ* electron microprobe, laser ablation inductively coupled plasma mass spectrometry, and synchrotron-based microanalyses were conducted on individual dolomite crystals in order to assess whether this mineral phase recorded differences in the chemical composition and redox state of the stabilization environment (Weber, 1964; Choquette and Hiatt, 2008). The resulting dataset is integrated into an organo-diagenetic model that is dependent on external forcing mechanisms, such as Milankovitch-scale orbital cycles.

3.2. Geological background information

During the late Triassic, present day western Venezuela and eastern Colombia consisted of a series of horst and graben systems, controlled by linear northeast-southwest-striking faults. The rates of displacement of these faults largely determined the deposition rates and thickness of syn- and post-rift deposits (Burke, 1976; Bartok, 1993). By the Valanginian (~136 Ma), these grabens had been infilled with alluvial continental red beds and fluvio-deltaic deposits, and then peneplained (Ford and Houbolt, 1963; González de Juana et al., 1980; Schubert, 1986; Bartok, 1993). Conditions favourable for carbonate deposition began mostly over continental rift deposits towards the Barremian (~125 Ma) (mid-Cretaceous dates after Malinverno et al., 2012), but in the Mérida Andes, the base of the mid-Cretaceous carbonate succession, referred in the literature as the Cogollo Group, locally overlies the igneous-metamorphic basement (González de Juana et al., 1980) (Fig. 3.2). By the early Aptian (~ 121 Ma), a distally steepened mixed carbonate-siliciclastic

ramp, referred to as the Maracaibo Platform (after Rod and Maync, 1954), was fully developed (Vahrenkamp et al., 1993). This ramp represents a very shallow (< 15 m; Bartok 1981) and episodically restricted epicontinental sea, developed in the most southern part of the mid-Cretaceous Central Atlantic Ocean (Fig. 3.2).

3.2.1. Aptian to early Albian

In the subsurface of the Maracaibo lake area, the Aptian to early Albian consists of a vertical succession of meter-scale shallow marine deposits that contain laterally continuous, dark-gray, organic-rich, fine-grained, laminar siliciclastic intervals. The succession exhibits systematic stacking patterns that build into complex intermediate-scale, high-frequency sequences (Bartok et al., 1981; Vahrenkamp et al., 1993; Yurewicz et al., 1998). Lithostratigraphically, the Aptian to early Albian succession has been named as the Apón Formation of the Cogollo Group. The formation averages ~120 m in thickness, but it exceeds 300 m towards the Perijá Range (Fig. 3.1). During deposition of the Apón Formation, a sub-basin affected by differential rates of subsidence, referred to as the Machiques trough, existed in what is now the Perijá Range (Sutton, 1946). This sub-basin was intermittently affected by periods of poor seawater circulation and stagnation (González de Juana et al., 1980; Bartok et al., 1981; Renz, 1981, 1982; Bartok, 1993).

The cyclic shallow marine deposits comprising the Apón Formation record variations in the amount of carbonate production, siliciclastic influx and organic matter accumulation, and therefore, the formation has been subdivided into three units: the lower (Tibú), middle (Machiques-Guáimaros) and upper (Piché) members (Renz, 1958). The Tibú Member consists of a cyclic lagoonal, mud-dominated facies assemblage, including pelecypod floatstone and miliolid wackestone, with minor amounts of glauconite wackestones and dolomitic shales towards the top. Deposition of the basal Tibú Member was followed, in the Perijá Range area, by a prominent interval known as the Machiques Member of the Apón Formation. This member is comprised of cyclic black shale - hemipelagic nodular floatstone couplets, and is areally restricted to the Machiques trough. The Machiques Member has a well-preserved late Aptian ammonite fauna belonging to the genus *Deshayesites* sp., and towards the top it also contains *Engonoceras* sp., which spans the uppermost Aptian to the middle Albian interval (Renz, 1982, p. 32).

Landwards the Machiques Member encroaches onto crinkled laminar lagoonal deposits, of variable thickness (5-22 m), known as the Guáimaros Member of the Apón Formation (Renz,

1958; Ford and Houbolt, 1963) (Fig. 3.2). This lithofacies can be recognized by being largely devoid of benthonic fauna, and by its dark grey to black colour and laminar nature (Renz, 1958, Ford and Houbolt, 1963; González de Juana et al., 1980). The main mineralogical feature of the Guáimaros Shale, as also referred in this study, is the abundance of dolomite and framboidal pyrite (see Ford and Houbolt, 1963), and it locally contains lenticular gypsum (González de Juana et al., 1980). According to Ford and Houbolt (1963), the microfacies associated to the Guáimaros Shale resembles modern marl sediments found in the Doha Lagoon in the Persian Gulf, whereas González de Juana et al. (1980, p. 236) indicate that the Guáimaros Shale may well represent tidal flat deposits. An extensive stratigraphic data set (resulting from more than 40 years of oil exploration in the Maracaibo lake area) demonstrates the widespread distribution of the Guáimaros Shale throughout western Venezuela (Ford and Houbolt, 1963; Renz, 1982).

Overlying the Guáimaros-Machiques Member is the Piché Member of the Apón Formation, which also exhibits a shallow marine stacking pattern, and contains the first appearance of the Albian foraminifera *Orbitolina texana concava* (Sutton, 1946; Renz, 1958). Early Albian ammonites are also present in the Piché Member (Renz, 1982), but most of its carbonate facies assemblage represents deposition in a subtidal to peritidal setting (Bartok et al., 1981).

In terms of sequence stratigraphy, three out of six mixed carbonate/clastic 'glacio-eustatic' sequences that have been recognized within the Cogollo Group (see Vahrenkamp et al., 1993) are within the Apón Formation; with three others pertaining to the overlying Lisure and Maraca formations (see below). By the time of the deposition of the Apón Formation, the accommodation space and facies architecture were largely controlled by the complex interplay between thermal subsidence and orbital forcing mechanisms, with differential subsidence controlling the development of paleobathymetric lows that were suitable for black shale deposition (Bartok, 1993; Figs. 3.1 and 3.2). By producing minor shifts in base sea level and controlling paleoclimate, variations in the Earth's eccentricity and precession would have controlled the extension and distribution of shallow marine facies within the mixed carbonate-siliciclastic ramp (see Vahrenkamp et al., 1993), and perhaps also the cyclic deposition of black shales-floatstone couplets infilling the Machiques sub-basin (for example Alberdi-Genolet and Tocco, 1999).

During relative sea level rises, the shallow marine environments were sites for the deposition of grainstone/rudstone interbar deposits. By contrast, the high sea level progradational

cycles produced extended low-energy restricted shallow-marine environments, represented by lagoonal sediments rich in organic matter (Bartok et al., 1981; Vahrenkamp et al., 1993). Within these facies, miliolid-rich foraminiferal wackestones and dolomitic shales represent restricted lagoonal and tidal flat settings (Bartok et al., 1981). An alternative view is that the carbonate ramp may also have been episodically affected by drowning, such that, in previously shallow-water areas, black shales rest on condensed basal transgressive lags or unconformities, which in turn, rest on shallow-water facies (Perez, 1996).

Although the lithofacies comprising the Apón Formation are generally thought to represent sedimentation in a humid climate zone (Vahrenkamp et al., 1993), by the time of deposition of the Guáimaros Shale, the ramp would have been affected by a more complex and dynamic climatic regime. A few lines of sedimentological evidence support such an interpretation:

i) When present, the impoverished faunal assemblage of the Guáimaros Shale consists of small-sized individuals (see Ford and Houbolt, 1963), suggestive of conditions not suitable for the colonization of stenohaline species.

ii) The presence of *Weichselia* sp. plant fragments (Renz, 1982, and references therein) — a xerophytic fossil of a fern-like angiosperm common in Aptian-to-Albian sedimentary successions of South America (Edwards, 1933). This is often interpreted as inhabiting coastal mudflats (Smith et al., 2001; Schweitzer et al., 2003), but would rather be representative of semi-arid climate regimes (see Sender et al., 2005 for details). *Weichselia* sp. would therefore, be a record of heterogeneities in the paleolittoral system that resulted in the colonization of the coastal zone by mangrove-like vegetation (Lacovara et al., 2000, 2003).

iii) The cryptomicrobial primary sedimentary features of Guáimaros lithology *sensu stricto* and the Guáimaros-like microfacies, includes crinkled laminar textures and is rarely bioturbated (Bartok et al., 1981), which suggests that its organic content (>1.1, up to 4.5 wt. % TOC, Table 3.3) would have partially resulted from the cyclic burial of microbial mats (for example Mazzullo and Friedman, 1977).

3.2.2 Late Albian - Early Cenomanian

Overlying the Apón Formation is the 80 m-thick Lisure Formation. The contact between Apón and Lisure formations is thought to represent a depositional hiatus (Rod and Maync, 1954), and the

unit is composed of a mixed carbonate-siliciclastic lithology, frequently glauconitic. Towards its base, the formation contains microfacies similar to the Guáimaros Shale, but these are much more limited in terms of their regional extent. Towards the top, the Lisure Formation contains abundant skeletal-oolitic grainstones that are often glauconitic (Renz, 1981). Overlying the Lisure Formation is the Maraca Formation, which consists of oncolithic floatstones that laterally grade to oolitic grainstones (Bartok, 1981). Towards the top of Maraca Formation, the shallow marine carbonate succession consists of floatstones and rudstones containing abundant *Exogyra* sp., *Ostrea* sp. and *Trigonia* sp., suggestive of an extended lagoonal subtidal environment (Bartok et al., 1981).

3.2.3 Cenomanian to Campanian

The demise of shallow water carbonate production in the Maracaibo ramp is marked by deposition of black shale and hemipelagic mudstones, which make up the La Luna Formation. These facies were deposited over a period of approximately 20 Myr from the Cenomanian to Campanian (Renz, 1981), and as suggested by a number of geochemical studies (see Bralower and Lorente, 2003 for a review), represents deposition in a persistently anoxic marine environment that characterized OAE 2 (Erlich, 1999).

3.2.4 Post-Campanian

The advance of a post-Campanian flexural forebulge moving landwards of the advancing thrust-belt caused an erosional event that may have exposed part of the Cretaceous succession in western Venezuela (Parnaud et al., 1995; Mann et al., 2006; Escalona and Mann, 2006). Based on seismic stratigraphy, however, Castillo and Mann (2006) suggest that such an erosional event did not lead to the exposure of the Lower Cogollo Group in the Maracaibo Lake area. Nonetheless, independent diagenetic studies by Méndez (1989) and Kummerow and Pérez de Mejía (1989) demonstrated that the carbonate rocks comprising the Apón Formation were locally affected by diagenesis in the mixing zone (see also Nelson et al., 2000). Yet, due their burial history (Yurewicz et al., 1998; Pöppelreiter et al., 2005) and differential compaction of marlstone/limestone alternations (Dewers and Ortoleva, 1994), the impermeable fine-grained rocks would have been minimally affected by epidiagenesis (Bartok, 1981, Pöppelreiter et al., 2005, 2008).

A phase of flexural down-warping followed the Paleogene emplacement of allochthonous lithospheric blocks of the Caribbean island arc over the passive continental margin of South

America (Escalona and Mann, 2006). Thereby, the base of the Cretaceous carbonate sequence reached depths in excess of 4 km (Yurewicz et al., 1998 and Popelreiter et al., 2005), only to be locally uplifted to their present day position in the subsurface of the Maracaibo Basin by Neogene transpressive strike-slip deformation (Audemard, 1991). The Neogene inversion of the Machiques and Uribante sub-basins also led to extraordinary exposures of the Cogollo Group in the Perijá Range and Mérida Andes (Fig. 3.1). The complex post-Eocene history of the Maracaibo Basin is beyond the scope of this paper (the interested reader is referred to Lugo and Mann, 2001; and Escalona and Mann, 2005 for details).

3.3. Methods

3.3.1. Samples

Our sampling focussed on the laterally continuous dolomite-bearing black shale microfacies known as the Guáimaros Shale. We also sampled analogous microfacies in the overlying lithological units (i.e., early Albian Piché Mb., and Lisure Fm.). Samples were retrieved from four exploration wells, most of which reached depths >4 km in the subsurface of the Maracaibo lake area (Figs. 3.1 and 3.2). The lateral distance between the studied boreholes ranges between 10 and 35 km (Fig. 3.1). Borehole TOT-3 was drilled between 1928 and 1930. Borehole Z26-D2 was drilled in 1955, and boreholes UD-171 and SOL-6 were drilled between 1982 and 1984.

The microfacies of interest are interbedded into peritidal cycles comprised of thick pelecypod floatstones, benthic foraminiferal (miliolids) wackestones, and mudstones which frequently show crinkled lamination (i.e., Ford and Houbolt, 1963; Bartok, 1981; Pöppelreiter et al., 2005). Prior to sampling, the intervals of interest were first identified by using gamma ray and resistivity well logs, followed by a visual inspection of the cores and standard petrography of 235 thin sections. The samples from the upper stratigraphic levels have less lateral extent than the Guáimaros Shale, which can be recognized across the study area (Fig. 3.2). All of the representative samples (n = 11; 9 dolomitic shales and 2 non-dolomitic black shales; Fig. 3.2), were taken from the central part of drill cores (150 mm in diameter). The sections of the cores sampled are not directly affected by faults and do not show evidence of post-depositional recrystallization.

3.3.2. Mineralogical and textural features

The mineralogical and textural features were analyzed via standard petrography, and Scanning Electron Microscopy (SEM) coupled to Electron Dispersive Spectrometry (EDS). Other analyses included X-ray Diffraction (XRD) to evaluate the mineralogy of the clay fraction, and Electron Probe Microanalyses to assess minor variations in the Mg:Ca ratio of dolomite crystals.

3.3.2.1. SEM-EDS

SEM observations were performed on a JEOL JSM-6301FXV that has an attached Norvar energy dispersive spectrometer system (PGT). Most photomicrographs were taken at 5 kV, but some involving complementary EDS were conducted at 20 kV. A constant working distance of 15 mm was used throughout our SEM-EDS analyses. Some samples were treated with 10 s immersion in 10% HCl, in order to reveal microtextural features resulting from the preferential dissolution of high Ca-dolomite (> 55 mol % $CaCO_3$; i.e., Jones et al., 2001).

3.3.2.2. Clay mineralogy

The <0.2 μm fraction of the clays were characterized via XRD at the Venezuelan Institute of Petroleum Technology (INTEVEP). Chemical pre-treatments performed prior to analysis included acetate buffer reaction to remove the carbonate fraction; organic matter removal via H_2O_2 reaction at 80°C; immersion into a sodium chloride, acetone, and methanol solution, to remove the amorphous organic fraction; and removal of iron oxides via dithionite. Oriented preparations were made by centrifugation followed by pressing the dried preparation upside down against absorbent paper, with one subsample previously wetted with ethylene glycol. The composites remained overnight in this position. XRD patterns were recorded from 2 to 35 (2θ) degrees using Ni-filtered Cu_Kα radiation. Slits were selected so that the X-ray beam divergence was less than the sample length. The patterns were collected automatically by step-scanning at 0.02° (2θ) intervals using a 1 s counting time per step. Quantitative analyses of the samples were determined by comparing the air-dried and glycol-solvated patterns (see Moore and Reynolds, 1989 for details).

3.3.2.3. EPMA

The major element distribution of the dolomite crystals comprising three representative samples was determined using Wavelength Dispersive Spectroscopy (WDS) in a JEOL JXA-8900

instrument operated at 15 kV accelerating voltage, focused beam diameter and an average current of 10 nA. WDS analyses were achieved by setting count times of 20 s on each peak and half the peak count time on each background. Detection limits (3σ) from the average of three analyses are ~250 ppm for both MgO and CaO oxides. A combination of natural minerals was used to reduce counts to weight percent concentrations using the CITZAF method, with matrix corrections as implemented by P. Carpenter (Caltech, 1993). The mineral crystals used as primary standards were Eugi (Spain) dolomite (MgO), and Big Horn (MO, USA) calcite (CaO).

3.3.3. Biomarkers

3.3.3.1 Microablation

Samples were processed according to the micro-ablation technique described by Jarrett et al. (2013). Laboratory blanks contained near-zero background levels, signifying that hydrocarbons detected in the samples are not cross contamination or instrumental contamination during experimental procedures.

3.3.3.2 Extraction and fractionation of extractable organic matter

Bitumen was extracted from 3 - 8 g of rock powder using an Automated Solvent Extractor (ASE 200, Dionex) with dichloromethane and methanol (9:1 v/ v) as solvents. Instrumental settings were as following: preheat 2 min, heat 5 min, static 2 min, flush 100%, purge 30 s, 5 cycles, 1000 PSI and 100 °C. The extracts were reduced in volume (< 1 ml) under a stream of purified nitrogen gas and then left to evaporate at room temperature.

Extractable organic matter (1 mg) was placed onto a dry-packed silica (annealed at 250°C/9h, grade 60, 70-230 mesh, ThermoFisher Scientific) column (4 mm internal diameter) and was air dried overnight. Extracts were separated by column chromatography into saturated, aromatic, and polar fractions. Saturated hydrocarbons were eluted with 1.5 dead volumes (DV) *n*-hexane, aromatic hydrocarbons with 2 DV *n*-hexane: dichloromethane (4:1 v/v) and polar compounds with 2.5 DV dichloromethane: methanol (1:1 v/v). Fractions were air-dried. Elemental sulfur was removed from the saturated fractions by filtration over freshly precipitated elemental copper (Brocks et al., 2005).

3.3.3.3 Gas chromatography-mass spectrometry (GC-MS)

Molecular components of saturated and aromatic hydrocarbon fractions were identified by a GC-MS system, consisting of a Waters AutoSpec Premier double-sector mass spectrometer interfaced with a 6890 GC (Agilent), fitted with a DB-5MS capillary column (60 m length, 0.25 mm internal diameter, 0.25 µm film thickness (J&W Scientific). Helium was used as the carrier gas at a constant flow of 1 ml/min. Samples were initially injected in splitless mode into a Gerstel PTV injector at a temperature of 60 °C, held for 0.1 min and then heated at 260 °C/min to 300 °C. For any run, the GC oven was programmed at 60 ^{0}C (4 min), heated to 315 °C at 4 °C/ min, with a final hold time of 22 to 52 min. The MS source was operated at 260 °C in EI+ mode at 70 eV ionization energy and with 8000 V acceleration voltage. Saturated and aromatic fractions were analysed in full scan mode over a mass range of 55-600 Da, with a scan duration of 0.7 s and interscan delay of 0.2 s. Saturated fractions were further analysed by multiple reaction monitoring (MRM) with a total cycle time of ~1.2 s for function 1 (~1.1 s cycle time, 0.1 s delay) and ~1.5 s for function (~1.4 s cycle time, 0.1 s inter-scan delay) for 42 transitions in total. Aromatic hydrocarbons were further analysed by selected ion recording (SIR) under magnet control with a total cycle time of ~0.85 s (0.75 s cycle time, 0.1 s inter-scan delay) for thirteen ions. All samples were injected in hexane to avoid deterioration of chromatographic signals due to the build-up of $FeCl_2$ in the ion source (see Brocks and Hope, 2014).

3.3.3.4 Peak identification and quantification

Polycyclic terpanes and steranes were identified by comparison with the AGSO-II industrial standard (Ahmed et al., 2013). Isoprenoid and aryl isoprenoid derivatives were identified by comparing spectra, elution times and patterns with laboratory reference material (Brocks and Summons, 2003; Brocks et al., 2005; Schinteie, 2011).

3.3.4. Major, minor and trace element analyses

3.3.4.1. Bulk analyses

3.3.4.1.1. Whole rock minor and trace element

Bulk rock minor and trace elements were determined after digestion with a 5:1 mixture of hydrofluoric and perchloric acids. A 1-g (dry weight) sample was first digested in a platinum

crucible with a solution of concentrated $HClO_4$ (2 mL) and HF (10 mL) to near dryness; subsequently a second addition of $HClO_4$ (1 mL) and HF (10 mL) was made and again the mixture was evaporated to near dryness. Finally, $HClO_4$ (1 mL) alone was added, and the samples were evaporated until the appearance of white fumes. The residue was then dissolved in 8 N HNO_3 and diluted to 25 mL and analyzed by Inductively Coupled Plasma Quadrupole Mass Spectrometry (ICPQ-MS), using a PerkinElmer Elan6000 instrument. None of the reported minor element values were corrected for non-lattice bound metal contamination, which would have required pore water measurements (Staudt et al., 1993). However, for some metals a comparison of bulk rock vs. intracrystalline concentrations, elements measured using laser ablation ICPQ-MS (see below), were used for that purpose. The total organic carbon (TOC) values were determined in carbonate-free samples using a combustion-infrared absorption method at a LECO CS-244 analyzer, and are composed of pyrolyzable carbon and additional CO and CO_2 groups released during oxidation of the residual organic carbon.

In order to facilitate comparison of rare earth elements (REE) patterns for different samples, the abundances of the individual REE were divided by the abundances in average post-Archean Shales (PAAS), with "SN" standing for PAAS-Normalized concentrations (Nance and Taylor, 1976). We focused mostly on the geochemistry of the redox-sensitive element cerium, and its neighbour elements La and Pr, but the ratio of heavy (HREE) vs. light (LREE) rare earths, Er/Nd, was also evaluated, as it offers a useful criterion to infer early diagenetic chemical changes likely to be caused by differential rates of siliciclastic input. The Ce anomaly was determined by evaluating the Pr/Pr* ratio of unity, where $(Pr^* = 0.5Ce + 0.5Nd)_{SN}$. This calculation (after Bau and Dulski, 1996) prevents biases caused by the occurrence of positive La anomalies in seawater-derived precipitates (for example, de Baar et al., 1991), which may result in an apparent Ce anomaly. The significance of the Ce anomaly, as an indicator of anoxicity, was further assessed by applying an alternative criteria, developed by de Baar et al., (1988), which states that only when the expression $Ce_{anom} = [3Ce/(2La + Nd)]_{SN} > 1.0$ would precipitation have occurred under anoxic conditions. The bulk sediment co-variation of Y/Ho and its neighbour element La was studied by using the expression Ce/Ce*. This parameter is useful to quantify the extent of detrital input to the plasma produced via laser ablation and evaluated using ICPQ-MS (see Kamber and Webb, 2004 for details).

3.3.4.1.2 Fe speciation

We used well-calibrated iron extraction techniques to explore the shallow marine redox conditions of deposition, where highly reactive iron (Fe_{HR}) represents the iron that may be geochemically and biologically active during early sediment diagenesis (Canfield et al., 1992; Poulton et al., 2004a). A sequential extraction scheme (Poulton and Canfield, 2005) was implemented to partition iron into its highly reactive components and its unreactive phases. This scheme recognizes a variety of operationally defined iron pools, comprising ferric oxides extracted with dithionite (Fe_{ox}), carbonate-associated Fe extracted with acetate (Fe_{carb}), and magnetite Fe extracted with oxalate (Fe_{mag}). Pyrite Fe (Fe_{Py}) was determined separately via chromous chloride distillation (Canfield et al., 1986). Highly reactive Fe was then calculated as $Fe_{HR} = Fe_{Py} + Fe_{carb} + Fe_{ox} + Fe_{mag}$ (Poulton et al., 2004b). The operational defined ratios from iron speciation, Fe_{HR} to total Fe (Fe_{HR}/Fe_T; Raiswell and Canfield, 1998) and Fe_{Py} to Fe_{HR} (Fe_{Py}/Fe_{HR}, Poulton et al., 2004) are presented in a cross-plot (after Shen et al., 2002).

3.3.4.1.3 Stable carbon and oxygen isotope analyses

Prior to analyses, the subsamples were treated for 48 hours with H_2O_2 (30%) to remove residual organic matter, rinsed three times with ultrapure water, and dried overnight in a vacuum oven at 30ºC. Stable C-isotope analyses of carbonates were performed by immersing whole-rock powders in 100% phosphoric acid while under vacuum (McCrea, 1950) and analyzing the released CO_2 on a Finnegan MAT 252 mass spectrometer. Since the samples investigated did not permit a physical separation of the dolomite from the minor amounts of calcite also present in the samples, a chemical separation technique was used which allowed CO_2 released from calcite and dolomite to be collected separately (see Epstein et al., 1963). This method is principally based on the marked difference in the relative rates of reaction between dolomite and calcite when treated with phosphoric acid. The carbon and oxygen isotopic data are reported with respect to deviation from V-PDB (Vienna Pee Dee Belemnite) using the standard δ-notation (Craig, 1957; Craig, 1961). Organic matter samples were acid cleaned to remove associated carbonate material according to the protocol of Hedges and Stern (1984). The demineralized organic matter was then analyzed by the closed-tube combustion method. Organic matter was placed in a quartz glass tube along with CuO, Cu and Ag metal, evacuated, and subsequently sealed with a torch and combusted over night

at 800 °C. The tubes were broken open in a vacuum line, and the CO_2 from combustion was purified cryogenically and analyzed.

3.3.4.1.4 Sr Isotope analyses

The small dolomite crystal size (average ~100 μm) precluded micro sampling of specific zones within crystals, and thus bulk samples were ground with an agate mortar and pestle. The powder samples were digested by using a dilute acid (6N HCl). During the measuring period, the NIST 987 standard yielded 0.710250 and the internal precision ('error') associated with the strontium isotopic analysis was from 0.000016 to 0.000018 (2σ level).

To provide an estimate of the initial Sr isotope signature of the carbonate fraction, we first evaluate to what extent the bulk Sr isotope composition of these rocks correlates with indicators of detrital contamination. This was accomplished by assessing the correlation between the $^{87}Sr/^{86}Sr$ signature of the samples and K, Zr, and rare earth elements (REEs) (Kamber et al., 2004). This test of isotopic integrity allowed us to establish the degree of correlation between the $^{87}Sr/^{86}Sr$ isotope ratios and such trace elements, with a high level of correlation indicating that the isotope (and trace element) systems remained closed during burial (see Kamber et al., 2004 for details). Then the isotope value of an uncontaminated sample can be inferred (see Kamber et al., 2004 for details).

3.3.4.2 In situ analyses

For the detection and spatial substantiation of subtle crystal-scale chemical differences in dolomite crystals, we used a combination of Laser Ablation Inductively Coupled Plasma Quadrupole Mass Spectrometry (LA-ICPQ-MS) and high-resolution photon microprobe analyses (see below). Analyses were performed using a Perkin-Elmer Elan6000 Quadrupole ICPQ-MS coupled to a New Wave UP-213 laser ablation system. The instrument parameters were as follows: RF power 1200 W, peak hopping acquisition, 50 ms dwell time. The crystals were ablated (60 μm spot, 15 Hz) in a discrete spot mode at laser fluence on target of ~4 J/cm^2. Ablation took place in a He atmosphere (850 ml/min continuous He flow) to which both Ar (~450 ml/min) and N_2 (6 ml/min) were added downstream of the LA cell. Quantitative results were obtained via calibration of relative element sensitivities against the pressed powder carbonate standard pellet USGS MACS-3, with [Ca] determined via EPMA as an internal standard. Although the complete range

of elemental masses certified in the MACS-3 standard were measured, here we focus predominately on results for V, Ni, Fe, Mn, Zn, Sr, REE and Y. Quantitative elemental analysis provides relative accuracy of better than 8%

The distribution of trace elements in dolomite crystals was assessed via spatially resolved synchrotron-based X-ray Fluorescence (μXRF). These analyses were conducted in the photon microprobe of the beamline 20ID at the Advanced Photon Source, Argonne National Laboratories (APS) in Argonne, IL. The analytical capabilities of this beamline not only allowed for an assessment of subtle micrometer-scale variations in the distribution of the first row transition metals, but also semi-quantitative analyses of their concentrations over a reduced analytical area; a highly desired feature when studying the geochemistry of fine dolomite crystals. X-rays tuned at 20.96 KeV were focused to a 5 × 6-micron spot using Kirkpatrick-Baez mirrors and rastered across an analytical area of a representative sample (UD-171 16 245.8'). The resulting fluorescence spectra were measured using a 4-element Vortex multi-element Si drift detector located at 90° to the incident beam in the direction of the polarization. The detector was calibrated to ~30 eV per channel. Full XRF spectra were collected for each pixel of both the sample and standard to quantify the amounts of metals present via the computer code PyMCA (Solé et al., 2007). Element-specific maps were then made to show hot spots of accumulation (for instance Sr, Y, and Mn enriched zones). A homogenous area at the microscale on the USGS' MACS-3 was used as an external standard.

3.4. Results

3.4.1. Authigenic minerals

Standard petrography reveals that the authigenic fraction of the microfacies studied here is dominated by dolomite (42 – 48%), with minor pyrite, and quartz. SEM-EDS show lesser amounts of gypsum, calcite, Ca-fluorapatite, and barite (Fig. 3.3). All of the minerals listed above are within a detrital clayey matrix.

3.4.1.1 Dolomite

Dolomite occurs as fine- to medium-crystalline (40-120 μm) interstitial cement. The mineral is euhedral to subhedral, and the samples contain no mimically replaced allochems. The contacts between fine dolomite and the clayey matrix are typically planar-e, but medium size dolomite crystals, typically exhibiting secondary overgrowths, may also have planar-s crystal boundaries (Fig. 3A). Fifty-four WDS analyses on such dolomite crystals indicate that their calcium composition ranges from 51.3 to 60.7 wt. % $CaCO_3$, with crystal cores showing Ca-enriched microzones (Fig. 3.3B). After a mild etching treatment with 10% HCl (10 s), the partial dissolution of these Ca-enriched crystal cores reveal spheroidal features similar to those observed on modern Ca-dolomite formed within mucilage sheaths (i.e., Fig. 3.3C). Crystal cortices, on the other hand, are relatively enriched in Mg, and do not exhibit spheroidal features after acid etching. In some samples, the cortices were also found to be chemically zoned, with some degree of Fe-enrichment and near stoichiometric Mg:Ca ratios (Fig. 3.3D).

3.4.1.2 Pyrite

Framboidal pyrite is a common mineral phase in the dolomitic shales from the Apón Formation ~ (5 – 8%). The framboids are often embedded in dolomite cement (Figs. 3.3A, 3.3E-F), and sometimes with Ca-F apatite (see below). Most of the individual framboids exhibit sizes averaging 8 to 12 μm, but small framboids (< 6 μm in diameter) were also observed. The crystals comprising the framboids are normally between 0.8 and 2 μm in size, but there are also aggregates of equant pyrite nanocrystals that are organized in an irregular non-spheroidal texture (Fig. 3.3G). The crystallites comprising these aggregates and the smaller framboids can be as small as ~300 nm (Fig. 3.3G). The small aggregates are more typically observed within the argillaceous matrix (Fig. 3.3H-I).

3.4.1.3 Quartz

Euhedral equant microquartz (15-20 μm in size) is commonly observed within the argillaceous matrix (for example Fig. 3.3G). Some samples also have chalcedony cement. As shown in Figure 3.3H-I, chalcedony did not develops as a mineral replacement fabric but as void filling rims within dolomite and clays (see below). Associated with the chalcedonic rims are nanometer-scale features such a globules and fine-scale lamination that suggest that they are silicified endolithic biofilms that grew over dolomite crystal surfaces (see Fig. 3.3I).

3.4.1.4 Calcite

Partial calcification of dolomite was observed in the sample from borehole Z26-D2. The calcite is low in Mg (< 4 wt. % $MgCO_3$), and occurs as sub-micrometer scale patches within the core of the crystals. The mineral also occurs as overgrowths adjoining multigenic dolomite that show corroded crystal faces (Figs. 3.4A-B). In this sample, gypsum (see below) is notably absent.

3.4.1.5 Gypsum

In samples from wells TOT-3 (14 210') and SOL-6 (18 008'), as well as in one sample from well UD-171 (16 245'), the dolomite crystals are not coated by silica but rather by equant gypsum microcrystals. The mineral was only observed as a cement infilling pre-compaction voids between euhedral dolomite crystals and their argillaceous matrix and is typically associated with fine (40-50 μm) dolomite crystals (Figs. 3.4C-D and 3.5B, D-E). The microcrystals show evidence of compaction (i.e., planar clay-gypsum interfaces) likely due to the pressure exerted by the crystallization force of gypsum growing against its surrounding. This chemical compaction caused planar intercrystalline boundaries of gypsum and produced local compaction with the clayey matrix forced aside. The textural features of gypsum indicates that this phase can be considered indigenous to these rocks, and not an artifact of pyrite oxidation or from the precipitation of evaporating pore waters after recovery of the cores (for example Patton et al., 1984). The microcrystalline gypsum rims do not show textural features that can be interpreted as mineralized biofilms, such as those observed on the chalcedonic rims described above.

3.4.1.6 Other accessory mineral phases

Ca-fluorapatite occurs as a pore-lining cryptocrystalline spheroidal phase, typically associated with the organic-rich clayey matrix. It also has a textural association with submicron-scale pyrite (Fig. 3.4E-F). SEM- EDS analysis also revealed the presence of subhedral micron-sized (10-30 μm) barite ($BaSO_4$) crystals (Fig. 3.4G).

3.4.2. Clay Minerals

Illite was identified by its characteristic d_{001} spacing at circa 10.0 Å. Kaolinite was identified by its characteristic air-dry basal spacing peaks at 7.1 and 3.6 Å, which remains invariant after glycol-solvation (Kirsimäe et al., 1999). When the diffractograms of ethylene glycol-treated and air-dried aliquots of the carbonate-removed samples are compared, the full widths at half-maximum of the

5.0 Å peak changed from 0.150 to 0.240 Å (Fig. 3.5A). Such a feature is indicative of the presence of discrete smectite layers (Battaglia et al., 2004). The illite-smectite mixed layers (I/S) gives a 001 peak at a d-value of ~12.9 Å, which expands to 16.7 Å after ethylene glycol treatment. The asymmetrical broadening of the air-dried aliquots is significantly diminished after ethylene-glycol treatment (Fig. 3.5A). When considered in terms of a broad peak at ca. 10.0 Å that has a tail towards lower angles, the clay matrix seems dominated by disordered I/S. Semi-quantitative XRD analysis of the <2 μm fraction revealed the following proportions (±2%): illite (38%), kaolinite (27%), and disordered I/S clay (35%); with illite accounting for up to 60% of that fraction (Fig. 3.5A). Figure 3.5 B shows the morphological features of the fine matrix material as observed in a representative freshly broken sample. A peak at 1,040.98 eV, attributed to Na, is frequently observed via EDS within the clay minerals (Fig. 3.5C). The presence of both Na and Cl suggests that the sodium peak probably represents halite impurities.

3.4.3. Elemental composition

3.4.3.1. Sodium

Na lattice-bound concentrations are useful to constrain the salinity of dolomitizing fluids and support observations regarding the genesis of dolomites and their environments of formation (Staudt et al., 1993). As the incorporation of Na in the dolomite lattice is related to the salinity of the dolomitizing brines, dolomite crystals formed in hypersaline supratidal environments would be expected to be enriched in Na (see Fritz and Katz, 1972), however, non-lattice bound Na contamination typically makes interpreting Na contents a questionable endeavour (see Budd, 1997).

The concentrations of Na were measured via bulk rock and LA-ICPQ-MS. Bulk sodium concentrations ranged between 355 and 2,866 ppm, with *in situ* values ranging from 658 ± 29 to 1,138 ± 93 ppm. The difference between the average *in situ* and bulk rock ICP-MS concentrations is ~23% (Tables 3.1 and 3.2). The lowest measured bulk [Na] occurs in borehole UD-171 at the base of Guáimaros shale. In the interval sampled on this core, bulk Na concentrations increase upwards from 355 to 1,476 ppm. Towards the top, the intracrystalline Na concentration averaged 1,067 ± 187 ppm. Intra-crystalline Na concentrations were also measured in borehole TOT-3,

where they averaged 1,138 ± 93 ppm while the $[Na]_{bulk}$ was found to be ~1,550 ppm. The difference between bulk rock and LA-ICPQ-MS measurements confirms that some of the Na is not associated with the carbonate phases. In any case, when our dolomite Na concentration dataset is compared with other uncorrected dolomite values, they seem to be in the range observed for evaporitic dolomites (see Budd, 1997).

3.4.3.2. Strontium and rare earth geochemistry

Sr concentrations are observed in primary dolomites, and result from its preferential substitution into Ca sites of poorly ordered Ca-rich dolomite. The bulk strontium concentrations of the dolomitic shale microfacies ranged from 143 to 744 ppm (Table 3.1). Average bulk Sr-concentrations consistently increases towards the Perijá Range. Concentrations peaked in well Z26D-2, with a minimum measured in samples from SOL-6 (Table 3.2). Intracrystalline strontium contents have the maximum values (467-744 ppm), whereas in samples exhibiting dolomite overgrowths, the crystal cortices were found to have relatively lower concentrations (143 – 211 ppm).

The dolomitic shales exhibit $^{87}Sr/^{86}Sr$ values that range from 0.70751 to 0.70812 (Table 3.2; Fig. 3.6A), and are thus enriched in ^{87}Sr with respect to the signature observed in biogenic allochems formed in equilibrium with late Aptian-Albian seawater (~0.70735; see McArthur et al., 2001)

A representative sample from core UD-171 (16 245.8') was targeted via μXRF, to investigate the spatial distribution of Sr in fine crystalline dolomite. The analysis reveals a relatively homogenous distribution of this element, which correlates with the measured distribution of Y (R^2 = 0.97; Fig. 3.6B). Y is considered indicative of the intracrystalline distribution of heavy rare earths (HREE), as it was not possible to measure the rare earth distribution by using the experimental setup of the beamline at the APS, which was rather optimized to detect first row transition metals.

The ratio of bulk rock heavy vs. light rare earths contents (HREE/LREE, Er/Nd) of the samples and their bulk concentrations of Zr and K (not shown) were found to be strongly correlated with the measured $^{87}Sr/^{86}Sr$ values (Fig. 3.6C). The high degree of correlation indicates that the observed shift of $^{87}Sr/^{86}Sr$ isotope ratio towards more heavy values, probably reflect variable rates of interaction of early diagenetic pore fluids with seawater containing a radiogenic Sr signature.

Following Kamber et al. (2004) we further evaluate the correlation of $^{87}Sr/^{86}Sr$ ratios and the bulk-Rb concentrations of the samples. The correlation between Rb and Zr contents ($R^2 = 0.73$ makes it possible to estimate that the Rb content of a sample uncontaminated with radiogenic Sr (i.e., Zr < D.L) is about 11 ppm Rb (Fig. 3.7A). Again, following the reasoning of Kamber et al. (2004), this value was extrapolated along a Sr-isotope vs. Rb concentration plot (Fig. 3.7B) to yield an initial $^{87}Sr/^{86}Sr$ ratio of ~ 0.70733. Such a value corresponds to the late Aptian-early Albian $^{87}Sr/^{86}Sr$ seawater curve (Bralower and Fullagar, 1994; McArthur et al., 2001).

3.4.3.3 Iron and manganese as redox indicators

3.4.3.3.1 Iron

The ratio of highly reactive to total iron (Fe_{HR}/Fe_T) can be used to recognize sediments deposited under an anoxic water column (see Raiswell and Canfield, 1998; Poulton and Raiswell, 2002; Poulton and Canfield, 2011). Accordingly, in sediments deposited beneath anoxic waters, Fe_{HR}/Fe_T ratios are commonly > 0.38, in contrast to oxic depositional conditions where Fe_{HR}/Fe_T below 0.22 are considered to provide a robust indication of oxic depositional conditions (Raiswell and Canfield, 1998; Raiswell et al., 2001; Poulton and Raiswell, 2002; Poulton and Canfield, 2011; Clarkson et al., 2014). Values of 0.22 – 0.38 can also occur during anoxic deposition due to either rapid sedimentation, or due to diagenetic conversion of Fe_{HR} minerals to poorly reactive sheet silicate minerals during early diagenesis (Poulton and Raiswell, 2002; Poulton et al., 2010; Poulton and Canfield, 2011), thus a Fe_{HR}/Fe_T threshold of > 0.38 provides a strong indication of anoxic deposition. All of the Fe_{HR}/Fe_T ratios in our samples are consistently greater than 0.50 (Fig. 3.8A). When such values are contrasted with modern and ancient anoxic deposits (Table 3.3), they point to a persistently oxygen-depleted depositional setting.

The amount of pyrite that can be formed in sediments is dependent on the availability of highly reactive Fe (Fe_{HR}). Thus, the chemistry of the anoxic water column at the time of deposition can be further evaluated by determining the extent to which the Fe_{HR} pool has been pyritized (Fe_{Py}/Fe_{HR}), this ratio distinguishes whether the water column was euxinic (i.e., sulfide-rich) or ferruginous (Fe-rich), with Fe_{Py}/Fe_{HR} > ~0.70 – 0.80 distinguishing euxinic from ferruginous conditions. This threshold was initially defined from analyses of euxinic Black Sea sediments by Anderson and Raiswell (2004), and redefined by Poulton et al. (2004) and März et al. (2008). The Fe_{Py}/Fe_{HR} values of the dolomitic shales are consistent with deposition under an anoxic ferruginous

water column, with a couple of samples possibly reflecting transient euxinic conditions (Fig. 3.8A). A non-dolomite bearing black shale level at the base of the Guáimaros member, borehole SOL-6 (18 051'), yields Fe_{Py}/Fe_{HR} of 0.85, indicating likely deposition under a euxinic water column. Below this level, at 18 082', this interval has, in addition to pyrite, an unusual hydroxide mineral identified via XRD as cobaltarhurite ($Co_2^{+}Fe_3^{2+}(AsO_4)_2(OH)_2 \cdot 4H_2O$), and also jarosite ($KFe_3^{+3}(OH)_2(SO4)_2$ — a phase that result from the oxidation of sulfide minerals. The localized occurrence of these minerals suggests subaerial exposure of the transgressive black shale horizon at some point during its early diagenetic history.

Pyrite oxidation may have potentially affected the original Fe speciation values, such that initially euxinic sediments now produce a ferruginous signal (i.e., they now exhibit relatively low Fe_{Py}/Fe_{HR}). To address this potential alteration issue, we applied a test that assumes — as an end member scenario — that all of the oxidised Fe_{HR} phases (i.e., Fe_{Ox}) derived from pyrite oxidation. Since iron is conservative through transformation of Fe_{Py} to Fe_{Ox}, and pyrite oxidation should not result in any significant change in Fe_{HR}/Fe_T, we recalculated the extent of pyritization by producing a Fe_{Py}^*/Fe_{HR} ratio, where $Fe_{Py}^* = Fe_{Py} + Fe_{Ox}$ (Fig. 3.8B). Accordingly, when a sample exhibiting relatively low Fe_{Py}/Fe_{HR} has $Fe_{Py}^*/Fe_{HR} > 0.70$, then that sample may have been oxidised, whereas if the Fe_{Py}^*/Fe_{HR} ratio remains below the 0.70 threshold, then the sample was indisputably deposited under a ferruginous water column. As shown in Figure 3.8B, our alteration test indicates that some samples may have been deposited below a euxinic water column. However, since this test assumes the extreme case that all Fe_{Ox} derives from pyrite oxidation (when, in fact, there was likely some Fe_{Ox} in the pre-oxidised sample), and oxidation of Fe(II) in carbonate minerals would also generate Fe_{Ox}, additional evidence must be sought to evaluate the potential for euxinic depositional conditions.

We also consider concentrations of the redox-sensitive element molybdenum, which is specifically drawn down into the sediment under anoxic sulfidic water column conditions (Helz et al., 1996; Zheng et al., 2000; Barling et al., 2001; Nägler et al., 2005). As seen in Table 3.1, in addition to the two samples that have high original Fe_{Py}/Fe_{HR} ratios indicative of euxinia (UD171 16 249' and SOL6 18 051'), two other samples with elevated Fe_{Py}^*/Fe_{HR} ratios from the Lisure Formation (SOL-6, 17 464' and Z26D-2 11 280') have significant Mo enrichment factors ($(Mo_{sample}/Mo_{shale})/(Al_{sample}/Al_{shale})$) when compared to average shale values (Wedepohl, 1978;

Fig. 8C). Other redox-sensitive transition metals such as Ni and V are also enriched in these samples (Table 3.1). These Mo enrichments (Mo_{EF} = 22 and 43) are consistent with values reported by Alberdi-Genolet and Tocco (1999) in black shales deposited in the Machiques trough, with this sub-basin exhibiting Mo_{EF} ranging from 5 to 320. Thus, we conclude that the redox interpretation of two samples has likely been affected by post-depositional oxidation, and our samples thus record a mixture of anoxic ferruginous and euxinic depositional conditions.

3.4.3.3.2 Manganese

The Mn* parameter ($Mn^* = \log ((Mn_{sample}/Mn_{shale}) \cdot (Fe_{sample}/Fe_{shale})^{-1}$; Machhour et al., 1994), where shale-normalization values are from Wedepohl (1978), has been used in the past as a proxy for the redox state of the precipitation environment of carbonates precipitated within organic-rich shales (for example Bellanca et al., 1996, 1997). The bulk Mn* index of the samples show a mean value of -0.51, with more negative values, of up to -0.82 (Table 3.1), indicating spatial variability in reducing conditions during deposition (i.e., Machhour et al., 1994). As shown in Figure 3.9A, the Mn* parameter systematically becomes more negative with increasing of the Al/ (Al+Fe+Mn) proportionality, and shows some degree of negative correlation with the HREE/LREE (Er/Nd) ratio of the samples (R^2 = 0.51).

In addition, there is some correlation between Pr/Pr* (as a measure of the Ce anomaly) and the total intracrystalline Mn concentration (Fig. 3.9C). Similarly to Bellanca et al. (1996), we also find a positive correlation between Mn* and the HREE/LREE ratio (R^2 =0.63). The spatial distribution of Mn vs. Fe, as observed in the representative sample (UD-171 16 245.8'), is shown in Figure 3.9D. Spatially resolved semi-quantitative analyses show a limited range of variability in iron and manganese concentrations of the fine euhedral dolomite, which indicates that the redox conditions during precipitation of such dolomite crystals were relatively constant.

3.4.3.4 Other redox-sensitive metals

3.4.3.4.1 Vanadium and Nickel

The proportionality of vanadium to nickel (V/V+Ni) was also analyzed to derive further information on the redox conditions of the depositional environment (Wignall, 1994, p. 45). The samples exhibit V/ (V+Ni) ratios greater than 0.65, with peaks as high as 0.92 (Tables 3.2 and 3.3) suggestive of deposition under anoxic conditions (Hatch and Leventhal, 1992).

3.4.3.4.2 Cerium

Ce anomalies (after De Baar et al., 1988) can probably be used to evaluate whether dolomite precipitated under anoxic conditions. In normal oxygenated seawater, Ce is less readily dissolved because of its co-precipitation with Fe and Mn-(oxy)hydroxides and complexation with the particulate organic matter. In this manner, authigenic carbonates formed in equilibrium with oxic to suboxic seawater would be expected to exhibit a negative Ce anomaly, which means depletion of Ce (see Kamber and Webb, 2001). By contrast, if authigenic carbonates formed in anoxic pore waters, they should be relatively enriched in Ce, and exhibit less negative to positive Ce anomalies (Wright et al., 1987). All of the laser ablated crystals showed Pr/Pr* ratios < 0.99 (Table 3.3; Fig. 3.10A) while the bulk rock has values that are above unity (Fig. 3.10A). The Ce signature of the crystals is not unlike that of Mn, with some degree of correlation indicating that the process of Ce incorporation into dolomite was linked to the redox cycling of Mn (Fig. 3.10B-C). As shown in Figure 3.10D, the Y/Ho values are somewhat spread, and there is some degree of correlation between these ratios and the La anomaly — inferred by using Ce/Ce* (Ce* = $(Ce/(0.5La + 0.5 Pr)_{SN})$. The laser ablated dolomite crystals (n= 46) display highly variable Ce/Ce* values ranging from 0.54 to 1.05 (Mean: 0.72; Median: 0.77; see Fig. 3.10D).

3.4.4. Biomarkers

Biomarker parameters can be particularly useful in terms of discriminating physicochemical variations in the depositional environment and specific modes of formation of an organic-rich fine-grained lithofacies. The total organic carbon content of our samples ranges from 1.1 to 4.5 (average 1.9) wt. %. The distribution of relevant biomarkers critical for determining depositional conditions, such as n-alkanes, terpanes, steranes, and other aromatic compounds (i.e., Didky et al., 1978), is described below.

3.4.4.1 n-alkanes

n-Alkanes in most samples ranged from *n*-C_{12} to *n*-C_{38} and have unimodal (samples 3, 4, 5, 6, 8, 9, 10), bimodal (1, 2) or trimodal (7) distribution patterns (sample numbers as referred in Table 3.4). In samples 2, 5, 6, 7 and 8, a dominance of *n*-alkanes with odd carbon numbers in the range C_{26} to C_{34} (CPI_{26-34}, 1.1 – 1.3) implies that organic matter was derived from waxes of terrestrial vascular plants (Eglinton et al., 1962; Bieger et al., 1997; Jeng, 2006). An odd-over-

even carbon preference for *n*-alkanes in the range C_{15} to C_{23} ($EOP_{15\text{-}23}$, 1.0), which is suggestive of an algal or cyanobacterial source (for example Gelpi et al., 1970), is only observed in sample 6. More common is an even-over-odd carbon number preference (Table 3.4). Possible causes for the dominance of even numbered *n*-alkanes are microbial degradation of higher molecular weight hydrocarbons, reduction of fatty acids in reducing environments or direct microbial input (Dembicki Jr et al., 1976; Shen et al., 1980; McKirdy et al., 1986; Grimalt and Albaigés, 1987; Elias et al., 1997).

3.4.4.2 Acyclic isoprenoid

Most samples contain regular (head-to-tail linked) acyclic isoprenoids (*i*-C_x) with 16 to 25 carbon atoms. Pseudohomologues with $\geq C_{21}$ carbon atoms are probably largely derived from archaea (Illich, 1983; Volkman, 1986), while pseudohomologues with C_{16} to C_{20} carbon atoms are predominantly regarded as degradation products of the phytol side chain of (bacterio)chlorophylls of phototrophic organisms. The acyclic isoprenoids pristane (Pr, *i*-C_{19}) and phytane (Ph, *i*-C_{20}) are oxidative and reductive products of the phytol side chain of chlorophyll, respectively (Powell and McKirdy, 1973). Thus, the ratio of pristane to phytane (Pr/Ph) is a useful parameter to interpret the redox conditions of the depositional environment (Didyk et al., 1978). Peters et al. (2005) suggests that high Pr/Ph ratios (>3.0), indicate a terrigenous organic matter input occurred under oxic conditions, while low values (<0.8) point to anoxic hypersaline carbonate environments. Thus, the range of relative abundances observed on these isoprenoids (Pr/Ph = 0.3 to 3.4, median 0.5, mean 1.0; Table 3.4) point to predominant anoxic hypersaline redox conditions during early diagenesis, with some degree of redox variability (i.e., Brooks et al., 1969).

Other tentatively identified isoprenoids have irregular head-to-head (C_{32} to C_{40}) and tail-to-tail (C_{20},crocetane; C_{25}, 2,6,10,15,19-pentamethylicosane, PMI; C_{30},squalane) branched structures, which are believed to be largely produced by archaea (Moldowan and Seifert, 1979; Rowland, 1990). However, crocetane can also be a degradation product of carotenoids and squalane precursors occur in organisms from all three domains of life (Maslen et al., 2009 and references therein)

3.4.4.3 Polycyclic terpanes

Similar to other reports for the mid-Cretaceous (Dumitrescu and Brassell, 2005 and references therein), our samples contained 13β(H),14α(H)-tricyclic terpanes in the range C_{19} to C_{26} (maximum at C_{23}) and a complete homologue series of 17α(H),21β(H)-hopanes with 27-35 carbon atoms (maximum at C_{30} or C_{31}). Minor components are C_{29} to C_{31} βα-hopanes (moretanes), 28,30-bisnorhopanes and C_{29} to C_{31} diahopanes (Table 3.4). Oleanane and bicadinane were also detected in trace amounts. These C_{30} pentacyclic terpanes are diagnostic for higher terrestrial plants (Moldowan et al., 1994) , but their abundance in the dolomitic shales is lower than reported in previous source rock studies of the Maracaibo Platform (Alberdi-Genolet and López, 2000).

Gammacerane (γ) is also present in all samples. This pentacyclic terpane is formed in sediments by defunctionalization of tetrahymanol (gammaceran-3β-ol) (Ten Haven et al., 1989; Sinninghe Damsté et al., 1995). Tetrahymanol occurs ubiquitously in marine sediments (Venkatesan, 1989). It has been found in nitrogen-fixing bacteria, purple non-sulfur bacteria, and in heterotrophic marine and lacustrine ciliates (Mallory et al., 1963; Zander et al., 1969; Kemp et al., 1984; Kleemann et al., 1990; Harvey and Mcmanus, 1991; Bravo et al., 2001). In stratified marine environments, anaerobic ciliates are probably the most significant source of tetrahymanol (Sinninghe Damsté et al., 1995). These organisms thrive at or beneath the chemocline in dense populations, causing elevated values of the gammacerane index (GI = γ/(γ+C_{30} αβ-hopane) in %). In the dolomitic shales from the Maracaibo ramp, values range from 1.1 to 18.0 % (Table 3.4). Although exact cut-off values are unknown, elevated GI ratios (> 5%) are regarded as an indicator of water column stratification, which can be sometimes associated with bottom water hypersalinity and reducing conditions (Ten Haven et al., 1988; Harvey and Mcmanus, 1991; Sinninghe Damsté et al., 1995).

A complete series of 2α and 3β C_{31} to C_{36} A-ring methylated hopanes is present with C_{32} as the most dominant homologue. The range of 2α (2MHI) and 3β-methylhopane indices (3MHI) for the C_{31} homologue (MHI = C_{31} methylhopane/(C_{31} methylhopane + C_{30} αβ S+R hopanes) in %), are 2.3 to 6.6 % and 1.5 to 7.3 %, respectively (Table 3.4). The precursor molecule of 2α-methylhopanes, 2-methylbacteriohopanetetrol, was initially proposed to be exclusively produced by photosynthesizing cyanobacteria (Summons et al., 1999). However, recent work argues that

sedimentary 2-methylhopanes are more typically associated with environmental niches with low oxygen levels, and a dominance of nitrogen-fixing organisms thriving within a sessile microbial community, such as microbial mats and stromatolites (Ricci et al., 2013). 3β-methylhopanes are indicative of microaerophilic methanotrophs (Neunlist and Rohmer, 1985) or acetobacteria (Simonin et al., 1994).

Another compound class detected in the mid-Cretaceous Venezuelan shales are C_{30} tetracyclic polyprenoids (TPP), which are believed to derive from freshwater algae. The ratio of these molecules with 27-nor(dia)cholestanes varies between 0.2 and 0.8. This range is commonly interpreted as a measure of the input of freshwater to marine environments (Holba et al., 2003).

3.4.4.4 Steranes

Steranes and aromatic steroids are abundant in all samples and comprise most of the known C_{26} to C_{30}-pseudohomologues, diasteranes, A-ring methylated steranes, and mono- and triaromatic steroids. Sterane abundances are similar to a study of the Machiques Member in the Perijá area (Alberdi-Genolet and Tocco, 1999). Both Cholestane (C_{27}) and stigmastane (C_{29}) are abundant in a similar range (32 to 45 % and 29 to 44 %, respectively), whereas ergostane (C_{28}) constitutes about 25 % in all but one sample. The ratio between eukaryotic steranes and bacterial hopanes (Ster/Hop) fluctuates widely between 0.1 and 1.4.

Although C_{27} steranes are particularly common in marine red algae (Patterson, 1971), as also are C_{29} steranes in higher land plants (Nishimura and Koyama, 1977), all three main steranes (C_{27}, C_{28}, C_{29}) have precursor sterols which are widely distributed in varying amounts, across eukaryotic lineages. This restricts their use as source-specific biomarkers (Volkman, 2003). Fluctuations in Mesozoic stigmastane (C_{29}) abundances are commonly best explained by variations in organic matter input from terrestrial plants that predominantly produce C_{29} sterols (Grantham and Wakefield, 1988). Abundant 24-*n*-propylcholestanes (C_{30} steranes, % $C_{30} = C_{30} \times 100/(\sum C_{27}\text{-}C_{30})$ are diagnostic marine indicators, since their precursor sterols are produced by marine foraminifera (Grabenstatter et al., 2013) and by marine benthic microalgae of the order Sarcinochrysidales (Raederstorff and Rohmer, 1984).

3.4.4.5 Carotenoid derivatives

The saturated hydrocarbon fraction contains the intact C_{40} carotenoid derivatives lycopane, β-carotane and γ-carotane, as well as further compounds that may represent structural isomers of γ- and β-carotane. The aromatic fractions contain aryl isoprenoids with a 2,3,6 trimethyl substitution pattern in the range C_{13} to C_{31}, and the C_{40} parent compound isorenieratane (III), as well as traces of chlorobactane (I) and β-isorenieratane (II).

The biogenic precursor of isorenieratane (III), isorenieratene, has two known biological sources: species of the bacterial phylum Actinobacteria and brown-pigmented strains of Chlorobiaceae (green sulfur bacteria) (Krügel et al., 1999; Ventura et al., 2007; Maresca et al., 2008). Actinobacteria show a wide variety of morphologies, as well as physiological and metabolic properties and are widely distributed in marine ecosystems (Ventura et al., 2007). Chlorobiaceae are strictly anaerobic, phototrophic bacteria that mainly use sulfide as electron donor, although some species can use ferrous iron (Heising et al., 1999; Frigaard and Bryant, 2006). Populations occur in stratified holomictic and meromictic water bodies, where their density is largest beneath the chemocline, which can be as deep as 100 m, but they also occur in shallow lagoons, stagnant seawater pools, and salt marshes (Overmann et al., 1992; Trüper and Pfennig, 1992 and references within; Manske et al., 2005). Chlorobiaceae also grow in microbial mats (Visscher and Stolz, 2005). In microbial mats as well as in the water column Chlorobiaceae usually thrive below purple sulfur bacteria (Chromatiaceae), which have higher light requirements (Biebl and Pfennig, 1978).

Aryl isoprenoids with a 2,3,6 trimethyl substitution pattern may be the cleavage products of aromatic carotenoids with the same substitution pattern, but may also form by aromatization of acyclic carotenoids such as β-carotane (Koopmans et al., 1997; Brocks and Schaeffer, 2008). The distribution of 2,3,6 breakdown products in the range $C_{30} – C_{31}$ can give clues about the precursor molecules. A linear correlation between C_{30} and C_{31} aryl isoprenoid abundances (R^2 =0.99) is evidence for an almost quantitative common biological origin for these two carotenoid breakdown products. The cleavage products of isorenieratane (III) are aryl isoprenoids with a 2,3,6 trimethyl substitution pattern. The loss of a terminal phenyl group through β-cleavage leads to fragments with 10 to 30 carbon atoms.

A homologue with 31 carbon atoms should not form, as this would require an energetically highly unfavourable cleavage in α-position to the aromatic ring. However, in the Maracaibo samples, 2,3,6 aryl isoprenoids include the C_{31} homologue, which is not produced by isorenieratane cleavage. Moreover, as shown in Table 3.4, C_{30} and C_{31} homologues are about equally abundant while higher homologues ($\geq C_{32}$) are not detected. The similar abundances indicate that the degradation of isorenieratene and its derivatives does not account for the bulk of the observed 2,3,6-trimethylated aryl isoprenoids. The pattern can also not be explained by the cleavage of chlorobactane (I), as this would also produce homologues with > 31 carbon atoms, which are lacking in the samples. Therefore, the source of the bulk of $\leq C_{31}$ aryl isoprenoids is neither isorenieratene nor chlorobactene but must be a carotenoid that readily loses a C_9 unit. One option is β-isorenieratene. However, its abundance is so low that it can be discounted as a plausible major source.

C_{13} to C_{31} 2,3,6-trimethylated aryl isoprenoid may also form by aromatization and cleavage of carotenoids with a β-carotene skeleton (Koopmans et al., 1996). The aromatization of one ring and cleavage of the second alicyclic ring can account for the observed aryl isoprenoid series, including the presence of abundant C_{31} and absence of higher pseudohomologues. ^{13}C of values of aryl isoprenoids can, in principle, help differentiating between the two major sources of 2,3,6 aryl isoprenoids: aromatic carotenoids or β-carotane derivatives (Koopmans et al., 1997), however, aryl isoprenoid concentrations were too low in the shale samples to perform isotopic measurements.

The ratio of short over long aryl isoprenoid fragments can be used as a measure of oxygen exposure, and is defined in this work as AIR-2 = $C_{13\text{-}19}/C_{20\text{-}26}$ (modified after Schwark and Frimmel, 2004). Low AIR-2 values are interpreted as a depositional environment with very stable redox stratification as there is virtually no exposure to oxygen. Conversely, high AIR-2 values are indicative of intermitted oxygenation or overturning of the water column. In the Maracaibo samples, AIR-2 ranges from 0.1 to 5.3 (mean 2.4, median 0.8).

3.4.4.6 Dibenzothiophene (DBT)

Dibenzothiophenes are also present in the dolomitic shale samples (Table 3.4). The sulfur-containing molecule DBT is an indicator for sulfur availability in the depositional environment. Phenanthrene (Phen), which is independent of sulfur levels, is commonly used in a ratio with DBT

(DBT/Phen) to characterize the depositional system (Zhu et al., 2011). DBT/Phen ratios can be used in combination with the redox indicator Pr/Ph to infer depositional environments and lithologies (Hughes et al., 1995). Based on the measured signals (DBT/Phen = 0.2 – 2.0, Pr/Ph = 0.3 – 3.4; Table 3.4), the environment at the time of deposition of the shales are consistent with variable interpretations from a sulfur-rich lagoonal to sulfur-poor mud flat.

3.4.4.7 Correlation of biomarker parameters

Principal Component Analysis (PCA) is a conventional multivariate technique founded on a correlation matrix, which cuts down a large number of geochemical variables to determine the components (groups of parameters) that influence the variance of multivariate data. Possible correlations between biogeochemical parameters were assessed by applying a PCA of scored data using Matlab R2014a. Because this study focuses in a specific microfacies, a stratigraphical analysis was not attempted but only the variability and correlation of parameters between samples were assessed in order to determine the environmental control(s) governing their deposition.

The first principal component explains most of the variance within the original data and each subsequent principal component describes the variance in progressively limited detail (1st PC = 41%, 2nd PC = 21%, 3rd PC = 14%). The 1st PCA also clusters the biomarkers ratios and some inorganic redox proxies (discussed below) in two distinct categories (see Table 3.5). The first category is characterized by elevated values for biomarker parameters that reflect high relative input of terrestrial and freshwater organic matter, such as the proportion of C_{29} steranes (% C_{29}), input of plant waxes ($CPI_{26\text{-}34} > 1$), and freshwater-derived organic matter (TPP). The first category is also defined by high AIR-2 and Pr/Ph, and clay-induced molecular rearrangements (diaC_{27}-C_{30}, C_{30} βα/αβ), both of which are consistent with a terrestrial source (Table 3.5). In contrast, biomarker values in the second category are typical for organic matter of marine origin, such as high C_{27} and C_{30} steranes proportions (% C_{27}, % C_{30}), high sterane versus hopane ratios (Ster/Hop), and high relative gammacerane abundances (GI). Moreover, the second category is also defined by higher sulfur availability (high DBT/Phen) and elevated biomarker ratios, typical of marine systems (28,30BNH, HHI) (Table 3.5). Samples in both of these categories do not follow a burial depth profile, ruling out maturity as a main component. Hence, controlling factors are thought to be biological and/or environmental. Thus, the 1st PC appears to be controlled by the relative influx of terrestrial organic matter into a marine depositional environment.

3.4.5. Stable isotope geochemistry

3.4.5.1. C isotope analyses

Figure 3.13A shows a compilation of previously reported bulk ^{13}C values of dolostones in the Apón Formation together with values determined in this study. While published data for the $\delta^{13}C$ of dolomites in the Apón Formation ranges from -5.2 to +4.0‰ (V-PDB), our dolomitic shales have $\delta^{13}C$ ranging from +1.19 to +4.0‰. The predominant signature seems to be from seawater-derived DIC, which by the time of precipitation was probably +2.5 ± 1.0‰ (see Menegatti et al., 1998). More negative $\delta^{13}C$ values were observed by Pöppelreiter et al. (2005) in fabric destructive dolostones with good reservoir properties, but such microfacies were not considered in this study, which focuses on dolomitic black shales. Figure 3.13B shows a discrimination of calcite and dolomite within the samples studied here. When calcite is present, $\delta^{13}C$ ranges from -0.1 to +2.2‰ (Fig. 3.13B). The sedimentary organic matter as measured in samples from UD-171 has a $\delta^{13}C_{org}$ of -22.5 ± 1.7‰.

3.4.5.2. O isotope analyses

Data from this study shows that oxygen isotopes in dolomite averaged -1.24‰ and largely follow the trend in carbon isotopes (R^2= 0.71). The covariance of $\delta^{18}O$ and $\delta^{13}C$ (Fig. 3.14B inset) might reflect a primary signal (Marshall, 1992). On the other hand, calcite reached δ-values as low as -10.0‰ V-PDB (average -5.2‰) and is uncorrelated with the measured O-isotope values (Fig. 3.13B). For all of the available oxygen isotope data, the magnitude of the negative excursions in $\delta^{18}O$ for calcite is about 5.6‰ lower than dolomite. This difference compares fairly well with values expected for equilibrium-paired phases (O'Neil and Epstein, 1966; but see Marshall, 1992).

3.5. Discussion

3.5.1. General aspects of Mid-Cretaceous ramp/shelf deposition

The mid-Cretaceous was a time of continuous epicontinental transgression and expansive epeiric basin formation (Budyko et al., 1987; Hay et al., 2006). These basins were predisposed to recording transient anoxic to euxinic conditions in the form of organic-rich condensed-levels (Schlager, 1989). The stratigraphic distribution of such intervals in mid-Cretaceous ramps/shelves was

conceivably controlled by the irregular paleotopography of post-rifted epicontinental basins. Accordingly, paleobathymetric lows with persistently anoxic bottom waters were sites favourable for black shale deposition, but as the nutrient-rich oxygen-depleted waters characterizing these sub-basins were episodically transported by upwelling processes to inner ramp/ shelf zones, eutrophication and demise in carbonate production would have also led to extended shallow marine black shale deposition (Wignall, 1991, 1994; Arthur and Sageman, 1994). It is likely that the deposition of these intervals were preceded by relative sea-level fall, and incidentally the most important episodes of base sea-level change during the mid-Cretaceous coincide with the episodes of major environmental perturbation comprising the OAE 1 (Föllmi, 2012) (Fig. 3.14).

The reestablishment of the carbonate factory in mid-Cretaceous ramps/ shelves affected by OAEs was only possible after the establishment of normal circulation patterns and water oxygen levels (Wignall, 1991; 1994), and the presence of black shale within shallow marine carbonate facies more likely reflects the sensitivity of carbonate depositional systems to Milankovitch-scale climate-forcing mechanisms (de Boer and Wonders, 1984; Herbert 1986; Goldhammer et al., 1987; Fisher et al., 1990; Erbacher, 1996; Herrle et al., 2003) Processes controlled by short-term Milankovitch-scale perturbations ($10^4 – 10^5$ Myr), such as major shifts in oceanic nutrient levels, temperature and circulation patterns, and organic productivity exerted a significant control on the type of sedimentation (see Burchette and Wright, 1992; James et al., 2001; see also Puga-Bernabéu et al., 2008).

Detailed stratigraphic analyses of mid-Cretaceous sequences (Lehmann et al., 1998; Herrle et al., 2003; Browning and Watkins, 2008; Föllmi, 2012; Wagner et al., 2013) have also shown that in tropical zones most ramp/shelf shallow marine environments were probably affected by episodic monsoonal events. Minor relative sea-level changes would have also exerted a substantial control on the intrabasinal circulation patterns by triggering the expansion of anoxic waters from adjacent sub-basins to middle (lagoonal-subtidal) and inner (peritidal) ramp/shelf settings (Wagner et al., 2013). However, how all of the interconnected variables mentioned above led to a paleooceanographic state favourable to the formation of interstitial dolomite within transgressive black shales has remained largely unexplored.

3.5.2. Paragenetic model

3.5.2.1. Stage I. Organic-rich clay deposition and pyrite authigenesis

3.5.2.1.1. Redox conditions at the time of deposition

A measure of the Eh regime is provided by the biomarker ratios DBT/Phen, Pr/Ph, HHI and AIR-2 (Table 3.5), as well as the iron speciation parameters Fe_{HR}/Fe_T and Fe_{Py}/Fe_{HR}. In principle, each of these parameters may be affected by late diagenetic or maturity-related processes or even oxidation during storage of the drill core material. However, AIR-2 correlates positively with Pr/Ph and negatively with DBT/Phen, HHI and Fe_{HR}/Fe_T (Fig 3.12), suggesting that the redox signals are largely primary. Interestingly, the extent of pyritization of highly reactive iron (Fe_{Py}/Fe_{HR}) does not correlate significantly with any other parameter, suggesting that pyritization was not influenced by the influx of terrestrial debris or that pyrite suffered some oxidation (see discussion below).

A principle component analysis clearly demonstrates that differences in biomarker redox parameters between samples are primarily driven my varying influx of oxidized terrestrial debris into a stratified reduced marine environment. This observation even extends to the AIR-2 ratio. As discussed in the 'Biomarkers' section, 2,3,6-AI in the Maracaibo samples are nearly quantitatively derived from the aromatization of carotenoids with a β-carotane skeleton, and AIR-2 is a measure of oxygen exposure of these molecules during early diagenesis. AIR-2 shows a wide range of values (0.1 to 8.1) consistent with highly variable redox conditions during early diagenesis. Traditionally, the variability would be explained by an unstable, overturning water column or oxygenation of bottom waters through waves or currents. However, the AIR-2 values can also be explained by a two component mixing effect. Carotenoids of terrestrial origin would suffer intense contact with oxygen in soil and during riverine transport, leading to strong cleavage and elevated AIR-2, whereas marine-derived β-carotenoid derivatives, predominantly of algal origin, would have been much less exposed to oxygen. This is because organic matter of dead algae settles quickly from the upper oxic part of the water column into the anoxic zone, protecting the carotenoids against oxidative cleavage and yielding low AIR-2. Therefore, in the dolomitic shales, the AIR-2 parameter probably does not reflect fluctuations in redox conditions in the marine realm, but simply changes in relative fluxes of terrestrial and marine organic matter into the depositional system.

Biomarkers also yield some information about redox stability within the marine system. The abundance of isorenieratane indicates anoxic conditions in the photic zone (Summons and Powell, 1987). As discussed earlier, cleavage of isorenieratene did not contribute significantly to the 2,3,6-AI pool, demonstrating that isorenieratene was never significantly exposed to oxygen. Consequently, the bottom waters remained anoxic throughout deposition of the analysed intervals, suggesting permanent and stable stratification with little to no oxygen availability except for perhaps the shallowest waters. This result is consistent with interpretations based on Fe speciation parameters, which suggest a stable anoxic environment with a dominantly ferruginous water column and transitory sulfidic conditions. Similarly, the Mo concentrations of the samples point to a mixture of anoxic ferruginous and euxinic depositional conditions.

A high gammacerane index (GI), a measure of the abundance of ciliates, is common in stable stratified aquatic ecosystems (Sinninghe Damsté et al., et al., 1995). In the Maracaibo samples, GI is lowered during periods of maximal terrestrial run-off (Fig. 3.12). This observation is counterintuitive as the influx of freshwater should intensify the density difference between deep and shallow waters and lead to rising GI values (for instance Erbacher et al., 2001). Decreasing GI values despite enhanced freshwater influx may have two explanations. Firstly, a decline in gammacerane production may be related to famine of ciliate populations. Ciliates commonly feed on anoxygenic phototrophs and other dense populations of bacteria that inhabit the chemocline within the photic zone. However, elevated terrestrial run-off probably caused turbid conditions. Towards the outer to middle ramp setting, it is plausible that the shading effect of suspended particles reduced the depth of the photic zone so that the base did not reach into anoxic bottom waters. This would have caused diminishing populations of anoxygenic phototrophs, thus affecting ciliate communities (Fig. 3.14). Secondly, GI values may be depressed during influx of terrestrial organic matter by a dilution effect. GI is defined as the ratio of gammacerane over C_{30} hopane. Thus, simple influx of hopanoid-rich soil material may have contributed to declining GI values. However, the very wide range of GI (1.1 to 18.2 %) suggests that ecological effects must have played a role as well.

3.5.2.1.2. Precipitation of pyrite

The discussion above point towards the bottom waters of the Maracaibo ramp at the time of shallow marine black shale deposition being permanently anoxic, and at times euxinic. As

illustrated in Figure 3.14, the expansion of oxygen-depleted nutrient-rich waters from the Machiques trough to the inner ramp may have caused the development of a transiently euxinic-ferruginous chemocline favourable for pyrite precipitation (Rickard and Luther, 2007). This chemocline was more persistent towards the Machiques trough, where a stagnant water column prevailed at times of relative sea level drops.

The upwelling of oxygen-depleted waters from the paleobathymetric low to the shallow ramp settings would have occurred shortly after relative sea level drops (early transgressive stage) (for example James et al., 2001). Upwelling of nutrient-rich waters in a general condition of restricted circulation would have been maintained only over relatively short time-scales (the time scale represented by each of our samples), but it caused a devastating effect on the carbonate-producing biota and was followed by a complete shutdown of the carbonate factory concomitant with black shale deposition and pyrite precipitation.

The ubiquity of relatively large pyrite framboids in the microfacies targeted here indicates that most pyrite precipitated in a transient euxinic-ferruginous redoxcline located at or below the sediment–water interface (Wilkin et al., 1996; Wignall and Newton, 1998) as compared with the redoxcline in the Machiques trough, which was persistently located in the water column (Fig. 3.14). In such disequilibrium zone, pyrite crystal growth was limited by the rapid reduction in concentration of reactive Fe and S species (Berner, 1984; Butler and Rickard, 2000), with a diffusion-limited supply of reactants (Rickard, 2012). The bimodal size distribution of pyrite would be explained by the transport of small pyrite aggregates formed in the water column. Accordingly, small framboids precipitated towards the outer ramp would have been transported and deposited in the lagoonal setting represented by our samples (for example Kershaw, 2015).

3.5.2.2 Stage II: Precipitation of dolomite

Dolomite is invariably associated with framboidal pyrite. The lateral persistence of this textural relation suggests that interstitial dolomite formed shortly after pyrite precipitation. Considering the intrinsic low permeability of the targeted intervals (see Bartok et al., 1981; Pöppelreiter et al., 2005), the textural relations between dolomite and other mineral phases, and the average size of the crystals (~80 μm), it is clear that interstitial dolomite grew prior to compaction.

The Maracaibo ramp had depositional surfaces that stayed near sea level for a few millions of years, and shows little evidence of major drops in sea level that would have exposed the depositional infill for long periods. Sea-level fluctuations of relatively low amplitude allowed extensive interstitial dolomite formation. These allowed repeated replenishment of pore waters by fluids favourable for dolomite formation over very extensive peritidal surfaces (Fig. 3.14). However, the planar-e chemically homogeneous, Ca-dolomite crystals described here are indicative of growth at low saturation conditions (see Sibley and Gregg, 1987). From bulk geochemical analyses, the interstitial dolomite precipitation microenvironment was more probably poised at a reducing Eh, with Fe(III)- and Mn(IV)-oxyhydroxides contained within the sediment matrix providing Fe^{2+} and Mn^{2+} by reductive dissolution. Ferrous iron, however, was rapidly fixed into coexisting pyrite framboids and Fe(II)-depleted pore waters evolved shortly after pyrite precipitation.

The rapid precipitation of framboidal pyrite favoured the biological utilization of Mn, to allow a dolomite stabilization mechanism relying on manganese recycling to operate effectively, such as envisioned in Chapter II. Manganese would have been recycled a number of times to be partially fixed into the dolomite crystals growing in equilibrium with iron-depleted pore waters. Supporting evidence for this assertion are the measured intracrystalline Ce-anomalies of dolomite, the observed differences of intracrystalline and bulk rock of such anomalies, and the degree of correlation of this parameter with Mn concentration and Mn* values. Additional evidence is the almost homogeneous distribution of Mn and Y in euhedral dolomite crystals, which suggests that the growth of dolomite as cement occurred in parallel with the biological reduction of Mn(IV)-oxyhydroxides during organic matter respiration. Mn(IV)-oxyhydroxides originally scavenged Y and REE of similar complexation behaviour (see Huang, 2010, and Schiff and Marshall, 2011). Therefore, the bioutilization of such phases could have also been responsible for the marked difference observed on the Pr/Pr* ratio of bulk sediments and the intracrystalline dolomite values (Fig. 3.10A-C), as well as the correlation between bulk Mn* and Er/Nd (Bellanca et al., 1999).

However, by the time of dolomite growth, diverse signals would have been recorded at different times, just as pore water chemistry is not tied to instantaneous simultaneous processes, but rather to a number of sequential controls. Hence, the presence of interlocking iron-bearing subhedral dolomite cortices might well represent a secondary oversaturation state of the pore

waters with regard to Fe-dolomite. The incorporation of iron onto dolomite lattices suggests that the overgrowths formed at a time marked by Fe^{2+} ion availability and low HS^- production, a condition that was likely enhanced by precipitation beneath a transient ferruginous-oxic chemocline that favoured settling and reductive dissolution of reactive Fe(III) oxyhydroxides from the water column. Accordingly, the Fe-enriched overgrowths more likely represent precipitation during or shortly after the influx of freshwaters to the lagoonal - tidal flat inner ramp setting. Such condition favourable for dolomite stabilization, has been referred in the literature as a schizohaline environment (Mazzullo and Friedman, 1977)

From the intracrystalline dolomite Na–concentrations (Table 3.2), it can be interpreted that dolomite precipitated under the influence of predominantly hypersaline pore waters, yet the oxygen isotope values of the samples do not point to extreme hypersalinity. Similarly, episodic perturbations of the precipitation environment were recorded by the spread and correlation of the non-redox sensitive Y/Ho and Ce/Ce* parameters (Fig. 3.10D, Table 3.1). Together all of these geochemical signals reflect a dolomite precipitation environment in which the influx of freshwater tended to dissolve the marine-derived inorganic signatures of the dolomite precipitates. The cross-plot of Rb and Zr vs. Sr isotopes values points, on the other hand, to increased $^{87}Sr/^{86}Sr$ values being the result of early diagenetic interactions of the dolomite precipitates with pore waters containing radiogenic Sr. The latter was derived from the weathering and transport of fine clastic material from granitic and post-Triassic arkosic sources in the hinterlands, which had initial values between 0.715 and 0.708, respectively (Maze, 1984). As observed in tropical and subtropical mid-Cretaceous sequences, it is possible that monsoonal forcing, with the higher influx of freshwater and finer-grained detritus, may have caused the development of the schizohaline environment. Nonetheless, the elemental ratios and biomarker parameters of the dolomitic shales support that the redox conditions in the middle to inner ramp remained constantly depleted in dissolved oxygen.

The picture that emerges is that after the upwelling of oxygen exhausted nutrient-rich waters, the shallow water column in the ramp consisted of euxinic upper waters overlying ferruginous bottom and pore waters. As discussed above, this condition favoured the precipitation of pyrite. By contrast, when the ramp was affected by monsoonal episodes, a short-lived, aperiodic bursts of molecular oxygen (O_2) accumulation probably led to an abundance of Fe_{HR} and was followed by a sudden increase in gross primary production. Our dataset indicates, however, that

the bottom waters remained anoxic and were not overturned. Therefore, the freshwater lids also overlaid the denser partially evaporated ferruginous bottom and pore waters. As the state of net surface heterotrophy was re-established, the freshwater lids would have become dysoxic (this is ~2.0 – 0.2 ml O_2/l) while the denser pore waters remained anoxic. Our combined dataset points to the development of such disequilibrium condition as the trigger of interstitial dolomite formation, with the thermodynamic drive and thus energy for microbial metabolisms being dictated by the sporadic transport of electron acceptors to the ramp.

3.5.2.3 Stage III: Inhibition of dolomite growth

The presence of equant gypsum as a minor authigenic component, and as small lenses in outcrops of the Guáimaros Member in the foothills of the Mérida Andes (González de Juana et al., 1980), probably reflects a local condition prevailing in the inner ramp early after the onset of dolomite crystal growth. In this regard, two non-mutually exclusive scenarios are envisioned as inhibitory of further dolomite growth: (1) washover events that led to dissolution of subaerial exposures of gypsum formed within supratidal sediments, and (2) the oxidation of abundant framboidal pyrite within exposed shales. The local presence of jarosite and cobaltarhurite within the non-dolomitic black shale level (SOL-6 18 082') attests to local subaerial exposure conditions of the fine-grained pyritic sediments.

As dissolved sulfate was replenished to the inner ramp, the mineral saturation conditions governing the sediment-pore water system were progressively changed towards a state of gypsum oversaturation. The precipitation of this phase probably occurred within biofilms that concentrated Ca (and some Mg) and developed interstitially over the dolomite surfaces. The high levels of dissolved sulfate led to these biofilms to act as nucleation centers for gypsum, which grew as equant microcrystals. In zones not affected by a significant flux of sulfate-bearing fluids, however, such biofilms rather acted as the locus for microcrystalline silica precipitation. Precipitation of silica allowed the preservation of delicate textural features that confirm that biofilms — once coating the early formed dolomite crystals, may have also produced the gypsum coats here described. Oversaturation of these biofilms with regard to silica and gypsum inhibited further dolomite growth.

The aluminosilicates comprising up to 56% of these rocks are considered major barium carriers, and barite can be only buried in sediments deposited under high productivity conditions and with sulfate availability (Dymond et al., 1992; Gingele and Dahmke, 1994; Paytan et al., 1996; Bellanca et al., 1996). Thus, the presence of barite confirms that some sulfate was locally available during the pre-compactional history of these sediments, as otherwise barite would have been readily dissolved (for example von Breymann et al., 1992; Torres et al., 1996; Gingele et al., 1999). Interestingly, the rocks in which barite is found also shows a DBT/Phen ratio <0.24. Dibenzothiophene (DBT) is considered an indicator for sulfur availability, and the DBT/Phen ratio is believed to be <1 in sulfate-deprived environments (Hughes et al., 1995). Thus, the low DBT/Phen ratio suggests that the influx of sulfate would have occurred in a shallow burial diagenetic realm shortly after deposition.

Finally, there would have been local supersaturation of the pore waters with regard to calcite, with dissolved bicarbonate being a by-product of sulfate reduction, and calcite replacing microcrystalline gypsum (see § 3.4.1.4 and § 3.4.5.2). The replacive calcite phase exhibit $\delta^{18}O$ values that are about 5.6‰ lower than coexisting dolomite, but have somewhat similar C isotope values (Fig. 3.13B), which indicates that there were no significant changes in the C isotope fractionation processes operating at the time of calcite precipitation, but oxygen limitation led to the accumulation of isotopically light bicarbonate (for example Harrison and Thode, 1958; Lloyd, 1968; Mizutani and Rafter, 1969).

3.6. Conclusions

The middle to inner ramp environment at the time of deposition of the dolomitic shales studied here is best described by a stratified water column in a restricted epicontinental marine basin with varying inputs of freshwater. The water body was defined by permanent photic zone anoxia, without major overturning events. During times of enhanced monsoonal precipitation (wet periods) the input of higher plant debris and freshwater algae as well as soil-derived clay and oxidatively degraded organic matter increased. In arid periods, the influx of euxinic upwelled waters was coupled with the dominance of marine organic matter signals.

In the microfacies targeted here, the omnipresence of framboidal pyrite in close textural relation with dolomite, and a number of redox-sensitive geochemical parameters, including biomarkers and Fe speciation data, as well as the elemental relation between bulk and *in situ* transition metal contents, collectively point to dolomite cementation in a persistently anoxic ferruginous and transiently euxinic environment episodically affected by freshwater influx. The textural and geochemical data of the resulting marlstones (dolomitic shales) indicate that early during burial, the interstices of the intervals interrogated became the locus of a very active elemental recycling process involving sulfide and reactive Fe and Mn species, with most dolomite precipitation occurring shortly after the onset of pyrite precipitation. As supported by the observed absolute and spatial correlation of intracrystalline Mn* and redox-sensitive rare earth Ce (Ce_{anom}, Pr/Pr*), the recycling of Mn and S would have been substantial at the time of dolomite growth. Accordingly, the progressive reduction of Mn-oxyhydroxides, which originally scavenged elements such as La, Ce, and Pr, may have had a significant influence on the incorporation of REE into interstitial dolomite.

Prior to compaction, and in the presence of seawater-derived fluids, the main limitation on dolomite formation was sustained alkaline conditions. Thus, orbital forcing mechanisms are thought critical for the stabilization process. These mechanisms allowed for the thermal expansion of nutrient-rich oxygen exhausted waters over the epicontinental ramp, which in turn lead to organic matter deposition. Cyclicity associated with Milankovitch-scale climate modulation would have also controlled the development of sudden shifts between semiarid and humid conditions. These shifts allowed for the periodic replenishment of electron acceptors, including sulfate and oxidized forms of Mn and Fe, which enhanced the rates of oxidation of the buried organic matter.

By sustaining elevated pore water alkalinity, the enhanced heterotrophy of the sedimentary organic matter allowed for stabilization of early formed Ca-dolomite precursors, which occurred in association with relatively high Mg:Ca ratios resulting from the generally hypersaline conditions governing the inner ramp.

As interstitial dolomite grew, the crystals developed distinctive textural relations with pyrite, which may have been locally oxidized, first leading to dissolution of metastable dolomite precursors and then to Fe-dolomite oversaturation. On the other hand, seasonality also operated to oversaturate the interstices of the sediments with regard to gypsum and/or silica, which precipitated intimately associated with dolomite, and ultimately inhibited further dolomite growth. Towards the Perijá Range, gypsum was replaced by isotopically light calcite, perhaps by deep subsurface sulfate reduction. Finally, the similarity in the mineral assemblage, geochemical signatures, and textural relationships of the microfacies studied here is thought indicative not of synchronicity, but of the resemblance of authigenic processes that acted in association with the multiple events comprising the OEA 1.

Table 3.1. Bulk rock inorganic geochemical data of the dolomitic shales.

Sample		Well (Depth)' Lithology	Z26D-2 (11280) Dol.Sh.	TOT-3 (14210) Dol.Sh.	UD-171 (16115) Argill.D.	UD-171 (16245.8) Dol.Sh.	UD-171 (16249) Dol.Sh.	SOL-6 (17464) Dol.Sh.	SOL-6 (17626) Dol.Sh.	SOL-6 (17631) Dol.Sh.	SOL-6 (18008) Argill.D.	SOL-6 (18051) Bl. Sh.	SOL-6 (18082) Sh.
Bulk rock	Isotope Ratios	$^{87}Sr/^{86}Sr_N$ (±0.00002)	0.707917	0.708127	0.707512	0.707843	0.707552	-	-	-	0.708552	-	-
		$\delta^{13}C$ (<0.05‰)	1.19 (D) -	2.77 (D) -	4.02 (D) 2.25 (C)	3.50 (D) -	-	-	-	-	2.89 (D) 2.26 (C)	-	-
		$\delta^{18}O$ (<0.05‰)	-2.97(D)	0.91 (D)	0.50 (D) -1.14(C)	1.29 (D)	-	-	-	-	-4.05 (D) -10.07 C)	-	-
	Minor and trace element concentrations (ppm)	**Na** (88)	1210	1555	1119	1476	858	5908	1934	2217	1127	827	2766
		Al (5967)	37766	34368	10575	18690	15537	94042	150100	159897	11782	166752	101715
		K (555)	5840	9478	4282	5211	4014	21738	23558	24765	4163	6758	23596
		Ti (380)	1303	1527	489	770	602	4223	6500	5736	485	5699	5523
		V (2)	143	31	16	16	23	135	96	108	20	47	102
		Cr (2)	130	31	16	21	33	109	86	88	50	60	74
		Fe (264)	18847	13976	5337	7807	6340	24258	22113	21984	6354	33480	28712
		Mn (2)	75	91	67	85	42	87	72	75	82	57	77
		Ni (0.3)	77	14	6	8	10	110	30	29	8	55	32
		Mo (0.2)	47	2	1	3	3	61	2	1	3	16	1
		Rb (10)	37	39	22	26	20	107	123	154	18.6	28	97
		Sr (11)	392	298	328	204	183	422	147	163	473	516	119
		Zr (3)	21	36	12	19	14	73	107	91.3	13.8	19	107
		LREE (6)	104	156	20	64	49	250	314	363	49	61	161
		HREE (0.1)	13	20	3	9	8	30	35	40	11	11	19
	Elemental ratios	**Fe/Al**	0.23	0.41	0.50	0.42	0.41	0.26	0.15	0.14	0.54	0.21	0.54
		Al/ (Al+Fe+Mn)	0.80	0.71	0.66	0.70	0.71	0.79	0.87	0.88	0.64	0.83	0.78
		Y/Ho	38.07	28.08	36.96	30.64	36.36	26.44	20.50	23.06	33.63	39.02	16.63
		Pr/Pr*$_{(SN)}$	1.10	0.99	1.03	1.01	1.06	1.05	1.00	0.99	1.02	1.12	1.05
		Ce/Ce*$_{(SN)}$	0.73	1.01	0.79	0.95	0.76	0.96	1.09	1.08	0.91	0.60	0.99
		Er/Nd $_{(SN)}$	0.073	0.045	0.093	0.061	0.077	0.045	0.048	0.041	0.081	0.074	0.048
	Redox Indicators	**Mn***	-0.32	-0.44	-0.15	-0.21	-0.43	-0.70	-0.74	-0.72	-0.14	-1.02	-0.82
		V/V+Ni	0.65	0.69	0.74	0.67	0.68	0.55	0.76	0.79	0.72	0.46	0.76
		Fe_T/Al	0.49	-	0.42	-	0.40	0.15	0.26	0.14	0.20	0.20	0.54
		Fe_{HR}/Fe_T	0.83	-	0.86	-	0.91	0.74	0.73	0.59	0.56	0.91	0.61
		Fe_{Py}/Fe_{HR}	0.68	-	0.46	-	0.73	0.13	0.63	0.56	0.48	0.85	0.33

Table 3.2 *In situ* elemental concentration data of dolomite

Sample		Well (Depth)	Z26D-2 11280	TOT-3 14210	UD-171 16245	UD-171 16248
Dolomite (LA-ICP-MS)	Minor and trace element concentrations	**Analyte** (DL)	Max. **Avg.** Min.			
		Na (200) ppm	1819 **728** 356	1787 **1139** 608	2865 **1067** 650	829 **657** 530
		K (0.01) wt.%	11.52 **2.89** 0.7	8.87 **4.45** 0.76	10.58 **2.16** 0.56	3.51 **1.82** 0.48
		Ti (0.1) ppm	105 **52** 42	1787.2 **1139** 608.3	91 **46** 37	57 **48** 40
		V (4) ppm	204 **108** 74	1787 **1139** 608	29 **7** 3	19 **11** 4
		Cr (21) ppm	180 **77** 41	28 **16** 5	35 **10** 5	25 **15** 6
		Fe (0.18) wt.%	1.38 **0.4** 0.13	1.98 **1.09** 0.54	2.14 **0.65** 0.15	0.47 **0.26** 0.07
		Mn (14) ppm	114 **79** 55	169 **125** 98	203 **139** 98	52 **41** 34
		Ni (5.4) ppm	143 **36** 15	20 **12** 5	23 **11** 4	11 **9** 4
		Y (3) ppm	49 **19** 12	29 **20** 14	19 **9** 6	36 **17** 11
		Ho (0.13) ppm	1.42 **0.5** 0.31	0.95 **0.71** 0.45	0.70 **0.32** 0.17	1.95 **0.55** 0.29
		Sr (19) ppm	591 **467** 398	744 **361** 256	334 **212** 43	220 **190** 163
	Elemental ratios	**Y/Ho**	50.37 **39.27** 34.49	31.16 **27.79** 23.30	38.26 **29.02** 24.41	45.34 **37.44** 31.53
		Pr/Pr*	0.98 **0.94** 0.80	0.90 **0.83** 0.75	0.94 **0.84** 0.77	0.97 **0.93** 0.89
		Er/Nd	0.10 **0.08** 0.06	0.08 **0.05** 0.04	0.08 **0.07** 0.05	0.32 **0.11** 0.08
		Ce/Ce*	1.03 **0.71** 0.63	1.21 **0.99** 0.91	0.98 **0.91** 0.85	0.74 **0.66** 0.64
		Ce_{anom}	0.92 **0.63** 34.49	1.06 **0.87** 0.78	0.85 **0.84** 0.71	0.65 **0.57** 0.54
		Mn*	0.50 **0.15** -0.34	0.12 **-0.17** -0.42	0.78 **0.21** -0.39	0.45 **0.01** -0.27

Table 3.3. Iron speciation data and average TOC values of dolomitic black shales of the Maracaibo Ramp, and comparison with the analogous variations in Holocene and Jurassic anoxic deposits.

Location	Fe_{HR}/Fe_T	Fe_{Py}/Fe_T	TOC (wt. %)
Modern sediments deposited beneath anoxic bottom waters. Cariaco Basin, Venezuela	0.30 to 0.68[a]	0.49 to 0.69[b]	Average 3.8[b]
Dolomitic shales, Late Aptian- early Albian Cogollo Group, Venezuela (this work)	0.56 to 0.91	0.13 to 0.85	1.1. to 5.0
Kimmeridge Clay (Upper Jurassic, U.K.)	0.27 to 0.90[c]	0.53 to 1.0[c]	1.1 to 7.0[d]

a. Raiswell and Canfield (1998); b. Lyons and others (2003) c. Raiswell and others (2001) d. Pearce and others (2010)

Table 3.4. Environmental biomarker parameters for the Maracaibo Basin shales

Core	**Sol6**	**Sol6**	**Sol6**	**Sol6**	**Sol-6**	**Sol6**	**UD171**	**UD171**	**UD171**	**Z26-D2**
Depth [feet]	**18008**	**18018**	**18051**	**17464**	**17626**	**17631**	**16115**	**16245**	**16249**	**11280**
Sample #	1	2	3	4	5	6	7	8	9	10
% C_{29}[a)]	36	37	35	29	40	44	36	38	35	30
dia C_{27}[b)]	0.66	3.1	1.6	0.11	2.4	1.6	0.74	1.1	0.64	0.15
dia C_{28} [b)]	0.61	2.7	1.3	0.09	1.7	1.9	0.68	0.99	0.54	0.21
dia C_{29}[b)]	0.44	2.5	0.95	0.05	1.5	1.5	0.64	0.77	0.38	0.12
dia $C_{27\text{-}29}$[c)]	0.57	0.50	0.60	0.58	0.46	0.44	0.46	0.50	0.58	0.55
$CPI_{26\text{-}34}$[d)]	0.98	1.1	0.94	0.93	1.2	1.3	1.1	1.1	0.90	(0.65)*
C_{26}/C_{25}[e)]	0.73	0.72	0.51	0.65	0.90	0.76	0.71	0.62	0.66	0.44
C_{30} βα/αβ[f)]	0.07	0.11	0.05	0.05	0.14	0.15	0.11	0.07	0.05	0.06
AIR-2[g)]	0.36	3.80	2.45	0.52	5.3	2.89	0.75	0.14	0.12	---
Pr/Ph[h)]	0.43	0.99	0.61	0.29	2.8	3.4	0.97	0.41	0.33	0.39
TPP[i)]	0.38	0.71	0.76	0.84	0.76	0.84	0.55	0.60	0.55	0.47
C_{31} 2α-MHI[j)]	4.9	3.9	3.0	3.4	3.4	3.2	6.6	3.3	2.3	4.0
C_{31} 3β-MHI[k)]	6.3	4.6	5.5	1.5	2.0	1.8	3.1	4.7	7.3	2.2
HHI[l)]	14	12	12	9.3	4.0	3.6	5.1	16	19	12
GI[m)]	5.9	2.8	18.2	7.9	1.1	1.4	2.8	12.3	12.9	9.2
Ster/Hop[n)]	0.81	0.94	1.1	0.46	0.14	0.13	0.15	1.0	0.50	0.42
% C_{27}[a)]	38	37	41	37	35	32	40	37	41	45
$EOP_{15\text{-}23}$[p)]	1.4	1.0	1.1	1.3	0.97	1.0	1.1	1.1	1.2	1.0
28,30 BNH[q)]	0.05	0.01	0.01	0.04	0.02	0.01	0.02	0.01	0.01	0.01
DBT/Phen[r)]	0.22	0.10	0.24	1.6	0.36	0.20	n/a	0.19	0.95	2.4
C_{30} nor[s)]	0.043	0.029	0.033	0.12	0.028	0.034	0.065	0.025	0.055	0.074

Table 3.4 (Cont.) Definition of organic parameters (foonotes)

[a)]% C_x	Ratio using diasterane (βα) and regular sterane (ααα+αββ) S+R isomers, % C_x = C_x / ∑ C_{27}-C_{29}, where x = 27, 28 or 29
[b)]dia C_x	Diasterane (βα) ratio, C_x= C_x βα (S+R) /C_x (ααα+αββ) (S+R), x = 27, 28, or 29 steranes
[c)]dia C_{27-}	Average of dia C_{27} – dia C_{29}
[d)]CPI_{26-34}	Carbon preference index, CPI = 2 x (C_{27}+C_{29}+C_{31}+C_{33}) / [C_{26}+2x(C_{28}+C_{30}+C_{32})+C_{34}], (PETERS et al., 2005)
[e)]C_{26}/C_{25}	Tricyclic hopane ratio
[f)]C_{30} βα/αβ	C_{30} βα/αβ = C_{30} moretane (βα) / C_{30} regular (αβ) hopane
[g)]AIR-2	2,3,6-trimethyl Aryl Isoprenoid Ratio, AIR-2 = ∑C_{13}-C_{19} AI/∑ C_{20}-C_{26} AI, modified from Schwark and Frimmel (2004)
[h)]Pr/Ph	Acyclic isoprenoid ratio of pristane (Pr) and phytane (Ph)
[i)]TPP ratio	C_{30} tetracyclic polyprenoid ratio, TPP ratio = 2xC_{30} TPP 18α(H),21R/(2xC_{30} TPP 18α(H),21R + 13β,17α,20(S+R)-27-nordiacholestane + 5α14α,17α(29S+R)-27-norcholestane + 5α14β,17β(20S+R)-27-norcholestane) (Holba et al., 2003)
[j)]2α-MHI	C_{31} 2α-methylhopane index, 2β-MHI = C_{31} 2α-methylhopane/(C_{31} 2α-methylhopane+C_{30} αβ hopane) x 100 (SUMMONS et al., 1999)
[k)]3β-MHI	C_{31} 3β- methylhopane index, 3α-MHI = 3β-C_{31} methylhopane / (3β-C_{31} methylhopane + C_{30} αβ hopanes) x 100 (BROCKS et al., 2005)
[l)]HHI	Homohopane index of 17α,21β(H)-homohopanes, HHI = C_{35} αβ (S+R) x 100 / ∑C_{31} - C_{35}αβ (S + R) expressed in % (PETERS et al., 2005)
[m)]GI	Gammacerane (γ) index, GI = γ/(γ+C_{30} αβ hopane) x 100
[n)]Ster/Hop	Ster/Hop = ∑ C_{27} to C_{30} (βα+ααα+αββ) S+R steranes / ∑ C_{27} - C_{35} (αβ + βα + dia) S+R hopanes
[o)]% C_{30}	sterane ratio as in a), but including all C_{30} 24-*n*-propylsterane isomers
[p)]EOP_{15-23}	Even-Over-Odd predominance, *n*-alkane ratio, EOP_{15-23} = [0.5x(C_{16}+C_{18}+C_{20}+C_{22})/(C_{15}+C_{17}+C_{19}+C_{21})]+ [0.5x(C_{16}+C_{18}+C_{20}+C_{22})/(C_{17}+C_{19}+C_{21}+C_{23})], modified from Bray & Evans (1961)
[q)]28,30 BNH	Ratio of 28,30 bisnorhopane (BNH), BNH = BNH/C_{30} αβ hopane
[r)]DBT/Phen	Ratio of dibenzothiophene (DBT) and phenanthrene (Phen), (HUGHES et al., 1995)
[s)] C_{30} nor	C_{30} 30-norhopane ratio, C_{30} nor = C_{30} 30-norhopane /C_{30} αβ hopane

* = low signal-to-noise level, n/a = not available, '---' = not detected

Table 3.5. Environmental biomarker parameters for the Maracaibo ramp shales.

	Proxy[a)]	Source and interpretation	References
Category 1	$\%C_{29}$	The terrestrial organic matter is characterized by high relative abundances of the C_{29} sterane that derives from higher plants.	(Huang and Meinschein, 1979)
	$diaC_{27-30}$	High clay relative to organic matter contents cause sterane rearrangement leading to elevated diasterane/sterane ratios, hence the ratio is commonly low in carbonates.	(Rubinstein et al., 1975; van Kaam-Peters et al., 1998)
	CPI_{26-34}	*n*-Alkanes in the carbon range C_{26} to C_{34} with an odd-over-even predominance are commonly derived from plants waxes. A ratio > 1 is indicative of terrestrial plant input.	(Bray and Evans, 1961; Tissot and Welte, 1984)
	C_{26}/C_{25}	This tricyclic ratio is observed to be > 1 in many lacustrine settings.	(Zumberge, 1987)
	C_{30} βα/αβ	The relative abundance of moretane can be influenced by the source of organic matter (for example ferns, lichen, nitrogen-fixing bacteria) and the depositional environment (peat, coal or hypersaline and lacustrine settings). It was hypothesized that elevated moretane ratios in marine sediments might be indicative of input of higher plant material.	(Hveding-Bergseth et al., 1983; Wang, 2007)
	AIR-2	Aryl isoprenoids originate from oxidative cleavage of molecules carotenoids. Under oxidative conditions, cleavage is enhanced and yields progressively shorter chains, which results in a higher ratio.	(Schwark and Frimmel, 2004)
	Pr/Ph	The phytol side chain of chlorophyll can either be reduced to phytane (Ph, C_{20}) or oxidised to pristane (Pr, C_{19}). The ratio is usually < 0.5 in reducing and > 1 in oxic depositional environments, although source input may play a role.	(Ten Haven et al., 1988)
	TPP ratio	Some algae thriving in fresh or brackish water appear to produce elevated levels of tetracyclic polyprenoids, TPP	(Holba et al., 2000; Holba et al., 2003)
Category 2	3β-MHI	3β-methylhopanoids are believed to be produced by microaerophilic methanotrophs. High 3β-MHI is indicative of a high input of these methanotrophs.	(Summons and Jahnke, 1992; Brocks et al., 2005)
	HHI	The homohopane index is high relative to total hopanes in carbonate source rocks and anoxic settings.	(Peters and Moldowan, 1991; Peters et al., 2005)
	GI	Gammacerane is produced mainly by ciliates that thrive at the chemocline and feed on anoxygenic phototrophs. A high ratio relative to C_{30} hopane is therefore usually observed in stratified systems.	(Sinninghe Damsté et al., 1995)
	Ster/ Hop	Terrestrial soil communities typically produce a higher proportion of bacterial hopanes than marine environments where eukaryotic steranes are more abundant. Marine settings usually have a Ster/Hop ratios >1.	(Moldowan et al., 1985)
	$\%C_{27}$	Marine plankton produces high C_{27} (cholestane) relative to C_{29} steranes. Therefore, this ratio is higher if marine algal biomass is abundant	Cao et al., 2009)
	$\%C_{28}$	Relative C_{28} sterol abundances are less source-specific, but suggest higher contribution of modern green algae	(Huang and Meinschein, 1979; Schwark and Empt, 2006)
	$\%C_{30}$	C_{30} sterols with *n*-propylcholestane skeleton occur in algae of the order *Sarcinocrysidales* and in foraminifera. They are diagnostic for marine organic matter.	(Moldowan et al., 1990; Grabenstatter et al., 2013)
	EOP_{15-23}	*n*-Alkanes in the carbon range C_{15} to C_{23} with an odd-over-even predominance are commonly derived from cyanobacteria or algae. Therefore, EOP_{15-23} may be low if algal or bacterial contributions are high	(Bray and Evans, 1961; Tissot and Welte, 1984)
	28,30 BNH	28,30 BNH was observed to be high in reducing conditions.	(Schoell et al., 1992)
	DBT/Phen	The sulfur-containing molecule DBT is an indicator for sulfur availability in the depositional environment. A ratio of > 1 is indicative for high-sulfur availability.	(Hughes et al., 1995)
	30nor	The relative abundance of C_{30} 30-norhopane is observed to be high in carbonate settings.	(Ten Haven et al., 1988)

a) A formal definition of all ratios is given in the footnotes of Table 3.4.

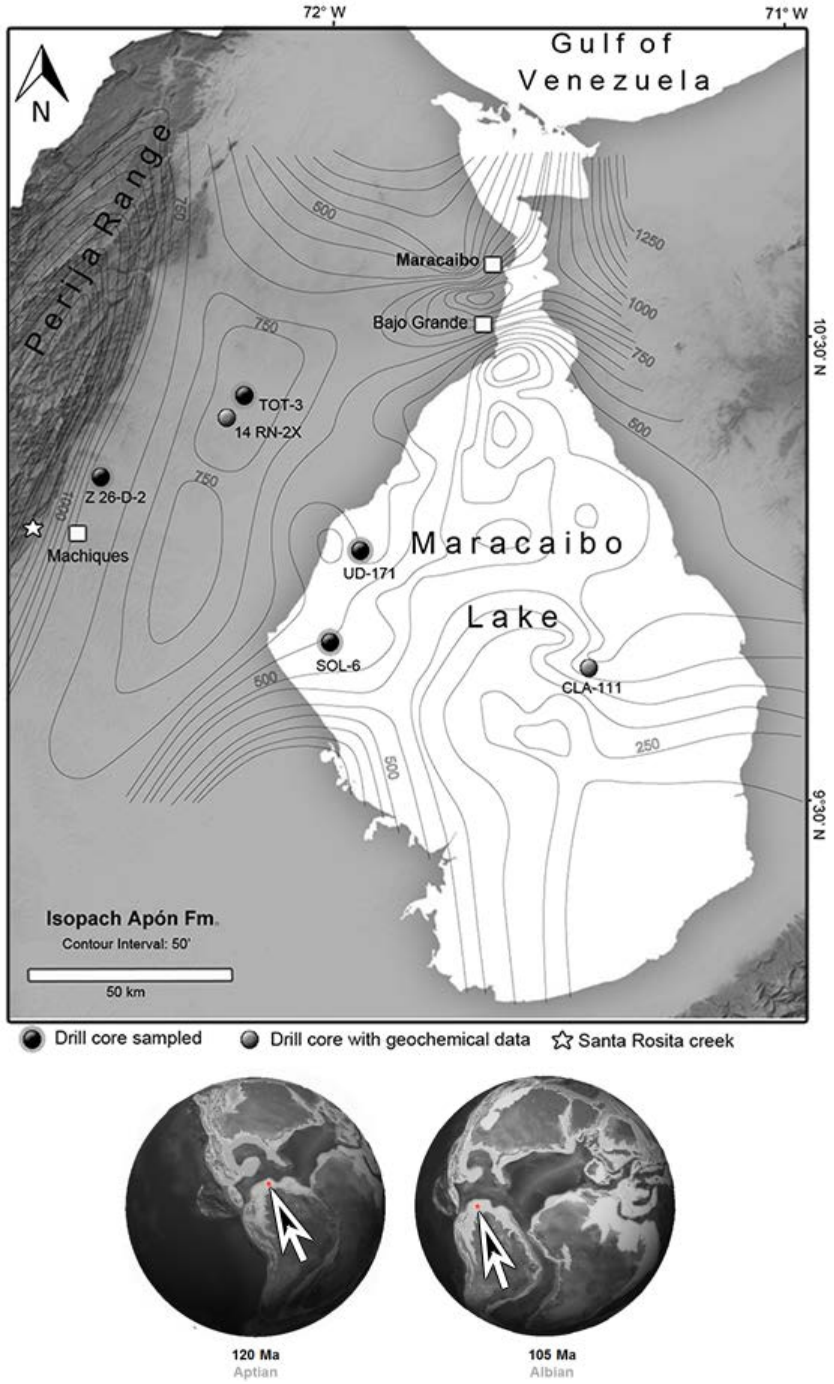

Figure 3.1. Study area and location of the well cores. The contour intervals (isopach map) approximate to the paleobathymetry at the time of deposition of the Apón Formation. It also shows the near equatorial paleogeographic location of the ramp during the Aptian to Albian transition (Paleogeography from Colourado Plateau Geosystems, http://www2.nau.edu/rcb7, July 2014).

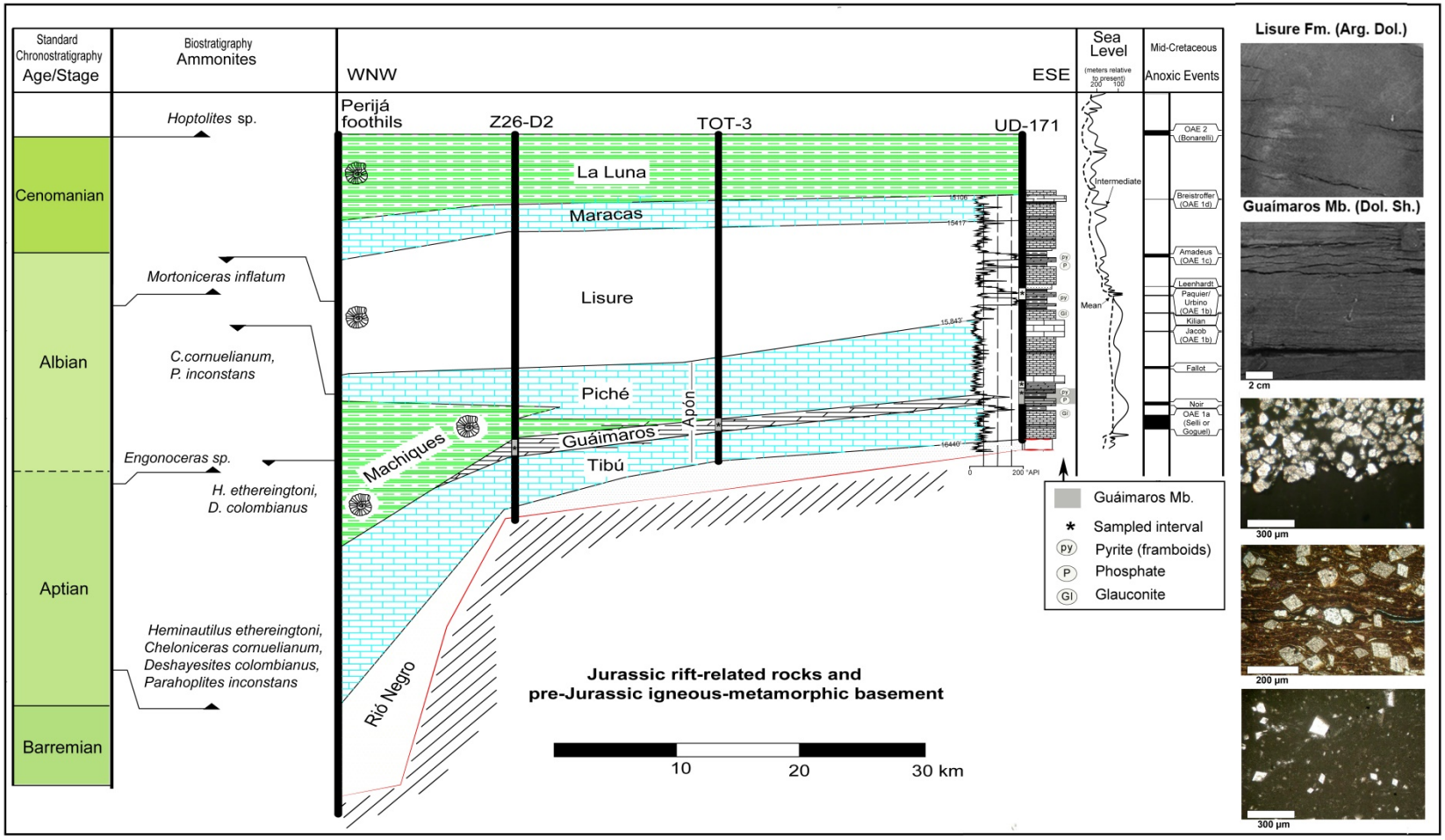

Figure 3.2. The mid-Cretaceous stratigraphic context of western Venezuela. Samples are from four oil exploration drill cores. Ammonite zonation is as defined by Renz (1982) with data from a section outcropping at Santo Rosita Creek in the Perijá Foothills. Also shown are two representative core sections and the range of lithologies from dolomitic shale to argillaceous dolomite.

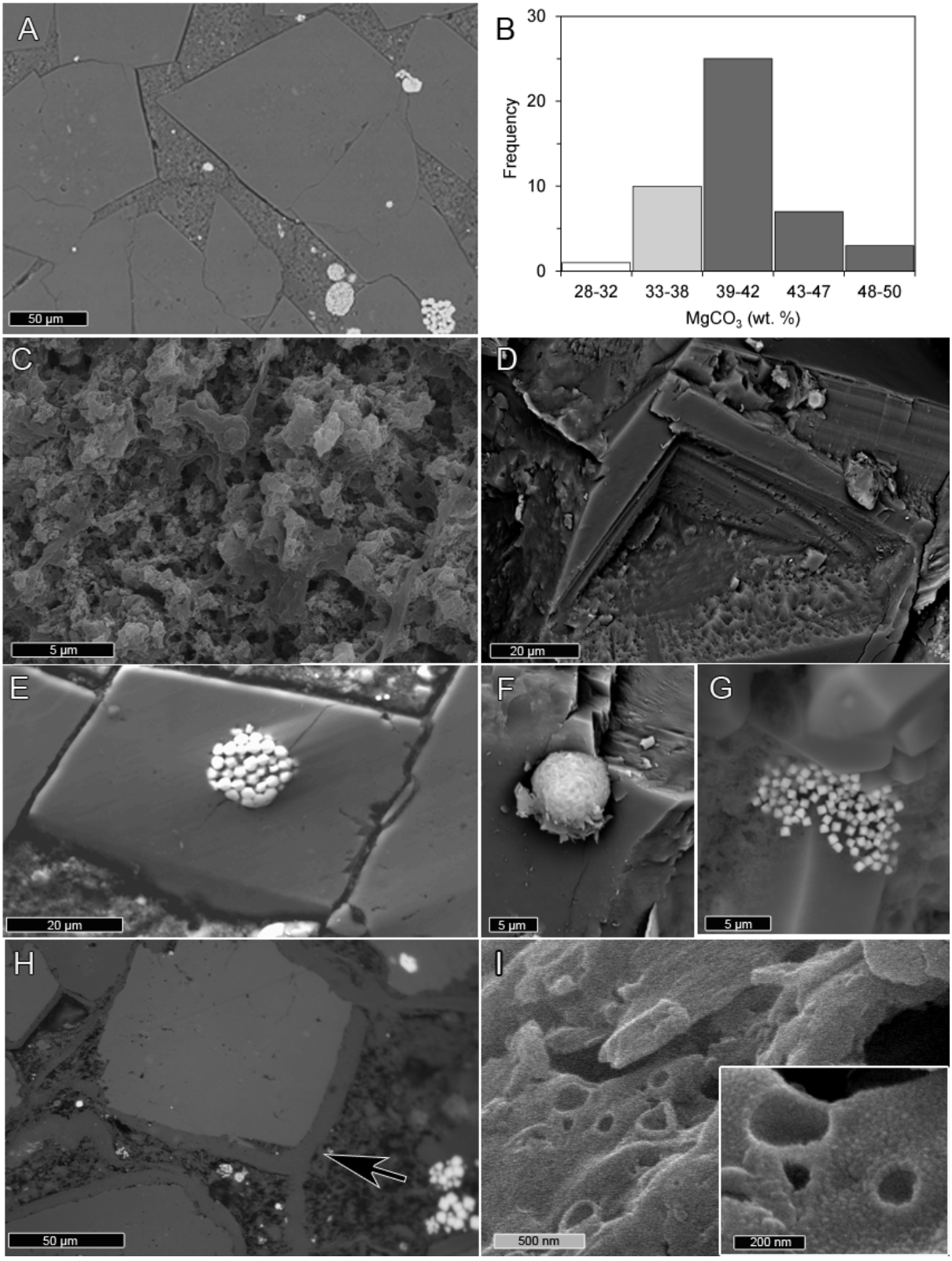
A
50 µm
B
30
20
10
0
Frequency
28-32
33-38
39-42
43-47
48-50
MgCO3 (wt. %)
C
5 µm
D
20 µm
E
20 µm
F
5 µm
G
5 µm
H
50 µm
I
500 nm
200 nm

Figure 3.3. Textural features. Dolomite crystals interfaces range from planar-e to planar-s (A). Note the abundance of framboidal pyrite. Most dolomite is Ca-enriched (B). After partial leaching with 10% HCl, the crystals exhibit features that are suggestive of multigenic origin. In the crystal cores, it is possible to observe features that look quite similar to modern Ca-dolomite (C); the crystal cortices, on the other hand, are less soluble (Mg enriched) and do not exhibit such features. Some cortices are also compositional heterogeneous, and might be Fe enriched (D). Pyrite framboids are often embedded within dolomite (E-F), these are also present in the matrix, which and also show aggregates of equant pyrite, which are here shown within authigenic quartz (G-H). Chalcedony can form thin micrometer scale veneers (arrow) around dolomite crystals (H). Within these veneers, there are microtextural features suggestive of an early silicification process of a biofilm (G).

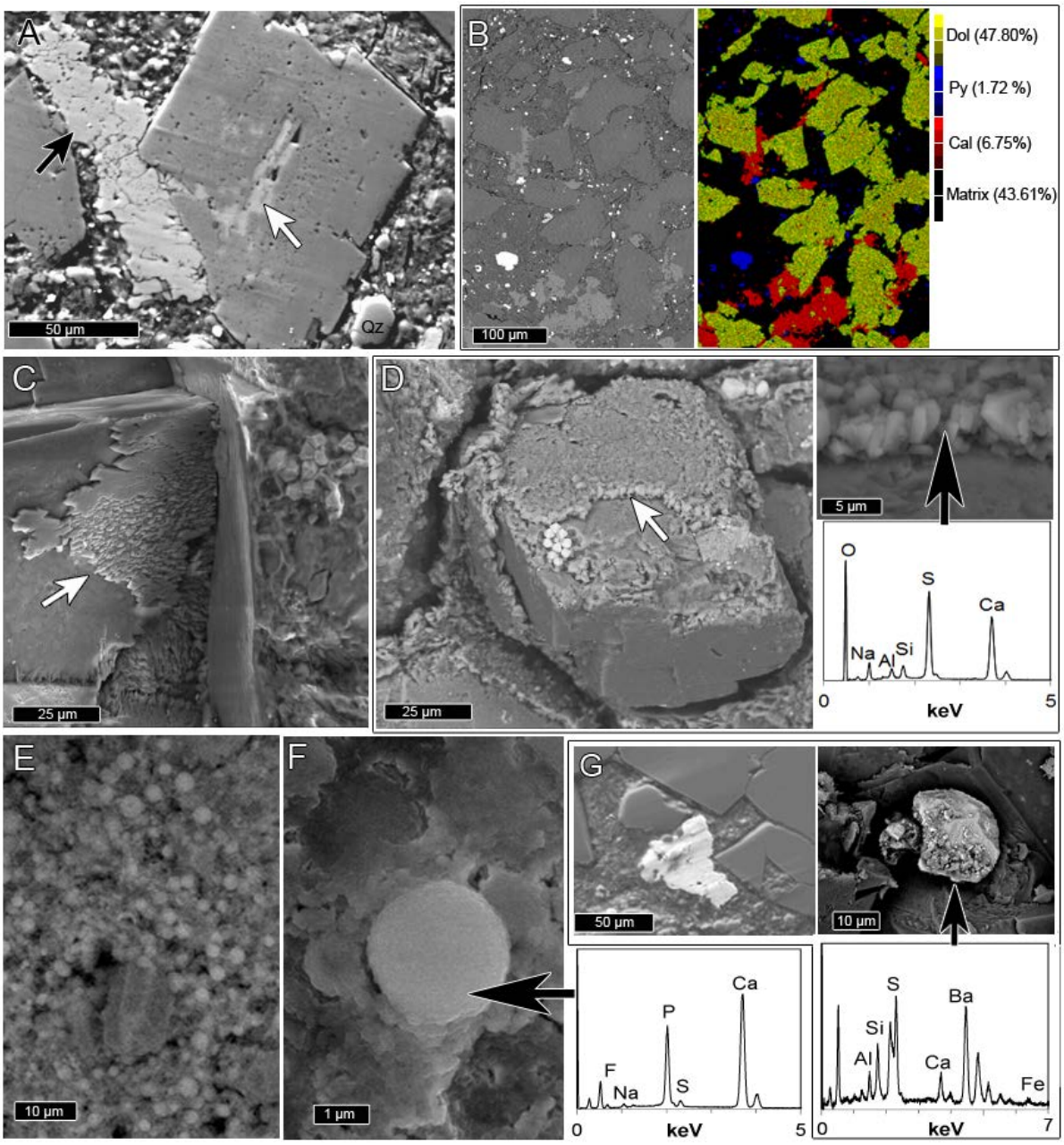

Figure 3.4. Textural features II. Calcite overgrowths might be associated with corroded dolomite crystals. In other wells, it was observed that the dolomite crystals are coated by equant gypsum overlays that show planar interfaces caused by normal stress across the gypsum-clay contacts (C-D). Cryptocrystalline Ca-fluorapatite is quite common within the matrix material (E-F). Subordinate amounts of barite have been also observed (G).

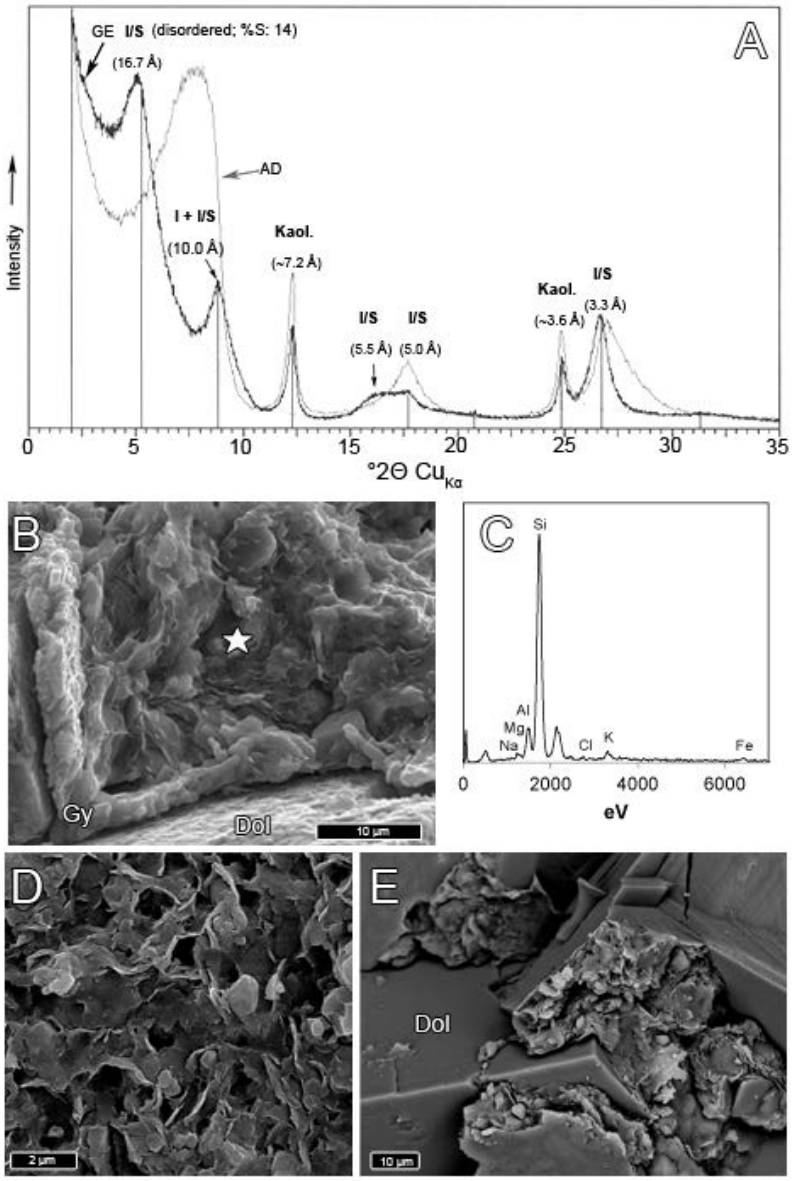

Figure 3.5. Clay X-ray powder diffraction analyses. The calculated X-ray powder diffraction profiles illustrate the identification procedures for illite, illite/smectite, and kaolinite; the d-spacing values from 2θ Cu_Kα radiation diffraction angles are labeled (A); the representative sample (TOT-3 14210) has 40% smectite within disordered I/S layers (GE: ethylene glycol spectrum; AD: air dried spectrum). Slightly crenulated sodium-bearing clay minerals, as shown via EDS (B-D), "D" is a zoom over the area analyzed via EDS (Gy: Gypsum, Dol: dolomite). Pore-filling clays are often packed within dolomite overgrowths (E).

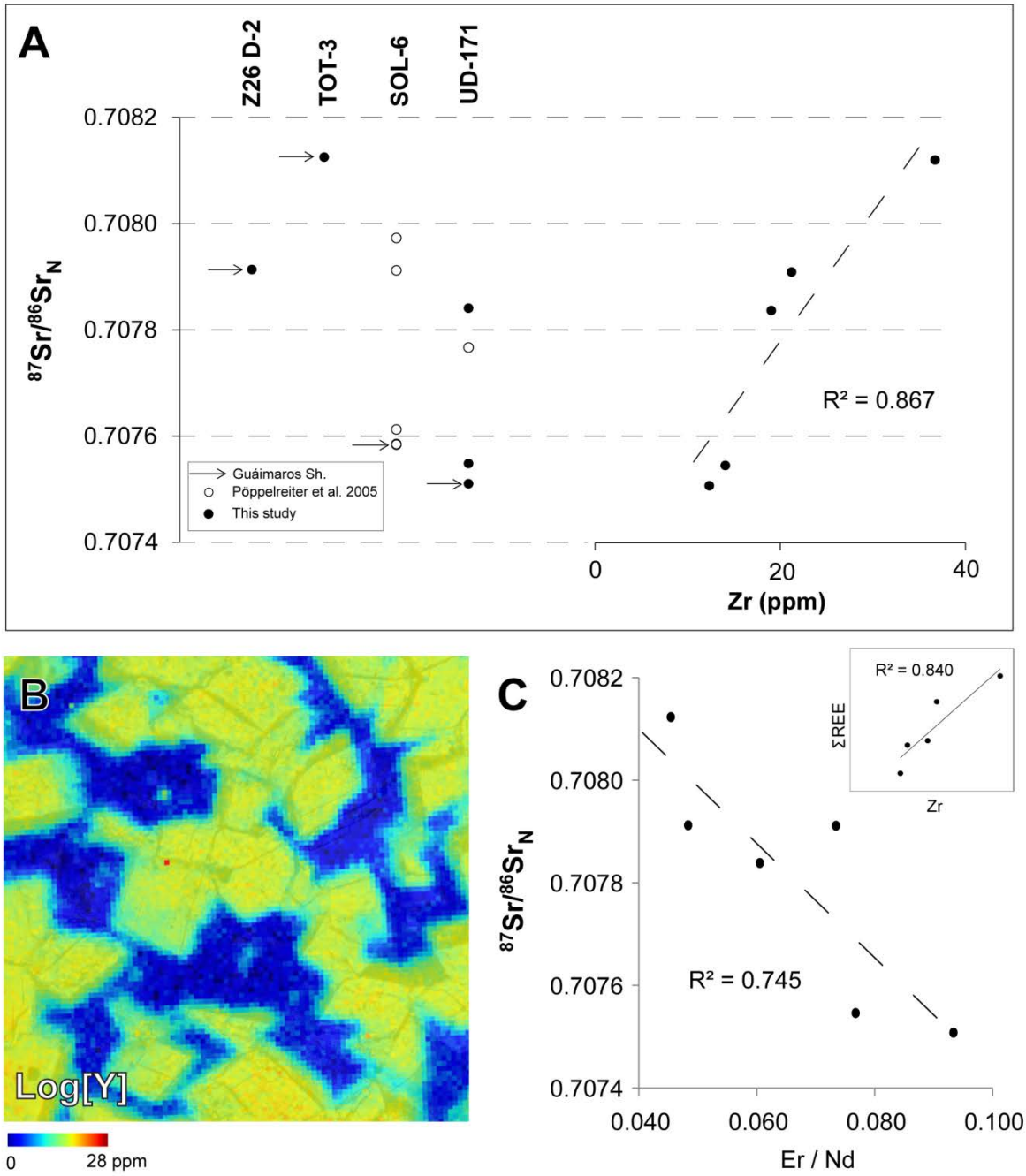

Figure 3.6. Strontium $^{87}Sr/^{86}Sr$ values range from 0.70751 to 0.70812, with higher values observed towards the Perijá Range. There is a strong correlation between bulk rock [Zr] and the Sr-isotope signatures of the samples (A). The open circles represent samples studied by Pöppelreiter et al. (2005); the filled circles represent the dolomitic shales targeted in this study. TAs observed via µXRF, dolomite crystals in sample UD-171-16 245.8' showed a relatively homogenous distribution of Y, which is expected to be similar to that of HREE. The HREE/

LREE ratio of the samples (estimated by using their PAAS-normalized Er/Nd ratio) and the bulk concentrations of elements such as Zr, and K (not shown), were found to be strongly correlated with the measured 87Sr/86SrN values (C). The inset in "C" shows that there is also a strong correlation between Total REE and Zr, which account for the detrital nature of the observed Sr-isotope trends.

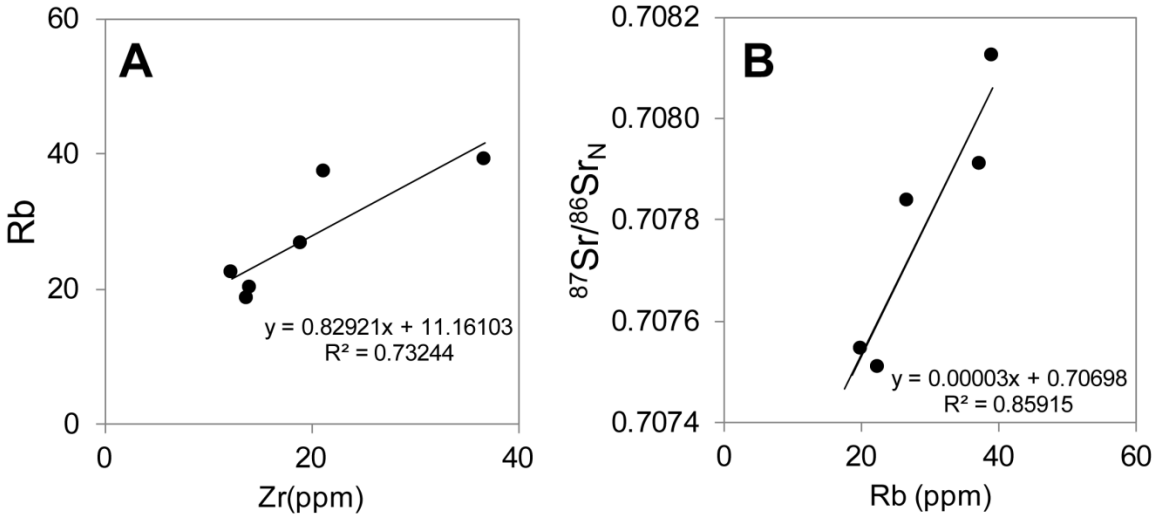

Figure 3.7. Binary plots of Rb vs. Zr and $^{87}Sr/^{86}Sr_N$ vs. Rb. A: Rb vs. Zr content. B: and 87Sr/86SrN vs. Rb content. This test of isotopic integrity is to establish whether initial isotope ratios correlate with trace element systematics (see Kamber et al., 2004 for details).

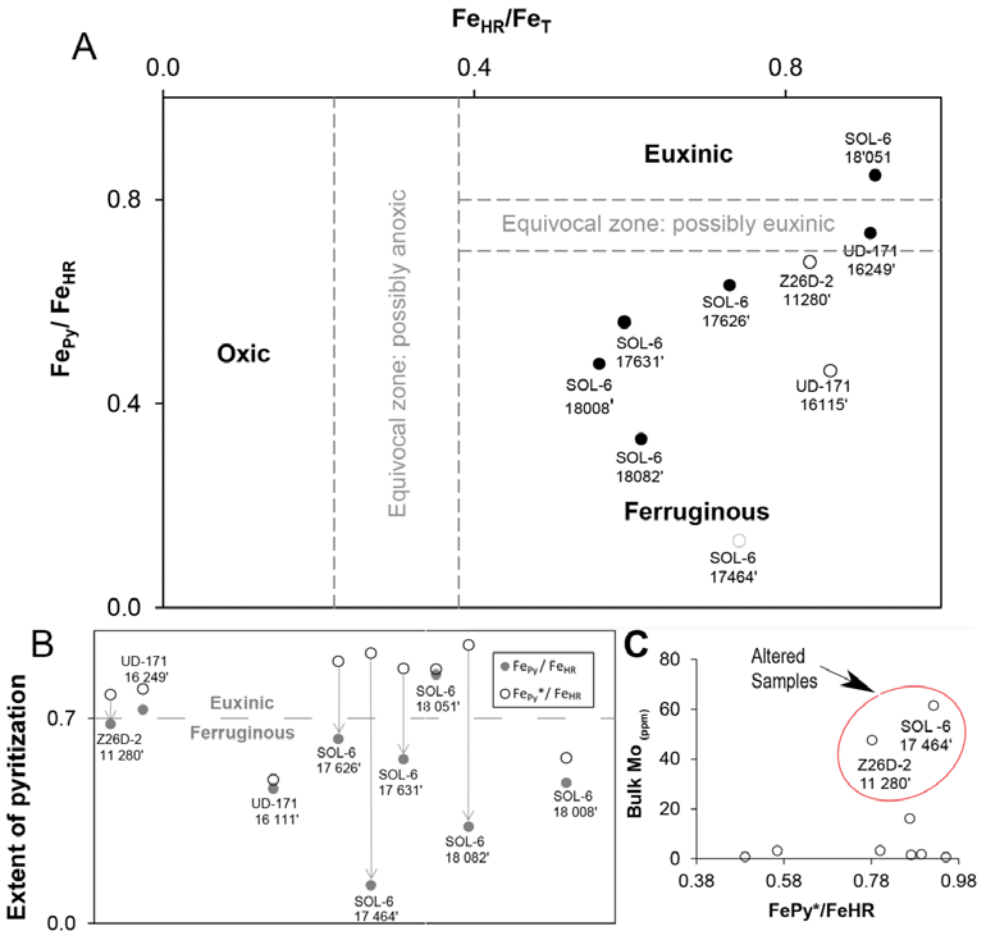

Figure 3.8. Iron Speciation data.Highly reactive iron to total iron ratios (Fe_{HR}/Fe_T) vs. the extent to which the Fe pool has been pyritized (Fe_{Py}/Fe_{HR}). Sediments deposited from anoxic waters commonly have Fe_{HR}/Fe_T greater than 0.38, while Phanerozoic sediments deposited under oxygenated waters have ratios below 0.22. In anoxic sediments with Fe_{HR}/Fe_T greater than 0.38, Fe_{Py}/Fe_{HR} values greater than ~0.70 indicate deposition from a sulfidic water column, and values less than ~0.70 indicate deposition from a ferruginous water column. Our data that the Guáimaros Shale and its analogues were dominantly deposited under anoxic (ferruginous) water columns (A). An alteration test suggest that samples exhibiting a Fe_{py}* above 0.7 may be reflective of subaerial alteration; the upwelling of euxinic mid-depth waters would have readily titrated Fe(II) as pyrite. This indicates that the formation of Fe_{Ox} from the oxidation of pyrite would have affected the original Fe_{Py}/Fe_{HR} to make appear initially euxinic samples as ferruginous (B). Only samples exhibiting relatively high [Mo] are considered as altered by pyrite oxidation and potentially deposited under euxinic conditions (C)

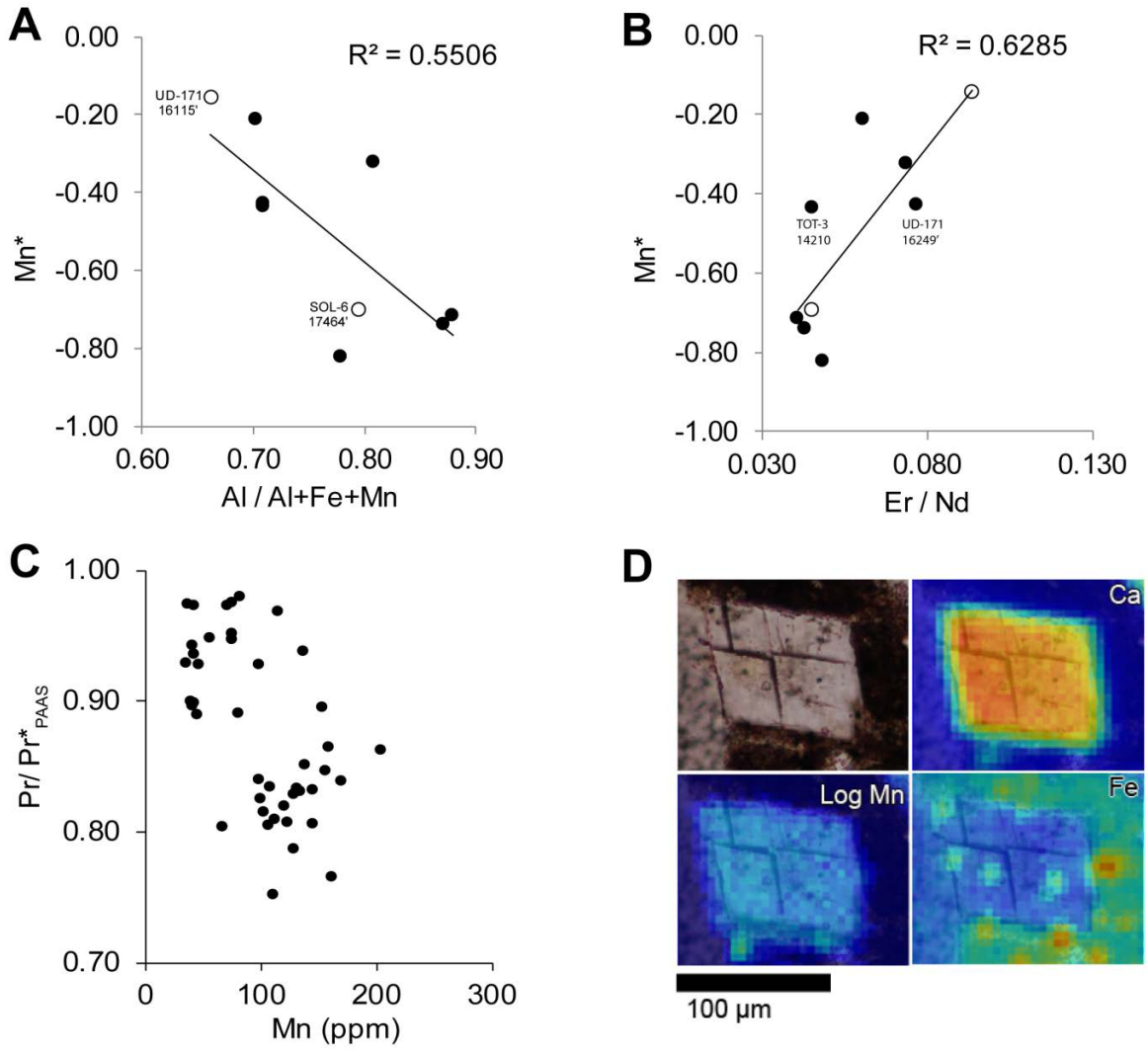

.

Figure 3.9. Mn* redox parameter and its relation to indicators of terrigenous influx. The samples characterized by a larger terrigenous supply [high Al/(Al + Fe + Mn) ratios], exhibit more negative Mn* values indicating strongly reducing conditions during deposition (A). The relation between the Mn* parameter and the HREE/LREE ratio may be due to the ability of detrital organic material and oxyhydroxide mineral phases to concentrate Nd (LREE) with respect to Er (HREE), as such the longer the sediment-water interface was under geochemical conditions involving utilization of these biologically reactive phases, the proportion of LREE into authigenic dolomite increase. The distribution of Mn vs. Fe as observed in sample UD-171-16 249' (D). The open circles represent samples from the Lisure Formation; the filled circles represent the dolomitic shales from the Guáimaros shale in the Apón Formation.

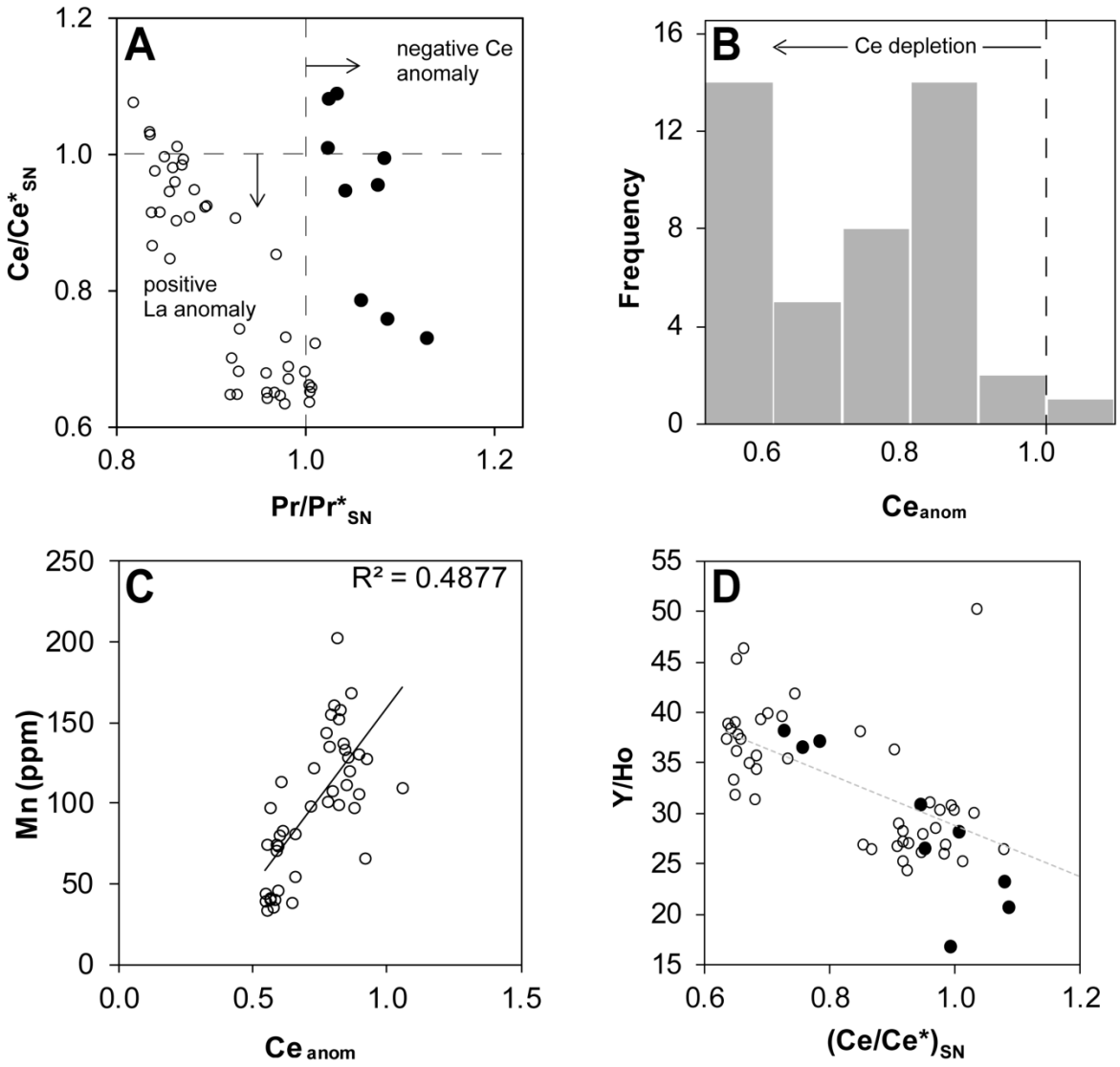

Figure 3.10. Cerium and lanthanum anomalies in the studied black shales. A binary plot help discriminates between apparent La and Ce anomalies. Most of the laser ablated dolomite phases reflect a positive La anomalies (A). It is possible to normalize the Ce abundances to those of its neighboring REE (Ce anomaly = 3 Ce/Ce_{SN}/ ($2La/La_{SN} + Nd/Nd_{SN}$)), yet it is important to mind that these are likely to be biased towards lower values due to the presence of the positive La anomaly. The arrow shows the direction of Ce depletion in seawater (i.e., complexation to particulate matter (B). There is some degree of correlation between Ce and Mn contents of dolomite (C). A variable degree of detrital contamination can be also inferred from the correlated variations between Y/Ho and La anomalies (D). The open circles represent samples analyzed via LA-ICP-MS; the filled circles represent solution-based ICP-MS measurements.

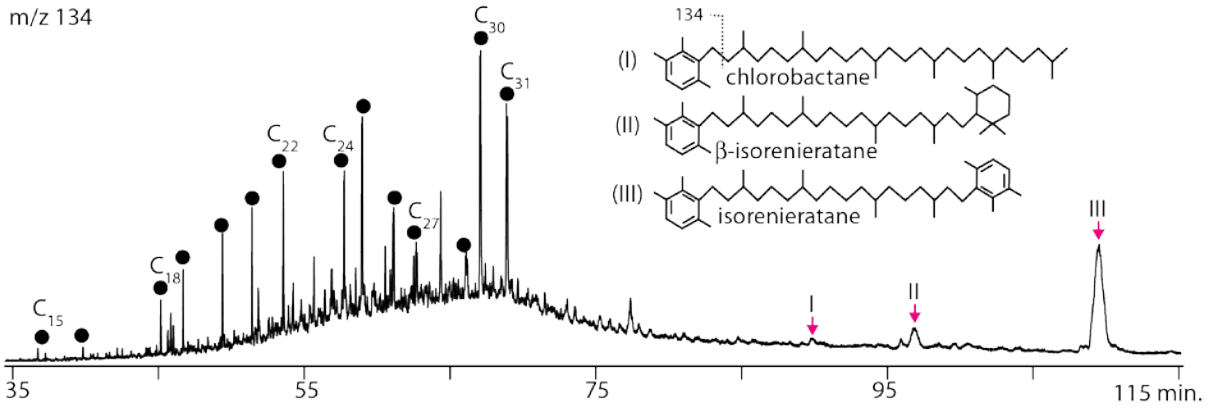

Figure 3.11. Aromatic carotenoids derivatives and 2,3,6 aryl isoprenoids (AI) in sample 08 (Table 3.3). In the Maracaibo ramp, the C_{31} homologue is presumably derived from oxidation and cleavage of a carotenoid with a β-carotene skeleton. C_x identifies the carbon number of AIs.

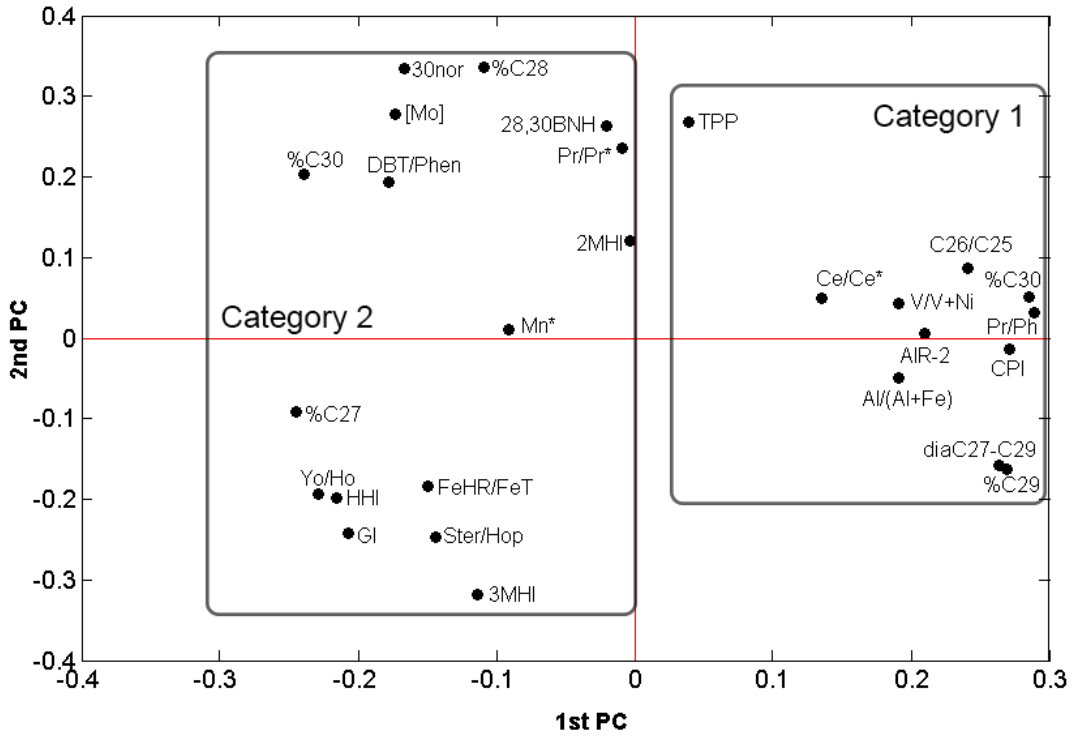

Figure 3.12. PCA of environmental proxies determined for samples from the Maracaibo ramp. See also Table 3.5

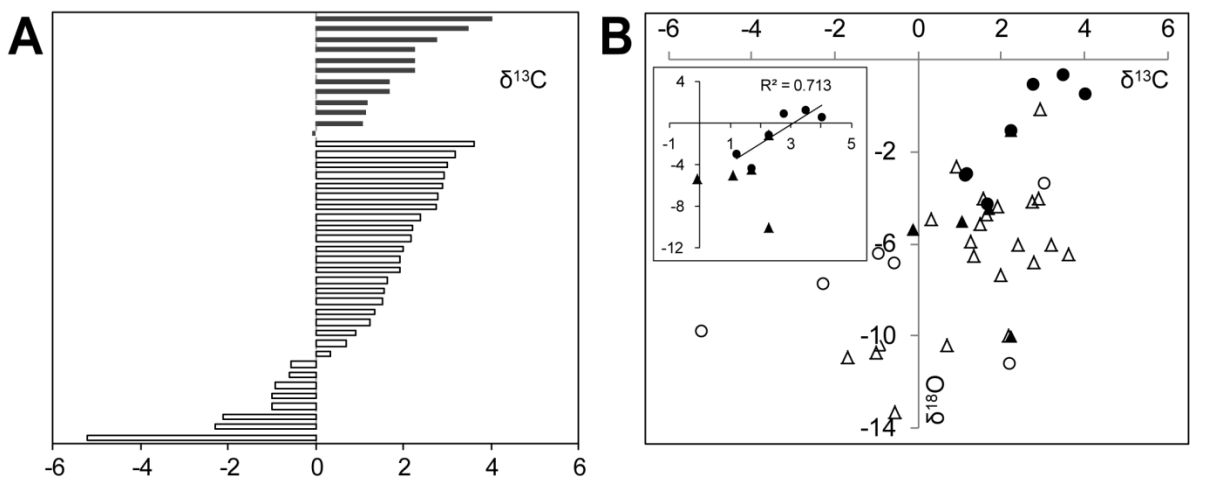

Figure 3.13. Stable C and O isotope signatures of the carbonate cements. Compiled carbonate C-isotope data from the Apón Formation (open bars) show a wider dispersion of $\delta_{13}C$ isotope values than values measured in the Guáimaros Shale. Carbonates in the Guáimaros Shale (filled bars) reflect a more significant contribution of marine-derived DIC (A). The binary plot shows $\delta^{13}C$ vs. $\delta^{18}O$ values of in the Apón Formation. Calcite coexisting with dolomite in calcified dolostones (triangles) and dolomitic shales (circles) shows ^{18}O depletion (about 5‰). Filled data points are data from the Guáimaros Shale.

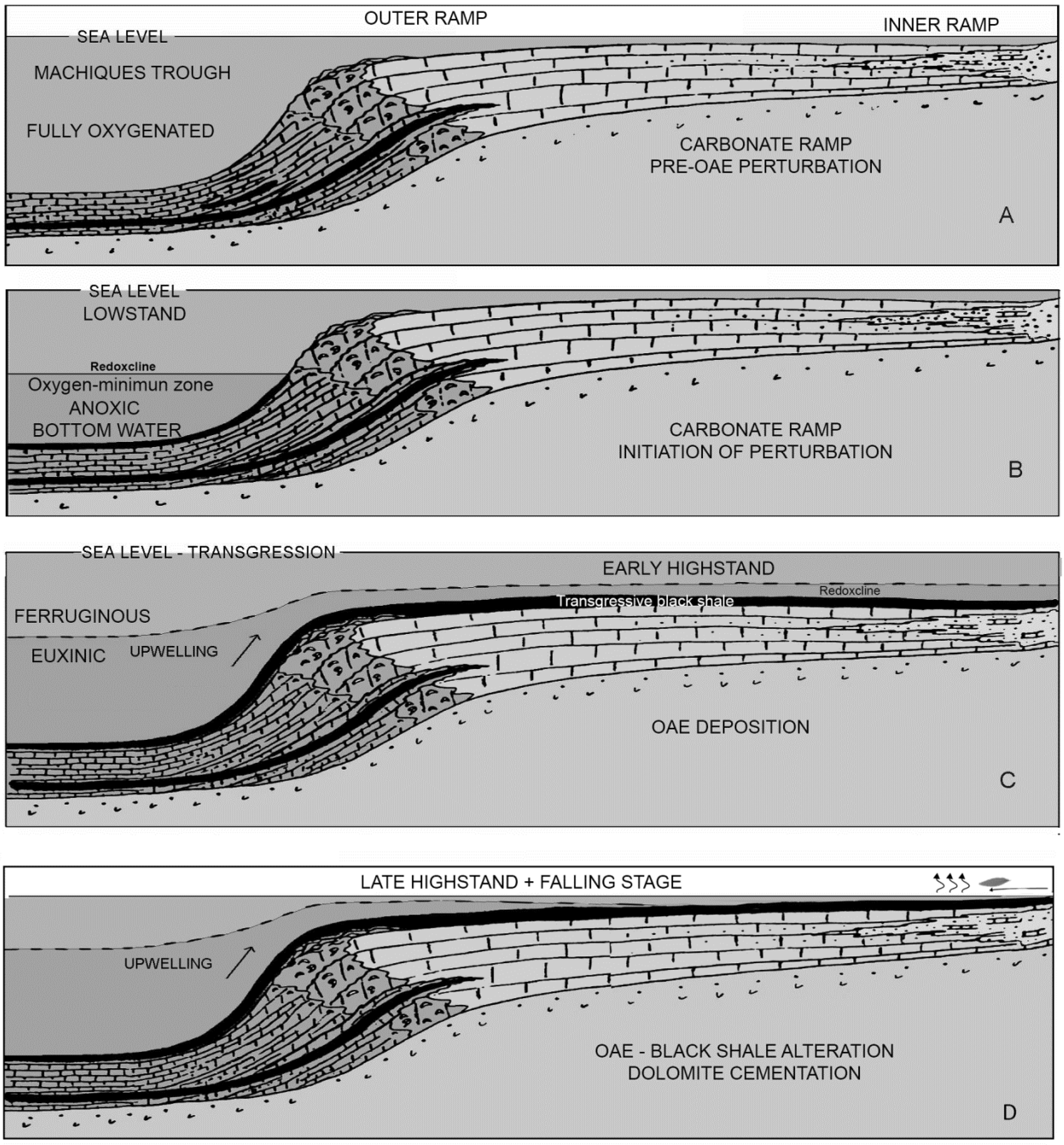

Figure 3.14. A model for the depositional environment of black shales in the mid-Cretaceous Maracaibo ramp throughout a single depositional cycle (After Mendez Dot et al., 2015). A pre-anoxic condition and normal oxygenation of the ocean waters in the Machiques sub-basin and Maracaibo ramp allowed for deposition of normal shallow marine carbonates (A). Initiation of anoxia is due to restriction of the basin followed by transgression, with oxygen exhausted euxinic waters transported from the sub-basin to the ramp by upwelling currents. This led to

transgressive black shale deposition in middle to inner ramp settings (B-C). As relative sea level felt, the organic rich fine-grained sediments were affected by extensive evaporation during semi-arid periods and transport of terrigenous and continental organic matter during wet monsoonal periods. The development of schizohaline conditions in the lagoonal setting favoured interstitial microbial dolomite formation (D).

3.7. References

Adams, D.D., Hurtgen, M.T., Sageman, B.B., 2010. Volcanic triggering of a biogeochemical cascade during Oceanic Anoxic Event 2. Nature Geoscience 3. doi:10.1038/ NGEO743.

Alberdi-Genolet, M. and Tocco, R., 1999. Trace metals and organic geochemistry of the Machiques Member (Aptian–Albian) and La Luna Formation (Cenomanian–Campanian), Venezuela. Chemical Geology 160, 19-38.

Alberdi-Genolet, M. and López, L., 2000. Biomarker 18α (H)-oleanane: a geochemical tool to assess Venezuelan petroleum systems. Journal of South American Earth Sciences 13, 751-759.

Anderson, T.F., Raiswell, R., 2004. Sources and mechanisms for the enrichment of highly reactive iron in euxinic Black Sea sediments. Am. J. Sci. 304 (3), 203–233.

Arthur, M.A. and Schlanger. S.O., 1979 Cretaceous "Oceanic Anoxic Events" as causal factors in development of reef-reservoir giant oil fields. Bulletin of the American Association of Petroleum Geologists 63,8704385

Arthur, M.A., Dean, W.E., and Stow, D.A.V.,1984. Models for the deposition of Mesozoic-Cenozoic fine-grained organic-carbon-rich sediment in the deep sea. In Stow, D.A.V. and Piper D.J.W Deep-water processes and facies (eds.), Geo- logical Society Special Publication 15, 527-562

Arthur, M.A., Dean, W.E., Schlanger, S.O., 1985. Variations in the global carbon cycle during the Cretaceous related to climate, volcanism, and changes in atmospheric CO_2. American Geophysical Union Monographs 32, 504-529.

Arthur, M. A., Jenkyns, H. C., Brumsack, H.J., and Schlanger, S. O. 1990. Stratigraphy, geochemistry, and paleoceanography of organic-carbon rich Cretaceous sequences. In: Ginsburg, R.N., and Beaudoin, B. (eds.) Cretaceous Resources, Events and Rhythms. Kluwer Academic, Dordrecht, NATO AS1 Series, 304, 75–119.

Arthur, M.A. Sageman, B.B., 1994. MARINE BLACK SHALES: Depositional Mechanisms and Environments of Ancient Deposits. Annual Reviews Earth & Planetary Sciences 22, 499–551. doi:10.1007/s13398-014-0173-7.2

Audemard, F. E., 1991, Tectonics of western Venezuela: Ph.D. dissertation, Rice University, Houston, Texas, 245 p.

Barclay, R. S., J. C. McElwain, and Sageman B. B., 2010. Carbon sequestration activated by a volcanic CO_2 pulse during Ocean Anoxic Event 2, Nature Geoscience, 3(3), 205–208.

Barling, J., Arnold, G.L. and Anbar, A.D., 2001. Natural mass-dependent variations in the isotopic composition of molybdenum. Earth and Planetary Science Letters 193, 447–457.

Bathurst, R.G.C., 1986. Diagenetically enhanced bedding in argillaceous platform limestones: stratified cementation and selective compaction. Sedimentology 34, 740-778.

Bartok, P., Reijers, T., and Juhasz, I., 1981. Lower Cretaceous Cogollo Group, Maracaibo Basin, Venezuela: sedimentology, diagenesis, and petrophysics. Am. Assoc. Pet. Geol. Bull. 65, 1110–1134.

Bartok, P., 1993. Pre-breakup geology of the Gulf of Mexico– Caribbean: Its relation to Triassic and Jurassic rift systems of the region: Tectonics 12, 441–459.

Bau, M., Dulski, P., 1996. Distribution of yttrium and rare-earth elements in the Penge and Kuruman iron-formations, Transvaal Supergroup, South Africa. Precambrian Res 79:37–55.

Bau, M., Schmidt, K., Koschinsky, a., Hein, J., Kuhn, T., Usui, a., 2014. Discriminating between different genetic types of marine ferro-manganese crusts and nodules based on rare earth elements and yttrium. Chem. Geol. 381, 1–9.

Bellanca, A., Claps, M., Erba, E., Masetti, D., 1996. Orbitally induced limestone/marlstone rhythms in the Albian—Cenomanian Cismon section (Venetian region, northern Italy): Sedimentology, calcareous and siliceous plankton. Palaeogeogr. Palaeoclimatol. Palaeoecol. 126, 227–260.

Bellanca, A., Masetti, D., Neri, R., 1997. Rare earth elements in limestone/marlstone couplets from the Albian-Cenomanian Cismon section (Venetian region, northern Italy): assessing REE sensitivity to environmental changes. Chem. Geol. 2541, 141–152.

Berner, R., 1984. Sedimentary pyrite formation: an update. Geochim. Cosmochim. Acta 48, 605–615.

Biebl, H., and Pfennig, N., 1978. Growth yields of green sulfur bacteria in mixed cultures with sulfur and sulfate reducing bacteria. Archives of microbiology 117, 9-16.

Bieger, T., Abrajano, T., and Hellou, J., 1997. Generation of biogenic hydrocarbons during a spring bloom in Newfoundland coastal (NW Atlantic) waters. Organic geochemistry 26, 207-218.

Bishop, W.F., 1975. Geology of Tunisia and Adjacent Parts of Algeria and Libya. Am. Assoc. Pet. Geol. Bull. 59, 413–450.

Bralower, T., Fullagar, P., 1997. Mid-Cretaceous strontium-isotope stratigraphy of deep-sea sections. GSA Bull. 109, 1421–1442.

Bralower, T., and Lorente, M., 2003, Paleogeography and stratigraphy of the La Luna Formation and related Cretaceous anoxic depositional systems. Palaios18, 301–304.

Bravo, J. M., Perzl, M., Härtner, T., Kannenberg, E. L., and Rohmer, M., 2001. Novel methylated triterpenoids of the gammacerane series from the nitrogen-fixing bacterium *Bradyrhizobium japonicum* USDA 110. European Journal of Biochemistry 268, 1323-1331.

Bray, E.E., and Evans, E.D., 1961. Distribution of n-paraffins as a clue to recognition of source beds. Geochimica et Cosmochimica Acta 22, 2-15.

Brocks, J. and Summons, R., 2003. Sedimentary hydrocarbons, biomarkers for early life.
Treatise on geochemistry 8, 63-115.

Brocks, J. J., Love, G. D., Summons, R. E., Knoll, A. H., Logan, G. A., and Bowden, S. A., 2005. Biomarker evidence for green and purple sulphur bacteria in a stratified Paleoproterozoic sea. Nature 437, 866-870

Brocks, J. J. and Schaeffer, P., 2008. Okenane, a biomarker for purple sulfur bacteria (Chromatiaceae), and other new carotenoid derivatives from the 1640Ma Barney Creek Formation. Geochimica et Cosmochimica Acta 72, 1396–1414.

Brooks, J., Gould, K., and Smith, J., 1969. Isoprenoid hydrocarbons in coal and petroleum. Nature 222, 257–259.

Browning, E.L., and Watkins, D.K., 2008. Elevated primary productivity of calcareous nannoplankton associated with ocean anoxic event 1b during the Aptian/Albian transition (Early Cretaceous), Paleoceanography, 23, PA2213.

Bottini, C., Erba, E., Tiraboschi, D., Jenkyns, H.C., Schouten, S., Sinninghe-Damsté, J.S., 2014. Climate variability and relationship with ocean fertility during the Aptian Stage. Clim. Past Discuss. 10, 689–738. doi:10.5194/cpd-10-689-2014

Budd, D., 1997. Cenozoic dolomites of carbonate islands: their attributes and origin. Earth-Science Rev. 42, 1–47

Budyko, M.I., Ronov, A.B., Yanshin, A.L., 1987. History of the Earth's Atmosphere. Springer Verlag, New York, USA, 139 pp.

Burke, K., 1976. Development of graben associated with the initial ruptures of the Atlantic Ocean. Tectonophysics 36, 93–112.

Butler, I., Rickard, D., 2000. Framboidal pyrite formation via the oxidation of iron (II) monosulfide by hydrogen sulphide. Geochim. Cosmochim. Acta 64, 2665–2672.

Canfield, D.E, Raiswell, R., Westrich, J., Reaves, C., Berner, R., 1986. The use of chromium reduction in the analysis of reduced inorganic sulfur in sediments and shales. Chem. Geol. 54, 149–155.

Canfield, D.E., Raiswell, R., Bottrell, S., 1992. The reactivity of sedimentary iron minerals toward sulfide. Am. J. Sci. 292, 659–683.

Cao, C., Love, G. D., Hays, L. E., Wang, W., Shen, S., and Summons, R. E., 2009. Biogeochemical evidence for euxinic oceans and ecological disturbance presaging the end-Permian mass extinction event. Earth and Planetary Science Letters 281, 188-201.

Castillo, M. V., and P. Mann, 2006, Cretaceous to Holocene structural and stratigraphic development in south Lake Maracaibo, Venezuela, inferred from well and three-dimensional seismic data: AAPG Bulletin 90, 529–564

Choquette, P.W., Hiatt, E.E., 2008. Shallow-burial dolomite cement: a major component of many ancient sucrosic dolomites. Sedimentology 55, 423–460.

Claps, M., Masetti, D., Pedrielli, E, Garavello, A.L., 1991. Analisi spettrale e cicli di Milankovitch in successione cretaciche del Sudalpino orientale. Riv. It. Strat. 92: 155-174.

Clarkson, M.O., Poulton, S.W., Guilbaud, R., Wood, R. a., 2014. Assessing the utility of Fe/Al and Fe-speciation to record water column redox conditions in carbonate-rich sediments. Chem. Geol. 382, 111–122.

Craig, H., 1957, Isotopic standards for carbon and oxygen and correction factors for mass-spectrometric analysis of carbon dioxide: Geochimica et Cosmochimica Acta, v. 12, p. 133-149.

Craig, H., 1961. Standards for reporting concentrations of deuterium and oxygen-18 in natural waters. Science, 133: 1833-1834.

de Baar, H., German, C., Elderfield, H., van Gaans, P., 1988. Rare earth element distributions in anoxic waters of the Cariaco Trench. Geochim. Cosmochim. Acta 52, 1203–1219.

de Baar, H.J.W., Schijf J., and Byrne, R.H., 1991. Solution chemistry of the rare earth elements in seawater. Euro. .I. Solid State Inorg. Chem 28, 357-373.

de Boer, P.L., and Wonders, A.A.H., 1984, Astronomically induced rhythmic bedding in Cretaceous pelagic sediments near Moria (Italy), in Berger, A., Imbrie, J., Hays, J., Kukla, G., and Saltzman, B., eds., Milankovitch and climate. Hingham, Massachusetts, Reidel, 177- 190.

Dembicki Jr, H., Meinschein, W. G., and Hattin, D. E., 1976b. Possible ecological and environmental significance of the predominance of even-carbon number C_{20}-C_{30} n-alkanes. Geochimica et Cosmochimica Acta 40, 203-208.

Davranche, M., Pourret, O., Gruau, G., Dia, A., Jin, D., Gaertner, D., 2008. Competitive binding of REE to humic acid and manganese oxide: impact of reaction kinetics on development of cerium anomaly and REE adsorption. Chem. Geol. 247, 154–170

Dewers, T., Ortoleva, P., 1994. Formation of stylolites, marl/limestone alternations, and dissolution (clay) seams by unstable chemical compaction of argillaceous carbonates.

Didky, B.M., Simoneit, B.R.T., Brassel, S.C., Eglinton, G., 1978. Organic geochemical indicators of palaeoenvironmental conditions of sedimentation. Nature 272, 216-222.

Dumitrescu, M. and Brassell, S. C., 2005. Biogeochemical assessment of sources of organic matter and paleoproductivity during the early Aptian Oceanic Anoxic Event at Shatsky Rise, ODP Leg 198. Organic geochemistry 36, 1002-1022.

Dymond, J., Suess, E. and Lyle, M., 1992. Barium in deep-sea sediment: A geochemical proxy for paleo-productivity. Paleoceanography, 7: 163-181.

Edwards, W., 1933. On the Cretaceous fern Paradoxopteris and its connexion with Weichselia. Ann. Bot.

Elias, V. O., Simoneit, B. R., and Cardoso, J. N., 1997. Even n-alkane predominances on the Amazon shelf and a Northeast Pacific hydrothermal system. Naturwissenschaften 84, 415-420.

Eglinton, G., Gonzalez, A. G., Hamilton, R. J., and Raphael, R. A., 1962. Hydrocarbon constituents of the wax coatings of plant leaves: A taxonomic survey. Phytochemistry 1, 89-102.

Erbacher, J., Thurow, J., Littke, R., 1996. Evolution patterns of radiolaria and organic matter variations: a new approach to identifying sea-level changes in mid-Cretaceous pelagic environments. Geology 24, 499–502.

Erbacher, J., Huber, B., Norris, R., Markey, M., 2001. Increased thermohaline stratification as a possible cause for an ocean anoxic event in the Cretaceous period. Nature 409, 325–327.

Erlich, R. N., Lorente, M.A.A., Palmer-Koleman, S., 1999. Geochemical characterization of oceanographic and climatic changes recorded in upper Albian to lower Maastrichtian strata, western Venezuela. Cretac. Res. 20, 547–581.

Escalona, A., Mann, P., 2006. An overview of the petroleum system of Maracaibo Basin. Am. Assoc. Pet. Geol. Bull. 90, 657–678.

Farrimond, P., Talbot, H., Watson, D., Schulz, L., and Wilhelms, A., 2004. Methylhopanoids: molecular indicators of ancient bacteria and a petroleum correlation tool. Geochimica et Cosmochimica Acta 68, 3873-3882.

Fisher, A. G. De Boer, P. L., and Premoli-Silva, I. 1990. Cyclostratigraphy. In: Ginsburg, R. N. and Beadoin, B., eds., Cretaceous Resources, Events and Rhythms: Background and Plans for Research. NATO ASI Series, Dordrecht, Klewer, 139-172.

Fisher, W. L., and Rodda, P. U., 1969. Edwards Formation (Lower Cretaceous), Texas: dolomitization in a carbonate platform system. AAPG Bulletin, 53(1), 55-72.

Föllmi, K.B.B., 2012. Early Cretaceous life, climate and anoxia. Cretac. Res. 35, 230–257.

Ford, A.B., Houbolt, J.J.H.C., 1963. The microfacies of the cretaceous of western Venezuela. EJ Brill, Leiden, 56 pp.

Frigaard, N.-U. and Bryant, D. A., 2006. Chlorosomes: antenna organelles in photosynthetic green bacteria, Complex intracellular structures in prokaryotes. Springer.

Fritz, P., Katz, A., 1972. The sodium distribution of dolomite crystals. Chem. Geol. 10.3 (1972): 237-244.

Gaona-Narvaez, T., Maurrasse, F.J.-M.R., Etayo-Serna, F., 2013. Geochemistry, palaeoenvironments and timing of Aptian organic-rich beds of the Paja Formation (Curiti, Eastern Cordillera, Colombia). Geol. Soc. London, Spec. Publ. 382, 31–48.

Gelpi, E., Schneider, H., Mann, J., and Oro, J., 1970. Hydrocarbons of geochemical significance in microscopic algae. Phytochemistry 9, 603-612.

Gingele, F.X. and Dahmke, A., 1994. Discrete barite particles and barium as tracers of paleoproductivity in South Atlantic sediments. Paleoceanography, 9: 151-168Gingele et al., 1999

Gingele, F.X., Zabel, M., Kasten, S., Bonn, W.J. and Nürnberg, C.C., 1999. Biogenic barium - methods and constraints of application as a proxy for paleoproductivity. In: Fischer G. and Wefer, G. (eds), Use of proxies in paleoceanography: examples from the South Atlantic. Springer, Berlin, pp. 345-364.

Given, R.K., Wilkinson, B.H., 1987. Dolomite Abundance and Stratigraphic Age: Constraints on Rates and Mechanisms of Phanerozoic Dolostone Formation: Perspectives 1068–1078.

Goldhammer, R.K, Dunn, P.A., Hardie, L.A., 1987, High frequency glacio-eustatic sea level oscillations with Milankovitch characteristics recorded in Middle Triassic platform carbonates in northern Italy: American Journal of Science 287, 853-828

González de Juana C., Arozena J. and Picard X.C., 1980. Geología de Venezuela y de sus Cuencas Petrolíferas, Ediciones Foninves, Caracas, 1031 pp.

Grabenstatter, J., Méhay, S., McIntyre-Wressnig, A., Giner, J.-L., Edgcomb, V. P., Beaudoin, D. J., Bernhard, J. M., and Summons, R. E., 2013. Identification of 24-n-propylidenecholesterol in a member of the Foraminifera. Organic geochemistry 63, 145-151.

Grantham, P. J. and Wakefield, L. L., 1988. Variations in the sterane carbon number distributions of marine source rock derived crude oils through geological time. Organic Geochemistry 12, 61-73.

Grimalt, J. and Albaigés, J., 1987. Sources and occurrence of C12 C22n-alkane distributions with even carbon-number preference in sedimentary environments. Geochimica et Cosmochimica Acta 51, 1379-1384.

Hallam, A., 1986. Origin of minor limestone-shale cycles: Climatically induced or diagenetic? Geology 14, 609–612.

Halley, R. B., 1985. Setting and geological summary of the Lower Cretaceous, Sunniland field, southern Florida. In Carbonate Petroleum Reservoirs (pp. 443-454). Springer New York.

Harrison, A.G, and Thode, H.G., 1958. Mechanism of the bacterial reduction of sulfate from isotopic fractionation studies Trans. Faraday Soc.54, 84–92.

Harvey, H. R. and Mcmanus, G. B., 1991. Marine ciliates as a widespread source of tetrahymanol and hopan-3β-ol in sediments. Geochimica et Cosmochimica Acta 55, 3387-3390.

Haq, B.U., Hardenbol, J., and. Vail, P.R., 1987, Chronology of fluctuating sea level since the Triassic: Science, 235, p. 1156–1167

Hatch, J.R. and Leventhal, J.S., 1992. Relationship between inferred redox potential of the depositional environment and geochemistry of the Upper Pennsylvanian (Missourian) Stark Shale Member of the Dennis Limestone, Wabaunsee County, Kansas, U.S.A. Chem. Geol. 99: 65-82

Hay, W.W., Migdisov, A., Balukhovsky, A.N., Wold, C.N., Flögel, S., Söding, E., 2006. Evaporites and the salinity of the ocean during the Phanerozoic: implications for climate, ocean circulation and life. In: Buggisch, W. (Ed.), Evolution of the System Earth in the Late Palaeozoic: Clues from Sedimentary Geochemistry. Palaeogeography, Palaeoclimatology, Palaeoecology 240, 3–46.

Heising, S., Richter, L., Ludwig, W., and Schink, B., 1999. *Chlorobium ferrooxidans* sp. nov., a phototrophic green sulfur bacterium that oxidizes ferrous iron in coculture with a Geospirillum sp. strain. Archives of microbiology 172, 116-124.

Helz, G.R., Miller, C. V., Charnock, J.M., Mosselmans, J.F.W., Pattrick, R. a D., Garner, C.D., Vaughan, D.J., 1996. Mechanism of molybdenum removal from the sea and its concentration in black shales: EXAFS evidence. Geochim. Cosmochim. Acta 60, 3631–3642.

Herbert, T. D., 1986. Milankovitch climatic origin of mid-Cretaceous black shale rhythms in central Italy. Nature, 321, 739-743.

Herrle, J.O., 2002. Paleoceanographic and paleoclimatic implications on mid-Cretaceous black shale formation in the Vocontian Basin and the Atlantic: evidence from calcareous nannofossils and stable isotopes. Tubinger Mikropalaontol. Mitt. 27, 114 pp.

Herrle, J., Pross, J., Friedrich, O., 2003. Forcing mechanisms for mid-Cretaceous black shale formation: evidence from the Upper Aptian and Lower Albian of the Vocontian Basin (SE France). Palaeogeogr. Palaeoclimatol. Palaeoecol. 190, 399–426.

Herrle, J. O., Kößler, P., Friedrich, O., Erlenkeuser, H., and Hemleben, C. 2004. High-resolution carbon isotope records of the Aptian to Lower Albian from SE France and the Mazagan Plateau (DSDP Site 545): a stratigraphic tool for paleoceanographic and paleobiologic reconstruction. Earth and Planetary Science Letters, 218, 149–161.

Holba, A., Dzou, L., Wood, G., Ellis, L., Adam, P., Schaeffer, P., Albrecht, P., Greene, T., and Hughes, W., 2003. Application of tetracyclic polyprenoids as indicators of input from fresh-brackish water environments. Organic geochemistry 34, 441-469.

Holba, A. G., Tegelaar, E., Ellis, L., Singletary, M., and Albrecht, P., 2000. Tetracyclic polyprenoids: Indicators of freshwater (lacustrine) algal input. Geology 28, 251-254.

Huang, C.H. 2010 Rare Earth Coordination Chemistry: Fundamentals and Applications. John Wiley and Sons, 575 pp.

Hughes, W., Holba, A., Dzou, L., 1995. The ratios of dibenzothiophene to phenanthrene and pristane to phytane as indicators of depositional environment and lithology of petroleum source rocks. Geochim Cosmochim Acta 59, 3581–98.

Hveding-Bergseth, N., Bruun T., and Kjoesen, H, 1983. Isolation of 30-nor-21 Hopan-22-one (lsoadlantone) from the lichen *Piatismatia glauca*. Phytochem., 22, 1826-1827.

Illich, H. A., 1983. Pristane, phytane, and lower molecular weight isoprenoid distributions in oils. AAPG bulletin 67, 385-393.

James, N., Bone, Y., Collins, L., Kyser, T., 2001. Surficial sediments of the Great Australian Bight: facies dynamics and oceanography on a vast cool-water carbonate shelf. J. Sediment. Res.

Jarrett, A. J., Schinteie, R., Hope, J. M., and Brocks, J. J., 2013. Micro-ablation, a new technique to remove drilling fluids and other contaminants from fragmented and fissile rock material. Organic geochemistry 61, 57-65.

Jeng, W.L., 2006. Higher plant n-alkane average chain length as an indicator of petrogenic hydrocarbon contamination in marine sediments. Marine Chemistry 102, 242-251.

Jenkyns, H.C., 2010. Geochemistry of oceanic anoxic events. Geochemistry, Geophys. Geosystems 11, doi:10.1029/2009GC002788.

Jones, B., Luth, R.W., MacNeil, A.J., 2001. Powder X-ray diffraction analysis of homogeneous and heterogeneous sedimentary dolostones. Journal of Sedimentary Research 71, 790-799.

Kamber, B.S., Webb, G.E., 2001. The geochemistry of late Archaean microbial carbonate: Implications for ocean chemistry and continental erosion history. Geochimica et Cosmochimica Acta 65, 2509–2525.

Kamber, B.S., Bolhar, R., Webb, G.E., 2004. Geochemistry of late Archaean stromatolites from Zimbabwe: evidence for microbial life in restricted epicontinental seas. Precambrian Research 132 (4), 379–399.

Karl, D.M., 2007. Microbial oceanography: paradigms, processes and promise. Nat. Rev. Microbiol. 5, 759–769.

Kemp, P., Lander, D. J., and Orpin, C. G., 1984. The lipids of the rumen fungus Piromonas communis. Journal of General Microbiology 130, 27-37.

Kleemann, G., Poralla, K., Englert, G., Kjøsen, H., Liaaen-Jensen, S., Neunlist, S., and Rohmer, M., 1990. Tetrahymanol from the phototrophic bacterium Rhodopseudomonas palustris: first report of a gammacerane triterpene from a prokaryote. Journal of General Microbiology 136, 2551-2553.

Kirsimäe, K., Jørgensen, P., Kalm, V., 1999. Low-temperature diagenetic illite-smectite in Lower Cambrian clays in North Estonia. Clay Miner. 94, 151–163.

Koopmans, M. P., Schouten, S., Kohnen, M. E., and Sinninghe-Damsté, J. S., 1996. Restricted utility of aryl isoprenoids as indicators for photic zone anoxia. Geochimica et Cosmochimica Acta 60, 4873-4876.

Koopmans, M. P., De Leeuw, J. W., and Damsté, J. S. S., 1997. Novel cyclized and aromatized diagenetic products of β-carotene in the Green River Shale. Organic geochemistry 26, 451-466.

Krügel, H., Krubasik, P., Weber, K., Saluz, H. P., and Sandmann, G., 1999. Functional analysis of genes from Streptomyces griseus involved in the synthesis of isorenieratene, a carotenoid with aromatic end groups, revealed a novel type of carotenoid desaturase. Biochimica et Biophysica Acta (BBA)-Molecular and Cell Biology of Lipids 1439, 57-64.

Kummerow, E., and Pérez de Mejía, D., 1989. Evolución diagenética de los carbonatos del Grupo Cogollo, cuenca del Lago de Maracaibo. VII Congreso Venezolano de Geología, Barquisimeto, Memorias 2, 745-771.

Kump, L.R., Arthur, M.A., 1999. Interpreting carbon-isotope excursions: carbonates and organic matter. Chem. Geol. 161, 181–198.

Kuypers, M.M., Blokker, P., Erbacher, J., Kinkel, H., Pancost, R.D., Schouten, S., Sinninghe Damste, J.S., 2001. Massive expansion of marine archaea during a mid-Cretaceous oceanic anoxic event. Science (80-.). 293, 92–5.

Kuypers, M.M.M., Blokker, P., Hopmans, E.C., Kinkel, H., Pancost, R.D., Schouten, S., Sinninghe Damsté, J.S., 2002. Archaeal remains dominate marine organic matter from the early Albian oceanic anoxic event 1b. Palaeogeogr. Palaeoclimatol. Palaeoecol. 185, 211–234.

Lacovara, K. J., Smith, J. R., Smith, J.B,. Lamanna, M.C., and Dodson. P., 2000. Paralic environments of the Cretaceous dinosaurs of Egypt: a discussion of uniformitarian analogs. Journal of Vertebrate Paleontology, 20. 53.

Lacovara, K. J., Smith, J. R., Smith, J. B., and Lamanna, M. C., 2003. The Ten Thousand Islands Coast of Florida: A modern analog to low-energy mangrove coasts of Cretaceous epeiric seas. In Davies, R.A.J., ed., Proceedings of the 5th International Conference on Coastal Sediments, Clearwater Beach, Florida. CD-ROM Published by World Scientific Publishing Corporation and East Meets West Productions, Corpus Christi, Texas, pp. 1773–1784.

Larson, R., Erba, E., 1999. Onset of the Mid-Cretaceous greenhouse in the Barremian-Aptian: Igneous events and the biological, sedimentary, and geochemical responses. Paleoceanography 14, 663–678.

Leckie, R.M., Bralower, T.J., Cashman, R., 2002. Oceanic anoxic events and plankton evolution: Biotic response to tectonic forcing during the mid-Cretaceous. Paleoceanography 17, 1–29.

Lehmann, C., Osleger, D.A., Montañez, I.P., Sliter , W., Arnaud- Vanneau, A., Banner, J., 1999. Evolution of the Cupido and Coahuila carbonate platforms, early Cretaceous, northeastern Mexico. Geol. Soc. Am. Bull. 111,1010–1029.

Lloyd, R.M., 1968. Oxygen isotope behaviour in the sulfate–water system J. Geophys. Res. 73. 6099–6110.

Lugo, J., and Mann, P. 1995, Jurassic–Eocene tectonic evolution of Maracaibo Basin, Venezuela, in A. Tankard, S. Suarez, and H. Welsink, eds., Petroleum basins of South America: AAPG Memoir 62, 699–725.

Lyons, T. W., Werne, J. P., Hollander, D. J., and Murray, R. W., 2003, Contrasting sulfur geochemistry and Fe/Al and Mo/Al ratios across the last oxic-to-anoxic transition in The Cariaco Basin, Venezuela: Chemical Geology 195, 131–157.

Machhour, L., Philip, J., Oudin, J.L., 1994, Formation of laminite deposits in anaerobic-dysaerobic marine environments. Mar. Geol. 117, 287–302.

McKirdy, D., Cox, R., Volkman, J., and Howell, V., 1986. Botryococcane in a new class of Australian non-marine crude oils. Nature 320, 57–59.

Malinverno, A., Hildebrandt, J., Tominaga, M., Channell, J.E.T., 2012. M-sequence geomagnetic polarity time scale (MHTC12) that steadies global spreading rates and incorporates astrochronology constraints. J. Geophys. Res. 117, B06104.

Mallory, F. B., Gordon, J. T., and Conner, R. L., 1963. The isolation of a pentacyclic triterpenoid alcohol from a protozoan. Journal of the American Chemical Society 85, 1362-1363.

Mann, P., Escalona, A., Verónica, M., 2006. Regional geological and tectonic setting of the Maracaibo supergiant basin, western Venezuela. Am. Assoc. Pet. Geol. Bull. 90, 445–477.

Manske, A. K., Glaeser, J., Kuypers, M. M., and Overmann, J., 2005. Physiology and phylogeny of green sulfur bacteria forming a monospecific phototrophic assemblage at a depth of 100 meters in the Black Sea. Applied and environmental microbiology 71, 8049-8060.

Maresca, J. A., Romberger, S. P., and Bryant, D. A., 2008. Isorenieratene biosynthesis in green sulfur bacteria requires the cooperative actions of two carotenoid cyclases. Journal of bacteriology 190, 6384-6391.

März, C., et al., 2008. Redox sensitivity of P cycling during marine black shale formation: dynamics of sulfidic and anoxic, non-sulfidic bottom waters. Geochim. Cosmochim. Acta 72 (15), 3703–3717.

Maslen, E., Grice, K., Gale, J. D., Hallmann, C., and Horsfield, B., 2009. Crocetane: a potential marker of photic zone euxinia in thermally mature sediments and crude oils of Devonian age. Organic Geochemistry, 40(1), 1-11.

Maze, W. B., 1984. Jurassic La Quinta Formation in the Sierra de Perijá, northwestern Venezuela: Geology and tectonic environment of red beds and volcanic rocks, in W. E. Bonini, Hargraves, R. B., and Shagam, R., eds., The Caribbean–South American plate boundary and regional tectonics: GSA Memoir 162, 263–282.

Mazzullo, S., Friedman, G., 1977. Competitive algal colonization of peritidal flats in a schizohaline environment: The Lower Ordovician of New York. J. of Sed. Res. 47, 398–410.

McArthur, J.M., Howarth, R.J., Bailey, T.R., 2007. Strontium Isotope Stratigraphy: LOWESS Version 3: Best Fit to the Marine Sr-Isotope Curve for 0–509 Ma and Accompanying Look-up Table for Deriving Numerical Age. J. Geol. 109, 155–170.

McCrea, J.M., 1950. On the isotopic chemistry of carbonates and a paleotemperature scale. The Journal of Chemical Physics 18, 849–857

McKirdy, D., Cox, R., Volkman, J., and Howell, V., 1986. Botryococcane in a new class of Australian non-marine crude oils.

Méndez Baamonde, J., 1989. Modelo depositacional del Grupo Cogollo, Talud externo, márgenes y plataforma interna. Memorias del VII Congreso Geológico Venezolano, Tomo II. Barquisimeto, Venezuela, pp. 827–850.

Méndez B, J., Baquero, M., Méndez Dot, J.A., 2009. Eventos Oceánicos Anóxicos OAE 1a y 1b en la Formación Apón del Grupo Cogollo durante el Cretácico Temprano. Cuenca de Maracaibo, Venezuela. Revista Latinoamericana de Geoquímica Orgánica 1, 6-18.

Méndez Dot, J. A., Méndez Baaamonde, J.,, Reyes, D., Wilchy, R., 2015. The Cogollo Group and the Oceanic Anoxic Events 1a y 1b, Maracaibo Basin, Venezuela. Brazilian Journal of Geology 45, 8-31.

Menegatti, A.P., Weissert, H., Brown, R.S., Tyson, R.V., Farrimond, P., Strasser, A., and Caron, M., 1998, High-resolution $\delta^{13}C$ stratigraphy through the Early Aptian "Livello Selli" of the Alpine Tethys: Paleoceanography 13, 530–545.

Mizutani, Y., and Rafter, T.A., 1969. Oxygen isotopic composition of sulfates: Part 4. Bacteria fractionation of oxygen isotopes in the reduction of sulfate and in the oxidation of sulfur Inst. of Nuclear Sciences, Lower Hutt, NZ. J. Sci. Technol. 12, 60–68.

Moldowan, J. M., Fago, F. J., Lee, C. Y., Jacobson, S. R., Watt, D. S., Slougui, N.-E., Jeganathan, A., and Young, D. C., 1990. Sedimentary 24-n-propylcholestanes, molecular fossils diagnostic of marine algae. Science 247, 309-312.

Moldowan, J. M. and Seifert, W. K., 1979. Head-to-head linked isoprenoid hydrocarbons in petroleum. Science 204, 169-171.

Moldowan, J. M., Seifert, W. K., Arnold, E., & Clardy, J., 1984. Structure proof and significance of stereoisomeric 28, 30-bisnorhopanes in petroleum and petroleum source rocks. Geochimica et Cosmochimica Acta 48, 1651-1661.

Monteiro, F.M., Pancost, R.D., Ridgwell, A., Donnadieu, Y., 2012. Nutrients as the dominant control on the spread of anoxia and euxinia across the Cenomanian-Turonian oceanic anoxic event (OAE2): Model-data comparison. Paleoceanography 27, PA4209.

Moore, D.M., and Reynolds, R.C., 1989. X-ray diffraction and the identification and analysis of clay minerals. Oxford University Press, 322 p.

Mutterlose, J., Pauly, S., Steuber, T., 2009. Temperature controlled deposition of early Cretaceous (Barremian-early Aptian) black shales in an epicontinental sea. Palaeogeography, Palaeoclimatology, Palaeoecology 273, 330 – 345.

Nägler, T.H., Siebert, C., Lüschen, H. and Böttcher, M.E., 2005. Sedimentary Mo isotope record across the Holocene fresh-brackish water transition of the Black Sea. Chem. Geol. 219, 283–295.

Nance, W.B., Taylor, S.R., 1976. Rare earth patterns and crustal evolution: I. Australian post-Archean sedimentary rocks, Geochimica et Cosmochimica Acta 40,1539–155.

Nelson, R., Moldovanyi, E., Matcek, C., Azpiritxaga, I., 2000. Production characteristics of the fractured reservoirs of the La Paz field, Maracaibo basin, Venezuela. Am. Assoc. Pet. Geol. Bull. 84, 1791–1809.

Neunlist, S. and Rohmer, M., 1985. Novel hopanoids from the methylotrophic bacteria Methylococcus capsulatus and Methylomonas methanica.(22S)-35-aminobacteriohopane-30, 31, 32, 33, 34-pentol and (22S)-35-amino-3 beta-methylbacteriohopane-30, 31, 32, 33, 34-pentol. Biochem. J 231, 635-639.

Nishimura, M. and Koyama, T., 1977. The occurrence of stanols in various living organisms and the behaviour of sterols in contemporary sediments. Geochimica et Cosmochimica Acta 41, 379-385.

Overmann, J., Cypionka, H., and Pfennig, N., 1992. An extremely low-light-adapted phototrophic sulfur bacterium from the Black Sea. Limnology and Oceanography, 150-155.

Patterson, G. W., 1971. The distribution of sterols in algae. Lipids 6, 120-127.

Patton, J. W., Choquette, P. W., Guennel, G. K., Kaltenback, A. J., and Moore, A. 1984. Organic geochemistry and sedimentology of lower to mid-Cretaceous deep-sea carbonates, Site-535 And Site-540, Leg-77. Initial Reports of the Deep Sea Drilling Project, 77, 417-443.

Paytan, A., Moore, W. S., & Kastner, M. (1996). Sedimentation rate as determined by ^{226}Ra activity in marine barite. Geochimica et Cosmochimica Acta, 60, 4313-4319.

Parnaud, Y., Gou, Y., Pascual, J., Truskowski, I., Gallango, O., and Passalacqua, H., 1995. Petroleum geology of the central part of the Eastern Venezuela Basin, in A. Tankard, S. Suarez, and H. Welsink, eds., Petroleum basins of South America: AAPG Memoir 62, 741–756.

Perez, J., 1996. Global and local controls upon the deposition of organic-rich Cretaceous sequences of Western Venezuela: a geochemical study. PhD Thesis. Fossil Fuels and Environmental Geochemistry Postgraduate Institute: NRG. University of Newcastle upon Tyne, UK.

Peters, K. E. and Moldowan, J. M. 1993. The biomarker guide: interpreting molecular fossils in petroleum and ancient sediments. Prentice-Hall, Englewood Cliffs, New Jersey, 363 pp.

Peters, K.E.,Walters, C.C., Moldowan, J.M., 2005. The Biomarker Guide: Biomarkers and Isotopes in Petroleum Systems and Earth History, second ed. Cambridge University Press, Cambridge.

Peterson, J.A., 1983, Petroleum geology and resources of south-eastern Mexico, northern Guatemala, and Belize: United States Geological Survey Circular 760, 44 p.

Piepgras, D.J., Jacobsen, S.B., 1992. The behaviour of rare earth elements in seawater: precise

Pöppelreiter, M., Balzarini, M.A., De Sousa, P., Engel, S., Galarraga, M., Hansen, B., Marquez, X., Morell, J., Nelson, R., Rodriguez, F., 2005. Structural control on sweet-spot distribution in a carbonate reservoir: Concepts and 3-D models (Cogollo Group, Lower Cretaceous, Venezuela). AAPG … 89, 1651–1676. doi:10.1306/08080504126

Pöppelreiter, M., 2008. Realizing complex carbonate facies, diagenetic and fracture properties with standard reservoir modelling software. Geol. Soc.309, 39–49.

Powell, T. and McKirdy, D., 1973. Relationship between ratio of pristane to phytane, crude oil composition and geological environment in Australia. Nature 243, 37-39.

Poulton, S.W., Raiswell, R., 2002. The low-temperature geochemical cycle of iron: from continental fluxes to marine sediment deposition. Am. J. Sci. 302, 774–805.

Poulton, S.W., Fralick, P.W., Canfield, D.E., 2004. The transition to a sulphidic ocean, 1 . 84 billion years ago. Nature 431, 173–177.

Poulton, S.E, Canfield, D.E., 2005. Development of a sequential extraction procedure for iron: implications for iron partitioning in continentally derived particulates. Chem. Geol. 214, 209–221.

Poulton, S.W., Fralick, P.W., Canfield, D.E., 2010. Spatial variability in oceanic redox structure 1.8 billion years ago. Nat. Geosci. 3 (7), 486–490.

Poulton, S.W., Canfield, D.E., 2011. Ferruginous Conditions : A Dominant Feature of the Ocean through Earth ’s History. Elements 107–112.

Puga-Bernabéu, Á., Betzler, C., 2008. Cyclicity in Pleistocene upper-slope cool-water carbonates: Unravelling sedimentary dynamics in deep-water sediments, Great Australian Bight, Odp Leg 182, Site 1131A. Sediment. Geol. 205, 40–52.

Raiswell, R., 1988. Chemical model for the origin of minor limestone-shale cycles by anaerobic methane oxidation. Geology 16, 641–644.

Raiswell, R., Canfield, D.E., 1998. Sources of iron for pyrite formation in marine sediments. Am. J. Sci. 219–245.

Raiswell, R., Newton, R., and Wignall, P.B., 2001. An indicator of water-column anoxia: resolution of biofacies variations in the Kimmeridge Clay (Upper Jurassic, U.K.): Journal of Sedimentary Research 71, 286–294.

Raiswell, R., Newton, R., Bottrell, S.H., Coburn, P., Briggs, D.E.G., Bond, D.P.G., Poulton, S.W., 2008. Turbidite depositional influences on the diagenesis of Beecher’s Trilobite Bed and the Hunsruck Slate: sites of soft tissue pyritization. American Journal of Science 308, 105-129.

Renz, O., 1958. Estratigrafía del cretáceo en Venezuela. Bol. Minist. Min. Hidrocarb. 5, 3–48.

Renz, O., 1981. Venezuela, in: Reyment, R.A., Bengtson., P. (Eds.), Aspects of Mid-Cretaceous Regional Geology, pp.197-220.

Renz, O., 1982. The Cretaceous ammonites of Venezuela. Birkhauser Verlag, Basel, 132. (+ 40 pl.).

Ricci, J. N., Coleman, M. L., Welander, P. V., Sessions, A. L., Summons, R. E., Spear, J. R., and Newman, D. K., 2013. Diverse capacity for 2-methylhopanoid production correlates with a particular ecological niche. The ISME journal 8, 675-684.

Rickard, D., Luther, G.W., 2007. Chemistry of iron sulfides. Chem. Rev. 107, 514–62.

Rickard, David. 2012. Sulfidic Sediments and Sedimentary Rocks. Dev. Sedimentol., Developments in Sedimentology 65. doi:10.1016/B978-0-444-52989-3.00006-4

Rod, E., and Maync, W. 1954. Revision of Lower Cretaceous stratigraphy of Venezuela: AAPG Bulletin 38, 93–283.

Rodgers, J., 1954. Terminology of limestone and related rocks: an interim report. J. Sediment. Res. 24.

Rowland, S., 1990. Production of acyclic isoprenoid hydrocarbons by laboratory maturation of methanogenic bacteria. Organic geochemistry 15, 9-16.

Rubinstein, I., Sieskind, O., and Albrecht, P., 1975. Rearranged sterenes in a shale: occurrence and simulated formation. Journal of the Chemical Society, Perkin Transactions 1, 1833-1836.

Sass, E., Katz, A., 1982. The origin of platform dolomites; new evidence. Am. J. Sci. 1184–1213.

Sass, E., and Bein, A., 1988. Dolomites and salinity: a comparative geochemical study. In Shukla, V. and Baker P.A., eds., Sedimentology and Geochemistry of Dolostones Spec. Publs SEPM 43,223-233.

Schinteie, R., 2011. Ancient Life at the Extremes: Molecular Fossils and Paleoenvironmental Contexts of Neoproterozoic and Cambrian Hypersaline Settings. American Geophysical Union, Fall Meeting 2011, abstract #B33L-01

Schijf, J., Marshall, K., 2011. YREE sorption on hydrous ferric oxide in 0.5 M NaCl solutions: a model extension. Mar. Chem. doi:10.1016/j.marchem.2010.09.003

Schlager, W., 1989. Drowning unconformities on carbonate platforms. In: Crevello, P.D., Wilson, J.L., Sarg, J.F., Read, J.F., eds., Controls on carbonate platform and basin development: SEPM Special Publication 44. SEPM, Tulsa, Oklahoma, U.S.A., pp. 15-2

Schlanger, S., Jenkyns, H., 1976. Cretaceous oceanic anoxic events: causes and consequences. Geol. en Mijnb. 55, 179–184.

Schoell, M., McCaffrey, M. A., Fago, F. J., and Moldowan, J. M., 1992. Carbon isotopic compositions of 28,30-bisnorhopanes and other biological markers in a Monterey crude oil. Geochimica et Cosmochimica Acta 56,1391-1399.

Schubert, C., 1986. Stratigraphy of the Jurassic La Quinta Formation, Mérida Andes, Venezuela: type sections Z. Deut. Geol. Ges., 137: 391-411.

Schwark, L. and Frimmel, A., 2004. Chemostratigraphy of the Posidonia black shale, SW-Germany: II. Assessment of extent and persistence of photic-zone anoxia using aryl isoprenoid distributions. Chemical Geology 206, 231-248.

Schweitzer, C.E., Lacovara, K.J., Smith, J.B., Lamanna, M.C., Lyon, M.A., Attia, Y., State, K., Nw, F.A., 2003. Mangrove-dwelling crabs (Decapoda: Brachyura: Necrocarcinidae) associated with dinosaurs from the upper Cretaceous (Cenomanian) of Egypt 77, 888–894.

Sender, L.M., Diez, J.B., Ferrer, J., Pons, D., Rubio, C., 2005. Preliminary data on a new Albian flora from the Valle del Río Martín, Teruel, Spain. Cretac. Res. 26, 898–905.

Shen, G., Fan, S., Lin, D., Su, N., and Zhou, H., 1980. The geochemistry of n-alkanes with an even-odd predominance in the Tertiary Shahejie Formation of northern China. Physics and Chemistry of the Earth 12, 115-121.

Shen, Y.N., Canfield, D.E., Knoll, A.H., 2002. Middle Proterozoic ocean chemistry: evidence from the McArthur Basin, northern Australia. Am. J. Sci. 302, 81–109

Sibley, D., Gregg, J., 1987. Classification of dolomite rock textures. J. Sediment. Res. 57, 967–975.

Simonin, P., Tindall, B., and Rohmer, M., 1994. Structure elucidation and biosynthesis of 31-methylhopanoids from Acetobacter europaeus. European Journal of Biochemistry 225, 765-771.

Sinninghe-Damsté, J. S., Kenig, F., Koopmans,M. P., Köstner, J.,Schouten, S., Hayes, J. M., and De Leeuw, J. W. 1995. Evidence for gammacerane as an indicator of water column stratification. Geochim. Cosmochim. Acta 59, 1895–1900.

Smith, J.B., Lamanna, M.C., Lacovara, K.J., Dodson, P., Smith, J.R., Poole, J.C., Giegengack, R., and Attia, Y., 2001. A giant sauropod dinosaur from an Upper Cretaceous mangrove deposit in Egypt. Science 292, 1704-1706.

Solé, V.A. Papillon, E. Cotte, M. Walter Ph., Susini, J. 2007, A multiplatform code for the analysis of energy-dispersive X-ray fluorescence spectra: Spectrochim. Acta Part B 62, 63-68.

Staudt, W., Oswald, E., Schoonen, M., 1993. Determination of sodium, chloride and sulfate in dolomites: a new technique to constrain the composition of dolomitizing fluids. Chem. Geol. 107, 97–109.

Summons, R. and Jahnke, L., 1992. Hopenes and hopanes methylated in ring-A: correlation of the hopanoids from extant methylotrophic bacteria with their fossil analogues. Biological markers in sediments and petroleum, 182-200.

Summons, R. and Powell, T., 1987. Identification of aryl isoprenoids in source rocks and crude oils: biological markers for the green sulphur bacteria. Geochimica et Cosmochimica Acta 51, 557-566.

Summons, R. E., Jahnke, L. L., Hope, J. M., and Logan, G. A., 1999. 2-Methylhopanoids as biomarkers for cyanobacterial oxygenic photosynthesis. Nature 400, 554-557.

Sun, S.Q., 1994. Perspective – A Reappraisal of Dolomite Abundance and Occurrence in the Phanerozoic. J. Sediment. Res. 64A, 396–404.

Sutton, F., 1946, Geology of Maracaibo Basin, Venezuela: AAPG Bulletin 30, 1621–1741.

Tejada, M.L.G., Suzuki, K., Kuroda, J., Coccioni, R., Mahoney, J.J., Ohkouchi, N., Sakamoto, T., Tatsumi, Y., 2009. Ontong Java plateau eruption as a trigger for the early Aptian oceanic anoxic event. Geology 37, 855–858.

Ten Haven, H., De Leeuw, J., Damsté, J. S., Schenck, P., Palmer, S., and Zumberge, J., 1988. Application of biological markers in the recognition of palaeohypersaline environments. Geological Society, London, Special Publications 40, 123-130.

Ten Haven, H., Rohmer, M., Rullkötter, J., and Bisseret, P., 1989. Tetrahymanol, the most likely precursor of gammacerane, occurs ubiquitously in marine sediments. Geochimica et Cosmochimica Acta 53, 3073-3079.

Tissot, B. P. and Welte, D. H., 1984. Petroleum formation and occurrence. *A New Approach Co Oil and GUS Exploration*. Springer-Verlag

Torres, M.E., Brumsack, H.J., Bohrmann, G. and Emeis, K.C., 1996. Barite fronts in continental margin sediments: A new look at barium remobilization in the zone of sulfate reduction and formation of heavy barites in diagenetic fronts. Chemical Geology, 127: 125-139.

Trüper, H. G. and Pfennig, N., 1992. The family Chlorobiaceae, The prokaryotes. Springer

Vahrenkamp, V. C., Franssen, R.C.W.M., Grötsch, J., Munoz, P. J., 1993, Maracaibo Platform (Aptian-Albian), northwestern Venezuela. In: Simo, J. A. T., Scott, R.W.,Masse,J.P., eds., Cretaceous Carbonate Platforms. AAPG Memoir 25, 25–33.

Van Kaam-Peters, H. M., Köster, J., De Leeuw, J. W., and Damsté, J. S. S., 1995. Occurrence of two novel benzothiophene hopanoid families in sediments. Organic geochemistry 23, 607-616.

Venkatesan, M.I., 1989. Tetrahymanol: Its widespread occurrence and geochemical significance. Geochimica et Cosmochimica Acta 53, 3095-3101.

Ventura, M., Canchaya, C., Tauch, A., Chandra, G., Fitzgerald, G. F., Chater, K. F., and van Sinderen, D., 2007. Genomics of Actinobacteria: tracing the evolutionary history of an ancient phylum. Microbiology and Molecular Biology Reviews 71, 495-548.

Visscher, P. T. and Stolz, J. F., 2005. Microbial mats as bioreactors: populations, processes, and products. Palaeogeography, Palaeoclimatology, Palaeoecology 219, 87-100.

Volkman, J., 2003. Sterols in microorganisms. Applied Microbiology and Biotechnology 60, 495-506.

Volkman, J. K., 1986. A review of sterol markers for marine and terrigenous organic matter. Organic geochemistry 9, 83-99.

Von Breymann, M.T.K., Emeis, K.C. and Suess, E., 1992. Water depth and diagenetic constraints on the use of barium as a paleoproductivity indicator. In: Summer-Hayes, C.P., editor, Upwelling Systems: Evolution since the Early Miocene. Geological Society Special Publication 64, pp 273-284.

Weber, J., 1964. Trace element composition of dolostones and dolomites and its bearing on the dolomite problem. Geochim. Cosmochim. Acta 28, 1817–1868.

Wedepohl, K.H., 1978. Manganese: abundance in common sediments and sedimentary rocks. In: Handbook of Geochemistry. Springer, Berlin, 1I/3, pp. 1-17.

Weedon, G.P., 1986, Hemi-pelagic shelf sedimentation and climatic cycles: The basal Jurassic (Blue Lias) of S. Britain: Earth and Planetary Science Letters, 76, p. 321-335.

Weedon, G. P., Hallam, A. 1987. Comment and reply on 'Origin of minor limestone-shale cycles'. Geology, 15, 92-94

Westphal, H., Munnecke, A., 2003. Limestone-marl alternations : A warm-water phenomenon? Geology 31, 263–266.

Wignall, P.B., 1991. Dysaerobic trace fossils and ichnofabrics in the Upper Jurassic Kimmeridge Clay of southern England. Palaios 6, 264–270.

Wignall, P., 1994. Black shales. Oxford University Press, Oxford, UK, 127 p.

Wignall, P.B., 2001. Large igneous provinces and mass extinctions. Earth-Science Reviews 53: 1-33.

Wignall, P.B., Newton, R., 1998. Pyrite framboid diameter as a measure of oxygen deficiency in ancient mudrocks. Amer. J. Sci. 298, 537–552.

Wignall, P.B., Bond, D.P.G., Kuwahara, K., Kakuwa, Y., Newton, R.J., Poulton, S.W., 2010. An 80 million year oceanic redox history from Permian to Jurassic pelagic sediments of the Mino-Tamba terrane, SW Japan, and the origin of four mass extinctions. Glob. Planet. Change 71, 109–123.

Wilkin, R.T., Barnes, H.L., Brantley, S.L., 1996. The size distribution of framboidal pyrite in modern sediments: an indicator of redox conditions. Geochim. Cosmochim. Acta 60, 3897–3912

Wright, J., Schrader, H., Holser, W.T., 1987. Paleoredox variations in ancient oceans recorded by rare earth elements in fossil apatite. Geochim. Cosmochim. Acta 51,631-644.

Yurewicz, D.A., Advocate, D.M., Lo, H., E.A., H., 1998. Source rocks and oil families, southwest Maracaibo basin (Catatumbo Subbasin), Colombia. Am. Assoc. Pet. Geol. Bull. 82, 1329–1352.

Zander, J. M., Caspi, E., Pandey, G. N., and Mitra, C. R., 1969. The presence of tetrahymanol in *Oleandra wallichii.* Phytochemistry 8, 2265-2267.

Zheng, Y., Anderson, R.F., van Geen, A. and Kuwabara, J., 2000. Authigenic molybdenum formation in marine sediments: a link to porewater sulphide in the Santa Barbara Basin. Geochim. Cosmochim. Acta 64, 4165–4178.

Zumberge, J. E., 1987. Prediction of source rock characteristics based on terpane biomarkers in crude oils: A multivariate statistical approach. Geochimica et Cosmochimica Acta 51, 1625-1637.

CHAPTER IV

Chemical and textural overprinting of ancient stromatolites: timing, processes, and implications for their use as paleoenvironmental proxies[3]

4.1. Introduction

The quest to quantitatively constrain the dynamic evolution of paleo-redox states in Precambrian oceans has led to the hypothesis that the trace metal content of ancient stromatolites can be used as valid proxies for ancient ocean chemistry (e.g., Kamber and Webb, 2001; Van Kranendonk et al., 2003; Bolhar et al., 2004, 2007; Kamber et al., 2004; Planavsky et al., 2009; Riding et al., 2014). In such studies, emphasis is placed on relative abundances of various bioactive trace element concentrations as well as shale-normalized Rare Earth Element (REE_{SN}) distributions in bulk samples. This approach is seemingly warranted by the observation that contemporary stromatolite communities robustly record modern seawater compositions (Webb and Kamber, 2000; Kamber and Webb, 2007). Broad consensus is that REE_{SN} and some transition metal signatures of ancient stromatolites are useful in the pursuit of an interpreTable 4.record of ancient seawater chemistry (see Riding et al., 2014).

An inherent difficulty with such models, however, is that Holocene stromatolites were affected only by shallow burial diagenesis. As such, it remains unquantified to what extent a far more complex diagenetic history within their ancient analogues overprinted original chemical signatures. Mechanisms that might promote disruption of such primary chemical indicators in ancient stromatolites include: diagenetic mobilization of trace metals; fractionation of transition elements and/or REE during secondary mineral precipitation; or contamination with metals derived from exogenous sources (e.g., Palmer, 1985; Elderfield and Pagett, 1986; Palmer and Elderfield, 1986; Sholkovitz and Shen, 1995; Bau et al., 1996; Reynard et al., 1999; Shields and Stille, 2001; Johannesson et al., 2006). In this regard, it is reasonable to evaluate to what extent the low trace metal concentrations typically found in these ancient putative organo-sedimentary

[3] A version of this manuscript was submitted for publication in *Precambrian Geology*

structures reflect a record of (albeit, poorly constrained) burial diagenesis and exhumation histories, rather than primary, marine-derived sources.

Under the generally oxygen-depleted conditions that accompanied Paleoproterozoic stromatolite accretion (e.g., Poulton et al., 2004), a number of trace elements are expected to have been variably enriched within minerals comprising these structures. This is because the redox sensitivity of transition metals and cerium, their preferential affinity for certain authigenic mineral phases, their complexation behaviour in the presence of reactive microbial biomass, and local scale paleoenvironmental factors, determined the magnitude of elemental enrichment in the different mineral phases. To investigate these various possibilities, we compared the textural, spectroscopic, and bulk-rock chemical signatures (transition metal and REE_{SN} abundances) of stromatolites of the Gunflint Formation from the region of Thunder Bay, Ontario, Canada (Fig. 4.1). It was previously recognized that these stromatolites are pervasively silicified even if they were essentially unmetamorphosed, which, in part, explains their remarkable microfossil content (Barghoorn and Tyler, 1965; Awramik and Barghoorn, 1977). It is also highly significant that their accretion occurred at a time in the evolution of marine chemical redox between the purported transition from largely ferruginous to sulfidic bottom water conditions (Poulton et al., 2004).

With regards to stromatolites thus far described from Archean-Proterozoic terranes, replacement of primary carbonates can range from slight to extensive, either by other carbonates (e.g., siderite, ankerite, calcite) or by non-carbonate minerals (e.g., amorphous silica). The sequence of events linked to the replacement process may be predictable, and in this regard, paragenetic relations between the cherty matrix (recrystallized amorphous silica) and dolomite offer insights into establishing the time during which silicification of the carbonates occurred (Dapples, 1979). Our goals here were to investigate the nature of silicification in the peritidal carbonates of the Gunflint Formation, with particular emphasis on the conditions necessary for silica permineralization. This will help elucidate any diagenetic bias on the bulk trace metal signatures of the secondarily silicified early diagenetic carbonate minerals. Conclusions drawn from this study are discussed in terms of the applicability of bulk-rock analyses of stromatolite samples to evaluate paleoceanographic conditions in deep geological time.

4.2. Geological Background

Rocks that comprise the sedimentary successions of the 1.88 Ga Gunflint Formation were deposited uncomformably on deformed Neoarchean greenstone-granite basement rocks of the Superior Province, and within the southward-thickening domain of the Animikie Basin (e.g., Pufhal, 1996, Fralick et al., 2002; Jirsa and Fralick, 2010). Following earlier stratigraphic studies (i.e., Broderick, 1920), Goodwin (1956) subdivided this formation into four members: the Basal Conglomerate, the Lower and Upper Cherty Member(s), and the Upper Limestone. With minor modifications, these terms remain in use today. The ~120 m thick formation crops out nearly continuously from Gunflint Lake on the Minnesota–Ontario border to the east of Thunder Bay (Fralick, 1989). A geochronological investigation of a euhedral zircon population from the Upper Cherty Member yielded a U-Pb isochron age of 1878 ± 1.3 Ma interpreted to define the depositional age of this stratigraphic member (Fralick et al., 2002).

We focus on stromatolites collected from the very base of the Lower Cherty Member that directly overlies the basal conglomerate. Relative to the other lithofacies of the Gunflint, this member represents the shallowest shoreward depositional facies of the succession (Winter and Knauth, 1992). In his pioneering work, Goodwin (1960) further subdivided the Lower Cherty Member into the following set of lithofacies: “algal chert” (i.e., stromatolites), tuffaceous shale, taconite, and banded chert-carbonates. At about the same time, Moorehouse (1960) pointed out that the Lower Cherty Member exhibits complex lateral variations of stromatolitic silicified grainstones, BIF, and shale microfacies: he further divided the unit into eleven distinct lithofacies to account for these differences. The lateral and vertical transition of lithofacies in the Gunflint superficially resembles shallow marine mixed clastic-carbonate depositional systems. Thus, it is thought to represent two marginal depositional cycles controlled by relative sea-level changes (Fralick and Barrett, 1995; Pufahl and Fralick, 2000).

The laminar internal structure of the stromatolites is defined by the presence of (dark) kerogen and/or iron oxides (Moreau and Sharp, 2004). Exceptionally well-preserved microfossils were first documented by Barghoorn and Tyler (1965) and Cloud (1965) from the Gunflint rocks. The microfossils may be coated with iron oxides, and have been interpreted to represent the remains of cyanobacteria (e.g., Awramik and Barghoorn, 1977) or chemolithotrophic Fe-oxidizing bacteria (e.g., Knoll, 2003; Planavsky et al., 2009). Understanding these rocks is important because both

the quality and quantity of Gunflint microfossil forms are the benchmark against which all other putative microscopic traces of early life are compared (Awramik and Barghoorn, 1977; Lowe, 1983; Schopf and Packer, 1987; Nudds and Selden, 2008; Planavsky et al., 2009; Wacey et al., 2012).

An early diagenetic silica permineralization process occurred shortly after stromatolite accretion to account for the exceptional preservation of the small microbial cell structures (Hesse, 1989; Knauth, 1994; Moreau and Sharp, 2004). The permineralization process probably involved the interaction of biofilms with seawater that was supersaturated at that time with respect to silica (i.e., Konhauser et al., 2001, 2004, 2005; Maliva et al., 2005). Other Precambrian stromatolites initially formed by processes of carbonate accretion, however, with the chert representing a secondary mineral phase formed during diagenesis (Buick and Dunlop, 1990; Grotzinger 1994). Such stromatolites, typically accreted in the peritidal zone, are characterized by the presence of unreplaced carbonates and the preservation of inclusions and ghosts of carbonate precursors, also with pseudomorphs and inclusions of evaporites (Maliva et al., 2005, their Table 4.1).

4.3. Samples and Methods

4.3.1. Samples

Samples from the Lower Gunflint Formation were collected in the Thunder Bay area. Locations for our collections occur along the northern shore of Lake Superior, at the Schreiber Channel Provincial Nature Reserve (Awramik and Barghoorn, 1977; Lanier, 1989), and the Frustration Bay locality (Awramik and Barghororn, 1977). The Frustration Bay samples were provided by Dr. Stanley Awramik (University of California at Santa Barbara). At the Schreiber Channel locality, we used previously collected stromatolitic cherts containing ooidal/peloidal intraclasts. Specimens came from unattached black chert cobbles found offshore, adjacent to the protected outcrop. For comparison purposes, we also sampled laminar hematite-rich digitate stromatolitic rocks from the Upper Cherty Member exposed at Mink Mountain (Planavsky et al., 2009; Shapiro and Konhauser, 2015) and a section of a large hemispheroid dome near Kakabeka Falls.

4.3.2 Methods

Petrographic thick- (250 μm) and thin-sections (30-40 μm) were systematically analyzed by standard and blue fluorescence petrography, as well as by Scanning Electron Microscope coupled to an Energy Dispersive Spectrometer (SEM-EDS) at the University of Alberta. These analyses were conducted on the petrographic sections and freshly broken samples, respectively. For descriptions of the quartz textures, we follow the terminology of Folk (1974). Accordingly, we used microquartz to refer to equant quartz crystals less than 20 μm in diameter, and megaquartz as that material with a crystal size greater than ~20 μm. Chalcedony is used herein for microcrystalline quartz with parallel- or radial-fibrous extinction, irrespective of the sign of elongation. Chert is used for any aggregate consisting of microquartz, megaquartz and/or chalcedony. Silica is a blanket term for any precipitate with the same chemical composition as quartz (e.g., Simonson 1987). For the description of dolomite/ankerite mineral textures, we followed the general scheme for naming these textures as outlined by Sibley and Gregg (1987).

Bulk-rock minor and trace elemental concentrations were determined at the University of Alberta. Initially a 0.2-g (dry weight) rock sample was digested in a platinum crucible with a solution of concentrated HNO_3 (2 mL) and HF (8 mL) to near dryness; subsequently a second addition of concentrated HCl (5 mL) and HNO_3 (5 mL) was made and again the mixture was evaporated to near dryness. The residue was then dissolved in 10 mL of 8 N HNO_3 and diluted to ~20 mL with 8.8 mL ultrapure water and 0.1 mL HNO_3. A 0.1 mL of a Br, In, and Sc spike was added. Samples were analyzed on an Perken Elmer Elan6000 Inductively Coupled Plasma Quadrupole Mass Spectrometer (ICPQ-MS) under the following operating conditions: RF power = 1200 W; dual detector mode; blank subtraction performed subsequent to internal standard correction; unit of measurement is cps (counts per second); auto lens on; use of 4-point calibration curves (0, 0.25, 0.50, and 1.00 ppm for Ca, Mg, and Fe; 0.005, 0.010, and 0.020 ppm for the remaining elements); sample uptake rate (using a peristaltic pump) was ~1 mL; sample analysis consisted of 35 sweeps/reading, 1 reading/replicate and 3 replicates; dwell times were 10 ms for Al, Mn, and U, and 20 ms for the remaining elements; and total intergration times (dwell time x number of sweeps) were 350 ms for Al, Mn, and U, and 700 ms for the remaining elements (Table 4.1). External reproducibility, based on repeated analysis of international whole rock standard (Granodiorite, Silver Plume, Colourado, GSP-2) is 5-10% (2σ level) for most elements. Internal

standards for Bi, Sc and In were also used. Determined REE data were corrected using both off-line and on-line correction methods for interferences of BaO on Eu and NdO on Tb (e.g., Cheatham et al 1993).

Following standard procedures, the La and Ce anomalies and measures of REE fractionation (i.e., (La/Yb), (Pr/Yb), (Nd/Yb), and (Gd/Yb)) were normalized against Post Archean Australian Shale (PAAS; Nance and Taylor, 1976; Taylor and McLennan, 1985). Normalization values (in ppm) for the REEs are: La (38), Ce (80), Pr (8.9), Nd (32), Sm (5.6), Eu (1.1), Gd (4.7), Tb (0.77), Dy (4.4), Ho (1.0), Er (2.9), Tm (0.4), Yb (2.8), and Lu (0.43). To evaluate for anomalous REE values, we used the approach developed by Bau and Dulski (1996) which prevents interpretations based on abnormal absolute concentrations of neighboring elements. For instance, the enrichment or depletion of Ce relative to La and Nd is widely used as a tracer for paleomarine redox conditions (Elderfield, 1988; De Baar et al., 1988). When only spider plots are used, however, the presence of Ce anomalies can be complicated by anomalous abundances of La.

Veizer et al. (1992) previously observed that the distribution of elements, such as Mn, Zn, and Y in Paleoproterozoic shelf sequences, is largely controlled by the carbonate fraction. To map the spatial distribution of yttrium at the scale of our digitate stromatolite samples, we employed synchrotron-based *in situ* micro-X-ray fluorescence (μXRF). These measurements were performed on the VESPERS microprobe beamline 07B2-1 at the Canadian Light Source (CLS) in Saskatchewan, and the 20ID-B beamline at the Advanced Photon Source (APS), Argonne National Laboratory (Illinois, USA). For both beamlines, the excitation energy was tuned at 20.2 keV, and a flux of 10^{10} – 10^{11} photons-per-second was micro-focused over an analytical area of ~30 μm^2 using Kirkpatrick-Baez (KB) mirrors. For both beamlines, the resulting fluorescence spectra were measured using a 4 element Vortex multi-element Si drift detector located 90° to the incident beam in the direction of the polarization, and the detector calibrated to ~30 eV per channel. Spatially resolved X-Ray Diffraction analyses (2D-XRD) were used to obtain small-scale mineralogical information. The experimental geometry was corrected and 2θ calibration done by measuring the reflection patterns of LaB_6 (NIST, SRM 660b). Calibration of the 2d-spacing of the targeted mineral was done by using the d_{101} peak of quartz.

Yttrium abundance was used to infer the distribution of REE for two reasons. Firstly, its $K\alpha_1$ emission line is at 14.9 keV, and thus within the detecTable 4.range of our synchrotron analyses (~5.5 −20.0 keV). In contrast, the other lanthanides have $K\alpha_1$ emission that range from 34.7 – 54.0 keV. This would mean that their detection would require tuning the instrument to much higher energies that are detrimental for determining the distribution of first row transition metals. Secondly, it is expected that the distribution of Y with the solid phases present in our samples, should be similar to Ho, and for that matter other HREEs. This is due to their similar complexation behaviour (e.g., Huang, 2010).

4.4. Results

4.4.1. Petrography and mineralogy

Detailed petrological descriptions of the stromatolitic rocks from the Gunflint Formation have a long history. Earlier studies reported fine-scale petrographic features reminiscent of microbial cellular structures (e.g., Barghoorn and Tyler, 1965; Awramik and Barghoorn, 1977; Moreau and Sharp, 2004), silica cements (e.g., Simonson, 1987; Simonson and Lanier, 1987; Marin et al., 2010, 2012), coated grains (e.g., Simonson, 1987; Lanier, 1989), and pyrite (e.g., Tyler and Barghoorn, 1963; cf. Papineau et al., 2005). Yet, studies of the carbonate fraction, and the possibility for some of the silica cements to be a replacement product after carbonates (e.g., Ricketts 1983; Grotzinger and Read, 1983; Grotzinger, 1986; Hofmann and Jackson, 1987; Buick and Dunlop, 1990), have received less attention (but see Markun and Randazzo, 1980; Sommers et al., 2000).

The stromatolite laminae from the Schreiber (Sch) and Frustration Bay (FB) outcrops contain an amorphous, dark-brown, organic-rich, silica matrix (Fig. 4.2A-B), which often includes fine euhedral to subhedral pyrite crystals that are typically 4-8 μm across (Figs. 4.2C-E). The pyrite may exhibit pyritohedral and octahedral morphologies, but cubic forms are more frequent. Individual pyrite crystals can reach 12-14 μm in size (Fig. 4.2D). The larger pyrite grains are concentrically zoned (Fig. 4.2E). In samples from FB, pyrite accounts for up to 6% of the bulk mineralogy. The stromatolitic Sch samples are relatively less abundant in pyrite (~3 %), but the walls of some ooids can be pervasively replaced by pyrite (Fig. 4.2F-G). This result contrasts with observations made on the correlative, but stratigraphically higher, Mink Mountain locality (MM),

where ooids are hematitic (Fig. 4.2H) and pyrite is generally absent (i.e., Planavsky et al., 2009; Shapiro and Konhauser, 2015). The primary porosity between peloid/ooid allochems is typically cemented by microquartz and megaquartz. Microquartz also comprises an isopachous cement infilling the original fenestral porosity (Figs. 4.2H and 4.3A-E).

In the Sch and FB locations, embedded within the isopachous cherty cement are fine (30-40 μm) rhombohedral crystals, which may also form mosaics within a microcrystalline silica matrix. High magnification SEM analyses of these cements reveal that the coarse rhombohedral crystals exhibit conchoidal fractures; they are silicified carbonates (Fig. 4.4B). When observed under blue light excitation, a first generation of microquartz cement surrounding the rhombs shows a dull luminescence with bright luminescent spots indicative of punctual accumulations of kerogen. The boundaries of the euhedral rhombs also display this characteristic bright luminescence (Fig. 4.4C), and these rhombohedral crystals are often in apparent optical continuity with the chert (Fig. 4.4D).

A second generation of radial-fibrous (or botryoidal) chalcedony cement infills the voids within the structures (Figs. 4.4D; 4.5A-B). This cement resembles the so-called submarine 'fan druse' as described by Shinn (1969) in the Persian Gulf, or 'spherulitic cement' described by Schroeder (1972) in Bermuda. The botryoidal chalcedony is length-slow as tested by insertion of the 550-nm full wave compensator (gypsum retardation plate) (i.e., it exhibits a high refractive index parallel to the crystallographic c-axis; see Fig. 4.5B). This is very different from primary authigenic chalcedony, which is known by exhibiting optical properties that result in a lower refractive index in the direction of the fibers; termed length-fast (Flörke et al., 1982; Graetsch, 1994; Wahl et al., 2002). In microfossiliferous stromatolites from the Proterozoic rocks of the Belcher Islands (central Hudson Bay, Canada), this kind of cement was defined as replacive chalcedony after aragonite (Hofmann and Jackson, 1987). Similar fabrics, now composed of calcite or dolomite, are also known from numerous Phanerozoic carbonate rocks and have been interpreted as replacement products of former submarine aragonite (i.e., Davies 1977; Mazzullo 1980; Given and Lohman 1981). Aissaoui (1985) provides details on the dissolution-precipitation processes that affect the mineralogy of Neogene examples of such fabrics.

Kerogen-rich patches that in cross-section delineate the various laminae often contain medium to coarse (60-140 μm), partially silicified, planar–e rhombohedral carbonate crystals (e.g.,

Fig. 4.5C). These carbonate cements are within a silica matrix and show corroded boundaries (Fig. 4.5D). When observed in SEM-EDX after an etching protocol that involved a 10-second immersion of polished samples into 6N HCl, the partially dissolved crystals reveal intracrystalline microfabrics that suggest that they predate the pervasive silicification process (Fig. 4.5E). It is noteworthy that, in samples from FB within the now silica cement, we also observed displacively replaced and isolated cubic molds and mineral casts (hoppers) (Fig. 4.5F-G). Such textures have not been previously described for the Gunflint Formation and point to localized precipitation of halite in an evaporitic peritidal zone.

Backscattered SEM shows that the medium- to coarsely-crystalline rhombs comprise chemically zoned crystals with a dolomitic composition and iron-rich cores (Fig. 4.6AB). Further 2D-XRD analyses of these rhombs show that the crystals are silicified Fe-rich members of the dolomite series, with ankeritic cores and Fe-dolomite cortices (Fig. 4.6C-D). This petrographic observation confirms previous reports of the "Lower Algal Chert Member" near the Schreiber location, where chemically zoned euhedral carbonates interspersed within the matrix were described by Simonson and Lanier (1987) and Moreau and Sharp (2004).

Using cement fabrics as a petrographic criterion, the stromatolites from the Lower Cherty Member of the Gunflint ought to have had a primary carbonate mineralogy that precipitated in a shallow peritidal and locally evaporitic setting. This correlates well with the earlier work of Markun and Randazzo (1980) which concentrated on stromatolitic cherts from the Schreiber locality. These concordant interpretations are at odds with that of Maliva et al. (2005), who extrapolated results from granular cherts that might (or might not) be representative of ooid shoal subtidal environments, to interpret the stromatolites from the Gunflint Formation.

4.4.2. Geochemistry

4.4.2.1. Trace elements

Figure 4.7 reports on the bulk rock concentrations of first row transition metals measured in Sch, FB, the hematite-bearing MM localities, and also (for comparison purposes) samples we collected from a large hemispheroid stromatolite cropping out near Kakabeka Falls (see Table 4.1). Vanadium was not detected in samples from Sch; measured V concentrations ([V]) in the FB reached 10.2 ± 0.7 ppm; while in the hematite-rich stromatolites from the MM, [V] are 3.3 ± 0.6

ppm. Chromium at Sch was 0.4 ± 0.1 ppm, and in the FB it reached 1.2 ± 0.3 ppm. The mean [Cr] value in MM was 17.7 ± 1.2 ppm. Iron was found in all samples analyzed; with hematitic specimens at MM averaging 3.14 ± 0.03 wt. %. In the dolomitic/ankeritic + pyritic samples, [Fe] ranges from 0.05 ± 0.01 (at Sch) to 2.02 ± 0.43 wt. % in FB stromatolites. Manganese was found in all of the samples, with larger contents appearing in the FB samples ([Mn] = 3,177.7 ± 908.4 ppm). Samples from MM have [Mn] = 780.6 ± 157.5 ppm. The lower contents were measured in Sch ([Mn] = 34.7 ± 1.3 ppm). In Sch, [Co] and [Ni] are consistently below 1 ppm (0.6 ± 0.1 ppm). In contrast, at FB, [Co] averaged 7.1 ± 2.8 ppm and Ni was 7.0 ± 0.4 ppm. Stromatolites at the MM are relatively enriched in [Ni] (18.3 ± 0.3 ppm) but not [Co] (3.4 ± 0.5 ppm). Copper was found relatively enriched in the hematitic stromatolites of MM (9.5 ± 1.8 ppm). The stromatolites from Sch and FB have [Cu] = 4.6 ± 1.2, and 8.7 ± 6.8 ppm, respectively. Similarly, we found that Zn is relatively enriched in the hematitic stromatolites of MM (9.5 ± 1.8 ppm). By contrast, the samples from the Sch and FB have [Zn] of 2.7 ± 1.6 ppm, and 3.6 ± 1.0 ppm. In summary, the samples from MM are consistently enriched in some transition metals, with a general depletion observed in samples from the Sch.

Figure 4.8 highlights a common feature in all dolomite/ankerite-bearing samples, where the distribution and abundance of some trace elements, such as Ni, Zn, and Fe, coincide with the carbonaceous laminae, and most Cu "hotspots" correspond to pyrite. The partially silicified, finely crystalline carbonate phases are reasonably homogeneous. Preferential concentrations of Mn, which does not readily form sulfides, are common in such carbonate phases. However, Mn is also predominantly found associated with kerogen/oxides-rich zones.

4.4.2.2. Rare earth elements

The REE systematics of ancient stromatolites has previously been used to: (1) investigate whether these elements reflect the evolving Precambrian ocean and the effects of widespread hydrothermal input (i.e., Eu anomalies, Kamber and Webb, 2001); (2) evaluate whether stromatolite accretion occurred under anoxic conditions (i.e., Ce anomalies; Van Kranendonk et al., 2003); and (3) define the environment of accretion of stromatolites (i.e., La anomalies; Bolhar and Van Kranendonk, 2007; Awramik and Buchheim, 2009). In the particular case of the Gunflint Formation, only the bulk rock REE geochemistry of hematite-bearing stromatolites has been used to evaluate the paleoenvironmental redox conditions at the time of accretion (Planavsky et al., 2009). Conversely,

there are no data for the REE signatures of dolomite- and pyrite-bearing stromatolites from the FB and Sch localities.

Figure 4.9 shows a comparison of our REE dataset and values previously reported for stromatolites of the Gunflint Formation (i.e., Planavsky et al., 2009). Our REE concentration data are also presented in Table 4.2. Except for La and Eu anomalies, the shale-normalized REE patterns are smooth, which indicates excellent analytical quality (Fig. 4.9A). The REE_{SN} data of stromatolites of Sch show characteristically flat, slightly HREE-depleted patterns (Sch: Pr/Yb_{SN} = 1.08 ± 0.24; Pr/Sm_{SN} = 0.74 ± 0.01; and Sm/Yb_{SN} = 1.45 ± 0.29), with significant positive Eu anomalies (Eu/Eu_{SN}^* = 2.03 ± 0.40). Lanthanum displays positive anomalous values (Ce/Ce_{SN}^* = 0.83 ± 0.14), and no analytically significant Ce-anomalies (Pr/Pr_{SN}^*= 0.90 ± 0.04). The stromatolitic rocks of FB (samples FB74g, A-2-75, 1-2-75) display less marked Eu anomalies (Eu/Eu_{SN}^* = 1.34 ± 0.13) than Sch, and positive La anomalies (Ce/Ce*= 0.87 ± 0.13), with slightly depleted HREE-patterns (Pr/Yb_{SN} = 1.61 ± 0.95; Pr/Sm_{SN} = 0.72 ± 0.04; Sm/Yb_{SN} = 1.45 ± 0.29). In both of these locations, Ce anomalies are not present (i.e., Pr/Pr_{SN}^* ~ 1.00) or are slightly positive (Fig. 4.9B). The samples from MM and Kakabeka Falls are characterized by Eu anomalous values (Eu/Eu_{SN}*= 1.96 ± 0.15 and 1.84 + 0.36, respectively; Fig 9A) and do not display conspicuous Ce anomalies (Fig. 4.9B-C).

We also evaluated via μXRF the distribution of Y as an indicator of the partitioning of REE within the different solid phases comprising the dolomite-bearing stromatolites. Our interest was in determining the association of this element with Ca- and Fe-bearing phases because these are the main sinks of REE and Y in such sediments (REE+Y; Bau et al., 2014). Phosphates are also important sinks of REE (e.g., Rasmussen, 1996), yet on the stromatolitic facies of the Gunflint Formation they only occur as accessory microcrystalline apatite associated to fossilized cells (Mojzsis and Arrhenius, 1998). This in contrast with observation of Hiatt et al. (2015) in the correlative Michigamme Formation, MI, USA, where phosphates are relatively more abundant. In sample FB74g from FB, the inter-correlation diagrams obtained from individual analyses conducted in steps of ~5 μm and at an analytical area of about 500 μm^2 revealed that most Y is associated with Ca-bearing phases (Fig. 4.8C). Our observations shows that the finely-crystalline carbonate phases also sequestered considerable amounts of Y, which, contrary to the zonation observed in coarse multigenic phases, seem to be homogenously distributed (at least at the scale

of our *in situ* μXRF analyses). The nature of fine crystalline dolomite within Ca-rich analytical areas makes it difficult to resolve the intracrystalline metal signatures of the small early formed carbonate phases preserved by the silicification of remnant microbial mats. Advances in micro-focussing technology, via sophisticated KB mirror setups, capable of reaching submicron-scale analytical areas, will permit future investigations of these phases, considered to be early diagenetic in origin (i.e., Ricketts, 1983).

4.5. Discussion

4.5.1. Mineral paragenesis on stromatolites of the Gunflint Formation

4.5.1.1. Petrographic and stable isotope insights

Contrary to the general model in which a viscous amorphous medium favors the growth of fibrous silica, such as silica gel (i.e., Graetsch et al., 1987), our petrographic data shows that most of the stromatolites from the Lower Gunflint Formation contain length-slow botryoidal chalcedony cement. This phase likely formed secondarily after the precipitation of fibrous carbonates (most probably aragonite). Another first generation isopachous cement appears to have been a Mg-rich carbonate, such as dolomite. As discussed above, an analogous observation was made in Paleoproterozoic stromatolites from the Belcher Islands (Hofmann and Jackson, 1987), and early formed dolomite has been also recently described in the correlative Michigamme Formation in Michigan, USA (Hiatt et al., 2015). The evidence shows that the primary carbonates precipitated subaqueously in close association with decaying organic matter, some of which was preserved as kerogen within the boundaries of rhombohedral crystals (e.g., Fig. 4.6C). The above interpretation is consistent with the process that would have governed the early stabilization process of these structures, which was presumably controlled by the breakdown of microbial biomass. Such microbially induced mechanisms often lead to a localized state of elevated pH and alkalinity, and thus to carbonate mineral oversaturation (see Gallagher et al., 2012).

Individual euhedral Fe-dolomite crystals locally corroded, silicified, and partially replaced by ankerite (i.e., Fig. 4.6) are found in the cherty matrix of the FB and Sch locations. This textural relation indicates that dolomite growth preceded precipitation of the silica as a post-depositional process (e.g., Dapples, 1979). Other early-formed carbonate cements were completely replaced by

silica due to a shallow burial silicification mechanism probably resulting from a silica oversaturated fluid permeating the structures after accretion. This early diagenetic fluid caused a coupled dissolution-precipitation reaction front, responsible for the pseudomorphic replacement of metastable carbonates. While silicification obliterated the metastable micritic and isopachous fabrics, leading to microquartz growth, it preserved the more stable rhombohedral dolomite inclusions. This is because aragonite and Mg-calcites are more soluble than dolomite under natural precipitation conditions (Morse and Mackenzie, 1990).

Replacement of primary carbonates is thought to have occurred under marine, probably evaporitic conditions, as indicated by the presence of cubic casts — interpreted here as halite — and length-slow chalcedony, which is thought to be the product of silicification of carbonate mineral phases formed under hypersaline Mg-rich conditions (Pittman and Folk, 1971; Folk and Siedlecka, 1974). Interestingly, length-slow chalcedony has been reported in other petrographic studies of the Lower Cherty Member (i.e., Markun and Randazzo, 1980), but was notably absent in oolitic chert microfacies studied by Maliva et al. (2005). Summers et al. (2000) also provided evidence pointing to a secondary silica replacement of primary carbonate ooids in rocks from the micro-fossiliferous Whitefish Falls locality in Nolalu, Ontario.

A general geochemical and thermodynamic requirement for silicification of carbonates is the existence of pore fluids supersaturated with respect to silica, and undersaturated with respect to the carbonate mineral that becomes dissolved (Hesse, 1989). Reported mechanisms for replacement of carbonates by silica are: (1) microbial metabolisms capable of locally lowering the pH, thus affecting metastable carbonate solubility and inducing silica precipitation (see Siever, 1962; Knoll, 1985; Clayton, 1986) and/or (2) the mixing of marine and continental waters, which can also induce a decrease in pore water pH (Knauth, 1979). The silicification process not only resulted in the fossilization of microbial cells beneath the surface, but also allowed for crystallographic orientations to be inherited from parent carbonate to product silica. Fluctuations in pH around the circumneutral and alkaline range in a hypersaline setting are thus considered crucial controlling factors for such silicification processes.

As proposed by Simonson and Hassler (1996), pervasive silicification was completed during shallow burial diagenesis, likely prompted by shifts in base sea level, which allowed for

the mixing of marine and continental waters. By locally affecting the chemistry of peritidal environments, such mixing process would have also shifted the saturation states of iron-bearing minerals, leading to replacement of the metastable dolomite cores by ankerite; while the less soluble Fe-dolomite crystal cortices prevailed (e.g., see Jones, 2013). In this regard, the multiple growth stages observed in pyrite suggest the partial oxidation of this phase as a likely mechanism for ankerite oversaturation of the internal precipitation environment within the stromatolites. Although some other iron-bearing minerals have been considered primary in origin (i.e., Planavsky et al., 2009), a more detailed study recently suggested instead that siderite might very well be a secondary carbonate mineral (Shapiro and Konhauser, 2015). Regarding hematite, these authors also pointed out that this mineral only dominates in areas where stromatolite-bearing horizons are in contact with Mesoproterozoic diabase sills and dikes of the Duluth Complex.

The abundance of siderite within hematitic stromatolite microfacies contrasts with its lack in ankerite/dolomite-bearing stromatolites and points to laterally variable paleoenvironmental chemistry and post-depositional diagenesis. These mineralogically dissimilar stromatolites, however, exhibit strikingly similar morphotypes, which suggests that these sedimentary structures represent a comparable accretionary setting but dissimilar diagenetic subenvironments. An early siderite phase would have formed from the enrichment in pore-water Fe(II) via subsurface Fe(III)-reducing microbes (Konhauser et al., 2005; Fisher et al., 2009), thus allowing Fe(II) to be in excess of biologically produced HS^-. Under this condition, Fe(II) was removed from solution in the presence of bicarbonate, leading to the formation of siderite (e.g., Coleman, 1985, Curtis et al., 1986). It should be recalled, however, that in the presence of moderate concentrations of sulfate, such as those characterizing most Paleoproterozoic continental margins (Partin et al., 2015), siderite precipitation promoted by Fe(III) reduction would be followed by the alteration of siderite to pyrite by sulfate reducers (e.g., Kenward et al., 2009). In this regard, *in situ* analyses of pyritized microfossils in stromatolites from the Schreiber locality suggest that these structures were stabilized in a diagenetic realm where the activity of sulfate reducers had initial significance, but were progressively limited by porosity occlusion linked to silica oversaturation and precipitation (Wacey et al., 2013). Our petrographic analyses of the FB and Sch samples further indicate that as silicification occurred, the early formed dolomite was preserved, but most, if not all, early formed siderite was dissolved.

Interestingly, as opposed to hematite that was previously reported in samples from the Schreiber Beach (Planavsky et al., 2009), our samples from this locality not only lack this phase, but the walls of some of the ooids are instead replaced by pyrite. Papineau et al. (2005) also report pyrite in cherts from Sch and measured their sulfur isotope signatures. Their study revealed a small range of $\delta^{34}S$ values (CDT) between +1.09 and +0.42‰ and $\Delta^{33}S$ values between +0.02 and +0.15‰. This range of values, however, does not allow for the identification of the sulfur source or inference on the oxygenation conditions at the time of precipitation (Papineau et al., 2005). At the correlative FB locality we observed that the majority of small pyrite grains occurred within kerogen-rich laminar areas (Fig. 4.5B, D). This could mean that either pyrite precipitated in association with the degradation of stromatolite-building microbial mats, or that it represents trapped crystals from desegregated framboids transported to the shallow shelf contemporaneous to stromatolite accretion. Based on textural evidence, and incorporating models that invoke a chemically stratified Animikie Basin (Poulton et al., 2004; 2010), an alternative mechanism for the localized abundance of pyrite is possible: transport of fine-grained pyrite precipitated in the water column to the shallow-marine loci of stromatolite accretion. Such a mechanism has been found capable of drawing pyrite in suspension from anoxic/euxinic deep redoxclines onto the shallow shelf, leading to the deposition of disaggregated framboids (see Kershaw et al., 2012; Kershaw, 2015).

Based on textural analyses, we propose that fluids undersaturated with respect to dolomite led to the partial dissolution of dolomite cores, and the precipitation of silicified ankerite may be associated with the diagenetic solubilization of iron from pyrite within the structures. The presence of disseminated chemically zoned-pyrite in specimens from FB suggests multiple post-depositional stages of pyrite dissolution and growth probably caused by repeated cycles of subaerial exposure and intertidal submergence. The ankerite cores precipitated inside hollow crystals that produced inside-out ankerite crystals that have an ankerite core encased by a Fe-dolomite cortex. The Fe-dolomite overgrowths may have precipitated under the influence of methanogenic and Fe(III) reducing bacterial communities operating in a near-surface diagenetic environment (e.g., Coleman, 1985; Curtis et al., 1986; Konhauser et al., 2005, Beal et al., 2009), but *in situ* carbonate $\delta^{13}C$ analyses would be required to test this hypothesis. Variations in pH linked to pyrite solubilisation would have caused dissolution of primary Ca-rich dolomite in the

cores of the crystals (see Jones, 2013, and references therein), which latter — in a HS^- limited, but alkaline re-precipitation environment — resulted in the co-precipitation of iron and manganese into the core-replacive ankerite phase. As observed by Marin et al. (2010), the petrographic evidence indicates that this process predates microquartz and megaquartz formation and occurs under silica-saturated pore water conditions. Recent nanoscale isotope analyses of pyritized microfossils in samples from the Sch location (Wacey et al., 2013), reveals that owing to coeval silicification, sulfate anion concentrations became rapidly depleted leading to dispersion of the sulfur isotope signature. Such a result places additional constrains on the timing of precipitation of the mineral assemblage.

Bulk rock measurements of $\delta^{13}C$ in carbonates from stromatolitic cherts of the Lower Gunflint also offer some insight, but their interpretation is not straightforward. Previous work has shown that they average -2.9‰ (Strauss and Moore, 1992), and in the microfossiliferous chert outcropping at the Frustration Bay locality, they exhibit near 0‰ values (Winter and Knauth, 1992). This $\delta^{13}C$ signature is also observed in early formed ankerite and siderite phases comprising analog facies of the Upper Gunflint, and has been interpreted as the result of a dominant marine bicarbonate source during carbonate mineral stabilization (e.g., Carrigan and Cameron, 1993). When this presumably seawater-derived signature ($\delta^{13}C \approx 0‰$) is contrasted with the *in situ* organic carbon isotope content of *bona fide* Gunflint microfossils (-32 to - 45‰; House et al., 2000), the organic $\delta^{13}C$ values seem too negative to be attributed to isotopic fractionation by cyanobacteria, and generally too positive to be attributed to isotopic fractionation by methanogens (Wacey et al., 2011). Nevertheless, elevated pCO_2 levels and hence high dissolved CO_2 concentrations in the surface Paleoproterozoic ocean (Sheldon, 2006) should have been concomitant with increased biological discrimination against ^{13}C during neritic microbial photosynthesis (see Hollander and McKenzie, 1991; also Riding, 2006). It is also the case that variations in the $\delta^{13}C$ values of marine organic matter can only be temporarily mirrored by the ^{13}C values of seawater DIC (e.g., Naafs et al., 2016). Therefore, not only would the $\delta^{13}C \approx 0‰$ of carbonates in the Gunflint Formation point directly to a predominant marine bicarbonate source during carbonate mineral stabilization, but the biological fractionation discussed by Wacey et al. (2011) is likely linked to redox stratification concurrent with fluctuations in the DIC and DOC reservoirs in the Precambrian ocean (i.e., Bekker, et al., 2008; Poulton et al., 2010).

Incidentally, in the Upper Gunflint member the $\delta^{13}C$ values of second generation carbonates are shifted toward lighter values (down to -7‰), suggesting a more significant incorporation of oxidized organic carbon during diagenesis (Carrigan and Cameron, 1993). The ^{13}C contents of such Fe-rich carbonate phases, however, contrast with the isotopic carbon signature that could be expected for Fe(III) reduction ($\delta^{13}C \approx$ -25 to -10‰; Coleman and Raiswell, 1993). As such, it was argued that the bulk rock carbon isotope data of the unmetamorphosed carbonates of the Gunflint Formation reflect the combined effect of a variable admixture of DIC influenced by microbial Fe(III) reduction (e.g., Bekker et al., 2010) and sulfate reduction (e.g., Wacey et al., 2013), with seawater bicarbonate and DIC evolved during shallow burial methanogenesis (e.g., Carrigan and Cameron, 1993). Bearing in mind that silicification likely minimized pore-water flow and hence closed these isotope systems early during diagenesis (Wacey et al., 2013), then a careful evaluation of the multi-isotope signals of carbonates in the stromatolites of the Gunflint Formation would offer insight into the problems in using carbon isotope signatures to recognize specific microbial processes (see Raiswell and Fisher, 2000 for details) and the apparent decoupling of the Paleoproterozoic carbonate and organic carbon records (Bekker et al., 2008). Probing such signatures in the range of carbonate mineralogies discussed here still presents an instrumental difficulty (see Riciputi et al., 1998 for details).

Overall, our petrographic insights and the evaluation of reported stable isotopes data allow us to propose the following mineralization sequence for the stromatolites of the Gunflint Formation:

1. Mg-calcite, aragonite, and minor dolomite co-precipitated subaqueously, infilling the void spaces of the organo-sedimentary structures. Their precipitation was linked to the degradation of labile organic matter of microbial origin, which may also have led to some primary pyrite precipitation. This was probably concomitant with early formed siderite dissolution followed by authigenic pyrite precipitation. Locally, halite co-precipitated with carbonates.

2. Early diagenetic replacement of metastable carbonate cements and halite by silica, with minor early formed dolomite crystals preserved.

3. Partial dissolution of primary dolomite in association with pyrite oxidation, followed by Fe-dolomite overgrowth and replacement of early formed dolomite cores by ankerite. The ankerite

precipitated prior to the onset of megaquartz formation infilling the remaining void space of the stromatolitic structures (cf. Marin et al., 2010).

4. In areas affected by Fe-rich pore waters that evolved after a Mesoproterozoic mafic intrusion (Shapiro and Konhauser, 2015), oxidation of Fe(II) first decreased the pH of the pore water system, and thus led to complete dissolution of both first and second generation carbonates, with subsequent precipitation, on a regional basis, of hematite (in the presence of pore-water O_2). As conditions favourable for Fe(III) reduction were progressively reinstated, a second stage of alkalinity production, with low biologically produced HS^-, allow for siderite precipitation (in the absence of pore-water O_2). There was also additional silicification.

4.5.1.2. Other geochemical insights

The various samples analyzed show insignificant (i.e., Ce/Ce* ~ 1.0) to positive La anomalies (mean: 0.95, median: 0.93). Variability in these anomalies between sites would have resulted from lateral variation in marine vs. continental influences in the peritidal realm, with areas affected by runoff probably exhibiting dilution of a seawater-derived La signature; although positive La anomalies might not be limited to marine settings (e.g., Johannesson et al., 2006, their Fig. 4.9).

Europium anomalies were not detected in our samples from the Sch, but are present in samples from the FB and MM, probably reflecting the local effects of exhalative hydrothermal input over the post-depositional redistribution of REE in both the Lower Cherty Member (i.e., FB) and the Upper Cherty Member (i.e., MM). Post-depositional alteration would have locally affected the primary REE contents and altered the initial Eu anomalies (Shields and Stille, 2001).

Siderite + hematite-bearing samples display REE series and Ce-anomalies (Pr/Pr*) patterns that are essentially similar to those of the samples composed of dolomite/ankerite + pyrite (Fig. 4.9A). Under the dissimilar physicochemical conditions controlling the precipitation of these purportedly primary mineral assemblages, the REE should have exhibited fundamentally different complexation behaviour, reflecting aqueous and mineral-specific REE fractionation during incorporation into their respective early diagenetic phase. This, in turn, should have produced dissimilar REE abundances and distribution trends (Kawabe et al., 1999; Bau and Koschinsky, 2008; Bau et al., 2009). For instance, in modern seawater, primary carbonate minerals exhibit a

preferential scavenging of light REE compared to heavy REE when compared to primary hydroxide minerals (Elderfield, 1988). Accordingly, the REE_{SN} patterns of Fe–oxide minerals should display different shale-normalized ratios and distribution patterns when compared with carbonate minerals (Bau et al., 1996; Bau et al., 2014), particularly if both of them precipitated from a Paleoproterozoic seawater source. Thus, our results suggest that bulk shale-normalized REE values of the Lower Gunflint stromatolites could not be a pristine record of the redox conditions prevailing at the time of early microbial mat mineralization.

By following the same line of thinking, and considering as well the dissimilar redox conditions that would have characterized the accretionary environments of our samples, then their similar anomalous bulk shale-normalized Pr/Pr* values represents an suspicious feature. This feature cannot be discriminated by using the stromatolite mineral assemblage as a criterion. Our combined dataset suggests that the mineral association siderite + hematite result from a ferruginous mineral stabilization environment probably influenced by exposure of Fe(II)-bearing exogenous fluids to rising atmospheric oxygen levels, and little to none biologically produced HS^-. As suggested by Shapiro and Konhauser (2015), this mineral association would have resulted from a post-depositional mixing process involving the localized Mesoproterozoic flow of reducing exogenous fluids trough the stromatolititic horizons now comprising the Upper Gunflint Formation. Hence, hematite precipitated when the Fe(II)-bearing pore water system came into contact with oxidizing meteoric fluids percolating the sequence; while siderite precipitated after Fe(II) reduction, when this pore water system affected by meteoric water admixture became alkaline and O_2 depleted (Shapiro and Konhauser, 2015).

On the other hand, and as discussed above, the dolomite/ankerite + pyrite bearing stromatolites could be considered a better-preserved early diagenetic precipitation environment, where the marine ferruginous conditions that interacted with biologically produced HS^- prior to silicification (Wacey et al., 2013), were not largely affected by the admixture process described above. Given that Ce is the only REE relevant for redox interpretations, our results suggest that bulk shale-normalized REEs values of the Lower Gunflint stromatolites indicate that the redox conditions prevailing at the time of early microbial mat mineralization were not responsible of the localized abundance of hematite.

By comparing the REE_{SN} signatures of carbonate- and pyrite-bearing stromatolites with those of their hematite- and siderite-bearing analogues, our bulk data reveal that rather than supporting a redox stratified shallow water column, the trace element inventories of these stromatolites reflect a dissimilar burial diagenetic history. Therefore, the textural features and chemical signals of stromatolite facies in the Gunflint Formation more likely reflect contrasting rates of continental runoff and solute delivery, or the temporarily and spatially variable evolution of diagenetic fluids due to mixing with exogenous fluids, rather than the vertical redox structure of shallow Precambrian seas.

4.5.2. Perspectives

By the late Archean and during the Paleoproterozoic, the range of early diagenetic reactions leading to marine authigenesis in ancient peritidal settings were increasingly influenced by inputs of oxidative weathering products, such as increasing fluxes of sulfate and trace metals (Konhauser et al., 2011). The fluxes were, in turn, controlled by various cyclic depositional controls, such as relative sea-level and climate changes (Eriksson et al., 1998; Sommers et al., 2000), that were capable of drastically affecting the chemical composition of pore-waters and the minerals precipitated in equilibrium with those waters. Hydrothermal fluids may have also been locally important for diagenetic mineral stabilization (see Walter, 1972; Still and Claure, 1986; Sommers and Awramik, 1996).

The detailed characterization of the style and extent of diagenetic alteration is a critical first step in evaluating the primary composition of ancient stromatolites, and hence the chemistry of the solutions once in equilibrium with the mineral comprising the accreting stromatolite structures (cf. Dickson, 2009). In this regard, similarities and/or differences between the REE distribution of these structures cannot solely be explained by the REE speciation in seawater, as the reactive solid phases originally stabilizing within the stromatolites had different scavenging properties (see Bau and Koschinsky, 2009). Moreover, because they were trapped, bound or precipitated within microbial mats, the REE content would have been progressively remobilized and incorporated into secondary phases only after the breakdown of the organometallic bonds and the reduction of the ferric oxyhydroxides took place. The remobilization of metals of interest is variable and proportional to the rates of disincorporation of these elements into their primary binding phase; while the rates of incorporation into secondary phases was not only a function of the preferential

affinity of these metals for the available organic ligands, but also of the variable physicochemical conditions governing the diagenetic alteration process within the structures (e.g., Petrash et al., 2012). Regarding REE, recent work by Johannesson et al. (2014) found a strong pH dependence of REE uptake by modern microbialites, which results from significant changes in La speciation in the circumneutral pH range. All of these factors can be further complicated by the fact that shallow burial diagenetic mixing of marine-derived and exogenous waters can also lead to elemental mobilization and partitioning (Shields and Stille, 2001).

From the discussion above we conclude that bulk rock datasets of Paleoproterozoic stromatolites do not permit unequivocal predictions on how the diagenetic fluids and silicifying solutions that were once in equilibrium with contemporaneous seawater interacted with the microbialite-constructing communities responsible for the "algal" (stromatolitic) facies, or how they affected the primary bulk-rock chemical signals. These fluids interacted with the microbialite-constructing communities responsible for the "algal" (stromatolitic) facies, such as those interrogated in the Gunflint Formation, where the preservation of a primary bulk-rock chemical signal seems unlikely. Clearly, more investigation of metal uptake by lithifying biological systems is necessary to evaluate whether or not the multigenic mineral assemblages comprising ancient stromatolites would have recorded a seawater-derived signature vs. the temporally and spatially variable diagenetic fluids that influenced their multi-step precipitation process (cf., Johannesson et al., 2014). In this regard, laboratory experiments (e.g., Robbins et al., 2015; Picard et al., 2015) offer an attractive avenue for further assessing the extent of preservation of primary transition metals and REE partition patterns under diagenetic conditions.

Furthermore, *in situ* analyses of chemical zoning of carbonates within the studied stromatolites using high-resolution spatial probes would be useful to clarify the early diagenetic picture that emerges from our re-assessment. These may offer an accurate record of progressive changes in the diagenetic redox conditions during crystal growth, but in most cases, their values are far from being a record of the concentration values of redox-sensitive elements in seawater at the time of precipitation. In this regard, only fine crystalline and well-preserved carbonates, such as those described here, or as detailed by Lepot et al. (2008) in stromatolites from Tumbiana Formation in Western Australia, are appropriate for use in the determination of paleo-seawater composition. Nonetheless, the small crystal size of such early formed crystals represents an

analytical challenge that can only be undertaken by applying emerging micro- and nano-focused methods and accurate instrumental calibration protocols.

4.6. Conclusions

Validating the model of stratification of Precambrian oceans requires detailed information on the redox-sensitive trace metal concentrations of Precambrian shallow marine rocks. Such successions are of paramount importance to resolving the spatial variability in ancient oceanic redox structure. Difficulties surrounding the application of bulk-rock chemical indicators to interpret the depositional conditions of peritidal facies include: (1) uncertainties on whether the elemental systematics of authigenic minerals comprising these structures reflect early biological vs. secondary abiological processes; (2) difficulties in elucidating the primary origin of specific elemental signatures of silica phases, some of which might be pseudomorphs after primary carbonates; (3) the general lack of understanding on how diverse syn- and post-depositional processes, that are dependent on poorly known sea level, burial, and exhumation histories, would have shifted the primary signatures of the early formed precipitates; and (4) variable circulations patterns and exogenous sources of elements, which may have also been responsible for significant post-depositional mineralogical variations.

Our data, taken together with the stratabound relation described by Shapiro and Konhauser (2015), show that the abundance of hematite and siderite within the Gunflint stromatolites might well represent a localized burial diagenetic condition. Were these minerals primary in origin as generally accepted (i.e., after Floran and Pipike, 1978), then the similitude of the bulk rock REE signatures of the stromatolite samples evaluated here suggests that shale-normalized Ce anomalies of these structures might not be amenable for regional scales redox paleoceanographic interpretations. In view of our results, interpretations of shallow marine redox stratification by solely using parameters such as Ce anomalies and poorly constrained isotope systems are not valid.

Should *in situ* transition metal signatures and REE data of stromatolites be used in further paleoenvironmental investigations, recrystallized carbonate phases must be avoided for interpretations of paleo-seawater composition. Perhaps the small size primary dolomite crystals described here offer such an opportunity. However, the presence of kerogen and other inclusions

together with the relatively low spatial resolution of currently available laser ablation techniques (e.g., 45 μm in diameter or above) make it difficult to target such primary phases. A more extended use of rapidly advancing photon and ion probes with a sub-micrometer scale resolution could provide a solution to this analytical challenge.

Table 4.1. Trace metal concentrations (ppm) and mineralogical and morphological features of the stromatolite samples

Sample name and locality	V	Cr	Mn	Fe	Co	Ni	Cu	Zn	Mineralogy/ Description
Frustration Bay (FB)									
FB74g1	9.0	0.7	2190	14778	4.2	7.29	1.6	2.3	Silicified multifurcate stromatolites and centimeter-scale hemispheroids with ankerite, pyrite, and minor fine crystalline dolomite.
FB74g1	10.2	1.1	2351	17076	4.4	7.55	2.2	3.0	
A.2-75	11.3	7.1	4992	28608	12.6	62.4	22.4	95.5	
Schreiber (Sch)									
Sch 1-2-1	<DL	0.4	36	557	0.6	0.7	5.7	3.8	Silicified multifurcate stromatolites with pyritized ooids/ peloids. Ankerite and minor fine crystalline dolomite
Sch 1-2-1	<DL	0.5	36	563	0.6	0.7	5.8	3.4	
Sch 1-4-1	<DL	0.3	32	491	0.5	0.6	2.2	1.5	
Mink Mountain (MM)									
MkM3	3.9	2.0	623	14737	1.7	1.2	6.2	11.2	Silicified hematite/ siderite-rich multifurcate stromatolite
MkM4	2.7	2.6	938	16058	1.2	1.6	3.7	7.7	
Kakabeka Falls									
Kaf 2-1	20.4	1.7	3436	53823	8.2	7.18	27.2	4.3	Large silicified hemispheroidal stromatolite with ankerite and calcite
Kaf 2-2	1.92	0.36	2681	28333	3.03	0.53	16.0	6.51	

Table 4.2. REE data (ppm) pertaining the studied stromatolites

Sample name and locality	La	Ce	Pr	Nd	Sm	Eu	Gd	Tb	Dy	Ho	Er	Tm	Yb	Lu
Frustration Bay (FB)														
FB74g1	6.51	17.17	2.56	11.21	2.24	0.60		0.26	1.37	0.27	0.65	0.06	0.33	0.04
FB74g1	5.82	14.82	2.08	8.89	1.72	0.46		0.23	1.29	0.26	0.66	0.07	0.36	0.05
A.2-75	3.69	4.38	0.49	2.10	0.46	0.14		0.12	0.71	0.16	0.41	0.05	0.27	<DL
Schreiber (Sch)														
Sch 1-2-1	2.03	3.53	0.39	1.62	0,33	0.12		0.05	0.30	0.06	0.16	0.02	0.10	<DL
Sch 1-2-2	1.98	3.52	0.38	1.61	0.32	0.11		0.04	0.29	0.05	0.15	0.03	0.10	<DL
Sch 1-4-1	2.17	3.70	0.46	1.69	0.40	0.19		0.05	0.36	0.07	0.22	0.03	0.18	0.03
Mink Mountain (MM)														
MkM3	1.91	3.61	0.39	1.46	0.26	0.10		0.03	0.21	0.04	0.12	<DL	0.11	<DL
MkM4	065	1.39	0.12	0.44	0.07	0.07		0.02	0.04	0.01	<DL	0.03	0.65	<DL
Kakabeka Falls														
Kaf 2-1	4.41	8.01	0.97	3.93	0.80	0.31		0.09	0.50	0.12	0.36	0.05	0.31	0.04
Kaf 2-2	0.28	0.67	0.06	0.26	0.06	0.02		0.01	0.07	0.02	0.05	0.01	0.01	0.01

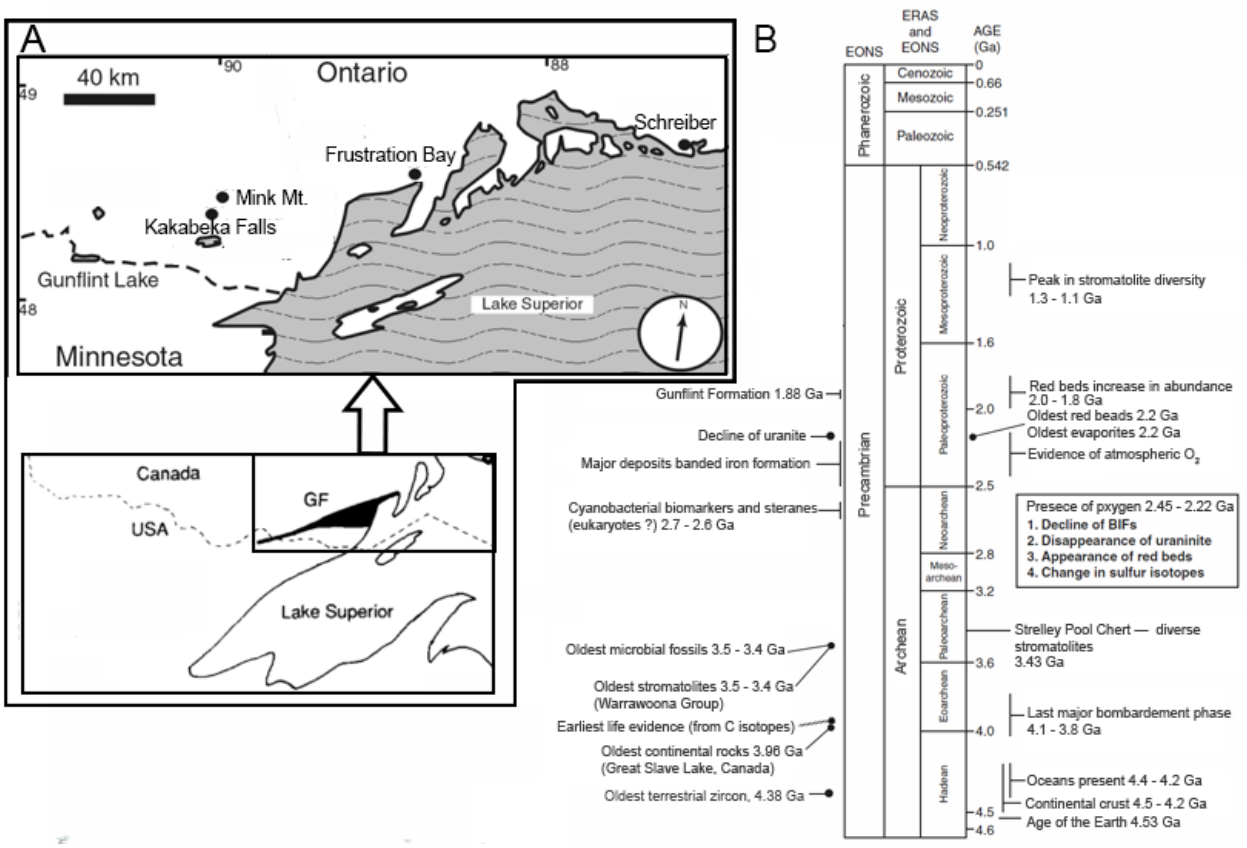

Figure 4.1. Location of the stromatolite occurrences studied here. On the right, the Gunflint Formation and its chronostratigraphic relevance within the general context of the oxygenation of the Earth's atmosphere and evolution of primitive life (After Taylor and Taylor, 1993; Farquhar et al., 2011, Mojzsis et al., 2014).

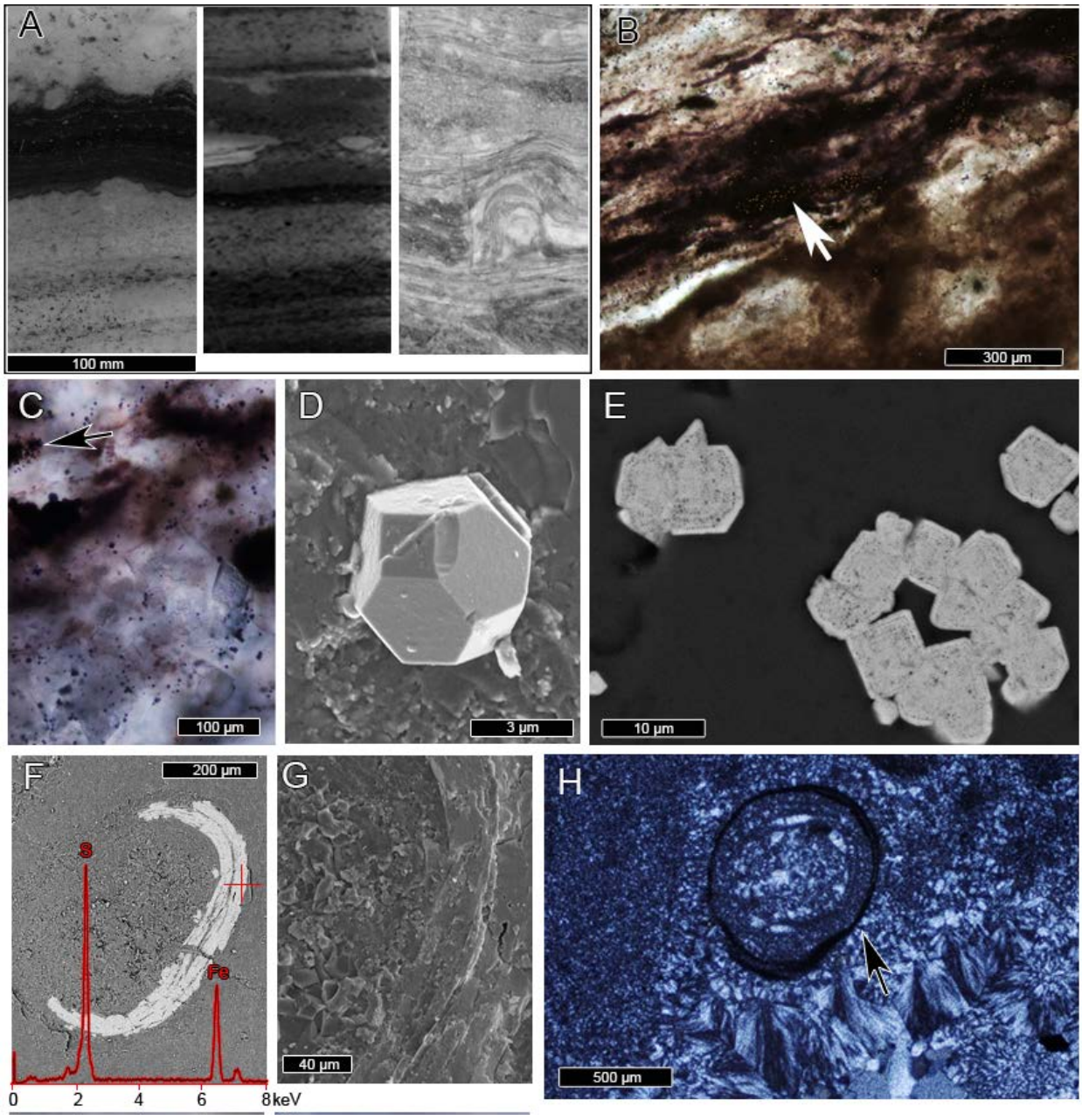

Figure 4.2. Textural features of the stromatolites from the Lower Gunflint Iron Formation (1/4). A-B: The laminae defining the stromatolites are widely defined by the abundance of carbonaceous organic matter, which is also finely disseminated throughout the matrix, and often contain accumulations of pyrite. C: Pyrite is also disseminated throughout the silica cements, but it is more abundant in the laminar carbonaceous patches (arrow). Note that this photomicrograph was optimized with a combination of transmitted and reflected light to show the abundance of pyrite. D-E: Pyrite crystals often exhibit pyritohedral habits and in some cases can be zoned. F-G: In the Schreiber locality, pyrite is often replacing the walls of ooidal features. The EDS shown in back scatter in F, was obtained in the area shown in "G". H: In samples from the MM location, iron oxides (arrow) occur in association with ooids cemented by microquartz.

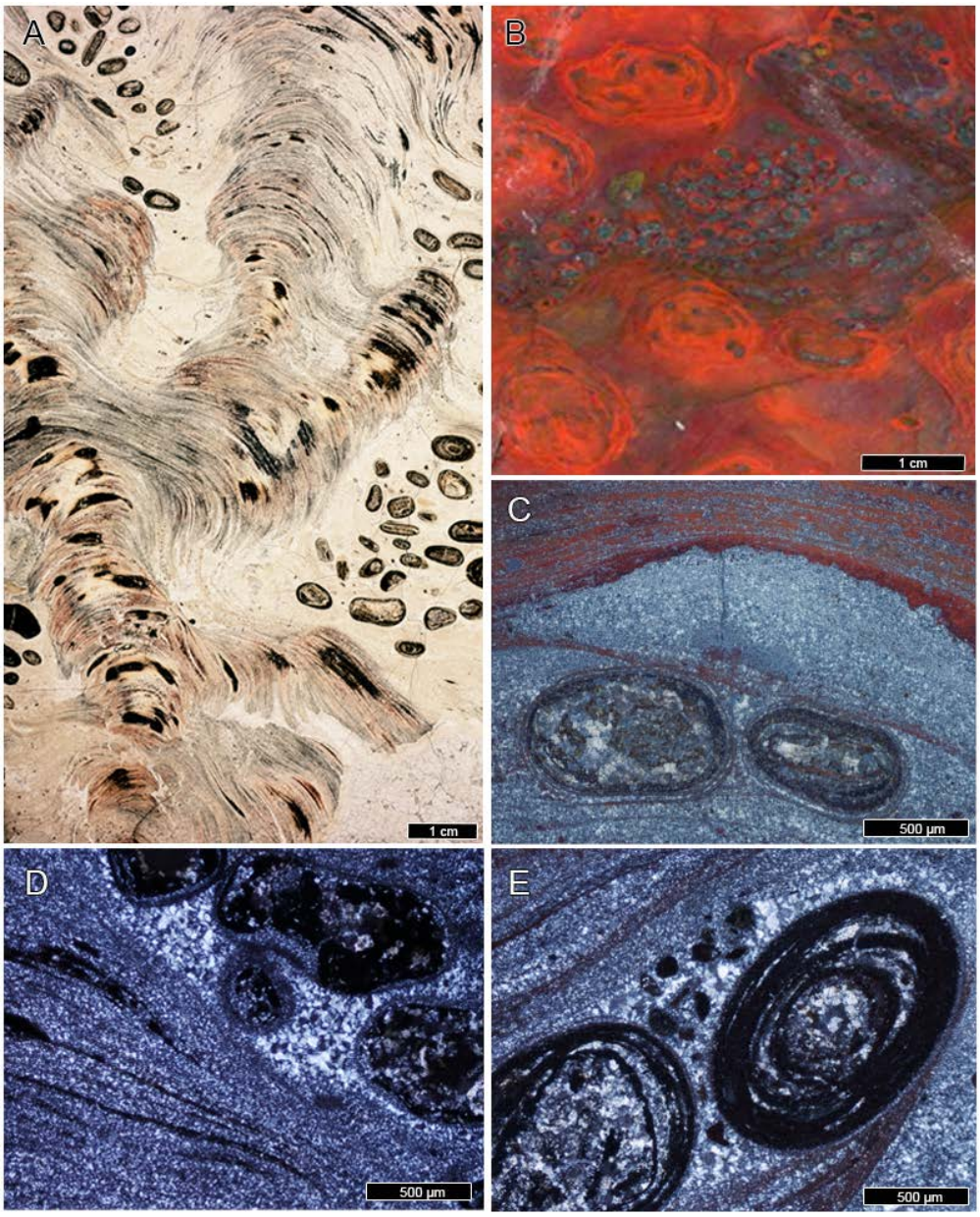

Figure 4.3. Textural features of the stromatolites from the Lower Gunflint Iron Formation (2/4). A-B: Columnar branching multifurcate stromatolites dominate the morphotypes on the Mink Mountain locality. C: the stromatolitic/ oolitic chert is hematite-rich. Note the abundance of coated grain infilling voids spaces among the laminar structures. D-E: These coated grains would be intraclasts trapped at the time of stromatolite accretion, their nuclei may also be comprised of chert fragments, requiring the nuclei to have formed within reach of erosion (i.e., near the sediment-water interface). The cortical laminae are hematitic/magnetitic; the interstices are filled with drusy megaquartz.

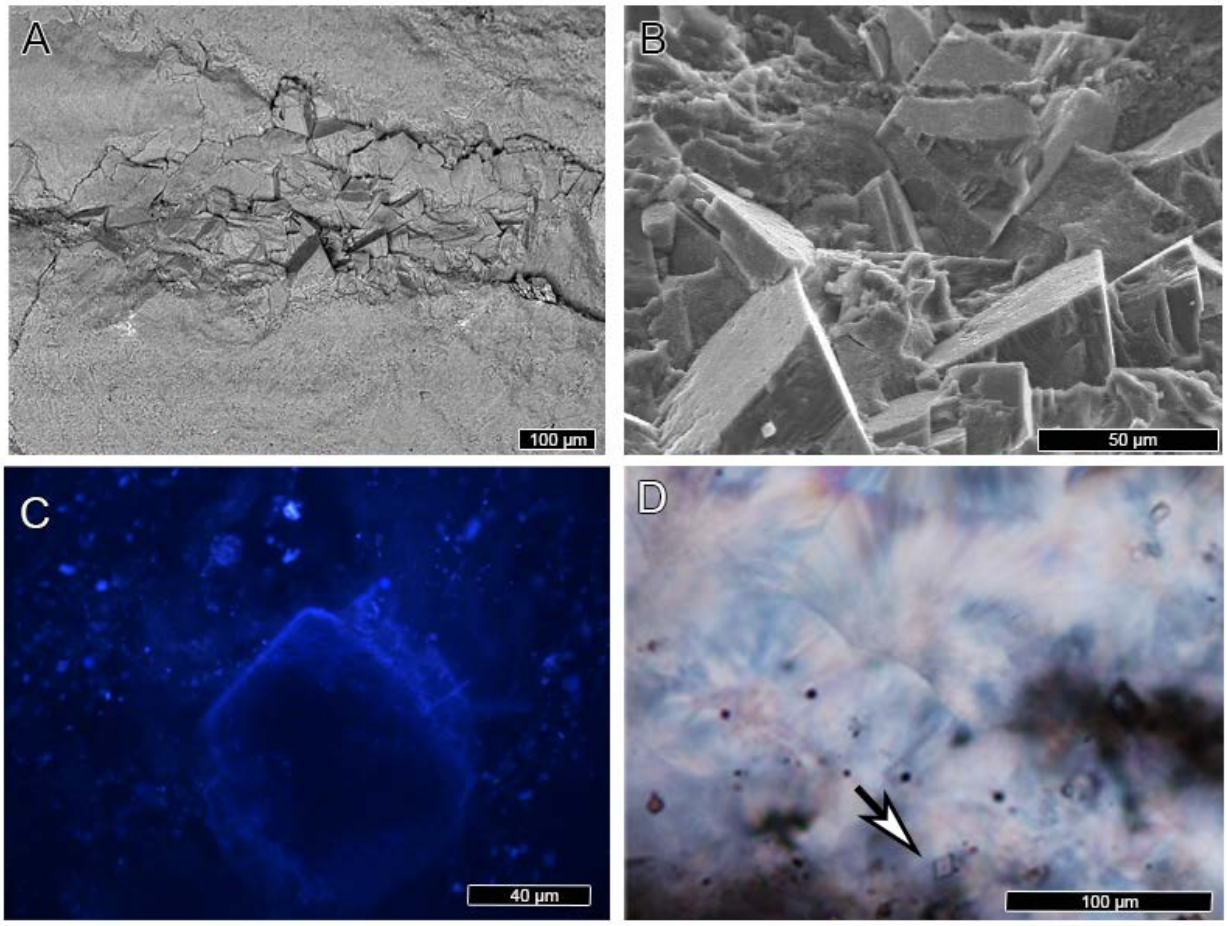

Figure 4.4. Textural features of the stromatolites from the Lower Gunflint Iron Formation (3/4). A-B: SEM photomicrographs are showing first generation isopach cements containing microquartz and fine crystalline rhombohedral silica phases. C: The rhombohedral features are coated by luminescent organic matter, which is also dispersed into areas dominated by microquartz, but not within the fibrous fabrics. D: Botryoidal slow-length chalcedony occurs in a textural relation that suggests that precipitation of this cement postdate the fine-scale rhombohedral features.

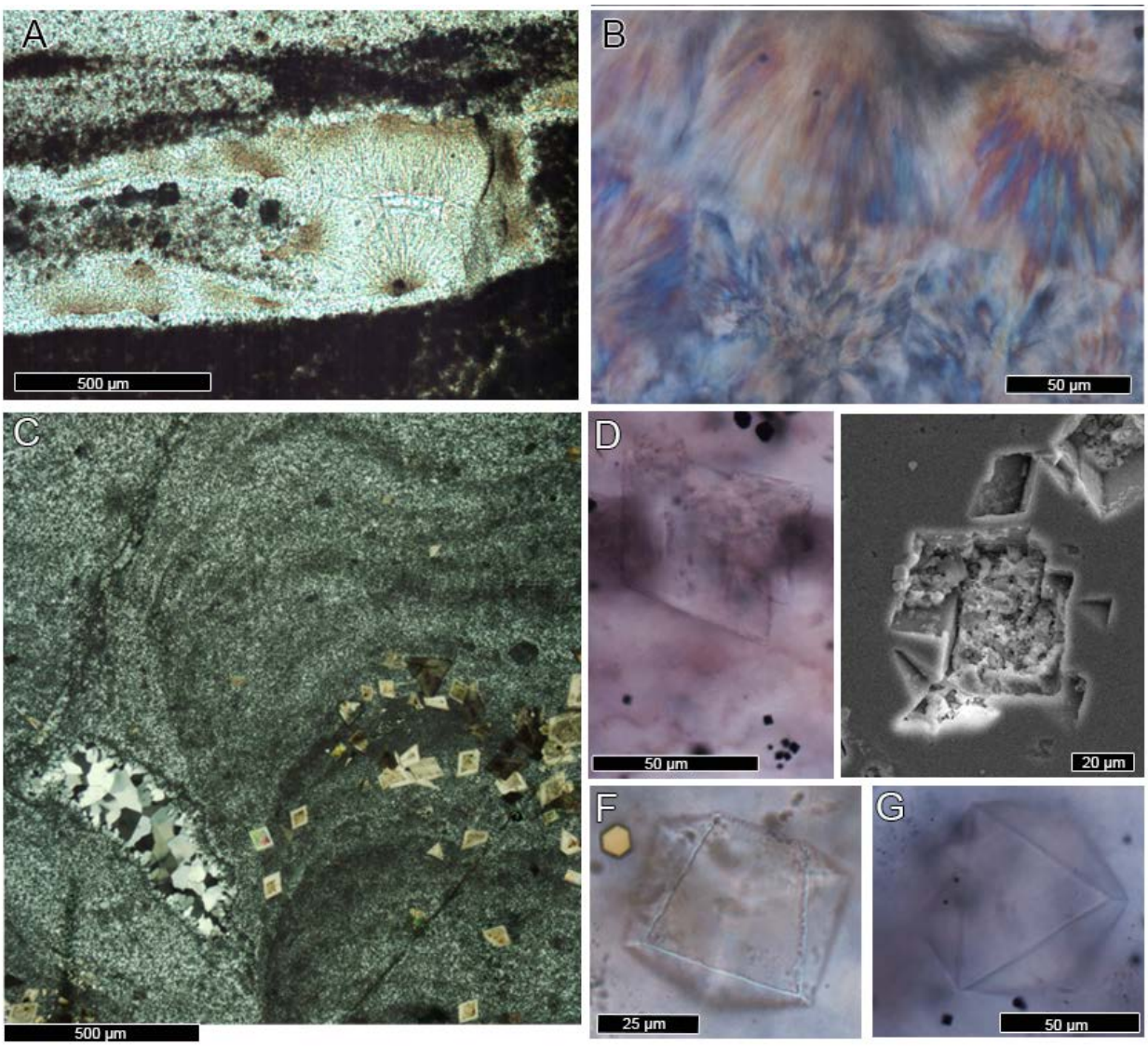

Figure 4.5. Textural features of the stromatolites from the Lower Gunflint Iron Formation (4/4). A-B: A first generation of cement is isopachously coating both laminar and ooidal/ peloidal allochems. Often a second generation of cement infilling the voids is radial-fibrous (botryoidal) chalcedony after aragonite. Notice the second order interference colours in the radiaxial cement (B: phase-contrast plus crossed nicols). C: Detail of a small silicified branching columnar stromatolite from the Schreiber locality. Notice the local abundance of carbonate rhombs, which are restricted to the structure. This sample exhibits a pore filling drusytexture comprised of first generation isopachous quartz followed my megaquartz cement infilling void spaces. D: Within the silica matrix on Frustration Bay samples, the silicification process preserved euhedral rhombs in apparent optical continuity with silica, these medium crystalline rhombs are often corroded. Notice pyrite crystals with different habits. E: The kerogen-rich patches contain partially silicified planar–e rhombohedral carbonate crystals, which in polished section become much more evident after dissolution with 6N HCl (10 s). F-G: cubic crystal cast morphologies in a silica matrix observed in the microfossiliferous sample Fb74g.

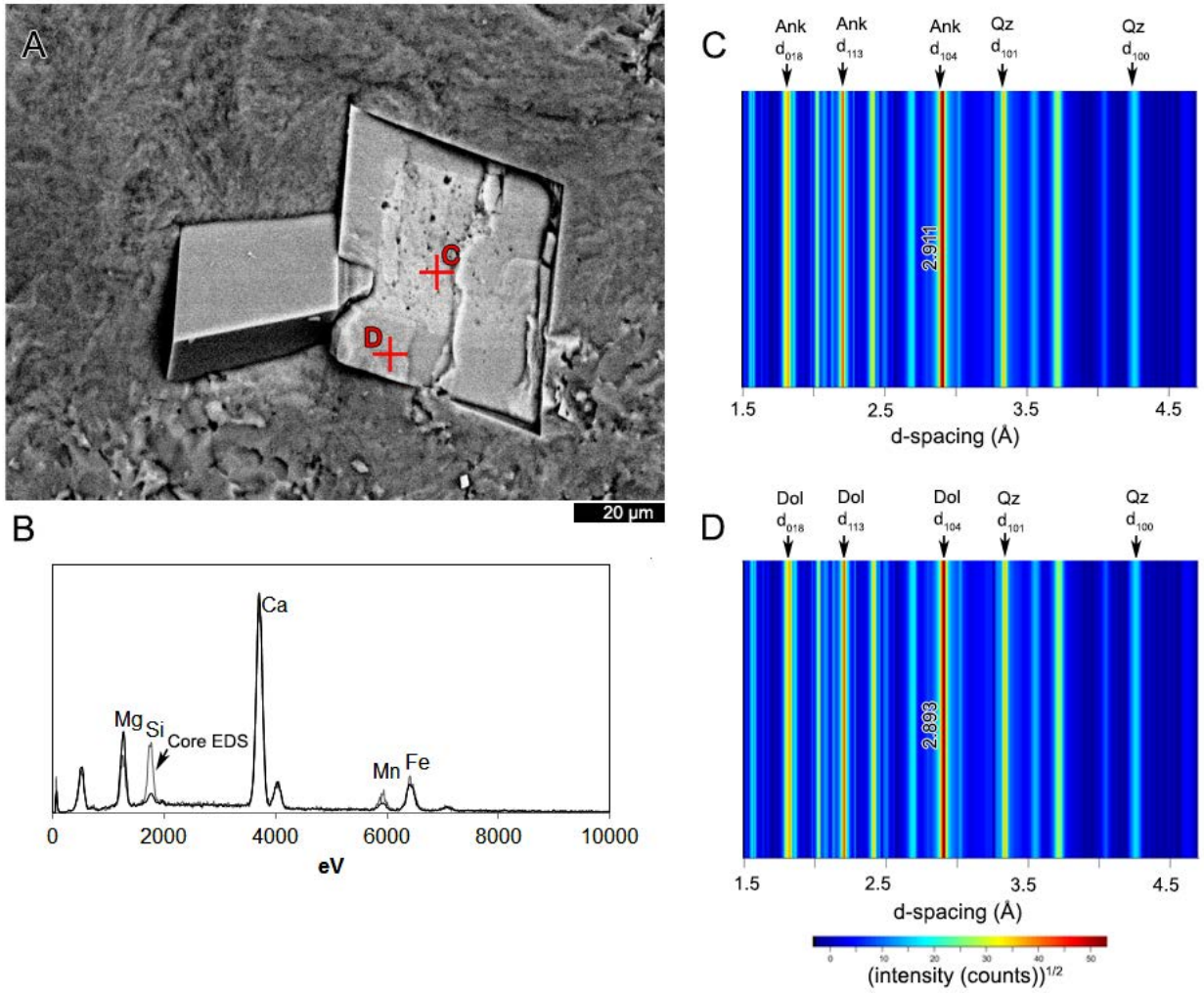

Figure 4.6. Synchrotron-based XRD results on zoned carbonate from a sample from the Frustration Bay locality. A-B: zoned carbonate crystal (BSEM + EDS). C-D: Fine-scale µXRD analyses of such crystals revealed that they are silicified Fe-rich members of the dolomite series, with ankeritic cores and Fe-dolomite cortices.

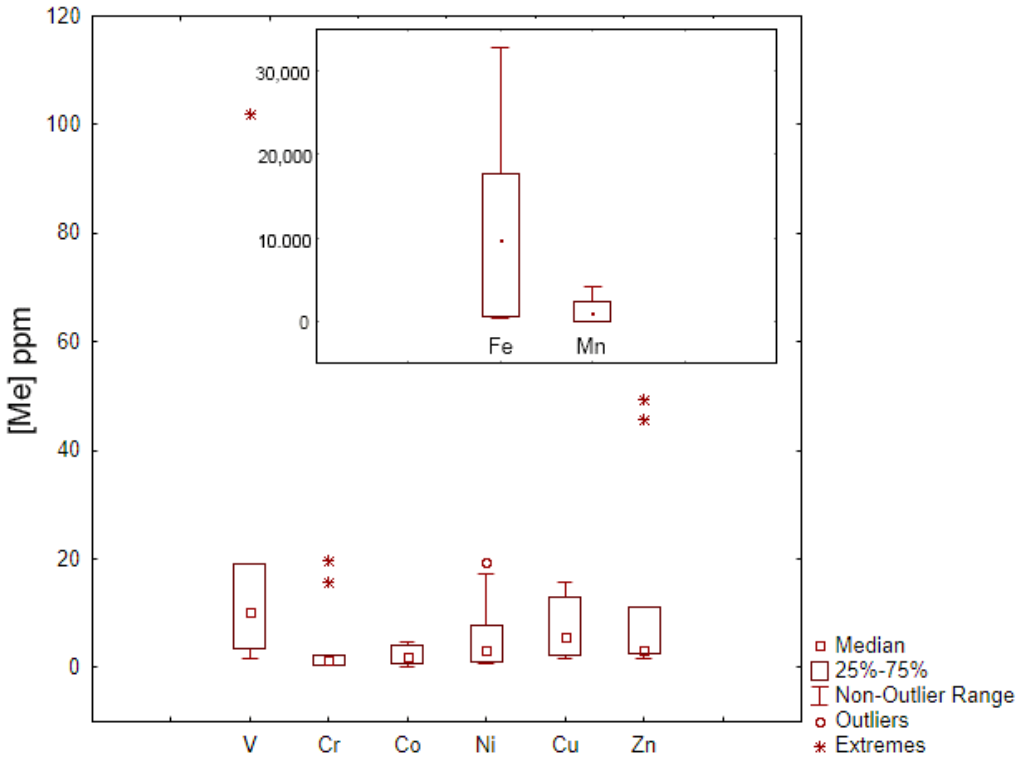

Figure 4.7. Box-plot diagram is showing the concentration range of the first row transition metals ([Me]) on the stromatolite samples. The inset displays the concentration range of Fe and Mn, which are in a larger range. See further explanation in the text.

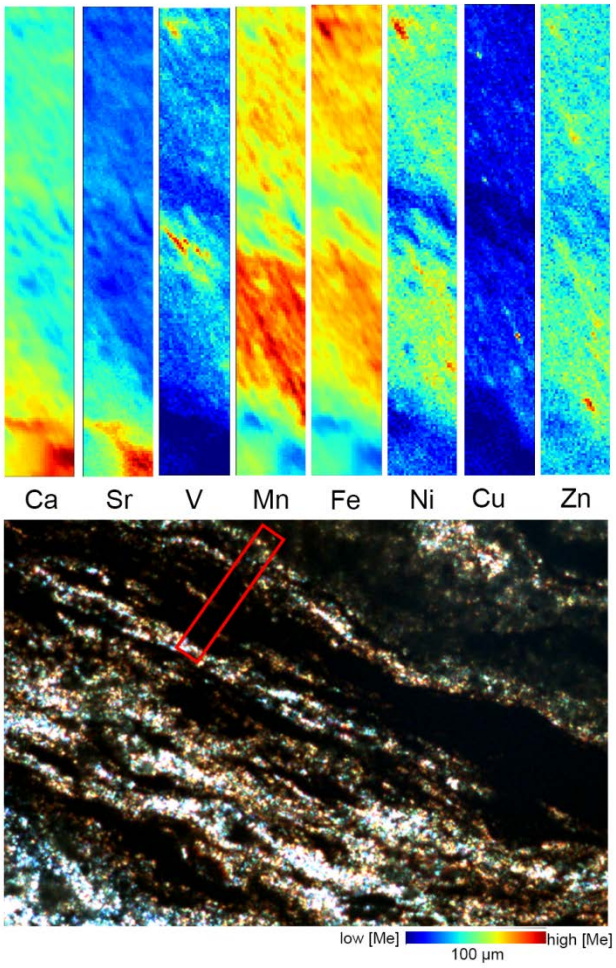

Figure 4.8. Micro-XRF map over a representative laminar zone of a stromatolite from the Frustration Bay microfossiliferous locality of the Gunflint Formation (sample is FB74g). The colour-coding convention assigns blue to the minimum and red to maximum deconvoluted peak area of the element. B-C: Elemental correlation plots, they show that most Y (and probably HREE, see main text) is associated with Ca-bearing phases. Note that an important fraction of Fe is within Fe-Ca carbonates (i.e., ankerite and ferroan dolomite).

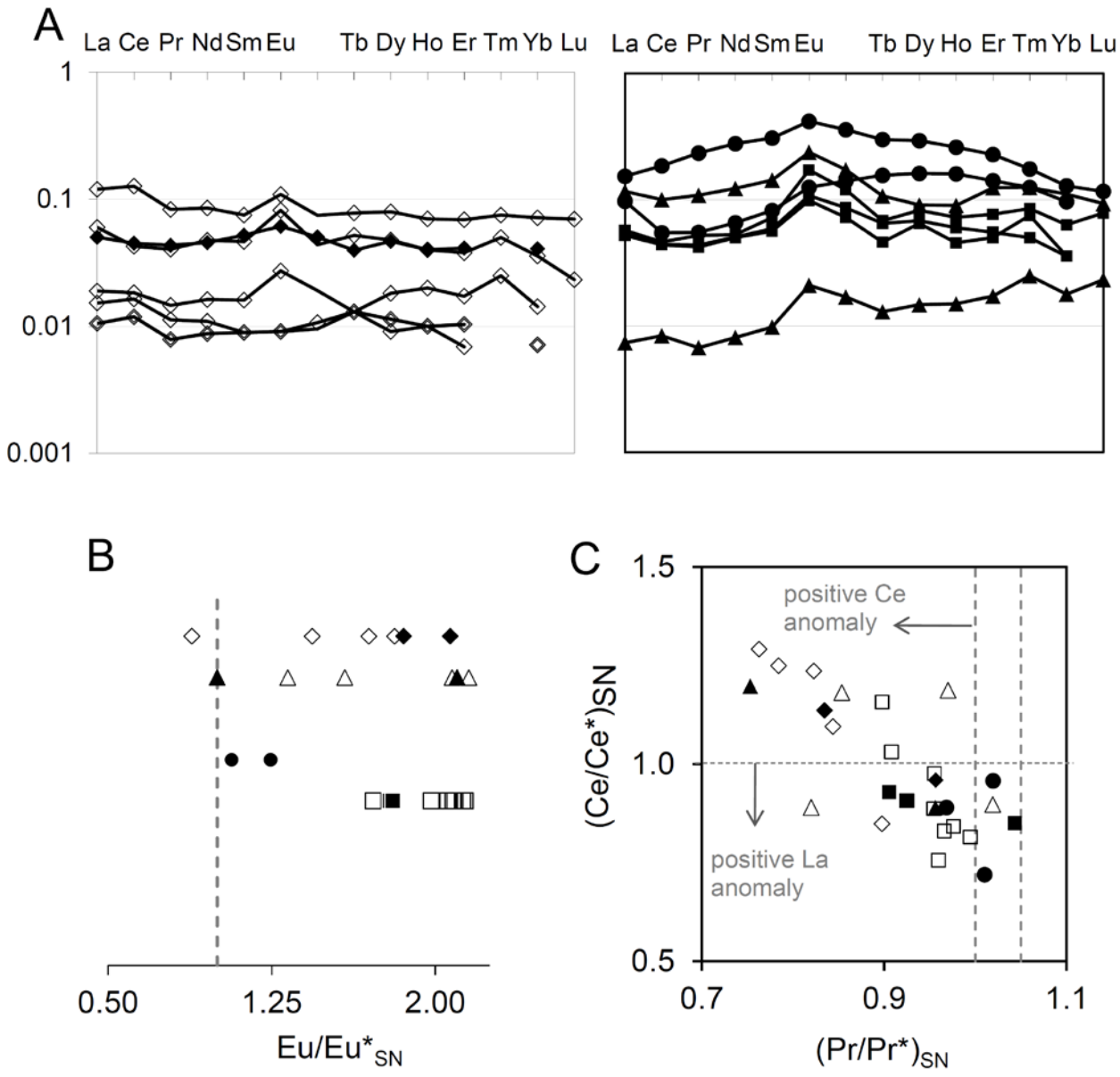

Figure 4.9. Shale-normalized REE diagrams (Post-Archean Australian Shale (PAAS) values of Taylor and McLennan (1985)). A: spider plots comparing values from representative nonhematitic and hematic stromatolites. B-C: Diagrams after Bau and Dulski (1996). Filled data points are data from this study; unfilled data points from Planavsky et al. (2009).

4.7 References

Aissaoui, D.M., 1985. Botryoidal aragonite and its diagenesis. Sedimentology 32, 345–361.

Awramik St. M., Barghoorn E. S. 1977. The Gunflint Microbiota. Precambrian Res. 5, 121-142.

Awramik, S.M., Buchheim, H.P., 2009. A giant, Late Archean lake system: The Meentheena Member (Tumbiana Formation; Fortescue Group), Western Australia. Precambrian Res. 174, 215–240.

Baragar,W., Scoates, F., 1981. The Circum-Superior belt: a Proterozoic plate margin? In: Kröner, A. (Ed.), Precambrian Plate Tectonics. Elsevier, Amsterdam, pp. 295–330.

Barghoorn, E.S., Tyler, S.A., 1965. Microorganisms from the Gunflint Chert. Science 147, 563–575.

Bau, M., and Möller, P. 1993. Rare earth element systematics of the chemically precipitated component in Early Precambrian iron formations and the evolution of the terrestrial atmosphere-hydrosphere-lithosphere system. *Geochimica et Cosmochimica Acta*, *57*(10), 2239-2249.

Bau, M., Dulski, P., 1996. Distribution of yttrium and rare-earth elements in the Penge and Kuruman iron-formations, Transvaal Supergroup, South Africa. Precambrian Res. 79, 37–55.

Bau, M., Koschinsky, A., 2009. Oxidative scavenging of cerium on hydrous Fe oxide: Evidence from the distribution of rare earth elements and yttrium between Fe oxides and Mn oxides in hydrogenetic ferromanganese crusts. Geochem. J. 43, 37–47. Bau, M., Schmidt, K., Koschinsky, a., Hein, J., Kuhn, T., and Usui, a., 2014, Discriminating between different genetic types of marine ferro-manganese crusts and nodules based on rare earth elements and yttrium: Chemical Geology, 381, 1–9.

Beal, E.J., House, C.H., and Orphan V.J., 2009. Manganese- and iron-dependent marine methane oxidation. Science 325, 184–187.

Bekker, A., Holmden, C., Beukes, N.J., Kenig, F., Eglingtone, B., Patterson, W.P., 2008. Fractionation between inorganic and organic carbon during the Lomagundi (2.22-2.1??Ga) carbon isotope excursion. Earth Planet. Sci. Lett. 271, 278–291.

Bekker, A., Slack, J., Planavsky, N., Krapez, B., Hofmann, A., Konhauser, K.O. and Rouxel, O.J., 2010. Iron formation: the sedimentary product of a complex interplay among mantle, tectonic, oceanic, and biospheric processes. Econ. Geol. 105, 467–508.

Bell, R., Jackson, G., 1974. Aphebian halite and sulphate indications in the Belcher Group, Northwest Territories. Can. J. Earth Sci. 11, 722–728.

Bolhar, R., Kamber, B.S., Moorbath, S., Fedo, C.M., Whitehouse, M.J., 2004. Characterization of early Archean chemical sediments by trace element signatures. Earth Planet. Sci. Lett. 222 (1), 43–60

Bolhar, R., Vankranendonk, M., 2007. A non-marine depositional setting for the northern Fortescue Group, Pilbara Craton, inferred from trace element geochemistry of stromatolitic carbonates. Precambrian Res. 155, 229–250.

Broderick, T. M., 1920. Economic geology and stratigraphy of the Gunflint iron district, Minnesota. Econ. Geol. 15, 422-452.Buick, R., Dunlop, J.S.R., 1990. Evaporitic sediments of Early Archean age from the Warrawoona Group, Western Australia. Sedimentology 37, 247–278.

Cheatham MM, Sangrey WF, White WM. 1993. Sources of error in external calibration ICPMS analysis of geological samples and an improved non-linear drift correction procedure. Spectrochim. Acta 48B:E487-506

Clayton, C.J., 1986. The chemical environment of flint formation in Upper Cretaceous chalks. In: Sieveking, G. de G., Hart, M.B.,Eds, , The Scientific Study of Flint and Chert. Cambridge University Press, Cambridge, pp. 43–54.

Coleman, M.L., Raiswell, R., 1993, Microbial mineralization of organic matter: mechanisms of self-organization and inferred rates of precipitation of diagenetic minerals. Philosophical Transactions of the Royal Society A: Mathematical, Physical and Engineering Sciences 344, 69–87.

Curtis, C.D., Coleman, M.L., Love L.G., 1986, Porewater evolution during sediment burial fromisotopic andmineral chemistry of calcite, dolomite and siderite concretions. Geochimica et Cosmochimica Acta 50, 2321–2334.

Dapples, E. C.,1979. Silica as an agent in diagenesis in Diagenesis, *in* Larsen, G. and Chilingar, G.V , eds., Diagenesis in sediments and sedimentary rocks. Developments in sedimentology 25A, Elsevier, 99-141.Davies, G.R., 1977. Former magnesian calcite and aragonite submarine cements in upper Paleozoic reefs of the Canadian arctic: a summary. Geology 5, 11-15.

De Baar, H.J.W., German, C.R., Elderfield, H., and van Gaans, P., 1988, Rare earth element distributions in anoxic waters of the Cariaco Trench: Geochimica et Cosmochimica Acta, v. 52, p. 1203−1219.

De Baar, H.J.W., Schijf, J., Byrne, R.H., 1991. Solution chemistry of the rare earth elements in seawater. Eur. J. Solid State Inorg. Chem. 28, 357–373

Derry, L. A., and Jacobsen, S. B. 1990. The chemical evolution of Precambrian seawater: Evidence from REEs in banded iron formations. *Geochimica et Cosmochimica Acta*, *54*(11), 2965-2977.

Dickson, J.A.D., 2009. Mississippian Paleocean Chemistry from Biotic and Abiotic Carbonate, Muleshoe Mound, Lake Valley Formation, New Mexico, U.S.A.- Discussion. J. Sediment. Res. 79, 42–43.

Elderfield, H., Pagett, R., 1986. Rare earth elements in ichthyoliths: variations with redox conditions and depositional environment. Sci. Total Environ. 49, 175–197

Elderfield, H., 1988. The oceanic chemistry of the rare earth elements. Phil. Trans. Roy. Soc. London A 325, 105–126.

Eriksson, P.G., Condie, K.C., Tirsgaard, H., Mueller, W.U., Altermann, W., Miall, a. D., Aspler, L.B., Catuneanu, O., Chiarenzelli, J.R., 1998. Precambrian clastic sedimentation systems. Sediment. Geol. 120, 5–53.

Farquhar, J., Zerkle, A., and Bekker, A., 2011, Geological constraints on the origin of oxygenic photosynthesis: Photosynthesis research 107, 11–36.Fischer, W.W., Schroeder, S., Lacassie, J.P., Beukes, N.J., Goldberg, T., Strauss, H., Horstmann, U.E., Schrag, D.P., and Knoll, A.H., 2009. Isotopic constraints on the Late Archean carbon cycle from the Transvaal Supergroup along the western margin of the Kaapvaal Craton, South Africa: Precambrian Research 169, p. 15–27.

Flörke, O. W., Graetsch, H., Martin, B., Röller, K. and Wirth, R. 1991. Nomenclature of microcrystalline and non-crystalline silica minerals, based on structure and microstructure. Neues Jahrbuch Für Mineralogie-Abhandlungen 163, 1, 19 - 42.

Floran, R.J., and Papike, J.J., 1978, Mineralogy and petrology of the Gunflint Formation, Minnesota-Ontario. J. Petrology, 19, 215-288

Fralick, P. 1989. Microbial bioherms, Lower Proterozoic Gunflint Formation, Thunder Bay, Ontario. In H.H.J. Geldsetzer, N.P. James, and G.E. Tebbutt, eds., Reefs: Canada and adjacent areas. Canadian Society of Petroleum Geologists, Memoirs, pp. 24–29.

Fralick, P., Barrett, T., 1995. Depositional controls on iron formation associations in Canada. Spec. Pub. Int. Ass. Sediment. 22, 137-156

Fralick, P., Davis, D., Kissin, S., 2002. The age of the Gunflint Formation, Ontario, Canada: single zircon U Pb age determinations from reworked volcanic ash. Can. J. Earth Sci. 39, 1091, 1085–1091. doi:10.1139/E02-028

Folk, R. L. 1974. The natural history of crystalline calcium carbonate: effect of magnesium content and salinity. J. Sedim. Petrol. 44, 40-53.

Folk, R.L., Siedlecka, A., 1974. The “schizohaline” environment: Its sedimentary and diagenetic fabrics as exemplified by Late Paleozoic rocks of Bear Island, Svalbard. Sediment. Geol. 11, 1–15.

Gallagher, K.L., Kading, T.J., Braissant, O., Dupraz, C., Visscher, P.T., 2012. Inside the alkalinity engine: the role of electron donors in the organomineralization potential of sulfate-reducing bacteria. Geobiology 10, 518–30.

Given, R.K., Lohmann, K.C., 1985. Derivation of the original isotopic composition of Permian marine cements. J. Sediment. Petrol. 55, 430–439

Graetsch, H., Flörke, O. W., Miehe, G. 1987. Structural Defects in Microcrystalline Silica. Phys. Chem. Minerals 14, 249 - 257.

Graetsch, H., 1994. Structural characteristics of opaline and micro-crystalline silica minerals. In: Heaney, P. J., Prewitt, C. T. & Gibbs, G. V. eds. Silica. Physical Behaviour, Geochemistry and Materials Applications, Reviews in Mineralogy 29, pp. 209 - 232.

Goodwin, A.M. 1956. Facies relations in the Gunflint Iron Forma- tion. Economic Geology, 51: 565–595. Goodwin, A.M. 1960. Gunflint Formation of the Whitefish Lake area. In Ontario Department of Mines Annual Report 69, pp. 41–63.

Grotzinger, J.P., 1986. Evolution of Early Proterozoic passive-margin carbonate platform, Rocknest Formation, Wopmay Orogen, Northwest Territories, Canada. J. Sediment. Petrol. 56, 831–847

Grotzinger, J.P., 1994, Trends in Precambrian carbonate sediments and their implication for understanding evolution, in Bengston, S., ed., Early life on Earth: New York, Columbia University Press, p. 245–258.

Grotzinger, J. P. and Read, J. F., 1983. Evidence for primary aragonite precipitation, lower Proterozoic (1.9 Ga) Rocknest dolomite, Wopmay orogen, Northwest Canada. Geology 11: 710-713.

Hesse, R., 1989. Silica diagenesis: origin of inorganic and replacement cherts. Earth-Sci. Rev. 26, 253–284.

Hiatt, E.E., Pufahl, P.K., Edwards, C.T., 2015. Sedimentary phosphate and associated fossil bacteria in a Paleoproterozoic tidal flat in the 1.85Ga Michigamme Formation, Michigan, USA. Sediment. Geol. 319, 24–39.

Hofmann, H.J., Jackson, G.D., 1987. Proterozoic ministromatolites with radial-fibrous fabric. Sedimentology 34, 963–971.

House, C.H., Schopf, J.W., McKeegan, K.D., Coath, C.D., Harrison, T.M., and Stetter, K.O., 2000, Carbon isotopic composition of individual Precambrian microfossils. Geology 28, 707–710.

Huang, C., 2010. Rare earth coordination chemistry: Fundamentals and applications. John Wiley & Sons (Asia), Singapore, 575 p.

Jirsa, M. and Fralick,P., 2010, Geology of the Gunflint Iron Formation and the Sudbury Impact Layer, Northeastern Minnesota, Institute on Lake Superior Geology, Field Trip 4, Field Trip Guidebooks 53, 77-92.

Jirsa, M. and Fralick,P., 2010, Geology of the Gunflint Iron Formation and the Sudbury Impact Layer, Northeastern Minnesota, Institute on Lake Superior Geology, Field Trip 4, Field Trip Guidebooks 53, 77-92.

Johannesson, K.H., Hawkins, D.L., Cortés, A., 2006. Do Archean chemical sediments record ancient seawater rare earth element patterns? Geochim. Cosmochim. Acta 70, 871–890.

Johannesson, K. H., Telfeyan, K., Chevis, D. A., Rosenheim, B. E., and Leybourne, M.I., 2014. Rare earth elements in stromatolites—1. Evidence that modern terrestrial stromatolites fractionate rare earth elements during incorporation from ambient waters. In In Y. Dilek, H. Furnes (eds.), Evolution of Archean Crust and Early Life, Modern Approaches in Solid Earth Sciences 7, DOI 10.1007/978-94-007-7615-9_14, © Springer Science+Business Media Dordrecht 2014.

Jones, B., 2013. Microarchitecture of dolomite crystals as revealed by subtle variations in solubility: Implications for dolomitization. Sediment. Geol. 288, 66-80.

Kamber, B,S., Webb, G.E., 2001. The geochemistry of late Archaean microbial carbonate: implications for ocean chemistry and continental erosion history. Geochim. Cosmochim. Acta 65, 2509–2525.

Kamber, B.S., Bolhar, R., Webb, G.E., 2004. Geochemistry of late Archaean stromatolites from Zimbabwe: evidence for microbial life in restricted epicontinental seas. Precambrian Res. 132, 379– 399.

Kamber, B.S., Webb, G.E., 2007. Transition metal abundances in microbial carbonate: a pilot study based on *in situ* LA-ICP-MS analysis. Geobiology 5, 375–389. doi:10.1111/j.1472-4669.2007.00129.x

Kawabe, I., Ohta, A., Miura, N., 1999. Distribution coefficients Fe oxyhydroxide of REE between precipitates and NaCl solutions affected by REE complexation. Geochem. Journal 33, 181–197.

Kenward, P.A, Goldstein, R.H., González, L.A, and Roberts, J.A, 2009, Precipitation of low-temperature dolomite from an anaerobic microbial consortium: the role of methanogenic Archaea, Geobiology 7, 556–65

Kershaw, S., Crasquin, S., Li, Y., Collin, P.-Y., Forel, M.-B., Mu, X., Baud, a, Wang, Y., Xie, S., Maurer, F., Guo, L., 2012. Microbialites and global environmental change across the Permian-Triassic boundary: a synthesis. Geobiology 10, 25–47.

Kershaw, S., 2015. Modern Black Sea oceanography applied to the end-Permian extinction event. J. Palaeogeogr. 4, 1–18.

Knauth, L.P., 1979. A model for the origin of chert in limestone. Geology 7, 274–277.

Knoll, A., 1985. Exceptional preservation of photosynthetic organisms in silicified carbonates and silicified peats. Philos. Trans. R. Soc. B 311, 111–122.

Knoll, A.H., 2003. Life on a Young Planet: the First Three Billion Years of Evolution on Earth. Princeton University Press, New Jersey.

Konhauser, K., Phoenix, V., 2001. Microbial–silica interactions in Icelandic hot spring sinter: possible analogues for some Precambrian siliceous stromatolites. Sedimentology 48, 415–433.

Konhauser, K.O., Jones, B., Phoenix, V.R., Ferris, G., and Renaut, R.W., 2004. The microbial role in hot spring silicification. Ambio 33, 552-558.

Konhauser, K.O., Newman, D.K., and Kappler, A., 2005. The potential significance of microbial Fe(III)-reduction during Precambrian banded iron formations. ***Geobiology***, 3:167-177.

Konhauser, K.O., Lalonde, S. V, Planavsky, N.J., Pecoits, E., Lyons, T.W., Mojzsis, S.J., Rouxel, O.J., Barley, M.E., Rosìere, C., Fralick, P.W., Kump, L.R., Bekker, A., 2011. Aerobic bacterial pyrite oxidation and acid rock drainage during the Great Oxidation Event. Nature 478, 369–73.

Lepot K., Benzerara K., Brown G. E. and Philippot P., 2008. Microbially influenced formation of 2,724 million years old stromatolites. Nat. Geosci. 1, 118–121.

Maliva, R.G., Knoll, A.H., Simonson, B.M., 2005. Secular change in the Precambrian silica cycle: Insights from chert petrology. Geol. Soc. Am. Bull. 117, 835.

Marin, J., Chaussidon, M., Robert, F., 2010. Microscale oxygen isotope variations in 1.9Ga Gunflint cherts: Assessments of diagenesis effects and implications for oceanic paleotemperature reconstructions. Geochim. Cosmochim. Acta 74, 116–130.

Marin, J., Chaussidon, M., Robert, F., 2012. Micrometer-scale chemical and isotopic criteria (O and Si) on the origin and history of Precambrian cherts: Implications for paleo-temperature reconstructions. Geochim. Cosmochim. Acta 92, 129–147.

Markun, C.D., Randazzo, A.F., 1980. Sedimentary structures in the Gunflint Iron Formation, Schreiber Beach, Ontario. Precambrian Reseacrh 12, 287–310.

Mazzullo, S.J., 1980. Calcite pseudospar replacive ofmarine acicular aragonite, and implications for aragonite cement diagenesis. Journal of Sedimentary Petrology 50, 409–422.

Mojzsis, S.J., and Arrhenius, G., 1998. Phosphates and carbon on Mars: Exobiological implications and sample return considerations. J. of Geophysical Research 103, 495–,511.

Mojzsis, S.J., Cates, N.L., Bleeker, W., Hopkins, M.D., Guitreau, M., Blichert-Toft, J., Trail, D. and Abramov, O., 2014. Component geochronology of the ca. 3960 Ma Acasta Gneiss. Geochimica et Cosmochimica Acta 133, 68-96.

Moorehouse, W.W. 1960. Gunflint Iron Range in the vicinity of Port Arthur. In Ontario Department of Mines Annual Report 69. pp. 1–40

Moreau, J., Sharp, T., 2004. A transmission electron microscopy study of silica and kerogen biosignatures in ~ 1.9 Ga Gunflint microfossils. Astrobiology 4, 196–210.

Morse, J.W., Mackenzie, F.T., 1990. Geochemistry of sedimentary carbonates. Elsevier Science Publishers B.V., Amsterdam, 706 p.

Naafs, B.D.A., Castro, J.M., De Gea, G.A., Quijano, M.L., Schmidt, D.N., and Pancost, R.D., 2016, Gradual and sustained carbon dioxide release during Aptian Oceanic Anoxic Event 1a: Nature Geoscience 9, 135–139.

Nance, W.B., Taylor, S.R., 1976. Rare earth patterns and crustal evolution: I. Australian post-Archean sedimentary rocks, Geochimica et Cosmochimica Acta 40,1539–1551

Nudds J.R., and Selden P.A., 2008. Fossil Ecosystems of North America: A Guide to the Sites and Their Extraordinary Biotas. University of Chicago Press, Chicago, IL, 288 pp.

Palmer, M.R., 1985. Rare earth elements in foraminifera tests. Earth Planet. Sci. Lett. 73, 285–298

Palmer, M.R., Elderfield, H., 1986. Rare earth elements and neodym- ium isotopes in ferromanganese oxide coatings pf Cenozoic foram- inifera from the Atlantic Ocean. Geochim. Cosmochim. Acta 50, 409–417.

Papineau, D., Mojzsis, S.J., Coath, C.D., Karhu, J. a., McKeegan, K.D., 2005. Multiple sulfur isotopes of sulfides from sediments in the aftermath of Paleoproterozoic glaciations. Geochim. Cosmochim. Acta 69, 5033–5060.

Partin, C.A., Bekker, A., Planavsky, N.J. and Lyons, T.W., 2015. Euxinic conditions recorded in the ca. 1.93 Ga Bravo Lake Formation, Nunavut (Canada): Implications for oceanic redox evolution. Chemical Geology, 417, 48-162.

Petrash, D.A., Gingras, M.K., Lalonde, S. V., Orange, F., Pecoits, E., Konhauser, K.O., 2012. Dynamic controls on accretion and lithification of modern gypsum-dominated thrombolites, Los Roques, Venezuela. Sediment. Geol. 245-246, 29–47. doi:10.1016/j.sedgeo.2011.12.006

Picard, A., Obst, M., Schmid, G., Zeitvogel, F., and Kappler, A., 2015. Limited influence of Si on the preservation of Fe mineral-encrusted microbial cells during experimental diagenesis. Geobiology 10.1111/gbi.12171.

Pittman Jr., J.S., Folk, R.L., 1971. Length-slow chalcedony after sulfate minerals in sedimentary rocks. Nat. Phys. Sci. 230, 64–65.

Planavsky, N., Rouxel, O., Bekker, A., Shapiro, R., Fralick, P., Knudsen, A., 2009. Iron-oxidizing microbial ecosystems thrived in late Paleoproterozoic redox-stratified oceans. Earth Planet. Sci. Lett. 286, 230–242.

Poulton, S.W., Fralick, P.W., Canfield, D.E., 2004. The transition to a sulphidic ocean similar to 1.84 billion years ago. Nature 431, 173–177.

Poulton, S.W., Fralick, P.W., Canfield, D.E., 2010. Spatial variability in oceanic redox structure 1.8 billion years ago. Nature Geosci. 3, 486–490.

Pufahl, P.K. 1996. Stratigraphic Architecture of a Paleoproterozoic iron formation depositional system: the Gunflint, Mesabi and Cuyuna iron ranges. Master's of Science Thesis, Lakehead University, Thunder Bay, Ont.

Pufahl, P.K., and Fralick, P.W., 2000, Depositional environments of the Paleoproterozoic Gunflint Formation: in Institute on Lake Superior Geology Proceedings, 46 Annual Meeting, Thunder Bay, Ontario, Part 2 Field Trip Guidebook 51.

Raiswell, R., and Fisher, Q.J., 2000, Mudrock-hosted carbonate concretions: a review of growth mechanism and their influence on chemical and isotopic composition. Journal of the Geological Society 157, 239–252.

Rasmussen, B., 1996, Early-diagenetic REE-phosphate minerals (florencite, gorceixite, crandallite, and xenotime) in marine sandstones; a major sink for oceanic phosphorus: American Journal of Science 296, 601–632.

Riciputi, L.R., Paterson, B.A., and Ripperdan, R.L., 1998, Measurement of light stable isotope ratios by SIMS: Matrix effects for oxygen, carbon, and sulfur isotopes in minerals. International Journal of Mass Spectrometry 178, 81–112.

Ricketts, B.D., 1983. The evolution of a middle Precambrian dolostone sequence: a spectrum of dolomitization regimes. SEPM J. Sediment. Res. 53, 565–586.

Riding, R., 2006. Cyanobacterial calcification, carbon dioxide concentrating mechanisms, and Proterozoic-Cambrian changes in atmospheric composition. Geobiology 4, 299–316.

Riding, R., Fralick, P., Liang, L., 2014. Identification of an Archean marine oxygen oasis. Precambrian Res. 251, 232–237.

Robbins, L.J., Swanner, E.D., Lalonde, S.V., Eickhoff, M., Paranich, M.L., Reinhard, C.T., Peacock, C.L., Kappler, A. and Konhauser, K.O., 2015. Limited Zn and Ni mobility during simulated iron formation diagenesis.Chemical Geology 402, 30-39.

Schroeder, J. H. 1972. Fabrics and sequences of submarine carbonate cements in Holocene Bermuda cup reefs. Geol Rundsch 61, 708-30.

Sibley, D., Gregg, J., 1987. Classification of dolomite rock textures. J. Sediment. Res. 57, 967–975.

Sheldon, N.D., 2006. Precambrian paleosols and atmospheric CO2 levels. Precambrian Res. 147, 148–155.

Shields, G., Stille, P., 2001. Diagenetic constraints on the use of cerium anomalies as palaeoseawater redox proxies: an isotopic and REE study of Cambrian phosphorites. Chem. Geol. 175, 29–48

Shinn, E.A., 1969, Submarine lithification of Ho- locene carbonate sediments in the Persian Gulf: Sedimentology 12, 109–144.

Sholkovitz, E.R., Shen, G.T., 1995. The incorporation of rare earth elements in modern coral. Geochim. Cosmochim. Acta 59, 2749–2756.

Schopf, J.W., Packer, B.M. 1987. Early Archean (3.3-billion to 3.5-billion-year-old) micro-fossils from Warrawoona Group, Australia. Science 237:70–73.

Shapiro, R.S., Konhauser, K.O., 2015. Hematite-coated microfossils : primary ecological fingerprint or taphonomic oddity of the Paleoproterozoic? Geobiology. doi:10.1111/gbi.12127

Siever, R., 1962. Silica solubility 0–2001C and the diagenesis of siliceous sediments. Journal of Geology 70, 127–150

Simonson, B.M. 1987. Early silica cementation and subsequent diagenesis in arenites from four Early Proterozoic iron formations in North America. J. Sed. Petrol., 57: 494–511.

Simonson, B.M., and Hassler, S.W. 1996. Was the deposition of large Precambrian iron formations linked to major marine transgressions? J. Geol. 104: 665–676.

Sommers, M.G., Awramik, S.M., and Woo, K.S., 2000, Evidence for initial calcite-aragonite composition of Lower Algal Chert Member ooids and stromatolites, Paleoproterozoic Gunflint Formation, Ontario, Canada: Canadian Journal of Earth Sciences, v. 1243, p. 1229–1243.

Sommers, M.G., and Awramik, S.M. 1996. Abiogenic "stromatolites" from the Gunflint Formation: Microstructural criteria for determining abiogenic vs. biogenic stromatolites. Abstracts with Programs, Geological Society of America. 28(7): 174

Taylor, T.N., and Taylor, E.L., 1993. The biology and evolution of fossil plants. New Jersey, USA: Prentice Hall. (pp. 384)

Taylor S.R., McLennan, S.M., 1985 The Continental Crust: Its Composition and Evolution. Blackwell, Malden, MA.

Tyler, S. A. and Barghoorn, E. S., 1963. Ambient pyrite grains in Precambrian cherts. Am. J. Sci. 261, 424-432.

Van Kranendonk, M.J., Webb, G.E., Kamber, B.S., 2003. New geological and trace element evidence from 3.45 Ga stromatolitic carbonates in the Pilbara Craton: support of a marine, biogenic origin and for a reducing Archaean ocean. Geobiology 1, 91–108

Veizer, J., Clayton, R. N., and Hinton, R. W.,1992. Geochemistry of Precambrian carbonates: IV. Early Paleoproterozoic (2.25 ± 0.25 Ga) seawater. Geochim.Cosmochim. Acta, 56(3), 875-885.

Wacey, D., Kilburn, M.M.R., Saunders, M., Cliff, J., and Brasier, M.D., 2011, Microfossils of sulphur-metabolizing cells in 3.4-billion-year-old rocks of Western Australia: Nature Geoscience 4, 1–5.

Wacey, D., Menon, S., Green, L., Gerstmann, D., 2012. Taphonomy of very ancient microfossils from the~ 3400Ma Strelley Pool Formation and~ 1900Ma Gunflint Formation: New insights using a focused ion beam. Precambrian Res. 220–221, 234–250.

Wacey, D., McLoughlin, N., Kilburn, M.R., Saunders, M., Cliff, J.B., Kong, C., Barley, M.E., Brasier, M.D., 2013. Nanoscale analysis of pyritized microfossils reveals differential heterotrophic consumption in the ~1.9-Ga Gunflint chert. Proc. Natl. Acad. Sci. U.S.A. 110, 8020–8024.Walter, M.R., 1972. Stromatolites and the biostratigraphy of the Australian Precam- brian and Cambrian. Special Papers in Palaeontology 11, 1–190

Wahl, C., Miehe, G. and Fuess, H. 2002. TEM characterisation and interpretation of fabric and structural degree of order in microcrystalline SiO_2 phases. Contrib. Mineral. Petrol. 143, 360 – 365.

Webb, G.E., Kamber, B.S., 2000. Rare earth elements in Holocene reefal microbialites: a new shallow seawater proxy. Geochim. Cosmochim. Acta 64, 1557–1565.

Winter, B.L., Knauth, L.P., 1992. STable 4.isotope geochemistry of cherts and carbonates from the 2.0 Ga gunflint iron formation: implications for the depositional setting, and the effects of diagenesis and metamorphism. Precambrian Res. 59, 283–313.

CHAPTER V

General Discussion and Conclusions

5.1. General Discussion

Over the past century, several models were developed to explain the stratigraphic abundance of dolomite. Ranging from hydrogeological to geomicrobiological interpretations, these models shed light on the kinetic constraints on low-temperature dolomite nucleation and the potential role of microbial metabolisms. Individually, these models fail to explain how completely dolomitized intervals, never subjected to elevated burial temperatures, that are often found in Neogene carbonate sequences form. The evidence supporting or arguing for the validity of any given dolomitization mechanism is generally a combination of textural and isotopic data. I chose to carefully investigate the redox-sensitive metal content of representative samples of modern, Creteceous, and Precambrian non-replacive dolomite to understand the paregenesis of this mineral in greater mechanistic detail and to place further constraints on the timing and biogeochemical environment of dolomite stabilization.

A significant problem with a direct comparison between modern sediments and sedimentary rocks, as implemented here, is that ancient carbonates often have metal concentrations that are significantly higher than any recent sediment. As a result, it has been argued that metal enrichments in carbonate rocks were not syngenetic but a result of burial diagenesis or epigenenesis — i.e., they resulted from rock interactions with thermally active brines or exogenous fluids long after deposition (Tucker, 1990). Similarly, a carbonate phase initially precipitated in organic and inorganic equilibrium with seawater may upon exposure to meteoric waters dissolve partially or entirely, exchange, and mix its trace elements with those in the diagenetically evolved interstitial pore water. The secondary phase will thus have a trace element composition shifted in the direction of equilibrium. Another important factor to take into consideration is that the distribution coefficients of trace metals in carbonates are precipitation=rate dependent, and, therefore, not representative of truly equilibrium conditions with seawater (Mackenzie and Morse, 1990).

Understanding the mineralogy, geochemistry, and petrogenesis of dolomite in modern sediments presents additional challenges: the sedimentary material is often comprised by a complex mixture at fine scales, and thus analyses require both microscale observations and chemostratigaphic integration. In spite of these complications, a comparison of dolomite in modern versus ancient sediments is useful as long as it is restricted to the mechanisms that control minor and trace element enrichments, or the physicochemical changes in pore waters that may have altered the partitioning and preservation of a given element into dolomite. For the purposes of this discussion, I consider the formation of dolomite from two perspectives: (1) the initial nucleation stage, when a number of compatible redox sensitive elements can be incorporated in the crystal lattice of Ca-rich dolomite precursors, and (2) the stage of crystal growth, when dissolution/ re-precipitation and re-equilibration with decaying organic matrices can change the initial pore water chemistry, and thus the solid phase concentrations of dolomite formed under such diagenetically evolved conditions.

5.1.1. Trace elements in peritidal dolomite: from nucleation to stabilization. Three case studies

5.1.1.1. General framework

Benthic microbes, and particularly the halophilic phototrophic communities that thrive in peritidal and lagoonal settings, produce vast amounts of exopolymeric substances (EPS) as an adaptive osmoregulating strategy that maintains optimal cytoplasmic hydration (Oren, 2000; Stal, 2000). Their EPS matrices are compositionally characterized by a high abundance of carboxyl-rich monomeric units, which are highly reactive towards dissolved metals under the hypersaline and alkaline conditions typically governing the peritidal zone of arid shallow carbonate systems. Upon burial, these organic substrates can be used by anoxygenic communities as a carbon source (King, 1988; Oren, 1990; Kempf and Bremer, 1998; Flemming and Wingender, 2001, 2010; Wood et al., 2001; Watkins 2014).

The last three decades of dolomite research have demonstrated that most modern dolomite nucleates in association with thick decaying biofilms — termed microbial mats (see Chapter II). These chemically stratified microbial ecosystems are comprised of up to 90% of metal reactive EPS (Flemming and Wingender, 2010). The physical (viscosity and elasticity) and chemical properties of EPS matrices can influence the morphological properties and composition of

carbonate minerals precipitated in organic equilibrium within them (Krumbein, 1986). The metal binding affinity of EPS along with their progressive enzymatic modification may lead to a self-re-arrangement of acidic functional groups and therefore to the development of nucleation templates suitable for Mg-carbonate growth. This mechanism of nucleation might have been of foremost importance in the geological past (Roberts et al., 2013), and can exert an important control over the trace metal content of dolomite (Petrash, 2010).

Due to stereochemical constraints, Mg does not bind directly with the acidic functional groups comprising EPS, but retains some water molecules after complexation. Thus, amorphous hydrated dolomite precursors usually predominate in the early stages of precipitation (Wang et al., 2009). Upon burial, however, these highly reactive amorphous precursors may transform into more crystalline dolomite (Riding, 2000; Wang et al., 2009). The stabilization of poorly crystalline Mg-carbonate phases as dolomite is strongly influenced by interactions between localized biogeochemical processes, capable of maintaining an elevated alkalinity over extended periods in the precipitation environment (Mazzullo, 2000). These biogeochemical processes should also exert a control over the activity of redox sensitive elements in sediments near buried organic substrates (this study).

The transition metal content of carbonates formed in equilibrium with reducing pore waters is a function of the redox potential and ionic activities of the precipitation environment, and thus should reflect chemical equilibrium with decaying organic matrices. By using three discrete case studies, this work shows that a detailed assessment of the abundance and distribution of redox-sensitive metals, when accompanied by comprehensive textural analyses, offers information useful to evaluate the conditions of dolomite growth.

5.1.1.2. Case Study I: modern dolomite

Chapter II postulates that in hypersaline peritidal settings, anaerobic biogeochemical processes involving coupled Mn and S cycling and organic matter respiration catalyze dolomite growth. This mechanism is an effective pH and alkalinity buffer and sustains carbon re-mineralization while shifting carbon speciation from HCO_3^- to CO_3^{2-}. By virtue of its greater translational or vibrational energy, excess carbonate anions can increase the dolomite saturation index (i.e., mineral precipitation potential) by displacing water dipoles bonded to abundant Mg ions. As the precursor Ca-dolomite phase grows — as part of a mixed phase cement, it incorporates

some Mn and other metals initially bound to coexisting Mn-oxyhydroxides, which are being actively reduced.

The enrichment of transition metals, such as Co, Ni, Zn, Cr, V, Mo, and Re in these modern dolomite-bearing sediments suggests that the chemostratigraphic patterns of augmentation or depletion of these elements can be used to infer precipitation under specific suboxic versus anoxic pore-water redox conditions. However, it must be emphasized that these elements are also removed from seawater by diffusion into anoxic sediments that lie below surficial suboxic horizons, and in continental margin deposits that receive significant mixed terrigenous fluxes — such as studied in the mid Cretaceous Maracaibo ramp, organic-rich horizons may also act as sinks for these metals.

5.1.1.3. Case Study II: Interstitial dolomite growth within mid-Cretaceous transgressive black shales

In Chapter III a bulk rock and *in situ* assessment of trace metal abundance was combined with iron speciation and biomarker analyses in order to interpret the variable redox states of pore waters at the time of shallow marine fine-grained sediment deposition and early diagenetic dolomite authigenesis in the mid-Cretaceous Maracaibo Platform. A paragenetic model was proposed in which environmental shifts associated with Milankovitch-scale cyclicity, led to the development of temporally and spatially restricted microenvironments favourable to early diagenetic dolomite formation.

In this model, minor modifications in the redox equilibrium conditions caused intense elemental recycling processes that involved enhanced microbial activity, organic matter re-mineralization and carbon fixation as dolomite. Orbital perturbations that occurred several times over periods of $10^5 – 10^4$ years are thought instrumental for widespread early diagenetic dolomite cementation. In this scenario, interstitial dolomite oversaturation resulted from the complex interplay between climatically driven drying and wetting events, high-frequency sea level changes, upwelling, and subsurface microbial activity. This variability produced specific trace metal enrichment trends, which are recorded in individual dolomite crystals.

In the dolomitic black shales, the magnitude of redox-sensitive element enrichment was found proportional to values generally measured in euxinic black shales, and a high Mo content in dolomite was found to be diagnostic of its partial precipitation in transiently euxinic pore waters.

However, the bulk and *in situ* iron-normalized Mn* parameter as well as measured Ce anomalies seem to produce conflicting data. Variability in Mn- and Fe-cycling processes at the time of dolomite precipitation is responsible for this behaviour. From the geochemical and textural dataset, it can be concluded that the ambiguity described above can be attributed to the fact that some redox sensitive metals are enriched in anoxic surface sediments, while others become enriched upon burial. A conservative approach is therefore to interpret the absence of enrichments as a reliable guide to precipitation under oxic conditions. In other words, the lack of enrichment of a group of redox sensitive metals in multigenic dolomite would strongly suggest that precipitation was linked to oxic/ dysoxic pore water rather than under anoxic/ euxinic conditions.

5.1.1.4. Case Study III: Carbonate cements within well-preserved Paleoproterozoic stromatolites

A bulk rock and *in situ* assessment of trace metals was combined with detailed textural analyses in order to interpret the variable redox states of pore waters at the time of stromatolite accretion and diagenetic mineral stabilization. In the paragenetic model, physicochemical shifts associated with exogenous water mixing, together with variable burial and exhumation histories, led to the development of temporarily and spatially restricted diagenetic fronts. This in turn led to silification of early formed carbonate cements, with pyrite oxidation, and localized secondary hematite and siderite formation. This general diagenetic model and its geochemical significance have implications for the use of stromatolite bulk-rock trace element data to interpret peleomarine chemistry. Accordingly, in ancient stromatolites, analyses of this nature can only concentrate on primary mineral phases, such as fine-crystalline dolomite and/or exceptionally rare aragonite (i.e., Lepot et al., 2008). However, due to the small size of such crystals, it is not possible to determine their trace element content and intracrystalline distribution by using currently available *in situ* laser ablation techniques. Further advances in micro-focusing capabilities of synchrotron photon microprobes would allow overcoming present-day analytical challenges.

5.2. Concluding remarks

Overall, this work demonstrates that chemical petrography via synchrotron-based photon microprobe provides insightful data to interpret the organically controlled early-diagenetic conditions of dolomite formation both in modern and ancient peritidal to lagoonal realms. Various

aspects of the co-precipitation of trace metals with Mg and Ca into dolomite were investigated. These aspects include:

1. Textural relations between primary dolomite and other authigenic minerals, and their significance for interpreting specific early and shallow burial diagenetic conditions.

2. Bulk concentration, speciation, and *in situ* distribution of redox-sensitive trace elements as proxy data of the dolomite precipitation environment.

3. Biogeochemical controls potentially exerted by subsurface chemosynthetic prokaryotes over the reactive metal stocks in the sediment pile and over the rates of sedimentary organic matter re-mineralization and carbon dioxide fixation.

4. High-frequency orbital cycles as regulators of biogeochemical reactions conducive to microbial dolomite growth.

5. Limitations on the use of ancient multigenic dolomites for interpreting paleooceanographic conditions.

5.2.1. Modern peritidal dolomite abundance

The study of dolomite in modern peritidal sediments from the Venezuelan Caribbean Sea supports the following general conclusion:

- In unconsolidated sediments, diffusion-limited transport of metabolites can lead to a significant 4D variation in redox conditions. This variation results from differing microbial respiration processes.
- In the peritidal zone of shallow marine sediments, anaerobic processes may occur within centimeters of aerobic zones, and the distribution of microbial communities may produce biogeochemical conditions outside of those based on thermodynamic predictions alone. Such geochemical disequilibrium conditions can be favourable for localized dolomite growth when their combined effects sustain high pore water alkalinity and elevated pH.
- In buried peritidal sediments, strong oxidants, such as Mn oxides, may reside in close proximity to reductants produced biotically or abiotically, leading to a tight redox cycle that

controls the fate and transport of some redox-sensitive elements and has the capacity to exert a strong control on the pH and the production of alkalinity from microbial respiration.

Other relevant finding worth to be mentioned here is:

- The spatial distribution of microbial communities in prograding sediments can be controlled by particular environmental shifts at the time of deposition.

Finally, although past studies have shown that sulfur oxidation and/or reduction may have an impact in dolomite authigenesis, there was a lack of information on competitive or coupled redox processes that occur concomitantly with native and evolved elemental sulfur bioutilization. A new hypothesis bridging these aspects posits that:

> In near-surface shallow marine diagenetic environments, the activity of microbial communities leads to dolomite formation as long as the combined effects of the production and consumption of by-products and the bioutilization of available metal and sulfur inventories sustain elevated pore water alkalinities. The reduction of Mn (IV) coupled with the oxidation of organic matter, the formation of Mn (III), and the reoxidation of the latter via intermediate forms of sulfur (Fig. 5.1) could be a critical driver of peritidal dolomite formation.

5.2.2. Mid-Cretaceous dolomite associated with black shales

In crystalline carbonate rocks (i.e., limestone/dolostone), the effects of late burial diagenesis can lead to multiple carbonate dissolution and re-precipitation stages that obliterate most of the primary textural features and chemical signals. In the late Aptian – early Albian dolomitic shale intervals studied here the flow of thermally active diagenetic fluids was prevented by differential compaction of the shale intervals. Combined with the continuous burial history of the mixed shallow marine carbonate-siliciclastic succession, these factors diminished the obliterating effects of recrystallization. Such diagenetic peculiarity allows for inferences regarding the elusive mechanisms of penecontemporaneous dolomite stabilization to be drawn. Results from this part of the research point to the following general conclusions:

- In well-preserved dolomites, the *in situ* distribution of redox-sensitive elements combined with detailed textural evaluations can be used for interpreting the variable pore water redox conditions at the time of dolomite growth.

- In coastal marine sediments, the 4D availability of oxidants and reductants, and the dynamics of all ongoing subsurface redox reactions may be controlled and afterward affected, over increasing time-scales, by seepage recharge, biological activity, climatically driven drying and wetting events, and high-frequency sea level changes.

- Environmental shifts associated with Milankovitch-scale cyclicity (i.e., orbital-forcing mechanisms) lead to the development of temporarily and spatially restricted diagenetic microenvironments in which microbial communities favourable to dolomite growth can flourish. Accordingly, short-term variations in sea level and climate can induce subtle changes in the availability of electron acceptors and donors in the sediment pile, and thus are capable of increasing the rates of CO_2 fixation into growing organogenic dolomite crystals.

The following findings are also important:

- Buried organic-rich levels containing reactive metal oxyhydroxides are the locus of authigenic dolomite precipitation. This is due to minor modifications in the redox equilibrium conditions that lead to intense elemental recycling processes involved in acetate turnover. This maybe an autocatalytic process linking the deep subsurface bioutilization of metal oxyhydroxides to the precipitation of dolomite.

- The bulk-rock shale-normalized Ce anomalies of multigenic dolomite would produce conflictive data that could mislead interpretations. The distribution of other redox sensitive elements within single crystals and the co-evaluation of bulk and *in situ* redox signals together with textural data are thus critical for paragenetic interpretations.

- The stratigraphic abundance of dolomite in peritidal sequences may correspond to a particular depositional condition triggered by the abundance and activity rates of native subsurface microbes and their influence over pore water alkalinity. Such a mechanistic link can become active multiple times during the pre-compaction history of the sediment, leading to dolomitization. It is thus necessary to examine Neogene dolomite-bearing sequences to advance this matter further.

5.2.3. Paleoproterozic dolomite associated with stromatolites

Petrographic and bulk rock geochemical comparisons of well-preserved stromatolites accreted in the intertidal zone of the Paleoproterozoic Animikie Basin shed an additional light on this work, allowing the following general conclusions:

- Elemental abundances of coeval stromatolites with similar morphotypes but dissimilar mineralogies provide hints of lateral changes in metal and sulfur bioavailability at the time of accretion, but these are unlikely to be directly related to paleocean chemistry.
- Diagenetic shifts associated with exogenous water mixing, together with variable burial and exhumation histories, led to the development of temporally and spatially restricted diagenetic fronts. This led to the silicification of early formed carbonate cements, pyrite oxidation, and localized secondary hematite and siderite formation; this has major consequeneces on attemps to determine the composition of ancient seawater from the trace metal chemistry of stromatolites.
- The source of data supporting oceanographic models of the past must be critically examined before any redox environment is inferred for a given shallow marine sedimentary deposit.
- Bulk rock data of ancient peritidal facies with poorly-know burial and exhumation histories must be avoided when the aim is to reconstruct the redox structure of Precambrian oceans.

When considering the Lower Algal Member of the Gunflint Formation, upcoming palaeoceanographic redox interpretations should only focus on small well-preserved and chemically homogeneous dolomite crystals. No other authigenic mineral phase on these structures can be unquestionably considered primary in origin. Such analyses, however, represent an analytical challenge that can only be overcame with a more extended use of ion and photon probes. The remarkable advances in the micro-focusing capabilities of modern synchrotron beamlines will likely provide the final, key dataset to advance on this matter.

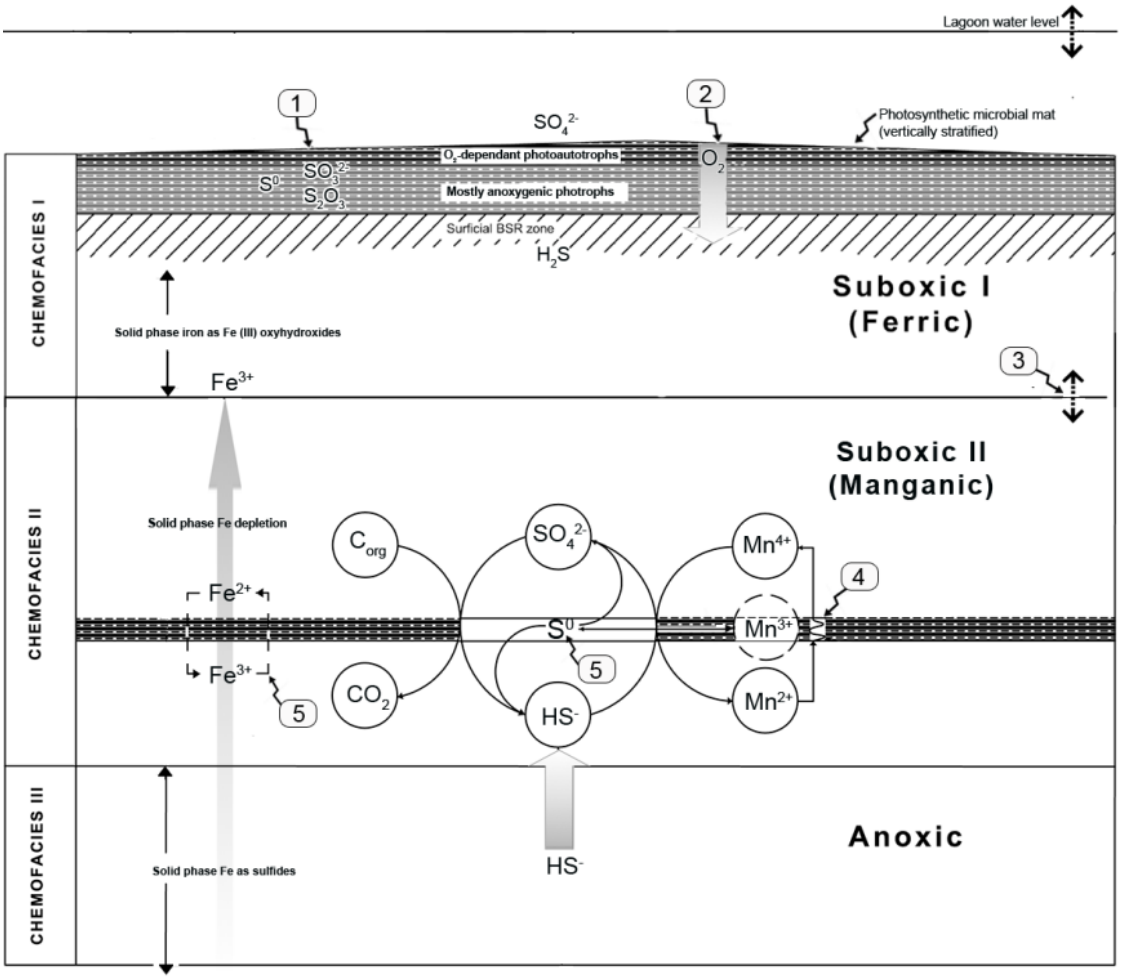

Figure 5.1. Schematic diagram showing a coupled sedimentary manganese - sulfur cycle, and interactions with iron cycling. In the suboxic manganic zone the upward flux of dissolved manganese (II) is oxidized to produce manganese (IV) oxides. 1: Dissolved Mn (II) can be bound by the organic functional groups comprising the EPS matrix, where it can be oxidized. Particulate Mn-bearing phases, formed in the water column are also trapped by mat, contributing to its overall reactivity. 2: O_2 penetration shifts on a diel and seasonally basis. 3: The vertical position of this dynamic interface change with seasonal shifts in lagoon water levels. 4: The buried organic substrate act as a diffusion barrier, localizing Mn(III) shuttle reactions. Other mechanisms (e.g., sulfate reduction) may also indirectly reduce Mn via sulfide production. 5: On these levels, there is also an active redox cycling of iron and sulfur.

5.3. References

Flemming, H.-C., Wingender, J., 2010. The biofilm matrix. Nat. Rev. Microbiol. 8, 623–633.

Kamber, B.S., Webb, G.E., 2007. Transition metal abundances in microbial carbonate: a pilot study based on *in situ* LA-ICP-MS analysis. Geobiology 5, 375–389.

King, G. M.,1988. Methanogenesis from methylated amines in a hypersaline algal mat. Applied and Environmental Microbiology 54, 130-136.

Kempf, B., Bremer, E., 1998. Uptake and synthesis of compatible solutes as microbial stress responses to high-osmolality environments. Arch. Microbiol. 170, 319–30.

Krumbein, W. E. (1986). Biotransfer of minerals by microbes and microbial mats. In Leadbeater, Barry SC, and Robert Riding, Eds., Biomineralization in lower plants and animals. Oxford University Press Biomineralization in lower plants and animals (pp. 55-72).

Lepot, K., Benzerara, K., Rividi, N., Cotte, M., Brown Jr., G.E., Philippot, P., Brown, G.E., 2009. Organic matter heterogeneities in 2.72Ga stromatolites: Alteration versus preservation by sulfur incorporation. Geochim. Cosmochim. Acta 73, 6579–6599. doi:10.1016/j.gca.2009.08.014

Oren, A. 1990. Formation and breakdown of glycine betaine and trimethylamine in hypersaline environments. Antonie van Leeuwenhoek 58, 291-298.

Oren, A. 1999, Bioenergetic aspects of halophilism, Microbiol. Mol. Biol. Rev., 63, 334–348

Petrash, D.A., 2010. Metal-enrichment in microbial carbonates : the role of carboxylated biomacromolecules. MSc Thesis, University of Alberta.

Soetaert, K., Hofmann, A., Middelburg, J., 2007. The effect of biogeochemical processes on pH. Mar. Chem 106, 380-401.

Stal, L.J., 2000. Cyanobacterial mats and stromatolites. In: BA Whitton and M Potts, Eds. The Ecology of Cyanobacteria: Their Diversity in Time and Space. Kluwer Academic Publishers, Dordrecht, pp. 61-120

Wang, D., Wallace, A.F., De Yoreo, J.J., Dove, P.M., 2009. Carboxylated molecules regulate magnesium content of amorphous calcium carbonates during calcification. Proceedings of the National Academy of Sciences 106:21511-21516

Watkins A.J., Roussel, E., Parkes, R.J., Sass, H., 2014. Glycine betaine as a direct substrate for methanogens (Methanococcoides spp.). Applied and Environmental Microbiology 8, 289-293.

Webb, G.E., and Kamber, B.S., 2000. Rare earth elements in Holocene reefal microbialites: a new shallow water proxy. Geochim Cosmochim Acta 64,1557–1565.

Wood, J.M., Bremer, E., Csonka, L.N., Kraemer, R., Poolman, B., van der Heide, T., and Smith, L.T., 2001. Osmosensing and osmoregulatory compatible solute accumulation by bacteria. Comparative Biochemistry and Physiology Part A: Molecular & Integrative Physiology, 130, 437-460.

BIBLIOGRAPHY

Adams, D.D., Hurtgen, M.T., Sageman, B.B., 2010. Volcanic triggering of a biogeochemical cascade during Oceanic Anoxic Event 2. Nature Geoscience 3. doi:10.1038/ NGEO743.

Aissaoui, D.M., 1985. Botryoidal aragonite and its diagenesis. Sedimentology 32, 345–361.

Alberdi-Genolet, M. and Tocco, R., 1999. Trace metals and organic geochemistry of the Machiques Member (Aptian–Albian) and La Luna Formation (Cenomanian–Campanian), Venezuela. Chemical Geology 160, 19-38.

Alberdi-Genolet, M. and López, L., 2000. Biomarker 18α (H)-oleanane: a geochemical tool to assess Venezuelan petroleum systems. Journal of South American Earth Sciences 13, 751-759.

Aller R. C., 1990. Bioturbation and manganese cycling in hemipelagic sediments. Philosophical Transactions of the Royal Society A 331, 51–68

Aller, R. C., 1994. The sedimentary Mn cycle in Long Island Sound. Its role as intermediate oxidant and the influence of bioturbation, O_2, and C_{org} flux on diagenetic reaction balances. J.Marine Research, 52, 259–295.

Aller, R.C., and Rude, P.D., 1988. Complete oxidation of solid phase sulfides by manganese and bacteria in anoxic marine sediments. Geochimica et Cosmochimica Acta 52, 751–765.

Anderson, T.F., Raiswell, R., 2004. Sources and mechanisms for the enrichment of highly reactive iron in euxinic Black Sea sediments. Am. J. Sci. 304 (3), 203–233.

Arthur, M.A. and Schlanger. S.O., 1979 Cretaceous "Oceanic Anoxic Events" as causal factors in development of reef-reservoir giant oil fields. Bulletin of the American Association of Petroleum Geologists 63,870-885

Arthur, M.A., Dean, W.E., and Stow, D.A.V.,1984. Models for the deposition of Mesozoic-Cenozoic fine-grained organic-carbon-rich sediment in the deep sea. In Stow, D.A.V. and Piper D.J.W Deep-water processes and facies (eds.), Geo- logical Society Special Publication 15, 527-562

Arthur, M.A., Dean, W.E., Schlanger, S.O., 1985. Variations in the global carbon cycle during the Cretaceous related to climate, volcanism, and changes in atmospheric CO_2. American Geophysical Union Monographs 32, 504-529.

Arthur, M. A., Jenkyns, H. C., Brumsack, H.J., and Schlanger, S. O. 1990. Stratigraphy, geochemistry, and paleoceanography of organic-carbon rich Cretaceous sequences. In: Ginsburg, R.N., and Beaudoin, B. (eds.) Cretaceous Resources, Events and Rhythms. Kluwer Academic, Dordrecht, NATO AS1 Series, 304, 75–119.

Arthur, M.A. Sageman, B.B., 1994. MARINE BLACK SHALES: Depositional Mechanisms and Environments of Ancient Deposits. Annual Reviews Earth & Planetary Sciences 22, 499–551. doi:10.1007/s13398-014-0173-7.2

Arvidson, R.S., MacKenzie, F.T., 1999. The dolomite problem: control of precipitation kinetics by temperature and saturation state. Amer. J. Sci. 299, 257–288.

Audemard, F. E., 1991, Tectonics of western Venezuela: Ph.D. dissertation, Rice University, Houston, Texas, 245 p.

Awramik St. M., Barghoorn E. S. 1977. The Gunflint Microbiota. Precambrian Res. 5, 121-142.

Awramik, S.M., Buchheim, H.P., 2009. A giant, Late Archean lake system: The Meentheena Member (Tumbiana Formation; Fortescue Group), Western Australia. Precambrian Res. 174, 215–240.

Ball, J.W., and Nordstrom, K., 1991. User's manual for WATEQ4F, with revised thermodynamic data base and test cases for calculating speciation of major, trace, and redox elements in natural waters. U.S. Geological Survey Open-File Report 91-183.

Baker, P.A., Kastner, M., 1981. Constraints on the formation of sedimentary dolomite. Science 213, 214–216

Baragar,W., Scoates, F., 1981. The Circum-Superior belt: a Proterozoic plate margin? In: Kröner, A. (Ed.), Precambrian Plate Tectonics. Elsevier, Amsterdam, pp. 295–330.

Barclay, R. S., J. C. McElwain, and Sageman B. B., 2010. Carbon sequestration activated by a volcanic CO_2 pulse during Ocean Anoxic Event 2, Nature Geoscience, 3(3), 205–208.

Bargar, J., Tebo, B., Villinski, J., 2000. *In situ* characterization of Mn (II) oxidation by spores of the marine *Bacillus* sp. strain SG-1. *Geochimica et Cosmochimica Acta* 64*,* 2775-2778

Barghoorn, E.S., Tyler, S.A., 1965. Microorganisms from the Gunflint Chert. Science 147, 563–575.

Barling, J., Arnold, G.L. and Anbar, A.D., 2001. Natural mass-dependent variations in the isotopic composition of molybdenum. Earth and Planetary Science Letters 193, 447–457.

Bartley, J.K., Knoll, A.H., Grotzinger, J.P., Sergeev, V.N., 1999. Lithification and fabric genesis in precipitated stromatolites and associated peritidal carbonates, Mesoproterozoic Billyakh Group, Siberia. Kah LC, Knoll AH. 1996. Microbenthic distribution of Proterozoic tidal flats: environmental and taphonomic considerations. Geology 24:79–82.

Bartok, P., Reijers, T., and Juhasz, I., 1981. Lower Cretaceous Cogollo Group, Maracaibo Basin, Venezuela: sedimentology, diagenesis, and petrophysics. Am. Assoc. Pet. Geol. Bull. 65, 1110–1134.

Bartok, P., 1993. Pre-breakup geology of the Gulf of Mexico– Caribbean: Its relation to Triassic and Jurassic rift systems of the region: Tectonics 12, 441–459.

Bathurst, R.G.C., 1986. Diagenetically enhanced bedding in argillaceous platform limestones: stratified cementation and selective compaction. Sedimentology 34, 740-778.

Bau, M., and Möller, P. 1993. Rare earth element systematics of the chemically precipitated component in Early Precambrian iron formations and the evolution of the terrestrial atmosphere-hydrosphere-lithosphere system. *Geochimica et Cosmochimica Acta*, *57*(10), 2239-2249.

Bau, M., Dulski, P., 1996. Distribution of yttrium and rare-earth elements in the Penge and Kuruman iron-formations, Transvaal Supergroup, South Africa. Precambrian Res. 79, 37–55.

Bau, M., Koschinsky, A., 2009. Oxidative scavenging of cerium on hydrous Fe oxide: Evidence from the distribution of rare earth elements and yttrium between Fe oxides and Mn oxides in hydrogenetic ferromanganese crusts. Geochem. J. 43, 37–47.

Bau, M., Schmidt, K., Koschinsky, a., Hein, J., Kuhn, T., and Usui, a., 2014, Discriminating between different genetic types of marine ferro-manganese crusts and nodules based on rare earth elements and yttrium: Chemical Geology, 381, 1–9.

Beal, E.J., House, C.H., and Orphan V.J., 2009. Manganese- and iron-dependent marine methane oxidation. Science 325, 184–187.

Bekker, A., Holmden, C., Beukes, N.J., Kenig, F., Eglingtone, B., Patterson, W.P., 2008. Fractionation between inorganic and organic carbon during the Lomagundi (2.22-2.1??Ga) carbon isotope excursion. Earth Planet. Sci. Lett. 271, 278–291.

Bekker, A., Slack, J., Planavsky, N., Krapez, B., Hofmann, A., Konhauser, K.O. and Rouxel, O.J., 2010. Iron formation: the sedimentary product of a complex interplay among mantle, tectonic, oceanic, and biospheric processes. Econ. Geol. 105, 467–508.

Bell, R., Jackson, G., 1974. Aphebian halite and sulphate indications in the Belcher Group, Northwest Territories. Can. J. Earth Sci. 11, 722–728.

Bellanca, A., Claps, M., Erba, E., Masetti, D., 1996. Orbitally induced limestone/marlstone rhythms in the Albian—Cenomanian Cismon section (Venetian region, northern Italy): Sedimentology, calcareous and siliceous plankton. Palaeogeogr. Palaeoclimatol. Palaeoecol. 126, 227–260.

Bellanca, A., Masetti, D., Neri, R., 1997. Rare earth elements in limestone/marlstone couplets from the Albian-Cenomanian Cismon section (Venetian region, northern Italy): assessing REE sensitivity to environmental changes. Chem. Geol. 2541, 141–152.

Berner, R., 1984. Sedimentary pyrite formation: an update. Geochim. Cosmochim. Acta 48, 605–615.

Bethke, C.M., Sanford, R. a., Kirk, M.F., Jin, Q., Flynn, T.M., 2011. The thermodynamic ladder in geomicrobiology. Am. J. Sci. 311, 183–210.

Biebl, H., and Pfennig, N., 1978. Growth yields of green sulfur bacteria in mixed cultures with sulfur and sulfate reducing bacteria. Archives of microbiology 117, 9-16.

Bieger, T., Abrajano, T., and Hellou, J., 1997. Generation of biogenic hydrocarbons during a spring bloom in Newfoundland coastal (NW Atlantic) waters. Organic geochemistry 26, 207-218.

Bishop, W.F., 1975. Geology of Tunisia and Adjacent Parts of Algeria and Libya. Am. Assoc. Pet. Geol. Bull. 59, 413–450.

Braissant, O., Decho, A. W., Dupraz, C., Glunk, C., Przekop, K. M., and Visscher, P. T., 2007. Exopolymeric substances of sulfate-reducing bacteria: Interactions with calcium at alkaline pH and implication for formation of carbonate minerals. *Geobiology* 5, 401–11.

Braissant, O., Decho, A.W., Przekop, K.M., Gallagher, K.L., Glunk, C., Dupraz, C., and Visscher, P.T., 2009. Characteristics and turnover of exopolymeric substances in a hypersaline microbial mat. *FEMS Microbial. Ecol.*67, 2005–2008.

Bralower, T., Fullagar, P., 1997. Mid-Cretaceous strontium-isotope stratigraphy of deep-sea sections. GSA Bull. 109, 1421–1442.

Bralower, T., and Lorente, M., 2003, Paleogeography and stratigraphy of the La Luna Formation and related Cretaceous anoxic depositional systems. Palaios18, 301–304.

Bravo, J. M., Perzl, M., Härtner, T., Kannenberg, E. L., and Rohmer, M., 2001. Novel methylated triterpenoids of the gammacerane series from the nitrogen-fixing bacterium *Bradyrhizobium japonicum* USDA 110. European Journal of Biochemistry 268, 1323-1331.

Bray, E.E., and Evans, E.D., 1961. Distribution of n-paraffins as a clue to recognition of source beds. Geochimica et Cosmochimica Acta 22, 2-15.

Breuker, A., Stadler, S., and Schippers, A., 2013. Microbial community analysis of deeply buried marine sediments of the New Jersey shallow shelf, IODP Expedition 313. *FEMS Microbial. Ecol.*, doi. 10.1111/1574-6941.12146.

Boetius, A., Ravenschlag, K., Schubert, C.J., Rickert, D., Widdel, F., Gieseke, A., Amann, R., Jørgensen, B.B., Witte, U., Pfannkuche, O., 2000. A marine microbial consortium apparently mediating anaerobic oxidation of methane. Nature 407, 623–6.

Bolhar, R., Kamber, B.S., Moorbath, S., Fedo, C.M., Whitehouse, M.J., 2004. Characterization of early Archean chemical sediments by trace element signatures. Earth Planet. Sci. Lett. 222 (1), 43–60

Bolhar, R., Vankranendonk, M., 2007. A non-marine depositional setting for the northern Fortescue Group, Pilbara Craton, inferred from trace element geochemistry of stromatolitic carbonates. Precambrian Res. 155, 229–250.

Bontognalli, T.R.R., Vasconcelos, C., Warthmann, R.J., Dupraz, C., Bernasconi, S.M., McKenzie, J. A., 2008. Microbes produce nanobacteria-like structures, avoiding cell entombment. Geology 36, 663-66.

Bontognalli, T.R.R., Vasconcelos, C., Warthmann, R.J., Bernasconi, S.M., Dupraz, C., Strohmenger, C.J., McKenzie, J.A., 2010. Dolomite formation within microbial mats in the coastal sabkha of Abu Dhabi (United Arab Emirates). Sedimentology 57, 824–844.

Böttcher, M., and Thamdrup, B., 2001. Anaerobic sulfide oxidation and stable isotope fractionation associated with bacterial sulfur disproportionation in the presence of MnO_2. *Geochimica et Cosmochimica Acta* 65, 1573–1581.

Boyanov, M.I., Kelly, S.D., Kemner, K.M., Bunker, B.A., Fein, J.B., and Fowle, D.A., 2003. Adsorption of cadmium to *Bacillus subtilis* bacterial cell walls: A pH-dependent X-ray absorption fine structure spectroscopy study. *Geochimica et Cosmochimica Acta* 67, 3299-3311.

Brady, P.V., Krumhansl, J.L., Papenguth, H.W., 1996. Surface complexation clues to dolomite growth. Geochim. Cosmochim. Acta 60, 727–731.

Brocks, J. and Summons, R., 2003. Sedimentary hydrocarbons, biomarkers for early life. Treatise on geochemistry 8, 63-115.

Brocks, J. J., Love, G. D., Summons, R. E., Knoll, A. H., Logan, G. A., and Bowden, S. A., 2005. Biomarker evidence for green and purple sulphur bacteria in a stratified Paleoproterozoic sea. Nature 437, 866-870

Brocks, J. J. and Schaeffer, P., 2008. Okenane, a biomarker for purple sulfur bacteria (Chromatiaceae), and other new carotenoid derivatives from the 1640Ma Barney Creek Formation. Geochimica et Cosmochimica Acta 72, 1396–1414.

Broderick, T. M., 1920. Economic geology and stratigraphy of the Gunflint iron district, Minnesota. Econ. Geol. 15, 422-452.Buick, R., Dunlop, J.S.R., 1990. Evaporitic sediments of Early Archean age from the Warrawoona Group, Western Australia. Sedimentology 37, 247–278.

Brooks, J., Gould, K., and Smith, J., 1969. Isoprenoid hydrocarbons in coal and petroleum. Nature 222, 257–259.

Browning, E.L., and Watkins, D.K., 2008. Elevated primary productivity of calcareous nannoplankton associated with ocean anoxic event 1b during the Aptian/Albian transition (Early Cretaceous), Paleoceanography, 23, PA2213.

Bottini, C., Erba, E., Tiraboschi, D., Jenkyns, H.C., Schouten, S., Sinninghe-Damsté, J.S., 2014. Climate variability and relationship with ocean fertility during the Aptian Stage. Clim. Past Discuss. 10, 689–738. doi:10.5194/cpd-10-689-2014

Buchbinder, B., and Friedman, G.M., 1971. Selective dolomitization of micrite envelopes: A possible clue to original mineralogy. Journal of Sedimentary 40, 514-517

Budd, D., 1997. Cenozoic dolomites of carbonate islands: their attributes and origin. Earth-Science Rev. 42, 1–47.

Burns, S.J., Baker, P.A., 1987. A Geochemical Study of Dolomite in the Monterey Formation, California. J. Sediment. Res. 57, 128.

Burns, S.J., Mckenzie, J.A., Vasconcelos, C., 2000. Dolomite formation and biogeochemical cycles in the Phanerozoic. Sedimentology 47, 49–61.

Budyko, M.I., Ronov, A.B., Yanshin, A.L., 1987. History of the Earth's Atmosphere. Springer Verlag, New York, USA, 139 pp.

Burdige, D.J., 1993. The biogeochemistry of manganese and iron reduction in marine sediments. Earth-Science Reviews 35, 249-284.

Burdige, D. J., and Nealson, K. H., 1985. Microbial manganese reduction by enrichment cultures from coastal marine sediments. Applied Environ. Microbiol. 50, 491–7.

Burke, K., 1976. Development of graben associated with the initial ruptures of the Atlantic Ocean. Tectonophysics 36, 93–112.

Butler, I., Rickard, D., 2000. Framboidal pyrite formation via the oxidation of iron (II) monosulfide by hydrogen sulphide. Geochim. Cosmochim. Acta 64, 2665–2672.

Calvert, S. E., and Pedersen, T. F., 1996. Sedimentary Geochemistry of Manganese: Implications for the Environment of Formation of Manganiferous Black Shales. Econ. Geol. 91, 36–47.

Canfield, D.E, Raiswell, R., Westrich, J., Reaves, C., Berner, R., 1986. The use of chromium reduction in the analysis of reduced inorganic sulfur in sediments and shales. Chem. Geol. 54, 149–155.

Canfield, D.E., Raiswell, R., Bottrell, S., 1992. The reactivity of sedimentary iron minerals toward sulfide. Am. J. Sci. 292, 659–683.

Canfield, D. E., Thamdrup, B., and Hansen, J. W., 1993a. The anaerobic degradation of organic matter in Danish coastal sediments: Iron reduction, manganese reduction, and sulfate reduction. Geochimica et Cosmochimica Acta 57, 3867–83.

Canfield, D.E., Jørgensen, B.B., Fossing, H., Glud, R., Gundersen, J., Ramsing, N.B., Thamdrup B., Hansen J.W., Nielsen L.P., Hall P.O.J., 1993b. Pathways of organic carbon oxidation in three continental margin sediments. Marine Geology 113, 27–40.

Cao, C., Love, G. D., Hays, L. E., Wang, W., Shen, S., and Summons, R. E., 2009. Biogeochemical evidence for euxinic oceans and ecological disturbance presaging the end-Permian mass extinction event. Earth and Planetary Science Letters 281, 188-201.

Carballo, J.D., Land, L.S., and Miser, D.E., 1987, Holocene dolomitization of supratidal sediments by active tidal pumping, Sugarloaf Key, Florida: Journal of Sedimentary Petrology 57, 153–165.

Castanier, S., Métayer-Levrel, G. Le, and Perthuisot, J., 1999. Ca-carbonate precipitation and limestone genesis —the microbiogeologist point of view. *Sed.Geol.*126, 9-23

Castillo, M. V., and P. Mann, 2006, Cretaceous to Holocene structural and stratigraphic development in south Lake Maracaibo, Venezuela, inferred from well and three-dimensional seismic data: AAPG Bulletin 90, 529–564

Cheatham MM, Sangrey WF, White WM. 1993. Sources of error in external calibration ICPMS analysis of geological samples and an improved non-linear drift correction procedure. Spectrochim. Acta 48B:E487-506.

Choquette, P.W., 1971, Late ferroan dolomite cement, Mississippian carbonates, Illinois Basin, U.S.A., m Bricker, O.P., editor, Carbonate Cements: Baltimore Johns Hopkins Univ. Studies in Geology 19, 339-346

Choquette, P.W., Hiatt, E.E., 2008. Shallow-burial dolomite cement: a major component of many ancient sucrosic dolomites. Sedimentology 55, 423–460.

Claps, M., Masetti, D., Pedrielli, E, Garavello, A.L., 1991. Analisi spettrale e cicli di Milankovitch in successione cretaciche del Sudalpino orientale. Riv. It. Strat. 92: 155-174.

Clarkson, M.O., Poulton, S.W., Guilbaud, R., Wood, R. a., 2014. Assessing the utility of Fe/Al and Fe-speciation to record water column redox conditions in carbonate-rich sediments. Chem. Geol. 382, 111–122.

Clayton, C.J., 1986. The chemical environment of flint formation in Upper Cretaceous chalks. In: Sieveking, G. de G., Hart, M.B.,Eds, , The Scientific Study of Flint and Chert. Cambridge University Press, Cambridge, pp. 43–54.

Craig, H., 1957, Isotopic standards for carbon and oxygen and correction factors for mass-spectrometric analysis of carbon dioxide: Geochimica et Cosmochimica Acta, v. 12, p. 133-149.

Craig, H., 1961. Standards for reporting concentrations of deuterium and oxygen-18 in natural waters. Science, 133: 1833-1834.

Coleman, M.L., Raiswell, R., 1993, Microbial mineralization of organic matter: mechanisms of self-organization and inferred rates of precipitation of diagenetic minerals. Philosophical Transactions of the Royal Society A: Mathematical, Physical and Engineering Sciences 344, 69–87.

Compton, J., 1992. Early diagenesis and the origin of diagenetic carbonate in sediment recovered from the Argo Basin, Northeastern Indian Ocean, Site 765. Proceedings of the Ocean Drilling Program, Site 765, 77–88.

Covington, A.K., Whitfield, M., 1988. Recommendations for the determination of pH in seawater and estuarine waters. Pure Appl. Chem. 60, 865–870.

Curtis, C.D., Coleman, M.L., Love L.G., 1986, Porewater evolution during sediment burial fromisotopic andmineral chemistry of calcite, dolomite and siderite concretions. Geochimica et Cosmochimica Acta 50, 2321–2334.

Curtis, C.D., Cope, J.C.W., Plant, D., and Macquaker, J.H.S., 2000. “Instantaneous” sedimentation, early microbial sediment strengthening and a lengthy record of chemical diagenesis preserved in Lower Jurassic ammonitiferous concretions from Dorset. J. Geol.Soc. 157, 165–72.

Dapples, E. C.,1979. Silica as an agent in diagenesis in Diagenesis, in Larsen, G. and Chilingar, G.V , eds., Diagenesis in sediments and sedimentary rocks. Developments in sedimentology 25A, Elsevier, 99-141.Davies, G.R., 1977. Former magnesian calcite and aragonite submarine cements in upper Paleozoic reefs of the Canadian arctic: a summary. Geology 5, 11-15.

Davies, P., Ferguson, J, and Bubela, B., 1975. Dolomite and organic material. Nature 255, 472–74.

de Baar, H.J.W., German, C.R., Elderfield, H., and van Gaans, P., 1988, Rare earth element distributions in anoxic waters of the Cariaco Trench: Geochimica et Cosmochimica Acta, v. 52, p. 1203−1219.

de Baar, H.J.W., Schijf, J., Byrne, R.H., 1991. Solution chemistry of the rare earth elements in seawater. Eur. J. Solid State Inorg. Chem. 28, 357–373

de Boer, P.L., and Wonders, A.A.H., 1984, Astronomically induced rhythmic bedding in Cretaceous pelagic sediments near Moria (Italy), in Berger, A., Imbrie, J., Hays, J., Kukla, G., and Saltzman, B., eds., Milankovitch and climate. Hingham, Massachusetts, Reidel, 177- 190.

Decho, A.W., 2000. Microbial biofilms in intertidal systems: an overview. *Continental Shelf Research* 20, 1257–1273.

Decho, A. W., Visscher, P. T., and Reid, R. P., 2005. Production and cycling of natural microbial exopolymers, EPS, within a marine stromatolite. *Palaeogeog., Palaeoclim., Palaeoecol.* 219, 71 – 86.

Défarge, C., Trichet, J., Jaunet, A.M., Robert, M., and Sansone, F.J., 1996. Texture of microbial sediments revealed by cryo-scanning electron microscopy. *J. Sed. Research* 66, 935–47.

Deffeyes, K.S., Lucia, F.J., and Weyl, P.K., 1964, Dolomitization: Observations on the island of Bonaire, Netherlands Antilles: Science, 143,678-679.

Dembicki Jr, H., Meinschein, W. G., and Hattin, D. E., 1976b. Possible ecological and environmental significance of the predominance of even-carbon number C_{20}-C_{30} n-alkanes. Geochimica et Cosmochimica Acta 40, 203-208.

Derry, L. A., and Jacobsen, S. B. 1990. The chemical evolution of Precambrian seawater: Evidence from REEs in banded iron formations. Geochimica et Cosmochimica Acta, 54(11), 2965-2977.

Des Marais, D. J., 2003. Biogeochemistry of hypersaline microbial mats illustrates the dynamics of modern microbial ecosystems and the early evolution of the biosphere. The Biological Bulletin 204, 160–16

Dickson, J.A.D., 2009. Mississippian Paleocean Chemistry from Biotic and Abiotic Carbonate, Muleshoe Mound, Lake Valley Formation, New Mexico, U.S.A.- Discussion. J. Sediment. Res. 79, 42–43.

Davranche, M., Pourret, O., Gruau, G., Dia, A., Jin, D., Gaertner, D., 2008. Competitive binding of REE to humic acid and manganese oxide: impact of reaction kinetics on development of cerium anomaly and REE adsorption. Chem. Geol. 247, 154–170

Dewers, T., Ortoleva, P., 1994. Formation of stylolites, marl/limestone alternations, and dissolution (clay) seams by unstable chemical compaction of argillaceous carbonates.

Didky, B.M., Simoneit, B.R.T., Brassel, S.C., Eglinton, G., 1978. Organic geochemical indicators of palaeoenvironmental conditions of sedimentation. Nature 272, 216-222.

Drever, J. I., 1988. The geochemistry of natural waters (2nd ed.). Englewood Cliffs, New Jersey, Prentice-Hall, 437 p.

Dumitrescu, M. and Brassell, S. C., 2005. Biogeochemical assessment of sources of organic matter and paleoproductivity during the early Aptian Oceanic Anoxic Event at Shatsky Rise, ODP Leg 198. Organic geochemistry 36, 1002-1022.

Dupraz, C., Reid, R.P., Braissant, O., Decho, A.W., Norman, R.S., Visscher, P.T., 2009. Processes of carbonate precipitation in modern microbial mats. Earth Science Reviews 96**,** 141–162.

Dymond, J., Suess, E. and Lyle, M., 1992. Barium in deep-sea sediment: A geochemical proxy for paleo-productivity. Paleoceanography, 7: 163-181.

Edwards, W., 1933. On the Cretaceous fern *Paradoxopteris* and its connexion with *Weichselia.* Ann. Bot. 47, 317-341.

Edwards, K. J., Becker, K., and Colwell, F., 2012. The deep, dark energy biosphere: Intraterrestrial life on Earth. Annual Reviews in Earth Planetary Sciences 40, 551–568.

Elderfield, H., Pagett, R., 1986. Rare earth elements in ichthyoliths: variations with redox conditions and depositional environment. Sci. Total Environ. 49, 175–197

Elderfield, H., 1988. The oceanic chemistry of the rare earth elements. Phil. Trans. Roy. Soc. London A 325, 105–126.

Elias, V. O., Simoneit, B. R., and Cardoso, J. N., 1997. Even n-alkane predominances on the Amazon shelf and a Northeast Pacific hydrothermal system. Naturwissenschaften 84, 415-420.

Eglinton, G., Gonzalez, A. G., Hamilton, R. J., and Raphael, R. A., 1962. Hydrocarbon constituents of the wax coatings of plant leaves: A taxonomic survey. Phytochemistry 1, 89-102.

Erbacher, J., Thurow, J., Littke, R., 1996. Evolution patterns of radiolaria and organic matter variations: a new approach to identifying sea-level changes in mid-Cretaceous pelagic environments. Geology 24, 499–502.

Erbacher, J., Huber, B., Norris, R., Markey, M., 2001. Increased thermohaline stratification as a possible cause for an ocean anoxic event in the Cretaceous period. Nature 409, 325–327.

Erlich, R. N., Lorente, M.A.A., Palmer-Koleman, S., 1999. Geochemical characterization of oceanographic and climatic changes recorded in upper Albian to lower Maastrichtian strata, western Venezuela. Cretac. Res. 20, 547–581.

Eriksson, P.G., Condie, K.C., Tirsgaard, H., Mueller, W.U., Altermann, W., Miall, a. D., Aspler, L.B., Catuneanu, O., Chiarenzelli, J.R., 1998. Precambrian clastic sedimentation systems. Sediment. Geol. 120, 5–53.

Escalona, A., Mann, P., 2006. An overview of the petroleum system of Maracaibo Basin. Am. Assoc. Pet. Geol. Bull. 90, 657–678.

Evans, E., Giglio, J., 1993. Interferences in inductively coupled plasma mass spectrometry. A review. J. Anal. At. Spectrom. 8, 1–18.

Fairbridge, R. W., 1957, The dolomite question, in R. J. Leblanc and J. C. Breeding, editors. Regional aspects of carbonate deposition: SEPM Spec. Pub. 5, 125-178

Farquhar, J., Zerkle, A., and Bekker, A., 2011, Geological constraints on the origin of oxygenic photosynthesis: Photosynthesis research 107, 11–36.

Fischer, W.W., Schroeder, S., Lacassie, J.P., Beukes, N.J., Goldberg, T., Strauss, H., Horstmann, U.E., Schrag, D.P., and Knoll, A.H., 2009. Isotopic constraints on the Late Archean carbon cycle from the Transvaal Supergroup along the western margin of the Kaapvaal Craton, South Africa: Precambrian Research 169, p. 15–27.

Farrimond, P., Talbot, H., Watson, D., Schulz, L., and Wilhelms, A., 2004. Methylhopanoids: molecular indicators of ancient bacteria and a petroleum correlation tool. Geochimica et Cosmochimica Acta 68, 3873-3882.

Fein, J., Daughney, C., Yee, N., and Davis, T., 1997. A chemical equilibrium model for metal adsorption onto bacterial surfaces. Geochimica et Cosmochimica Acta 61, 3319–3328.

Filzmoser, P., and Hron, K. 2008. Outlier detection for compositional data using robust methods. Mathematical Geoscience. 40, 233–248.

Fisher, A. G. De Boer, P. L., and Premoli-Silva, I. 1990. Cyclostratigraphy. In: Ginsburg, R. N. and Beadoin, B., eds., Cretaceous Resources, Events and Rhythms: Background and Plans for Research. NATO ASI Series, Dordrecht, Klewer, 139-172.

Fisher, W. L., and Rodda, P. U., 1969. Edwards Formation (Lower Cretaceous), Texas: dolomitization in a carbonate platform system. AAPG Bulletin, 53(1), 55-72.

Flemming, H.-C., Wingender, J., 2010. The biofilm matrix. Nat. Rev. Microbiol. 8, 623–633.

Flörke, O. W., Graetsch, H., Martin, B., Röller, K. and Wirth, R. 1991. Nomenclature of microcrystalline and non-crystalline silica minerals, based on structure and microstructure. Neues Jahrbuch Für Mineralogie-Abhandlungen 163, 1, 19 - 42.

Floran, R.J., and Papike, J.J., 1978, Mineralogy and petrology of the Gunflint Formation, Minnesota-Ontario. J. Petrology, 19, 215-288

Föllmi, K.B.B., 2012. Early Cretaceous life, climate and anoxia. Cretac. Res. 35, 230–257.

Folk, R. L. 1974. The natural history of crystalline calcium carbonate: effect of magnesium content and salinity. J. Sedim. Petrol. 44, 40-53.

Folk, R.L., Siedlecka, A., 1974. The “schizohaline” environment: Its sedimentary and diagenetic fabrics as exemplified by Late Paleozoic rocks of Bear Island, Svalbard. Sediment. Geol. 11, 1–15.

Ford, A.B., Houbolt, J.J.H.C., 1963. The microfacies of the cretaceous of western Venezuela. EJ Brill, Leiden, 56 pp.

Fralick, P. 1989. Microbial bioherms, Lower Proterozoic Gunflint Formation, Thunder Bay, Ontario. In H.H.J. Geldsetzer, N.P. James, and G.E. Tebbutt, eds., Reefs: Canada and adjacent areas. Canadian Society of Petroleum Geologists, Memoirs, pp. 24–29.

Fralick, P., Barrett, T., 1995. Depositional controls on iron formation associations in Canada. Spec. Pub. Int. Ass. Sediment. 22, 137-156

Fralick, P., Davis, D., Kissin, S., 2002. The age of the Gunflint Formation, Ontario, Canada: single zircon U Pb age determinations from reworked volcanic ash. Can. J. Earth Sci. 39, 1091, 1085–1091. doi:10.1139/E02-028.

Fraústo da Silva, J.J.R., Williams, R.J.P., 2001. The Biological Chemistry of the Elements, second ed. Oxford University Press, Oxford, UK, 575 pp.

Frigaard, N.-U. and Bryant, D. A., 2006. Chlorosomes: antenna organelles in photosynthetic green bacteria, Complex intracellular structures in prokaryotes. Springer.

Fritz, P., Katz, A., 1972. The sodium distribution of dolomite crystals. Chem. Geol. 10.3 (1972): 237-244.

Fredickson, J. K., Garland, T. R., Hicks, R. J., Thomas, J. M., Li, S. W., and McFadden, K. M., 1989. Lithotrophic and heterotrophic bacteria in deep subsurface sediments and their relation to sediment properties. Geomicrobiology Journal 7, 53–66.

Fredickson, J. K., and Fletcher, M., 2001, Subsurface Microbiology and Biogeochemistry: New York, Wiley & Sons, p. 341.

Friedman, G. M., and Sanders, J. E., 1967, Origin and occurrence of dolostones, in Chilingar, G. V., Bissell, H. J., and Fairbridge, R. W., editors., Carbonate Rocks; Origin, Occurrence and Classification: Amsterdam, Developments in Sedimentology, 9A, Elsevier, 267-348.

Fritz, P., Katz, A., 1972. The sodium distribution of dolomite crystals. Chem. Geol.

Froelich, P.N., Klinkhammer, G.P., Bender, M.L., Luedtke, N.A., Heath, G.R., Cullen, D., Dauphin, P., Hammond, D., Hartman, B., and Maynard, V., 1979. Early oxidation of organic-matter in pelagic sediments of the eastern equatorial Atlantic: Suboxic diagenesis: Geochimica et Cosmochimica Acta 43, 1075–1090.

Gaines, A.M., 1974. Protodolomite synthesis at 100 °C and atmospheric pressure. Science 183, 518-520.

Gaines, A.M., 1977. Protodolomite redefined. J. Sediment. Petrol. 47, 543-546

Gallagher, K.L., Kading, T.J., Braissant, O., Dupraz, C., Visscher, P.T., 2012. Inside the alkalinity engine: the role of electron donors in the organomineralization potential of sulfate-reducing bacteria. Geobiology 10, 518–30.

Gaona-Narvaez, T., Maurrasse, F.J.-M.R., Etayo-Serna, F., 2013. Geochemistry, palaeoenvironments and timing of Aptian organic-rich beds of the Paja Formation (Curiti, Eastern Cordillera, Colombia). Geol. Soc. London, Spec. Publ. 382, 31–48.

Gebelein, C.D., and Hoffman, P., 1973. Algal origin of dolomite laminations in stromatolitic limestone. Journal of Sedimentary Petrology 43, 603–613.

Geesey, G.G., and Jang, L., 1989. Interactions between metal ions and capsular polymers. In Beveridge, T.J., and Doyle R., eds., Metal ions and bacteria, 325-357.

Gilbert, P., Abrecht, M., and Frazer, B.H., 2005. The organic-mineral interface in biominerals. Reviews in Mineralogy and Geochemistry 59, 157-185.

Gellatly, A., Lyons, T., 2005. Trace sulfate in mid-Proterozoic carbonates and the sulfur isotope record of biospheric evolution. Geochim. Cosmochim. Acta 69, 3813–3829.

Gelpi, E., Schneider, H., Mann, J., and Oro, J., 1970. Hydrocarbons of geochemical significance in microscopic algae. Phytochemistry 9, 603-612.

Gingele, F.X. and Dahmke, A., 1994. Discrete barite particles and barium as tracers of paleoproductivity in South Atlantic sediments. Paleoceanography, 9: 151-168Gingele et al., 1999.

Gingele, F.X., Zabel, M., Kasten, S., Bonn, W.J. and Nürnberg, C.C., 1999. Biogenic barium - methods and constraints of application as a proxy for paleoproductivity. In: Fischer G. and Wefer, G. (eds), Use of proxies in paleoceanography: examples from the South Atlantic. Springer, Berlin, pp. 345-364.

Given, R.K., Lohmann, K.C., 1985. Derivation of the original isotopic composition of Permian marine cements. J. Sediment. Petrol. 55, 430–439.

Given, R.K., Wilkinson, B.H., 1987. Dolomite Abundance and Stratigraphic Age: Constraints on Rates and Mechanisms of Phanerozoic Dolostone Formation: Perspectives 1068–1078.

Glew, J.R., 1991. Miniature gravity corer for recovering short sediment cores. Journal of Paleolimnology 5, 285-287.

Goldhammer, R.K, Dunn, P.A., Hardie, L.A., 1987, High frequency glacio-eustatic sea level oscillations with Milankovitch characteristics recorded in Middle Triassic platform carbonates in northern Italy: American Journal of Science 287, 853-828

González de Juana C., Arozena J. and Picard X.C., 1980. Geología de Venezuela y de sus Cuencas Petrolíferas, Ediciones Foninves, Caracas, 1031 pp.

Goodwin, A.M. 1956. Facies relations in the Gunflint Iron Forma- tion. Economic Geology, 51: 565–595. Goodwin, A.M. 1960. Gunflint Formation of the Whitefish Lake area. In Ontario Department of Mines Annual Report 69, pp. 41–63.

Grabenstatter, J., Méhay, S., McIntyre-Wressnig, A., Giner, J.-L., Edgcomb, V. P., Beaudoin, D. J., Bernhard, J. M., and Summons, R. E., 2013. Identification of 24-n-propylidenecholesterol in a member of the Foraminifera. Organic geochemistry 63, 145-151.

Graetsch, H., Flörke, O. W., Miehe, G. 1987. Structural Defects in Microcrystalline Silica. Phys. Chem. Minerals 14, 249 - 257.

Graetsch, H., 1994. Structural characteristics of opaline and micro-crystalline silica minerals. In: Heaney, P. J., Prewitt, C. T. and Gibbs, G. V. eds. Silica. Physical Behaviour, Geochemistry and Materials Applications, Reviews in Mineralogy 29, pp. 209 - 232.

Graf, D., Goldsmith, J., 1956. Some hydrothermal syntheses of dolomite and protodolomite. J. Geol. 64, 173–186.

Grantham, P. J. and Wakefield, L. L., 1988. Variations in the sterane carbon number distributions of marine source rock derived crude oils through geological time. Organic Geochemistry 12, 61-73.

Gregg, J.M. and Shelton, K.L., 1990. Dolomitization and dolomite neomorphism in the backreef facies of the Bonterre and Davis formations (Cambrian), southeastern Missouri. Sediment. Petrol. 60: 549-562.

Grotzinger, J.P., 1986. Evolution of Early Proterozoic passive-margin carbonate platform, Rocknest Formation, Wopmay Orogen, Northwest Territories, Canada. J. Sediment. Petrol. 56, 831–847.

Grotzinger J.P., 1989. Facies and evolution of Precambrian carbonate depositional systems: emergence of the modern platform archetype. In Crevello, P.D., Wilson, J.L., Sarg, J.F, Read, J.F., eds., Controls on Carbonate Platform and Basin Development, Soc. Econ.Paleontol. Mineral. Spec. Publ. 44, 79–106.

Grotzinger, J.P., 1994, Trends in Precambrian carbonate sediments and their implication for understanding evolution, in Bengston, S., ed., Early life on Earth: New York, Columbia University Press, p. 245–258.

Grotzinger, J. P. and Read, J. F., 1983. Evidence for primary aragonite precipitation, lower Proterozoic (1.9 Ga) Rocknest dolomite, Wopmay orogen, Northwest Canada. Geology 11: 710-713.

Grotzinger, J.P., Knoll, a H., 1999. Stromatolites in Precambrian carbonates: evolutionary mileposts or environmental dipsticks? Annu. Rev. Earth Planet. Sci. 27, 313–58.

Grimalt, J. and Albaigés, J., 1987. Sources and occurrence of C12 C22n-alkane distributions with even carbon-number preference in sedimentary environments. Geochimica et Cosmochimica Acta 51, 1379-1384.

Haack, E.A., Warren, L.A., 2003. Biofilm Hydrous Manganese Oxyhydroxides and Metal Dynamics in Acid Rock Drainage. Environ. Sci. Technol. 37, 4138–4147.

Hallam, A., 1986. Origin of minor limestone-shale cycles: Climatically induced or diagenetic? Geology 14, 609–612.

Halley, R. B., 1985. Setting and geological summary of the Lower Cretaceous, Sunniland field, southern Florida. In Carbonate Petroleum Reservoirs (pp. 443-454). Springer New York.

Hammersley A.P., Svensson, S.O., Han, M., Fitch A.N., and Hausermann D., 1996. Two-dimensional detector software: from real detector to idealized image or two-theta scan: High Pressure Research 14, 235-248.

Han, Y. J., Aizenberg, J., 2003. Effect of magnesium ions on oriented growth of calcite on carboxylic acid functionalized self-assembled monolayer. J. Am. Chem. Soc. 125, 4032–3.

Hardie, L.A., and Shinn, E.A., 1986. Carbonate depositional environments - modern and ancient – part 3. tidal flats. Colourado School of Mines Quarterly 81, 1-74.

Harrison, A.G, and Thode, H.G., 1958. Mechanism of the bacterial reduction of sulfate from isotopic fractionation studies Trans. Faraday Soc.54, 84–92.

Harvey, H. R. and Mcmanus, G. B., 1991. Marine ciliates as a widespread source of tetrahymanol and hopan-3β-ol in sediments. Geochimica et Cosmochimica Acta 55, 3387-3390.

Haq, B.U., Hardenbol, J., and. Vail, P.R., 1987, Chronology of fluctuating sea level since the Triassic: Science, 235, p. 1156–1167

Hatch, J.R. and Leventhal, J.S., 1992. Relationship between inferred redox potential of the depositional environment and geochemistry of the Upper Pennsylvanian (Missourian) Stark Shale Member of the Dennis Limestone, Wabaunsee County, Kansas, U.S.A. Chem. Geol. 99: 65-82

Hay, W.W., Migdisov, A., Balukhovsky, A.N., Wold, C.N., Flögel, S., Söding, E., 2006. Evaporites and the salinity of the ocean during the Phanerozoic: implications for climate, ocean circulation and life. In: Buggisch, W. (Ed.), Evolution of the System Earth in the Late Palaeozoic: Clues from Sedimentary Geochemistry. Palaeogeography, Palaeoclimatology, Palaeoecology 240, 3–46.

Heising, S., Richter, L., Ludwig, W., and Schink, B., 1999. *Chlorobium ferrooxidans* sp. nov., a phototrophic green sulfur bacterium that oxidizes ferrous iron in coculture with a Geospirillum sp. strain. Archives of microbiology 172, 116-124.

Helz, G.R., Miller, C. V., Charnock, J.M., Mosselmans, J.F.W., Pattrick, R. a D., Garner, C.D., Vaughan, D.J., 1996. Mechanism of molybdenum removal from the sea and its concentration in black shales: EXAFS evidence. Geochim. Cosmochim. Acta 60, 3631–3642.

Herbert, T. D., 1986. Milankovitch climatic origin of mid-Cretaceous black shale rhythms in central Italy. Nature, 321, 739-743.

Herrle, J.O., 2002. Paleoceanographic and paleoclimatic implications on mid-Cretaceous black shale formation in the Vocontian Basin and the Atlantic: evidence from calcareous nannofossils and stable isotopes. Tubinger Mikropalaontol. Mitt. 27, 114 pp.

Herrle, J., Pross, J., Friedrich, O., 2003. Forcing mechanisms for mid-Cretaceous black shale formation: evidence from the Upper Aptian and Lower Albian of the Vocontian Basin (SE France). Palaeogeogr. Palaeoclimatol. Palaeoecol. 190, 399–426.

Herrle, J. O., Kößler, P., Friedrich, O., Erlenkeuser, H., and Hemleben, C. 2004. High-resolution carbon isotope records of the Aptian to Lower Albian from SE France and the Mazagan Plateau (DSDP Site 545): a stratigraphic tool for paleoceanographic and paleobiologic reconstruction. Earth and Planetary Science Letters, 218, 149–161.

Hesse, R., 1989. Silica diagenesis: origin of inorganic and replacement cherts. Earth-Sci. Rev. 26, 253–284.

Hiatt, E.E., Pufahl, P.K., Edwards, C.T., 2015. Sedimentary phosphate and associated fossil bacteria in a Paleoproterozoic tidal flat in the 1.85Ga Michigamme Formation, Michigan, USA. Sediment. Geol. 319, 24–39.

Hoehler, T.M., Jørgensen, B.B., 2013. Microbial life under extreme energy limitation. Nat. Rev. Microbiol. 11, 83–94.

Hofmann, H.J., Jackson, G.D., 1987. Proterozoic ministromatolites with radial-fibrous fabric. Sedimentology 34, 963–971.

Holba, A., Dzou, L., Wood, G., Ellis, L., Adam, P., Schaeffer, P., Albrecht, P., Greene, T., and Hughes, W., 2003. Application of tetracyclic polyprenoids as indicators of input from fresh-brackish water environments. Organic geochemistry 34, 441-469.

Holba, A. G., Tegelaar, E., Ellis, L., Singletary, M., and Albrecht, P., 2000. Tetracyclic polyprenoids: Indicators of freshwater (lacustrine) algal input. Geology 28, 251-254.

Holail, H., Lohmann, K.C , Sanderson, I., 1988, Dolomitization and dedolomitization of Upper Cretaceous carbonates: Bahariya Oasis, Egypt, in Shukla, V., and Baker, P. A., editors, Sedimentology and geochemistry of dolostones: SEPM Spec. Publ. 43, 191-207

Holland, H., Zimmermann, H. 2000. The Dolomite Problem Revisited. International Geology Review, 37–41.

Holmden, C., 2009. Ca isotope study of Ordovician dolomite, limestone, and anhydrite in the Williston Basin: Implications for subsurface dolomitization and local Ca cycling. Chem. Geol. 268, 180–188.

House, C.H., Schopf, J.W., McKeegan, K.D., Coath, C.D., Harrison, T.M., and Stetter, K.O., 2000, Carbon isotopic composition of individual Precambrian microfossils. Geology 28, 707–710.

Huang, C., 2010. Rare earth coordination chemistry: Fundamentals and applications. John Wiley & Sons (Asia), Singapore, 575 p.

Hughes, W., Holba, A., Dzou, L., 1995. The ratios of dibenzothiophene to phenanthrene and pristane to phytane as indicators of depositional environment and lithology of petroleum source rocks. Geochim Cosmochim Acta 59, 3581–98.

Hveding-Bergseth, N., Bruun T., and Kjoesen, H, 1983. Isolation of 30-nor-21 Hopan-22-one (lsoadlantone) from the lichen *Piatismatia glauca*. Phytochem., 22, 1826-1827.

Illich, H. A., 1983. Pristane, phytane, and lower molecular weight isoprenoid distributions in oils. AAPG bulletin 67, 385-393.

Ingerson E., 1962. Problems of the geochemistry of sedimentary carbonate rocks. Geochim. et Coamochim. Acta 26, 815-847.

Irwin, M.L., 1965. General theory of epeiric clear water sedimentation. Am. Assoc. Pet. Geol. Bull., 49: 445-459.

Irwin, H., Curtis, C., and Coleman, M., 1977. Isotopic evidence for source of diagenetic carbonates formed during burial of organic-rich sediments. Nature, 269:209-213.

James, N., Bone, Y., Collins, L., Kyser, T., 2001. Surficial sediments of the Great Australian Bight: facies dynamics and oceanography on a vast cool-water carbonate shelf. J. Sediment. Res.

Jarrett, A. J., Schinteie, R., Hope, J. M., and Brocks, J. J., 2013. Micro-ablation, a new technique to remove drilling fluids and other contaminants from fragmented and fissile rock material. Organic geochemistry 61, 57-65.

Jeng, W.L., 2006. Higher plant n-alkane average chain length as an indicator of petrogenic hydrocarbon contamination in marine sediments. Marine Chemistry 102, 242-251.

Jenkyns, H.C., 2010. Geochemistry of oceanic anoxic events. Geochemistry, Geophys. Geosystems 11, doi:10.1029/2009GC002788.

Jirsa, M. and Fralick,P., 2010, Geology of the Gunflint Iron Formation and the Sudbury Impact Layer, Northeastern Minnesota, Institute on Lake Superior Geology, Field Trip 4, Field Trip Guidebooks 53, 77-92.

Jirsa, M. and Fralick,P., 2010, Geology of the Gunflint Iron Formation and the Sudbury Impact Layer, Northeastern Minnesota, Institute on Lake Superior Geology, Field Trip 4, Field Trip Guidebooks 53, 77-92.

Johannesson, K.H., Hawkins, D.L., Cortés, A., 2006. Do Archean chemical sediments record ancient seawater rare earth element patterns? Geochim. Cosmochim. Acta 70, 871–890.

Johannesson, K. H., Telfeyan, K., Chevis, D. A., Rosenheim, B. E., and Leybourne, M.I., 2014. Rare earth elements in stromatolites—1. Evidence that modern terrestrial stromatolites fractionate rare earth elements during incorporation from ambient waters. In In Y. Dilek, H. Furnes (eds.), Evolution of Archean Crust and Early Life, Modern Approaches in Solid Earth Sciences 7, DOI 10.1007/978-94-007-7615-9_14, © Springer Science+Business Media Dordrecht 2014.

Johnson, C.M., Mclennan, S.M., Mcsween, H.Y., Summons, R.E., 2013. Smaller , better , more : Five decades of advances in geochemistry. Geol. Soc. Am. Special Pub, 1–44. doi:10.1130/2013.2500(08).

Jones, B., 2013. Microarchitecture of dolomite crystals as revealed by subtle variations in solubility: Implications for dolomitization. Sediment. Geol. 288, 66-80.

Jones, B., Luth, R.W., MacNeil, A.J., 2001. Powder X-ray diffraction analysis of homogeneous and heterogeneous sedimentary dolostones. Journal of Sedimentary Research 71, 790-799.

Jørgensen B. B. and Kasten S., 2006. Sulfur cycling and methane oxidation. In Marine Geochemistry. In Schulz H. D., Zabel M., eds. Springer, Berlin, pp. 271–309

Jørgensen, B. B., Boetius, A., 2007. Feast and famine — microbial life in the deep-sea bed: Nature Reviews Microbiology, 5, 770–781.

Kah, L.C., Knoll, A.H., 1996. Microbenthic distribution of Proterozoic tidal flats: environmental and taphonomic considerations. Geology 24, 79–82.

Kallmeyer, J., Pockalny, R., Adhikari, R. R., Smith, D. C., and D'Hondt, S., 2012, Global distribution of microbial abundance and biomass in subseafloor sediment: PNAS 109, 16213–16216.

Kamber, B,S., Webb, G.E., 2001. The geochemistry of late Archaean microbial carbonate: implications for ocean chemistry and continental erosion history. Geochim. Cosmochim. Acta 65, 2509–2525.

Kamber, B.S., Bolhar, R., Webb, G.E., 2004. Geochemistry of late Archaean stromatolites from Zimbabwe: evidence for microbial life in restricted epicontinental seas. Precambrian Res. 132, 379– 399.

Kamber, B.S., Webb, G.E., 2007. Transition metal abundances in microbial carbonate: a pilot study based on *in situ* LA-ICP-MS analysis. Geobiology 5, 375–389. doi:10.1111/j.1472-4669.2007.00129.x

Kappler A., Emerson D., Edwards, K.J., Amend, J.P., Gralnick, J.A, Grathwohl, P., Hoehler, T.M., Straub, K.L., 2005. Microbial activity in biogeochemical gradients - new aspects of research. Geobiol 3, 229-233.

Karl, D.M., 2007. Microbial oceanography: paradigms, processes and promise. Nat. Rev. Microbiol. 5, 759–769.

Kastner, M., Hollander, D., and Garrison, R., 1984. The association of dolomite-phosphorite-chert: causes and possible diagenetic sequences. In Garrison, R. E., Kastner, R. E., and Zenger, D. H., editors, Dolomites of the Monterey Formation and Other Organic-Rich Units. Pac. Sect., Soc. Econ. Paleontol. Mineral. Spec. Publ. 41,75-86.

Kawabe, I., Ohta, A., Miura, N., 1999. Distribution coefficients Fe oxyhydroxide of REE between precipitates and NaCl solutions affected by REE complexation. Geochem. Journal 33, 181–197.

Kelts, K. R., and McKenzie, J. A., 1982. Diagenetic dolomite formation in Quaternary anoxic diatomaceous muds of Deep Sea Drilling Project Leg 64, Gulf of California. In Curray, J.R., Moore, D., et al., Init. Reports. DSDP, 64: Washington (U.S. Govt. Printing Office), 553-569

Kemp, P., Lander, D. J., and Orpin, C. G., 1984. The lipids of the rumen fungus Piromonas communis. Journal of General Microbiology 130, 27-37.

Kempf, B., Bremer, E., 1998. Uptake and synthesis of compatible solutes as microbial stress responses to high-osmolality environments. Arch. Microbiol. 170, 319–30.

Kendall, C.G.St.C., and Skipwith P.S. 1968. Recent algal mats of a Persian Gulf lagoon. *Journal of Sedimentary Petrology* 38, 1040–1058.

Kenward, P.A, Goldstein, R.H., González, L.A, and Roberts, J.A, 2009, Precipitation of low-temperature dolomite from an anaerobic microbial consortium: the role of methanogenic Archaea, Geobiology 7, 556–65.

Kenward, P., Fowle, D. A., Goldstein, R.H., Ueshima, M., González, L.A., and Roberts, J. A., 2013. Ordered low-temperature dolomite mediated by carboxyl-group density of microbial cell walls. *AAPG Bulletin* 97, 2113–2125.

Kershaw, S., Crasquin, S., Li, Y., Collin, P.-Y., Forel, M.-B., Mu, X., Baud, a, Wang, Y., Xie, S., Maurer, F., Guo, L., 2012. Microbialites and global environmental change across the Permian-Triassic boundary: a synthesis. Geobiology 10, 25–47.

Kershaw, S., 2015. Modern Black Sea oceanography applied to the end-Permian extinction event. J. Palaeogeogr. 4, 1–18.

King, G. M.,1988. Methanogenesis from methylated amines in a hypersaline algal mat. Applied and Environmental Microbiology 54, 130-136.

Kirkland, B., Lynch, F., Rahnis, M., 1999. Alternative origins for nannobacteria-like objects in calcite. Geology 27, 347–350.

Kleemann, G., Poralla, K., Englert, G., Kjøsen, H., Liaaen-Jensen, S., Neunlist, S., and Rohmer, M., 1990. Tetrahymanol from the phototrophic bacterium Rhodopseudomonas palustris: first report of a gammacerane triterpene from a prokaryote. Journal of General Microbiology 136, 2551-2553.

Kirsimäe, K., Jørgensen, P., Kalm, V., 1999. Low-temperature diagenetic illite-smectite in Lower Cambrian clays in North Estonia. Clay Miner. 94, 151–163.

Knauth, L.P., 1979. A model for the origin of chert in limestone. Geology 7, 274–277.

Knoll, A., 1985. Exceptional preservation of photosynthetic organisms in silicified carbonates and silicified peats. Philos. Trans. R. Soc. B 311, 111–122.

Knoll, A., 2003. Biomineralization and evolutionary history. Rev. Mineral. Geochemistry 329–356.

Knoll, A., Swett, K., 1990. Carbonate deposition during the late Proterozoic Era: an example from Spitsbergen. Am. J. Sci. 290, 104–132.

Knoll, A.H., 2003. Life on a Young Planet: the First Three Billion Years of Evolution on Earth. Princeton University Press, New Jersey.

Konhauser, K.O. 2007. Introduction to Geomicrobiology. Blackwell Publishing. 433 p.

Konhauser, K., Phoenix, V., 2001. Microbial–silica interactions in Icelandic hot spring sinter: possible analogues for some Precambrian siliceous stromatolites. Sedimentology 48, 415–433.

Konhauser, K.O., Jones, B., Phoenix, V.R., Ferris, G., and Renaut, R.W., 2004. The microbial role in hot spring silicification. Ambio 33, 552-558.

Konhauser, K.O., Newman, D.K., and Kappler, A., 2005. The potential significance of microbial Fe(III)-reduction during Precambrian banded iron formations. ***Geobiology***, 3:167-177.

Konhauser, K.O., Lalonde, S. V, Planavsky, N.J., Pecoits, E., Lyons, T.W., Mojzsis, S.J., Rouxel, O.J., Barley, M.E., Rosìere, C., Fralick, P.W., Kump, L.R., Bekker, A., 2011. Aerobic bacterial pyrite oxidation and acid rock drainage during the Great Oxidation Event. Nature 478, 369–73.

Konhauser, K.O. , Gingras, M.K., and Kappler, A., 2011. Diagenesis – Biologically Controlled. In: J. Reitner and V. Thiel, editors, *Encyclopedia of Geobiology*. Springer, Berlin, p. 777-784.

Koopmans, M. P., Schouten, S., Kohnen, M. E., and Sinninghe-Damsté, J. S., 1996. Restricted utility of aryl isoprenoids as indicators for photic zone anoxia. Geochimica et Cosmochimica Acta 60, 4873-4876.

Koopmans, M. P., De Leeuw, J. W., and Damsté, J. S. S., 1997. Novel cyclized and aromatized diagenetic products of β-carotene in the Green River Shale. Organic geochemistry 26, 451-466.

Kraft, S., Stümpel, J., Becker, P., Kuetgens, U. 1996. High-resolution x-ray absorption spectroscopy with absolute energy calibration for the determination of absorption edge energies. Review of scientific instruments 67, 681–687.

Krügel, H., Krubasik, P., Weber, K., Saluz, H. P., and Sandmann, G., 1999. Functional analysis of genes from Streptomyces griseus involved in the synthesis of isorenieratene, a carotenoid with aromatic end groups, revealed a novel type of carotenoid desaturase. Biochimica et Biophysica Acta (BBA)-Molecular and Cell Biology of Lipids 1439, 57-64.

Krumbein, W. E. (1986). Biotransfer of minerals by microbes and microbial mats. In Leadbeater, Barry SC, and Robert Riding, Eds., Biomineralization in lower plants and animals. Oxford University Press Biomineralization in lower plants and animals (pp. 55-72).

Kummerow, E., and Pérez de Mejía, D., 1989. Evolución diagenética de los carbonatos del Grupo Cogollo, cuenca del Lago de Maracaibo. VII Congreso Venezolano de Geología, Barquisimeto, Memorias 2, 745-771.

Kump, L.R., Arthur, M.A., 1999. Interpreting carbon-isotope excursions: carbonates and organic matter. Chem. Geol. 161, 181–198.

Kuypers, M.M., Blokker, P., Erbacher, J., Kinkel, H., Pancost, R.D., Schouten, S., Sinninghe Damste, J.S., 2001. Massive expansion of marine archaea during a mid-Cretaceous oceanic anoxic event. Science (80-.). 293, 92–5.

Kuypers, M.M.M., Blokker, P., Hopmans, E.C., Kinkel, H., Pancost, R.D., Schouten, S., Sinninghe Damsté, J.S., 2002. Archaeal remains dominate marine organic matter from the early Albian oceanic anoxic event 1b. Palaeogeogr. Palaeoclimatol. Palaeoecol. 185, 211–234.

Kwak, S. Y., DiMasi, E., Han, Y.-J., Aizenberg, J., and Kuzmenko, I., 2005. Orientation and Mg Incorporation of Calcite Grown on Functionalized Self-Assembled Monolayers. A Synchrotron X-ray Study. *Crystal Growth and Design* 5, 2139–2145.

Lacovara, K. J., Smith, J. R., Smith, J.B,. Lamanna, M.C., and Dodson. P., 2000. Paralic environments of the Cretaceous dinosaurs of Egypt: a discussion of uniformitarian analogs. Journal of Vertebrate Paleontology, 20. 53.

Lacovara, K. J., Smith, J. R., Smith, J. B., and Lamanna, M. C., 2003. The Ten Thousand Islands Coast of Florida: A modern analog to low-energy mangrove coasts of Cretaceous epeiric seas. In Davies, R.A.J., ed., Proceedings of the 5th International Conference on Coastal Sediments, Clearwater Beach, Florida. CD-ROM Published by World Scientific Publishing Corporation and East Meets West Productions, Corpus Christi, Texas, pp. 1773–1784.

Lalonde, S.V., Konhauser, K.O., Reysenbach, A.-L., and Ferris, F.G., 2005. Thermophilic silicification: The role of *Aquificales* in hot spring sinter formation. *Geobiology* 3, 41-52.

Lalonde, S.V., Amskold, L, McDermott, T.R., Inskeep, W.P., and Konhauser, K.O., 2007. Chemical reactivity of microbe and mineral surfaces in hydrous ferric oxide depositing hydrothermal springs. *Geobiology* 5, 219–234.

Lalonde, S.V., Dafoe, L.T., Pemberton, S.G., Gingras, M.K., and Konhauser, K.O., 2010. Investigating the geochemical impact of burrowing animals: Proton and cadmium adsorption onto the mucus lining of Terebellid polychaete worms. *Chemical Geology* 271, 44–51.

Land, L. S., and Epstein, S., 1970, Late Pleistocene diagenesis and dolomitization, North Jamaica: Sedimentology 14, 187-200.

Land, L.S., 1973. Holocene meteoric dolomitization of Pleistocene limestones, North Jamaica. Sedimentology 20, 411– 424

Land, L.S., 1985. The origin of massive dolomite. J. Geol. Educ, 33:112-125.

Land, L S., Salem, M. R. I., and Morrow, D. W., 1975. Paleohydrology of ancient dolomites: geochemical evidence: Am. Assoc. Petroleum Geologists Bull. 59, 1602-1625.

LaRowe, D.E., Amend, J.P., 2015. Catabolic rates, population sizes and doubling/replacement times of microorganisms in natural settings. Am. J. Sci. 315, 167–203.

Larson, R., Erba, E., 1999. Onset of the Mid-Cretaceous greenhouse in the Barremian-Aptian: Igneous events and the biological, sedimentary, and geochemical responses. Paleoceanography 14, 663–678.

Lasemi, Z., Boardman, M.R., Sandberg, P.A., 1989. Cement origin of supratidal dolomite, Andros Island, Bahamas. J. Sediment. Petrol. 59, 249–257.

Leckie, R.M., Bralower, T.J., Cashman, R., 2002. Oceanic anoxic events and plankton evolution: Biotic response to tectonic forcing during the mid-Cretaceous. Paleoceanography 17, 1–29.

Lehmann, C., Osleger, D.A., Montañez, I.P., Sliter , W., Arnaud- Vanneau, A., Banner, J., 1999. Evolution of the Cupido and Coahuila carbonate platforms, early Cretaceous, northeastern Mexico. Geol. Soc. Am. Bull. 111,1010–1029.

Lenders, J.J.M., Dey, A., Bomans, P.H.H., Spielmann, J., Hendrix, M.M.R.M., de With, G., Meldrum, F.C., Harder, S., Sommerdijk, N.A.J.M., With, G. De, 2012. High-Magnesian Calcite Mesocrystals: A Coordination Chemistry Approach. J. Am. Chem. Soc. 134, 1367–73.

Lepot K., Benzerara K., Brown G. E. and Philippot P., 2008. Microbially influenced formation of 2,724 million years old stromatolites. Nat. Geosci. 1, 118–121.

Lepot, K., Benzerara, K., Rividi, N., Cotte, M., Brown Jr., G.E., Philippot, P., Brown, G.E., 2009. Organic matter heterogeneities in 2.72Ga stromatolites: Alteration versus preservation by sulfur incorporation. Geochim. Cosmochim. Acta 73, 6579–6599. doi:10.1016/j.gca.2009.08.014.

Lippmann, F., 1973. Sedimentary carbonate minerals. Berlin, Springer-Verlag, 228

Lloyd, R.M., 1968. Oxygen isotope behaviour in the sulfate–water system J. Geophys. Res. 73. 6099–6110.

Lomstein, B. A., Langerhuus, A. T., D'Hondt, S., Jørgensen, B. B., and Spivack, A. J., 2012, Endospore abundance, microbial growth and necromass turnover in deep sub-seafloor sediment: Nature 484, 101–104.

Lorens, B., 1980. Sr, Cd, Mn and Co distribution coefficients in calcite as a function of calcite precipitation rate 45.

Lugo, J., and Mann, P. 1995, Jurassic–Eocene tectonic evolution of Maracaibo Basin, Venezuela, in A. Tankard, S. Suarez, and H. Welsink, eds., Petroleum basins of South America: AAPG Memoir 62, 699–725.

Lyons, T. W., Werne, J. P., Hollander, D. J., and Murray, R. W., 2003, Contrasting sulfur geochemistry and Fe/Al and Mo/Al ratios across the last oxic-to-anoxic transition in The Cariaco Basin, Venezuela: Chemical Geology 195, 131–157.

Lumsden, D.N., 1985. Secular variations in dolomite abundance in deep marine sediments. Geology 13, 766.

Lumsden, D.N., 1988. Characteristics of Deep-Marine Dolomite. J. Sediment. Res 58, 1023-1031

Lumsden, D., Lloyd, R., 1997. Three dolomites. J. Sediment. Res. 67, 391–396.

Machhour, L., Philip, J., Oudin, J.L., 1994, Formation of laminite deposits in anaerobic-dysaerobic marine environments. Mar. Geol. 117, 287–302.

Machel, H.G., 2004. Concepts and models of dolomitization: a critical reappraisal. Geol. Soc. London, Spec. Publ. 235, 7–63. doi:10.1144/GSL.SP.2004.235.01.02

Machel, H., Mountjoy, E., 1986. Chemistry and environments of dolomitization—a reappraisal. Earth-Science Rev. 23, 175–222.

Machel, H.G., Mountjoy, E.W. and Amthor, J.E. 1996b. Mass balance and fluid flow constraints on regional-scale dolomitization, Late Devonian, Western Canada Sedimentary Basin. Bulletin of Canadian Petroleum Geology 44, 566-571.

Macquaker, J.H.S., Taylor, K.G., Keller, M., and Polya, D., 2014. Compositional controls on early diagenetic pathways in fine-grained sedimentary rocks: Implications for predicting

unconventional reservoir attributes of mudstones. Am. Assoc. Pet. Geol. Bull. 98, 587–603. doi:10.1306/08201311176

Madison, A.S., Tebo, B.M., Mucci, A., Sundby, B., and Luther, G.W. 2013. Abundant porewater Mn (III) is a major component of the sedimentary redox system. *Science* 341, 875-878.

McKirdy, D., Cox, R., Volkman, J., and Howell, V., 1986. Botryococcane in a new class of Australian non-marine crude oils. Nature 320, 57–59.

Major, R.P., Lloyd, R.M., Lucia, F.J., Friedman, G.M., 1992. Oxygen isotope composition of Holocene dolomite formed in a humid hypersaline setting: Comment and Reply. Geology 20, 586.

Malinverno, A., Hildebrandt, J., Tominaga, M., Channell, J.E.T., 2012. M-sequence geomagnetic polarity time scale (MHTC12) that steadies global spreading rates and incorporates astrochronology constraints. J. Geophys. Res. 117, B06104.

Maliva, R.G., Knoll, A.H., Simonson, B.M., 2005. Secular change in the Precambrian silica cycle: Insights from chert petrology. Geol. Soc. Am. Bull. 117, 835.

Mallory, F. B., Gordon, J. T., and Conner, R. L., 1963. The isolation of a pentacyclic triterpenoid alcohol from a protozoan. Journal of the American Chemical Society 85, 1362-1363.

Manceau, A., Marcus, M., and Grangeon, S., 2012. Determination of Mn valence states in mixed-valent manganates by XANES spectroscopy. American Mineralogist 97, 816-827.

Mann, S., Sparks N.H.C., Scott, G.H.E., and deVrind-deJong E.W., 1988. Oxidation of manganese and formation of Mn_3O_4 (hausmannite) by spore coats of a marine *Bacillus* sp. *Applied Environmental Microbiology* 54, 2140-2143.

Mann, P., Escalona, A., Verónica, M., 2006. Regional geological and tectonic setting of the Maracaibo supergiant basin, western Venezuela. Am. Assoc. Pet. Geol. Bull. 90, 445–477.

Mansfield, C., 1980. A urolith of biogenic dolomite—Another clue in the dolomite mystery. Geochim. Cosmochim. Acta 44, 829–839.

Manske, A. K., Glaeser, J., Kuypers, M. M., and Overmann, J., 2005. Physiology and phylogeny of green sulfur bacteria forming a monospecific phototrophic assemblage at a depth of 100 meters in the Black Sea. Applied and environmental microbiology 71, 8049-8060.

Maresca, J. A., Romberger, S. P., and Bryant, D. A., 2008. Isorenieratene biosynthesis in green sulfur bacteria requires the cooperative actions of two carotenoid cyclases. Journal of bacteriology 190, 6384-6391.

Marin, J., Chaussidon, M., Robert, F., 2010. Microscale oxygen isotope variations in 1.9Ga Gunflint cherts: Assessments of diagenesis effects and implications for oceanic paleotemperature reconstructions. Geochim. Cosmochim. Acta 74, 116–130.

Marin, J., Chaussidon, M., Robert, F., 2012. Micrometer-scale chemical and isotopic criteria (O and Si) on the origin and history of Precambrian cherts: Implications for paleo-temperature reconstructions. Geochim. Cosmochim. Acta 92, 129–147.

Markun, C.D., Randazzo, A.F., 1980. Sedimentary structures in the Gunflint Iron Formation, Schreiber Beach, Ontario. Precambrian Reseacrh 12, 287–310.

Marlow, J.J., Steele, J.A., Case, D.H., Connon, S,A., Levin, L.A., and Orphan, V.J., 2014. Microbial Abundance and Diversity Patterns Associated with Sediments and Carbonates from the Methane Seep Environments of Hydrate Ridge, OR. Front. Mar. Sci. 1:44.

Maslen, E., Grice, K., Gale, J. D., Hallmann, C., and Horsfield, B., 2009. Crocetane: a potential marker of photic zone euxinia in thermally mature sediments and crude oils of Devonian age. Organic Geochemistry, 40(1), 1-11.

Maze, W. B., 1984. Jurassic La Quinta Formation in the Sierra de Perijá, northwestern Venezuela: Geology and tectonic environment of red beds and volcanic rocks, in W. E. Bonini, Hargraves, R. B., and Shagam, R., eds., The Caribbean–South American plate boundary and regional tectonics: GSA Memoir 162, 263–282.

Mazzullo, S., 1992. Geochemical and neomorphic alteration of dolomite: a review. Carbonates and Evaporites 7, 21–37.

Mazzullo, S., 2000. Organogenic Dolomitization in Peritidal to Deep-Sea Sediments: Perspectives. J. Sediment. Res. 70, 10–23.

Mazzullo, S., Friedman, G., 1977. Competitive algal colonization of peritidal flats in a schizohaline environment: The Lower Ordovician of New York. J. of Sed. Res. 47, 398–410.

Mazzullo, S.J., 1980. Calcite pseudospar replacive ofmarine acicular aragonite, and implications for aragonite cement diagenesis. Journal of Sedimentary Petrology 50, 409–422.Mojzsis, S.J., and Arrhenius, G., 1998. Phosphates and carbon on Mars: Exobiological implications and sample return considerations. Journal of Geophysical Research 103, 28,495–28,511.

Mazzullo, S.J., Reid, A. M., and Gregg, J.M., 1987. Dolomitization of Holocene Mg-calcite supratidal deposits, Ambergris Cay, Belize. Geological Soc. of America Bull. 98, 224–231.

McArthur, J.M., Howarth, R.J., Bailey, T.R., 2007. Strontium Isotope Stratigraphy: LOWESS Version 3: Best Fit to the Marine Sr-Isotope Curve for 0–509 Ma and Accompanying Look-up Table for Deriving Numerical Age. J. Geol. 109, 155–170.

McCrea, J.M., 1950. On the isotopic chemistry of carbonates and a paleotemperature scale. The Journal of Chemical Physics 18, 849–857.

McKenzie, J. A., 1991. The dolomite problem: an outstanding controversy. Controversies in Modern Geology, 37-54.

McKirdy, D., Cox, R., Volkman, J., and Howell, V., 1986. Botryococcane in a new class of Australian non-marine crude oils. Nature 320, 57 – 59.

McHargue, T., and Price, R., 1982. Dolomite from clay in argillaceous or shale-associated marine carbonates. J. Sediment. Petrol 52, 873–886.

Meister, P., 2013. Two opposing effects of sulfate reduction on carbonate precipitation in normal marine, hypersaline, and alkaline environments. Geology 41, 499–502.

Melim, L., Scholle, P., 2002. Dolomitization of the Capitan Formation forereef facies (Permian, West Texas and New Mexico): seepage reflux revisited. Sedimentology 49, 1207–1227.

Méndez Baamonde, J., 1989. Modelo depositacional del Grupo Cogollo, Talud externo, márgenes y plataforma interna. Memorias del VII Congreso Geológico Venezolano, Tomo II. Barquisimeto, Venezuela, pp. 827–850.

Méndez B, J., Baquero, M., Méndez Dot, J.A., 2009. Eventos Oceánicos Anóxicos OAE 1a y 1b en la Formación Apón del Grupo Cogollo durante el Cretácico Temprano. Cuenca de Maracaibo, Venezuela. Revista Latinoamericana de Geoquímica Orgánica 1, 6-18.

Méndez Dot, J. A., Méndez Baaamonde, J.,, Reyes, D., Wilchy, R., 2015. The Cogollo Group and the Oceanic Anoxic Events 1a y 1b, Maracaibo Basin, Venezuela. Brazilian Journal of Geology 45, 8-31.

Menegatti, A.P., Weissert, H., Brown, R.S., Tyson, R.V., Farrimond, P., Strasser, A., and Caron, M., 1998, High-resolution $\delta^{13}C$ stratigraphy through the Early Aptian "Livello Selli" of the Alpine Tethys: Paleoceanography 13, 530–545.

Middelburg, J., de Lange, G.J., and Kreulen, R., 1990. Dolomite formation in anoxic sediments of Kau Bay, Indonesia. Geology 18, 399-492

Mizutani, Y., and Rafter, T.A., 1969. Oxygen isotopic composition of sulfates: Part 4. Bacteria fractionation of oxygen isotopes in the reduction of sulfate and in the oxidation of sulfur Inst. of Nuclear Sciences, Lower Hutt, NZ. J. Sci. Technol. 12, 60–68.

Mojzsis, S.J., Cates, N.L., Bleeker, W., Hopkins, M.D., Guitreau, M., Blichert-Toft, J., Trail, D. and Abramov, O., 2014. Component geochronology of the ca. 3960 Ma Acasta Gneiss. Geochimica et Cosmochimica Acta 133, 68-96.

Moldowan, J. M., Fago, F. J., Lee, C. Y., Jacobson, S. R., Watt, D. S., Slougui, N.-E., Jeganathan, A., and Young, D. C., 1990. Sedimentary 24-n-propylcholestanes, molecular fossils diagnostic of marine algae. Science 247, 309-312.

Moldowan, J. M. and Seifert, W. K., 1979. Head-to-head linked isoprenoid hydrocarbons in petroleum. Science 204, 169-171.

Moldowan, J. M., Seifert, W. K., Arnold, E., Clardy, J., 1984. Structure proof and significance of stereoisomeric 28, 30-bisnorhopanes in petroleum and petroleum source rocks. Geochimica et Cosmochimica Acta 48, 1651-1661.

Monteiro, F.M., Pancost, R.D., Ridgwell, A., Donnadieu, Y., 2012. Nutrients as the dominant control on the spread of anoxia and euxinia across the Cenomanian-Turonian oceanic anoxic event (OAE2): Model-data comparison. Paleoceanography 27, PA4209.

Montero-Serrano, J.C., Palarea-Albaladejo, J., Martín-Fernández, J.A., Martínez-Santana, M., and Gutiérrez-Martín, J. V.,2010. Sedimentary chemofacies characterization by means of multivariate analysis. Sedimentary Geology 228, 218-228.

Moore, C.H., 1989. Dolomitization associated with meteoric and mixed meteoric and marine waters, in: Moore, C.H. (Ed.), Developments in Sedimentology 46: Carbonate Diagenesis and Porosity. Elsevier, pp. 219–235.

Moore, D.M., and Reynolds, R.C., 1989. X-ray diffraction and the identification and analysis of clay minerals. Oxford University Press, 322 p.

Moore, T. S., Murray, R. W., Kurtz, A. C., and Schrag, D. P., 2004. Anaerobic methane oxidation and the formation of dolomite. *Earth and Planetary Science Letters*, 229, 141–154.

Moorehouse, W.W. 1960. Gunflint Iron Range in the vicinity of Port Ar- thur. In Ontario Department of Mines Annual Report 69. pp. 1–40

Moreau, J., Sharp, T., 2004. A transmission electron microscopy study of silica and kerogen biosignatures in ~ 1.9 Ga Gunflint microfossils. Astrobiology 4, 196–210.

Moreira, N.F., Walter, L.M., Vasconcelos, C., McKenzie, J.A., and Mccall, P.J., 2004. Role of sulfide oxidation in dolomitization: sediment and porewater geochemistry of a modern hypersaline lagoon system. Geology 32, 701–704.

Morrow, D.W., Ricketts, B.D., 1988. Experimental investigation of sulfate inhibition of dolomite and its mineral analogues. In: Shukla, V., Baker, P.A. (Eds.), Sedimentology and Geochemistry of Dolostones. Society of Economic Paleontologists and Mineralogists, Tulsa, pp. 25–38.

Morse, J.W., Mackenzie, F.T., 1990. Geochemistry of sedimentary carbonates. Elsevier Science Publishers B.V., Amsterdam, 706 p.

Mucci, A. and Morse, J.W., 1983. The incorporation of Mg 2+ and Sr 2+ into calcite overgrowths: influences of growth rate and solution composition. Geochim. Cosmochim. Acta, 47: 217-223.

Mucci, A., 1988. Manganese uptake during calcite precipitation from seawater: conditions leading to the formation of a pseudokutnahorite. *Geochimica et Cosmochimica Acta* 52, 1859–1868.

Muller, G., Scoll, W. V., and Tietz, G., 1973, Diagenetic development of a Precambrian limestone as interpreted from a modern analogue: Sedimentology 20, 529-538

Murray, J.W. and Brewer, P.G., 1977. Mechanism of removal of manganese, iron and other trace metals from seawater, in Glasby, G.P., ed., Marine manganese deposits. Elsevier, Amsterdam, 291- 325.

Mutterlose, J., Pauly, S., Steuber, T., 2009. Temperature controlled deposition of early Cretaceous (Barremian-early Aptian) black shales in an epicontinental sea. Palaeogeography, Palaeoclimatology, Palaeoecology 273, 330 – 345.

Myers, C. R., and Nealson, K.H., 1988. Microbial reduction of manganese oxides. Interactions with iron and sulfur. *Geochimica et Cosmochimica Acta* 52, 2727–2732.

Naafs, B.D.A., Castro, J.M., De Gea, G.A., Quijano, M.L., Schmidt, D.N., and Pancost, R.D., 2016, Gradual and sustained carbon dioxide release during Aptian Oceanic Anoxic Event 1a: Nature Geoscience 9, 135–139.

Nadson, G. A., 1928. Breitag zur kenntnis der bakteriogenen kalkablagerungen. Archiv fuer Hydrobiologie, 19, 154–164.

Nägler, T.H., Siebert, C., Lüschen, H. and Böttcher, M.E., 2005. Sedimentary Mo isotope record across the Holocene fresh-brackish water transition of the Black Sea. Chem. Geol. 219, 283–295.

Nadson, G. A., 1928. Breitag zur kenntnis der bakteriogenen kalkablagerungen. Archiv fuer Hydrobiologie, 19, 154–164.

Nance, W.B., Taylor, S.R., 1976. Rare earth patterns and crustal evolution: I. Australian post-Archean sedimentary rocks, Geochimica et Cosmochimica Acta 40,1539–1551.

Nelson, R., Moldovanyi, E., Matcek, C., Azpiritxaga, I., 2000. Production characteristics of the fractured reservoirs of the La Paz field, Maracaibo basin, Venezuela. Am. Assoc. Pet. Geol. Bull. 84, 1791–1809.

Neunlist, S. and Rohmer, M., 1985. Novel hopanoids from the methylotrophic bacteria Methylococcus capsulatus and Methylomonas methanica.(22S)-35-aminobacteriohopane-30, 31, 32, 33, 34-pentol and (22S)-35-amino-3 beta-methylbacteriohopane-30, 31, 32, 33, 34-pentol. Biochem. J 231, 635-639.

Nickel, E.H. and Grice, J.D., 1998. The IMA Commission on new minerals and mineral names: Procedures and guidelines on mineral nomenclature, 1998. Canadian Mineralogist 36, 913-926

Nishimura, M. and Koyama, T., 1977. The occurrence of stanols in various living organisms and the behaviour of sterols in contemporary sediments. Geochimica et Cosmochimica Acta 41, 379-385.

Nordeng, S., Sibley, D., 1996. A crystal growth rate equation for ancient dolomites: Evidence for millimeter-scale flux-limited growth. J. Sediment. Res. 66, 477–481.

Nordstrom, D.K., Plummer, L.N., Langmuir, D., Busenberd, E, May, H. M., Jones, B.F., and Parkhurst, D.L., 1990, Revised chemical equilibrium data for major water-mineral reactions and their limitations, in Melchior, D. C, and Bassett, R. L., eds., Chemical modeling of aqueous systems II: *American Chemical Society Symposium Series* 416, 398-413.

Nudds J.R., and Selden P.A., 2008. Fossil Ecosystems of North America: A Guide to the Sites and Their Extraordinary Biotas. University of Chicago Press, Chicago, IL, 288 pp.

Nyman, S.L., Nelson, C.S., Campbell, K.A., 2010. Miocene tubular concretions in East Coast Basin, New Zealand: analogue for the subsurface plumbing of cold seeps. Marine Geology 272 (1–4), 319–336.

Orcutt, B. N., Sylvan, J. B., Knab, N. J., and Edwards, K. J., 2011. Microbial ecology of the dark ocean above, at, and below the seafloor. Microbiology and Molecular Biology Reviews 75, 361–422.

Oren, A. 1990. Formation and breakdown of glycine betaine and trimethylamine in hypersaline environments. Antonie van Leeuwenhoek 58, 291-298.

Oren, A. 1999, Bioenergetic aspects of halophilism, Microbiol. Mol. Biol. Rev., 63, 334–348.

Overmann, J., Cypionka, H., and Pfennig, N., 1992. An extremely low-light-adapted phototrophic sulfur bacterium from the Black Sea. Limnology and Oceanography, 150-155.

Palmer, M.R., 1985. Rare earth elements in foraminifera tests. Earth Planet. Sci. Lett. 73, 285–298

Palmer, M.R., Elderfield, H., 1986. Rare earth elements and neodym- ium isotopes in ferromanganese oxide coatings pf Cenozoic foram- inifera from the Atlantic Ocean. Geochim. Cosmochim. Acta 50, 409–417.

Papineau, D., Mojzsis, S.J., Coath, C.D., Karhu, J. a., McKeegan, K.D., 2005. Multiple sulfur isotopes of sulfides from sediments in the aftermath of Paleoproterozoic glaciations. Geochim. Cosmochim. Acta 69, 5033–5060.

Parkes, R., Cragg, B., Wellsbury, P., 2000. Recent studies on bacterial populations and processes in subseafloor sediments: A review. Hydrogeol. J. 8, 11–28

Parkes, R.J., Wellsbury, P., Mather, I.D., Cobb, S.J., Cragg, B.A., Hornibrook, E.R.C., Horsfield, B., 2007. Temperature activation of organic matter and minerals during burial has the potential to sustain the deep biosphere over geological time scales. Organic Geochemistry 38, 845–85.

Parkes, R., Linnane, C., Warthmann, G., Sass, H., Weightman, A., Hornibrook, E., Horsfield, B., 2011. Prokaryotes stimulate mineral H_2 formation for the deep biosphere and subsequent thermogenic activity. Geology 39, 219–222.

Parkes, R.J., Cragg, B., Roussel, E., Webster, G., Weightman, A., Sass, H., 2014. A review of prokaryotic populations and processes in sub-seafloor sediments, including biosphere: geosphere interactions. Mar. Geol. 352, 409–425.

Partin, C.A., Bekker, A., Planavsky, N.J. and Lyons, T.W., 2015. Euxinic conditions recorded in the ca. 1.93 Ga Bravo Lake Formation, Nunavut (Canada): Implications for oceanic redox evolution. Chemical Geology, 417, 48-162.

Patterson, G. W., 1971. The distribution of sterols in algae. Lipids 6, 120-127.

Patton, J. W., Choquette, P. W., Guennel, G. K., Kaltenback, A. J., and Moore, A. 1984. Organic geochemistry and sedimentology of lower to mid-Cretaceous deep-sea carbonates, Site-535 And Site-540, Leg-77. Initial Reports of the Deep Sea Drilling Project, 77, 417-443.

Paytan, A., Moore, W. S., & Kastner, M. (1996). Sedimentation rate as determined by ^{226}Ra activity in marine barite. Geochimica et Cosmochimica Acta, 60, 4313-4319.

Parnaud, Y., Gou, Y., Pascual, J., Truskowski, I., Gallango, O., and Passalacqua, H., 1995. Petroleum geology of the central part of the Eastern Venezuela Basin, in A. Tankard, S. Suarez, and H. Welsink, eds., Petroleum basins of South America: AAPG Memoir 62, 741–756.

Perez, J., 1996. Global and local controls upon the deposition of organic-rich Cretaceous sequences of Western Venezuela: a geochemical study. PhD Thesis. Fossil Fuels and Environmental Geochemistry Postgraduate Institute: NRG. University of Newcastle upon Tyne, UK.

Peters, K. E. and Moldowan, J. M. 1993. The biomarker guide: interpreting molecular fossils in petroleum and ancient sediments. Prentice-Hall, Englewood Cliffs, New Jersey, 363 pp.

Peters, K.E.,Walters, C.C., Moldowan, J.M., 2005. The Biomarker Guide: Biomarkers and Isotopes in Petroleum Systems and Earth History, second ed. Cambridge University Press, Cambridge.

Peterson, J.A., 1983, Petroleum geology and resources of south-eastern Mexico, northern Guatemala, and Belize: United States Geological Survey Circular 760, 44 p.

Petrash, D.A., 2010. Metal-enrichment in microbial carbonates : the role of carboxylated biomacromolecules. MSc Thesis, University of Alberta.

Petrash, D.A., Gingras, M., and Lalonde, S.V., Orange, F., Pecoits, E., and Konhauser, K.O., 2012. Dynamic controls on accretion and lithification of modern gypsum-dominated thrombolites, Los Roques, Venezuela. *Sedimentary Geology* 245–246, 29–47.

Petrash, D.A., Lalonde, S.V., Raudsepp, M., Konhauser, K.O. 2011a. Assessing the importance of organic matrix materials in biofilm chemical reactivity: insights from proton and cadmium

adsorption onto the commercially available biopolymer alginate. *Geomicrobiology Journal* 28, 266-273

Petrash, D.A., Lalonde, S.V., Gingras, M.K., and Konhauser, K.O., 2011b. A surrogate approach to studying the chemical reactivity of burrow mucous linings in marine sediments. *Palaios* 26, 594–600.

Picard, A., Obst, M., Schmid, G., Zeitvogel, F., and Kappler, A., 2015. Limited influence of Si on the preservation of Fe mineral-encrusted microbial cells during experimental diagenesis. Geobiology 10.1111/gbi.12171.

Piepgras, D.J., Jacobsen, S.B., 1992. The behaviour of rare earth elements in seawater: precise

Pittman Jr., J.S., Folk, R.L., 1971. Length-slow chalcedony after sulfate minerals in sedimentary rocks. Nat. Phys. Sci. 230, 64–65.

Planavsky, N., Rouxel, O., Bekker, A., Shapiro, R., Fralick, P., Knudsen, A., 2009. Iron-oxidizing microbial ecosystems thrived in late Paleoproterozoic redox-stratified oceans. Earth Planet. Sci. Lett. 286, 230–242.

Pöppelreiter, M., 2008. Realizing complex carbonate facies, diagenetic and fracture properties with standard reservoir modelling software. Geol. Soc.309, 39–49.

Powell, T. and McKirdy, D., 1973. Relationship between ratio of pristane to phytane, crude oil composition and geological environment in Australia. Nature 243, 37-39.

Poulton, S.W., Raiswell, R., 2002. The low-temperature geochemical cycle of iron: from continental fluxes to marine sediment deposition. Am. J. Sci. 302, 774–805.

Poulton, S.W., Fralick, P.W., Canfield, D.E., 2004. The transition to a sulphidic ocean, 1 . 84 billion years ago. Nature 431, 173–177.

Poulton, S.E, Canfield, D.E., 2005. Development of a sequential extraction procedure for iron: implications for iron partitioning in continentally derived particulates. Chem. Geol. 214, 209–221.

Poulton, S.W., Fralick, P.W., Canfield, D.E., 2010. Spatial variability in oceanic redox structure 1.8 billion years ago. Nat. Geosci. 3 (7), 486–490.

Poulton, S.W., Canfield, D.E., 2011. Ferruginous Conditions : A Dominant Feature of the Ocean through Earth ’s History. Elements 107–112.

Pufahl, P.K. 1996. Stratigraphic Architecture of a Paleoproterozoic iron formation depositional system: the Gunflint, Mesabi and Cuyuna iron ranges. Master’s of Science Thesis, Lakehead University, Thunder Bay, Ont.

Pufahl, P.K., and Fralick, P.W., 2000, Depositional environments of the Paleoproterozoic Gunflint Formation: in Institute on Lake Superior Geology Proceedings, 46 Annual Meeting, Thunder Bay, Ontario, Part 2 Field Trip Guidebook 51.

Pufahl, P., Hiatt, E., Kyser, T., 2010. Does the Paleoproterozoic Animikie Basin record the sulfidic ocean transition? Geology 98, 659-662.

Puga-Bernabéu, Á., Betzler, C., 2008. Cyclicity in Pleistocene upper-slope cool-water carbonates: Unravelling sedimentary dynamics in deep-water sediments, Great Australian Bight, Odp Leg 182, Site 1131A. Sediment. Geol. 205, 40–52.

Raiswell, R., 1988. Chemical model for the origin of minor limestone-shale cycles by anaerobic methane oxidation. Geology 16, 641–644.

Raiswell, R., Canfield, D.E., 1998. Sources of iron for pyrite formation in marine sediments. Am. J. Sci. 219–245.

Raiswell, R., and Fisher, Q.J., 2000, Mudrock-hosted carbonate concretions: a review of growth mechanism and their influence on chemical and isotopic composition. Journal of the Geological Society 157, 239–252.

Raiswell, R., Newton, R., and Wignall, P.B., 2001. An indicator of water-column anoxia: resolution of biofacies variations in the Kimmeridge Clay (Upper Jurassic, U.K.): Journal of Sedimentary Research 71, 286–294.

Raiswell, R., Newton, R., Bottrell, S.H., Coburn, P., Briggs, D.E.G., Bond, D.P.G., Poulton, S.W., 2008. Turbidite depositional influences on the diagenesis of Beecher's Trilobite Bed and the Hunsruck Slate: sites of soft tissue pyritization. American Journal of Science 308, 105-129.

Rasmussen, B., 1996, Early-diagenetic REE-phosphate minerals (florencite, gorceixite, crandallite, and xenotime) in marine sandstones; a major sink for oceanic phosphorus: American Journal of Science 296, 601–632.

Ravel B. and Newville M., 2005, Athena, Artemis, Hephaestus: data analysis for X-ray absorption spectroscopy using IFEFFIT: *J. Synchrotron Rad.* 12, 537-541.

Raz, S., Weiner, S., and Addadi, L., 2000. Formation of High-Magnesian Calcites via an amorphous precursor phase: possible biological implications. *Advanced Materials* 12, 38–42.

Renz, O., 1958. Estratigrafía del cretáceo en Venezuela. Bol. Minist. Min. Hidrocarb. 5, 3–48.

Renz, O., 1981. Venezuela, in: Reyment, R.A., Bengtson., P. (Eds.), Aspects of Mid-Cretaceous Regional Geology, pp.197-220.

Renz, O., 1982. The Cretaceous ammonites of Venezuela. Birkhauser Verlag, Basel, 132. (+ 40 pl.).

Ricci, J. N., Coleman, M. L., Welander, P. V., Sessions, A. L., Summons, R. E., Spear, J. R., and Newman, D. K., 2013. Diverse capacity for 2-methylhopanoid production correlates with a particular ecological niche. The ISME journal 8, 675-684.

Riciputi, L.R., Paterson, B.A., and Ripperdan, R.L., 1998, Measurement of light stableisotope ratios by SIMS: Matrix effects for oxygen, carbon, and sulfur isotopes in minerals. International Journal of Mass Spectrometry 178, 81–112.

Rickard, D., Luther, G.W., 2007. Chemistry of iron sulfides. Chem. Rev. 107, 514–62.

Rickard, David. 2012. Sulfidic Sediments and Sedimentary Rocks. Dev. Sedimentol., Developments in Sedimentology 65. doi:10.1016/B978-0-444-52989-3.00006-4

Ricketts B.D., 1982. Comment on Pecambrian dolomites: Petrographic isotopic evidence that they differ from Phanerozoic dolomites: Geology 10, 663

Ricketts, B.D., 1983. The evolution of a middle Precambrian dolostone sequence: a spectrum of dolomitization regimes. SEPM J. Sediment. Res. 53, 565–586.

Riding, R., 2006. Cyanobacterial calcification, carbon dioxide concentrating mechanisms, and Proterozoic-Cambrian changes in atmospheric composition. Geobiology 4, 299–316.

Riding, R., Fralick, P., Liang, L., 2014. Identification of an Archean marine oxygen oasis. Precambrian Res. 251, 232–237.

Robach, J., Stock, S., Veis, A., 2006. Mapping of magnesium and of different protein fragments in sea urchin teeth via secondary ion mass spectroscopy. J. Struct. Biol. 155, 87–95.

Robbins, L.J., Swanner, E.D., Lalonde, S.V., Eickhoff, M., Paranich, M.L., Reinhard, C.T., Peacock, C.L., Kappler, A. and Konhauser, K.O., 2015. Limited Zn and Ni mobility during simulated iron formation diagenesis.Chemical Geology 4

Roberts, J, A., Bennett, P.C., Gonzalez, L.A., Macpherson, G,L, Milliken, K.L., 2004. Microbial precipitation of dolomite in methanogenic groundwater. Geology 32, 277–280.

Roberts, J. A, Kenward, P. A, Fowle, D. A, Goldstein, R.H., González, L. A, and Moore, D.S., 2013. Surface chemistry allows for abiotic precipitation of dolomite at low temperature. *PNAS* 6–11, doi. 10.1073/pnas.1305403110.

Rod, E., and Maync, W. 1954. Revision of Lower Cretaceous stratigraphy of Venezuela: AAPG Bulletin 38, 93–283.

Rodgers, J., 1954. Terminology of limestone and related rocks: an interim report. J. Sediment. Res. 24.

Rowland, S., 1990. Production of acyclic isoprenoid hydrocarbons by laboratory maturation of methanogenic bacteria. Organic geochemistry 15, 9-16.

Rubinstein, I., Sieskind, O., and Albrecht, P., 1975. Rearranged sterenes in a shale: occurrence and simulated formation. Journal of the Chemical Society, Perkin Transactions 1, 1833-1836.

Sánchez-Román, M., C. Vasconcelos, T. Schmid, M. Dittrich, J. A. McKenzie, R. Zenobi, and M. A. Rivadeneyra, 2008. Aerobic microbial dolomite at the nanometer scale: Implications for the geological record: Geology 36, 879–882.

Sánchez-Román, M., Mckenzie, J.A., de Luca Rebello, A., Rivadeneyra, M.A., and Vasconcelos, C., 2009, Presence of sulfate does not inhibit low-temperature dolomite precipitation. *Earth and Planetary Science Letters* 285, 131–139.

Sass, E., Katz, A., 1982. The origin of platform dolomites; new evidence. Am. J. Sci. 1184–1213.

Sass, E., and Bein, A., 1988. Dolomites and salinity: a comparative geochemical study. In Shukla, V. and Baker P.A., eds., Sedimentology and Geochemistry of Dolostones Spec. Publs SEPM 43,223-233.

Sass, E., Bein, A., Almogi-Labin, A., 1991. Oxygen isotope composition of diagenetic calcite in organic-rich rocks: evidence for 18O depletion in marine anaerobic porewater. Geology 19, 839–842.

Schinteie, R., 2011. Ancient Life at the Extremes: Molecular Fossils and Paleoenvironmental Contexts of Neoproterozoic and Cambrian Hypersaline Settings. American Geophysical Union, Fall Meeting 2011, abstract #B33L-01

Schijf, J., Marshall, K., 2011. YREE sorption on hydrous ferric oxide in 0.5 M NaCl solutions: a model extension. Mar. Chem. doi:10.1016/j.marchem.2010.09.003.

Schippers, A., and Jørgensen, B., 2001. Oxidation of pyrite and iron sulfide by manganese dioxide in marine sediments. *Geochimica et Cosmochimica Acta* 65, 915–922.

Schlager, W., 1989. Drowning unconformities on carbonate platforms. In: Crevello, P.D., Wilson, J.L., Sarg, J.F., Read, J.F., eds., Controls on carbonate platform and basin development: SEPM Special Publication 44. SEPM, Tulsa, Oklahoma, U.S.A., pp. 15-2

Schlanger, S., Jenkyns, H., 1976. Cretaceous oceanic anoxic events: causes and consequences. Geol. en Mijnb. 55, 179–184.

Schmoker JW, Krystinik KB, and Halley RB (1985) Selected characteristics of limestone and dolomite reservoirs in the United States. Bulletin American Association Petroleum 69, 733-741

Schoell, M., McCaffrey, M. A., Fago, F. J., and Moldowan, J. M., 1992. Carbon isotopic compositions of 28,30-bisnorhopanes and other biological markers in a Monterey crude oil. Geochimica et Cosmochimica Acta 56,1391-1399.

Schofield, J. C., and Nelson, C. S., 1978, Dolomitization and Quaternary climate of Niue Island, Pacific Ocean. Pacific Geology 13, 37-48.

Schroeder, J. H. 1972. Fabrics and sequences of submarine carbonate cements in Holocene Bermuda cup reefs. Geol Rundsch 61, 708-30.

Schubert, C., 1986. Stratigraphy of the Jurassic La Quinta Formation, Mérida Andes, Venezuela: type sections Z. Deut. Geol. Ges., 137: 391-411.

Schwark, L. and Frimmel, A., 2004. Chemostratigraphy of the Posidonia black shale, SW-Germany: II. Assessment of extent and persistence of photic-zone anoxia using aryl isoprenoid distributions. Chemical Geology 206, 231-248.

Schweitzer, C.E., Lacovara, K.J., Smith, J.B., Lamanna, M.C., Lyon, M.A., Attia, Y., State, K., Nw, F.A., 2003. Mangrove-dwelling crabs (Decapoda: Brachyura: Necrocarcinidae) associated with dinosaurs from the upper Cretaceous (Cenomanian) of Egypt 77, 888–894.

Sender, L.M., Diez, J.B., Ferrer, J., Pons, D., Rubio, C., 2005. Preliminary data on a new Albian flora from the Valle del Río Martín, Teruel, Spain. Cretac. Res. 26, 898–905.

Shen, G., Fan, S., Lin, D., Su, N., and Zhou, H., 1980. The geochemistry of n-alkanes with an even-odd predominance in the Tertiary Shahejie Formation of northern China. Physics and Chemistry of the Earth 12, 115-121.

Shen, Y.N., Canfield, D.E., Knoll, A.H., 2002. Middle Proterozoic ocean chemistry: evidence from the McArthur Basin, northern Australia. Am. J. Sci. 302, 81–109.

Shima, S., Krueger, M., Weinert, T., Demmer, U., Kahnt, J., Thauer, R.K., Ermler, U., 2012. Structure of a methyl-coenzyme M reductase from Black Sea mats that oxidize methane anaerobically. Nature 481, 98–101. doi:10.1038/nature10663

Shinn E. A., Ginsburg, R. N., and Lloyd, R. M., 1965, Recent supratidal dolomite from Andros Island, Bahamas, in Pray, L. C., and Murray, R. C., eds., Dolomitization and Limestone Diagenesis: SEPM Spec. Publ. 13, 112-123.

Shinn, E.A., 1983, Tidal flat environments, in Scholle, P.A., Bebout, D.G., and Moore, C.H., eds., Depositional Environments in Carbonate Rocks: American Association of Petroleum Geologists, Memoir 33, 172–210

Sheldon, N.D., 2006. Precambrian paleosols and atmospheric CO2 levels. Precambrian Res. 147, 148–155.

Shields, G., Stille, P., 2001. Diagenetic constraints on the use of cerium anomalies as palaeoseawater redox proxies: an isotopic and REE study of Cambrian phosphorites. Chem. Geol. 175, 29–48

Shinn, E.A., 1969, Submarine lithification of Ho- locene carbonate sediments in the Persian Gulf: Sedimentology 12, 109–144.

Sholkovitz, E.R., Shen, G.T., 1995. The incorporation of rare earth elements in modern coral. Geochim. Cosmochim. Acta 59, 2749–2756.

Schopf, J.W., Packer, B.M. 1987. Early Archean (3.3-billion to 3.5-billion-year-old) micro-fossils from Warrawoona Group, Australia. Science 237:70–73.

Shapiro, R.S., Konhauser, K.O., 2015. Hematite-coated microfossils : primary ecological fingerprint or taphonomic oddity of the Paleoproterozoic? Geobiology. doi:10.1111/gbi.12127.

Shukla, 1988. Sedimentology and geochemistry of a regional dolostones: correlation of trace elements with dolomite fabrics, in V.J. Shukla and P.A. Baker, editors, Sedimentology and geochemistry of dolostones.SEPM Spec. Publ., 43, 129–144.

Sibley, D., Gregg, J., 1987. Classification of dolomite rock textures. J. Sediment. Res. 57, 967–975.

Sibley, D.F., 1991. Secular changes in the amount and texture of dolomite. Geology 19, 151–154.

Siever, R., 1962. Silica solubility 0–2001C and the diagenesis of siliceous sediments. Journal of Geology 70, 127–150

Simonin, P., Tindall, B., and Rohmer, M., 1994. Structure elucidation and biosynthesis of 31-methylhopanoids from Acetobacter europaeus. European Journal of Biochemistry 225, 765-771.

Simonson B.M., 1985. Sedimentological constraints on the origins of Precambrian iron-formations. Geol. Soc. Am. Bull. 96, 244– 252.

Simonson, B.M. 1987. Early silica cementation and subsequent diagenesis in arenites from four Early Proterozoic iron formations in North America. J. Sed. Petrol., 57: 494–511.

Simonson, B.M., and Hassler, S.W. 1996. Was the deposition of large Precambrian iron formations linked to major marine transgressions? J. Geol. 104: 665–676.

Sinninghe-Damsté, J. S., Kenig, F., Koopmans,M. P., Köstner, J.,Schouten, S., Hayes, J. M., and De Leeuw, J. W. 1995. Evidence for gammacerane as an indicator of water column stratification. Geochim. Cosmochim. Acta 59, 1895–1900.

Slaughter, M., Hill, R.J., 1991. The influence of organic matter in organogenic dolomitization. J. *Sediment. Petrol.* 61, 296–303.

Smith, J.B., Lamanna, M.C., Lacovara, K.J., Dodson, P., Smith, J.R., Poole, J.C., Giegengack, R., and Attia, Y., 2001. A giant sauropod dinosaur from an Upper Cretaceous mangrove deposit in Egypt. Science 292, 1704-1706.

Soetaert, K., Hofmann, A., Middelburg, J., 2007. The effect of biogeochemical processes on pH. Mar. Chem 106, 380-401.

Solé, V.A. Papillon, E. Cotte, M. Walter Ph., Susini, J. 2007, A multiplatform code for the analysis of energy-dispersive X-ray fluorescence spectra: Spectrochim. Acta Part B 62, 63-68.

Sommers, M.G., Awramik, S.M., and Woo, K.S., 2000, Evidence for initial calcite-aragonite composition of Lower Algal Chert Member ooids and stromatolites, Paleoproterozoic Gunflint Formation, Ontario, Canada: Canadian Journal of Earth Sciences, v. 1243, p. 1229–1243.

Sommers, M.G., and Awramik, S.M. 1996. Abiogenic "stromatolites" from the Gunflint Formation: Microstructural criteria for determining abiogenic vs. biogenic stromatolites. Abstracts with Programs, Geological Society of America. 28(7): 174

Stal, L.J., 2000. Cyanobacterial mats and stromatolites. In: BA Whitton and M Potts, Eds. The Ecology of Cyanobacteria: Their Diversity in Time and Space. Kluwer Academic Publishers, Dordrecht, pp. 61-120.

Staudt, W., Oswald, E., Schoonen, M., 1993. Determination of sodium, chloride and sulfate in dolomites: a new technique to constrain the composition of dolomitizing fluids. Chem. Geol. 107, 97–109.

Summons, R. and Jahnke, L., 1992. Hopenes and hopanes methylated in ring-A: correlation of the hopanoids from extant methylotrophic bacteria with their fossil analogues. Biological markers in sediments and petroleum, 182-200.

Summons, R. and Powell, T., 1987. Identification of aryl isoprenoids in source rocks and crude oils: biological markers for the green sulphur bacteria. Geochimica et Cosmochimica Acta 51, 557-566.

Summons, R. E., Jahnke, L. L., Hope, J. M., and Logan, G. A., 1999. 2-Methylhopanoids as biomarkers for cyanobacterial oxygenic photosynthesis. Nature 400, 554-557.

Sun, S.Q., 1994. Perspective – A Reappraisal of Dolomite Abundance and Occurrence in the Phanerozoic. J. Sediment. Res. 64A, 396–404.

Sunda, W.G. Huntsman, S.A., 1988. Effect of sunlight on redox cycles of manganese in the southwestern Sargasso Sea. *Deep-Sea Res.* 35, 1297-1317.

Sunda, W.G. Huntsman, S.A., 1990. Diel cycles in microbial manganese oxidation and manganese redox speciation in coastal waters of the Bahama Islands. *Limnol. Oceanogr.* 35, 325-328.

Sunda, W.G., Kieber, D.J., 1994. Oxidation of humic substances by manganese oxides yields low-molecular-weight organic substrates. *Nature* 367, 62–64

Sutton, F., 1946, Geology of Maracaibo Basin, Venezuela: AAPG Bulletin 30, 1621–1741.

Taylor, T.N., and Taylor, E.L., 1993. The biology and evolution of fossil plants. New Jersey, USA: Prentice Hall. (pp. 384)

Taylor S.R., McLennan, S.M., 1985. The Continental Crust: Its Composition and Evolution. Blackwell, Malden, MA.

Tebo, B.M., 1991. Manganese(II) oxidation in the suboxic zone of the Black Sea. *Deep-Sea Research* 38 *(Suppl. 2)*, S883-S905

Tebo, B. M., Bargar, J. R., Clement, B. G., Dick, G. J., Murray, K. J., Parker, D., Verity, R., and Webb, S.M., 2004. Biogenic Manganese Oxides: Properties and Mechanisms of Formation. *Annual Rev. Earth Planet. Sci.*32, 287–328.

Tejada, M.L.G., Suzuki, K., Kuroda, J., Coccioni, R., Mahoney, J.J., Ohkouchi, N., Sakamoto, T., Tatsumi, Y., 2009. Ontong Java plateau eruption as a trigger for the early Aptian oceanic anoxic event. Geology 37, 855–858.

Ten Haven, H., De Leeuw, J., Damsté, J. S., Schenck, P., Palmer, S., and Zumberge, J., 1988. Application of biological markers in the recognition of palaeohypersaline environments. Geological Society, London, Special Publications 40, 123-130.

Ten Haven, H., Rohmer, M., Rullkötter, J., and Bisseret, P., 1989. Tetrahymanol, the most likely precursor of gammacerane, occurs ubiquitously in marine sediments. Geochimica et Cosmochimica Acta 53, 3073-3079.

Tissot, B. P. and Welte, D. H., 1984. Petroleum formation and occurrence. *A New Approach Co Oil and GUS Exploration*. Springer-Verlag

Thamdrup, B, and Finster, K., 1993. Bacterial disproportionation of elemental sulfur coupled to chemical reduction of iron or manganese. *Applied Environ. Microbiol.* 59, 101–108.

Thamdrup, B, Rosselló-Mora, R., and Amann, R., 2000. Microbial manganese and sulfate reduction in Black Sea shelf sediments. *Applied Environ. Microbiol.* 66, 2888–2897.

Thamdrup, B., Fossing, H., and Jørgensen, B., 1994. Manganese, iron and sulfur cycling in a coastal marine sediment, Aarhus Bay, Denmark. Geochimica et Cosmochimica Acta 58, 5115–29.

Torres, M.E., Brumsack, H.J., Bohrmann, G. and Emeis, K.C., 1996. Barite fronts in continental margin sediments: A new look at barium remobilization in the zone of sulfate reduction and formation of heavy barites in diagenetic fronts. Chemical Geology, 127: 125-139.

Tribovillard, N., Algeo, T. J., Lyons, T., and Riboulleau, A., 2006. Trace metals as paleoredox and paleoproductivity proxies: An update. Chemical Geology 232, 12–32.

Trouwborst, R. E., Clement, B. G., Tebo, B. M., Glazer, B. T., and Luther, G. W., 2006. Soluble Mn, III, in suboxic zones. Science 313, 1955-57.

Trüper, H. G. and Pfennig, N., 1992. The family Chlorobiaceae, The prokaryotes. Springer.

Tucker, M., 1982. Precambrian dolomites: petrographic and isotopic evidence that they differ from Phanerozoic dolomites. Geology 7–12.

Tucker, M., 1983. Diagenesis, geochemistry, and origin of a Precambrian dolomite: the Beck Spring Dolomite of eastern California. J. Sediment. Res. 53.

Tucker, M.E., 1992. The Precambrian-Cambrian boundary: seawater chemistry, ocean circulation and nutrient supply in metazoan evolution, extinction and biomineralization. J. Geol. Soc. London. 149, 655–668.

Tucker, M. E., and Wright, V. P., 2009. Carbonate sedimentology. John Wiley & Sons.

Turchyn, A.V., Brüchert, V., Lyons, T.W., Engel, G.S., Balci, N., Schrag, D.P., Brunner, B., 2010. Kinetic oxygen isotope effects during dissimilatory sulfate reduction: a combined theoretical and experimental approach. Geochimica et Cosmochimica Acta 74, 2011–2024.

Tyler, S. A. and Barghoorn, E. S., 1963. Ambient pyrite grains in Precambrian cherts. Am. J. Sci. 261, 424-432.

Van Lith Y., Warthmann R., Vasconcelos C. and McKenzie J. A., 2003. Sulfate-reducing bacteria induce low-temperature Ca-dolomite and high Mg-calcite formation. Geobiology 1, 71–79.

Vahrenkamp, V. C., Franssen, R.C.W.M., Grötsch, J., Munoz, P. J., 1993, Maracaibo Platform (Aptian-Albian), northwestern Venezuela. In: Simo, J. A. T., Scott, R.W.,Masse,J.P., eds., Cretaceous Carbonate Platforms. AAPG Memoir 25, 25–33.

Van Kaam-Peters, H. M., Köster, J., De Leeuw, J. W., and Damsté, J. S. S., 1995. Occurrence of two novel benzothiophene hopanoid families in sediments. Organic geochemistry 23, 607-616.

Van Kranendonk, M.J., Webb, G.E., Kamber, B.S., 2003. New geological and trace element evidence from 3.45 Ga stromatolitic carbonates in the Pilbara Craton: support of a marine, biogenic origin and for a reducing Archaean ocean. Geobiology 1, 91–108

Van Lith, Y., Warthmann, R., Vasconcelos, C., and McKenzie, J. A., 2003. Sulphate-reducing bacteria induce low-temperature Ca-dolomite and high Mg-calcite formation. Geobiology 1, 71–79.

Vasconcelos, C., McKenzie, J.A., Bernasconi, S., Grujic, D., and Tien, A.J., 1995, Microbial mediation as a possible mechanism for natural dolomite formation at low temperatures: Nature 377, 220–222.

Vasconcelos, C. and McKenzie, J. A., 1997. Microbial mediation of modern dolomite precipitation and diagenesis under anoxic conditions (Lagoa Vermelha, Rio de Janeiro, Brazil). J. Sed. Research 67, 378–390.

Veizer J. 1983. Trace elements and isotopes in sedimentary carbonates. *In* Reeder R.J., ed., Carbonates: Mineralogy and Chemistry, Reviews in Mineralogy, I, pp. 265-300. Mineral. Soc. America, Book Crafters, Incorporated, Chelsea, MI

Veizer, J., Clayton, R. N., and Hinton, R. W.,1992. Geochemistry of Precambrian carbonates: IV. Early Paleoproterozoic (2.25 ± 0.25 Ga) seawater. Geochim.Cosmochim. Acta, 56(3), 875-885.

Venkatesan, M.I., 1989. Tetrahymanol: Its widespread occurrence and geochemical significance. Geochimica et Cosmochimica Acta 53, 3095-3101.

Ventura, M., Canchaya, C., Tauch, A., Chandra, G., Fitzgerald, G. F., Chater, K. F., and van Sinderen, D., 2007. Genomics of Actinobacteria: tracing the evolutionary history of an ancient phylum. Microbiology and Molecular Biology Reviews 71, 495-548.

Visscher, P. T. and Stolz, J. F., 2005. Microbial mats as bioreactors: populations, processes, and products. Palaeogeography, Palaeoclimatology, Palaeoecology 219, 87-100.

Volkman, J., 2003. Sterols in microorganisms. Applied Microbiology and Biotechnology 60, 495-506.

Volkman, J. K., 1986. A review of sterol markers for marine and terrigenous organic matter. Organic geochemistry 9, 83-99.

Von Breymann, M.T.K., Emeis, K.C. and Suess, E., 1992. Water depth and diagenetic constraints on the use of barium as a paleoproductivity indicator. In: Summer-Hayes, C.P., editor, Upwelling Systems: Evolution since the Early Miocene. Geological Society Special Publication 64, pp 273-284.

von der Borch, C.C. and Jones, J.B., 1976. Spherular modern dolomite from the Coorong area, South Australia. Sedimentology 23, 587–591.

von der Borch, C.C., and Lock, D., 1979. Geological significance of Coorong dolomites: Sedimentology 26, 813–824.

Wacey, D., Kilburn, M.M.R., Saunders, M., Cliff, J., and Brasier, M.D., 2011, Microfossils of sulphur-metabolizing cells in 3.4-billion-year-old rocks of Western Australia: Nature Geoscience , 1–5.

Wacey, D., Menon, S., Green, L., Gerstmann, D., 2012. Taphonomy of very ancient microfossils from the~ 3400Ma Strelley Pool Formation and~ 1900Ma Gunflint Formation: New insights using a focused ion beam. Precambrian Res. 220–221, 234–250.

Wacey, D., McLoughlin, N., Kilburn, M.R., Saunders, M., Cliff, J.B., Kong, C., Barley, M.E., Brasier, M.D., 2013. Nanoscale analysis of pyritized microfossils reveals differential heterotrophic consumption in the ~1.9-Ga Gunflint chert. Proc. Natl. Acad. Sci. U.S.A. 110, 8020–8024.Walter, M.R., 1972. Stromatolites and the biostratigraphy of the Australian Precam- brian and Cambrian. Special Papers in Palaeontology 11, 1–190

Wahl, C., Miehe, G. and Fuess, H. 2002. TEM characterisation and interpretation of fabric and structural degree of order in microcrystalline SiO_2 phases. Contrib. Mineral. Petrol. 143, 360 – 365.

Wang, D., Wallace, A.F., De Yoreo, J.J., Dove, P.M., 2009. Carboxylated molecules regulate magnesium content of amorphous calcium carbonates during calcification. Proceedings of the National Academy of Sciences 106:21511-21516.

Wanless, H. R., 1979, Limestone response to stress: pressure solution and dolomitization: Jour. Sed. Petrology 49, 437-462.

Warren, J., 2000. Dolomite: occurrence, evolution and economically important associations. Earth-Science Rev. 52, 1–81.

Warthmann, R., Van Lith, Y., Vasconcelos, C., McKenzie, J.A., and Karpoff, A., 2000, Bacterially induced dolomite precipitation in anoxic culture experiments. *Geology* 28, 1091–1094.

Watkins A.J., Roussel, E., Parkes, R.J., Sass, H., 2014. Glycine betaine as a direct substrate for methanogens (Methanococcoides spp.). Applied and Environmental Microbiology 8, 289-293.

Webb, G.E., and Kamber, B.S., 2000. Rare earth elements in Holocene reefal microbialites: a new shallow water proxy. Geochim Cosmochim Acta 64,1557–1565.

Weber, J., 1964. Trace element composition of dolostones and dolomites and its bearing on the dolomite problem. Geochim. Cosmochim. Acta 28, 1817–1868.

Wedepohl, K.H., 1978. Manganese: abundance in common sediments and sedimentary rocks. In: Handbook of Geochemistry. Springer, Berlin, 1I/3, pp. 1-17.

Weedon, G.P., 1986, Hemi-pelagic shelf sedimentation and climatic cycles: The basal Jurassic (Blue Lias) of S. Britain: Earth and Planetary Science Letters, 76, p. 321-335.

Weedon, G. P., Hallam, A. 1987. Comment and reply on 'Origin of minor limestone-shale cycles'. Geology, 15, 92-94

Westphal, H., Munnecke, A., 2003. Limestone-marl alternations : A warm-water phenomenon? Geology 31, 263–266.

Whitman, W. B., Coleman, D. C., and Wiebe, W. J., 1998, Prokaryotes: The unseen majority: Proceedings of the National Academy of Sciences of the United States of America, v. 95, n. 12, p. 6578–6583.

Wignall, P.B., 1991. Dysaerobic trace fossils and ichnofabrics in the Upper Jurassic Kimmeridge Clay of southern England. Palaios 6, 264–270.

Wignall, P., 1994. Black shales. Oxford University Press, Oxford, UK, 127 p.

Wignall, P.B., 2001. Large igneous provinces and mass extinctions. Earth-Science Reviews 53: 1-33.

Wignall, P.B., Newton, R., 1998. Pyrite framboid diameter as a measure of oxygen deficiency in ancient mudrocks. Amer. J. Sci. 298, 537–552.

Wignall, P.B., Bond, D.P.G., Kuwahara, K., Kakuwa, Y., Newton, R.J., Poulton, S.W., 2010. An 80 million year oceanic redox history from Permian to Jurassic pelagic sediments of the Mino-Tamba terrane, SW Japan, and the origin of four mass extinctions. Glob. Planet. Change 71, 109–123.

Wilkin, R.T., Barnes, H.L., Brantley, S.L., 1996. The size distribution of framboidal pyrite in modern sediments: an indicator of redox conditions. Geochim. Cosmochim. Acta 60, 3897–3912.

Windom, H.L., Schropp, S.J., Calder, F.D., Ryan, J.D., Smith Jr., R.G., Burney, F.G., Lewis, L.C., Rawlinson, C.H., 1989. Natural trace metal concentrations in estuarine and coastal marine sediments of the southeastern United States. *Environ. Sci. Technol*. 23, 314–320.

Winter, B.L., Knauth, L.P., 1992. STable 4.isotope geochemistry of cherts and carbonates from the 2.0 Ga gunflint iron formation: implications for the depositional setting, and the effects of diagenesis and metamorphism. Precambrian Res. 59, 283–313.

Wood, J.M., Bremer, E., Csonka, L.N., Kraemer, R., Poolman, B., van der Heide, T., and Smith, L.T., 2001. Osmosensing and osmoregulatory compatible solute accumulation by bacteria. Comparative Biochemistry and Physiology Part A: Molecular & Integrative Physiology, 130, 437-460.

Wright, J., Schrader, H., Holser, W.T., 1987. Paleoredox variations in ancient oceans recorded by rare earth elements in fossil apatite. Geochim. Cosmochim. Acta 51,631-644.

Wright, D.T., and Wacey, D., 2005. Precipitation of dolomite using sulphate-reducing bacteria from the Coorong Region, South Australia: significance and implications. Sedimentology 52, 987–1008.

Wright, J.E., Wyld, S.J., 2011. Late Cretaceous subduction initiation on the eastern margin of the Caribbean-Colombian Oceanic Plateau. One Great Arc of the Caribbean (?). Geosphere 7, 468–493.

Yang, Y., Sahai, N., Romanek, C.S., and Chakraborty, S., 2012. A computational study of Mg^{2+} dehydration in aqueous solution in the presence of HS^{-} and other monovalent anions – Insights to dolomite formation. Geochimica et Cosmochimica Acta 88, 77–87.

Yurewicz, D.A., Advocate, D.M., Lo, H., E.A., H., 1998. Source rocks and oil families, southwest Maracaibo basin (Catatumbo Subbasin), Colombia. Am. Assoc. Pet. Geol. Bull. 82, 1329–1352.

Zander, J. M., Caspi, E., Pandey, G. N., and Mitra, C. R., 1969. The presence of tetrahymanol in

Zenger, D. H., 1972. Dolomitization and uniformitarianism: Journal of Geological Education 20, 107-124.

Zhang, F., Xu, H., Konishi, H., Kemp, J.M., Roden, E.E., and Shen, Z., 2012. Dissolved sulfide-catalyzed precipitation of disordered dolomite: Implications for the formation mechanism of sedimentary dolomite. Geochimica et Cosmochimica Acta 97, 148–165.

Zheng, Y., Anderson, R.F., van Geen, A. and Kuwabara, J., 2000. Authigenic molybdenum formation in marine sediments: a link to porewater sulphide in the Santa Barbara Basin. Geochim. Cosmochim. Acta 64, 4165–4178.

Zumberge, J. E., 1987. Prediction of source rock characteristics based on terpane biomarkers in crude oils: A multivariate statistical approach. Geochimica et Cosmochimica Acta 51, 1625-1637.